Technical feasibility of a quick bridge replacement strategy with minimal traffic hindrance

On the retainment of existing foundations and the application of Advanced Cementitious Materials in an Accelerated Bridge Construction method

by

M.A.G. (Merijn) Stap

- Graduation Thesis -

in partial fulfilment of the requirements for the degree of

Master of Science
in Civil Engineering

at Delft University of Technology,
to be defended publicly on Tuesday 12 December 2017 at 16:00 pm.

Student number: 4022025
Date: December 2017

Thesis committee:
Prof. dr. ir. D.A. Hordijk, TU Delft, chairman
Prof. dr. K.G. Gavin, TU Delft
Dr. ir. C. van der Veen, TU Delft
Ir. A.D. Reitsema, TU Delft and Heijmans, daily supervisor
Ing. L. Tiggelman, Heijmans

An electronic version of this thesis is available at http://repository.tudelft.nl/.

TU Delft Delft University of Technology

heijmans

PREFACE

Dear reader,

This research study is submitted in partial fulfilment of the requirements for the degree of Master of Science in Civil Engineering.

The Dutch infrastructure market faces a large replacement challenge in the near future. The highway closures required during these construction works will stress the already overloaded Dutch highway network even more, leading to higher congestion rates and more economic damage.
In my opinion, it is our duty as civil engineers to not only deal with the technical challenges at hand but to this by respecting and improving the interfaces with society. This requires sustainable solutions that cause minimal hindrance and can be fit in the current circular economy. That is why the cooperation of knowledge institutes like the TU Delft and companies with market experience is so important.
In this thesis I aim to give insight into the possibilities for time-reducing construction methods and their potential incorporation in a tender strategy, while respecting the boundary conditions given by society.

I would like to thank my graduation committee for the advice and remarks that I have received on my graduation results and process. Special thanks goes out to prof.dr.ir. D.A. Hordijk for his enthusiasm and extensive feedback and my daily supervisor, ir. A.D Reitsema, for his frequent remarks and comments. I am thankful for prof.dr. K.G. Gavin for his view on the geotechnical challenges and for dr.ir. C. van der Veen for sharing his knowledge on concrete bridges and their structural behaviour. Furthermore, I would like to thank ing. L. Tiggelman, prof.ir. A.F. van Tol and ing. H.J. Everts for their input on the retainment of existing foundations, an area of expertise that is not common knowledge to me.
And finally, I would like to express my gratitude towards Heijmans, for the opportunity to incorporate practical market experience in my theoretical research study and for providing me with all the necessary support. Thanks to the enthusiasm of my direct colleagues and their willingness to always help me out, I have experienced my graduation period as very pleasant.

M.A.G. (Merijn) Stap
Delft, December 2017

SUMMARY

Bridges are a crucial part of the dense Dutch highway network. Almost 50% of the current bridges are built between 1960 and 1980 for an intended service life of 50 years and thus they might reach the end of their lifetime in the near future. This strongly indicates that a large challenge can be expected regarding infrastructural replacement.
In current practice, the replacement of bridges within the highway network often leads to substantial traffic hindrance, which has a large negative impact on the Dutch economy. Therefore reduction of traffic hindrance – together with sustainability – is generally an important quality criteria in MEAT-procedures (Most Economic Advantageous Tender) for tender assignments. In order to prepare for the upcoming replacement challenge, there is a need for contractors, the government and product suppliers to invest in the development of a sustainable tender strategy now.

The main objective of this thesis was to propose a tender strategy that incorporates sustainability and in particular the reduction of traffic hindrance into a technically feasible design. An extensive literature review has led to a quick bridge replacement strategy consisting of three time-reducing actions, listed according to their potential profit in construction time:

1. **Select the Accelerated Bridge Construction (ABC) approach**
   By means of lateral sliding or transportation by SPMTs (Self-Propelled Modular Transporters) entire superstructures can be constructed off-site and transported to their final location in a matter of hours.
2. **Retain the existing foundations**
   In terms of on-site construction time it would be beneficial to retain the existing foundations. Additionally, theory suggests that a profit in bearing capacity can be obtained compared to the current design codes, which might lead to the total elimination of additional foundation elements required.
3. **Avoid intermediate supports**
   Less elements are required if intermediate supports are avoided in the new bridge design. This does however lead to longer spans, and to prevent additional groundwork activities from an increase in deck height a higher slenderness must be obtained. Furthermore, the new superstructure design must be as light as possible, not only to allow for foundation retainment, but also to facilitate transportation and speed of erection.

In particular, the technical feasibility of these actions - both separately and combined - required more research. A case study considering a two-span plate bridge was used to investigate these strategy actions. The results show that in theory, a substantial profit in pile bearing capacity can be obtained. The largest contributors to this increase are the pile group effects, the governing CPTs (Cone Penetration Tests) and the set-up of soil over time. Part of this profit can be easily applied in practice but in most cases additional research into the mechanisms and practical applicability is required. Furthermore it was found that a trough bridge concept with open structure elements in UHPC (Ultra-High Performance Concrete) is very suitable as a slender and lightweight superstructure. The relatively low support reactions that follow from superstructure weight reduction allow for a combination with the retained existing foundation, without the need for additional foundation strengthening. However, due to the reduced cross-sectional area of the trough bridge the challenge no longer consists of obtaining the required slenderness, but of providing an adequate shear and torsion capacity following a limited compressive strut strength.
The study was put into a broader perspective by analysing a dataset of plate bridges consisting of multiple spans, which is the most commonly applied bridge type in practice. For most cases it was found that more research into the obtainable bearing capacity profit is required, in order to obtain an adequate design.
By combining the strategy actions and comparing the required on-site construction time to conventional bridge replacement practices, traffic hindrance was reduced from 85 days to a closure of just one weekend.

It was concluded that the proposed tender strategy has a high potential. Not only is the on-site reduction time diminished but the retainment of the existing foundations and the application of UHPC in a slender and lightweight superstructure may also lead to a highly sustainable design.

NOMENCLATURE

ABBREVIATIONS

ABC	Accelerated Bridge Construction
ACM	Advanced Cementitious Material
CPT	Cone Penetration Test
KEL	Knife-Edge Load
LM	Load Model
MEAT	Most Economic Advantageous Tender
NAP	Normaal Amsterdams Peil (Amsterdam Ordnance Datum)
NSC	Normal Strength Concrete
OCR	Over-Consolidation Ratio
PTL	Pile Tip Level
RWS	Dutch Federal Highway Administration (Rijkswaterstaat)
SLS	Serviceability Limit State
SPMT	Self-Propelled Modular Transporter
UDL	Uniformly Distributed Load
UHPC	Ultra-High Performance Concrete
UHPFRC	Ultra-High Performance Fibre-Reinforced Concrete
ULS	Ultimate Limit State

LIST OF SYMBOLS

Latin symbols:

A_i	Cross-sectional area
b_i	Width of an element
c_{nom}	Minimum concrete cover
d_i	Thickness of an element
D_p	Pile diameter
D_{eq}	Equivalent pile diameter
D_{max}	Maximum aggregate size
d_i	Depth of an element
E_i	Modulus of elasticity for material i
$f_{1,2}$	Densification factors for pile installation
f_{cd}	Concrete design compressive strength
f_{ck}	Concrete characteristic compressive strength
f_{ctd}	Concrete design tensile strength
F_{id}	Design load force
F_{ik}	Characteristic load force
f_{pd}	Prestress design tensile strength
f_{yd}	Steel design yield strength
g	Gravitational acceleration
h_i	Height of an element
K	Factor of lateral earth pressure *or* fibre orientation factor
L	Length of an element
l_c	Characteristic length
l_f	Individual fibre length
n	Number of elements
q_c	Cone resistance

q_{id}	Design distributed load per meter length
q_{ik}	Characteristic distributed load per meter length
Q_{id}	Design distributed load per squared meter
Q_{ik}	Characteristic distributed load per squared meter
r	Distance between two elements
R_{id}	Design resistance capacity
R_{ik}	Characteristic resistance capacity
t	Time
V_i	Volume
w	Settlement *or* crack width
w_0	Kerb width
w_1	Theoretical traffic lane width
z	Depth

Greek symbols:

α_{cc}	Long-term effects coefficient for concrete compressive strength
α_p	Pile tip resistance factor
α_s	Pile shaft resistance factor
γ_i	Specific weight *or* safety factor
Δ	Difference
$\Delta\epsilon_p$	Increase of strain in prestressing
ϵ_c	Applied concrete strain
ϵ_{c3}	Maximum linear concrete compressive strain
ϵ_{cu3}	Ultimate concrete compressive strain
ϵ_s	Applied steel strain
λ	Slenderness ratio
ν	Poissons ratio
ξ_i	Correlation factors
ρ_i	Material density
σ_i	Stress *or* area pressure
σ_{pm0}	Prestress at t = 0
$\sigma_{pm\infty}$	Prestress at t = ∞
τ_i	Shear stress
$\phi_{cc}(t)$	Concrete creep factor
Φ_i	Diameter

Contents

Part I

Main report

1 INTRODUCTION

1.1. PROBLEM DESCRIPTION

Bridges are a crucial part of the Dutch national and regional infrastructure network. With increasing mobility after the Second World War, the total length of highways has increased substantially, with the largest growth between 1960 and 1980 (Figure 1.1a). Simultaneously with the expansion of our road network, a large amount of bridges were constructed to accommodate a continuous and safe traffic flow. A dataset provided by the Dutch Federal Highway Administration (RWS) shows that almost 50% of the currently existing bridges is built in this time period between 1960 and 1980, as shown in Figure 1.1b *[Reitsema et al., 2015]*.

At time of construction, the applied design codes prescribed an intended service life of 50 years. Nevertheless many of these bridges still stand nowadays, despite the increase of traffic load over the last decades in both weight and intensity. Through conservative designs and strengthening by for example ongoing hydration of the concrete residual capacity is provided. It depends on their state during inspection whether the constructions can be re-approved or whether they have to be replaced.
However, irrespective of the possible increase of design life for individual bridges, there is a strong indication that in the near future a large challenge regarding infrastructural replacement will occur.

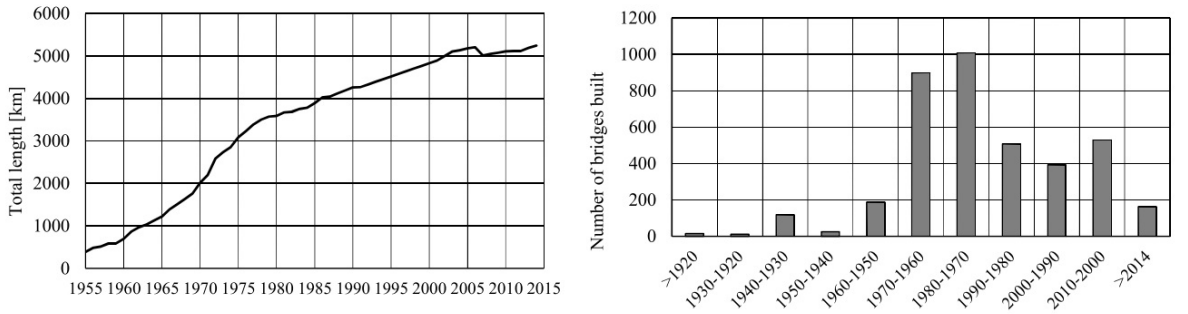

(a) Historical overview of length of Dutch main road network.

(b) Historical overview of constructed Dutch bridges in last decades.

FIGURE 1.1: Historical overview of the Dutch infrastructure *[Reitsema et al., 2015]*

In current practice, when a bridge needs to be replaced, contractors can submit their tender designs to the client (in this case RWS) which will then be assessed according to a so-called MEAT-procedure. MEAT stands for Most Economic Advantageous Tender, a procedure in which predefined award criteria based on quality requirements are taken into account as a price reduction. Designs that fulfil (part of) the quality requirements will receive a discount on their tender price and at the end the project is assigned to the design with the lowest overall price (Figure 1.2).

Especially in large infrastructural projects, the reduction of traffic hindrance is an important criterion in the MEAT-procedure. Hindrance of traffic flow has a large direct and indirect economic impact, depending on the traffic intensity and duration of hindrance. Furthermore, the overall traffic intensity has increased over

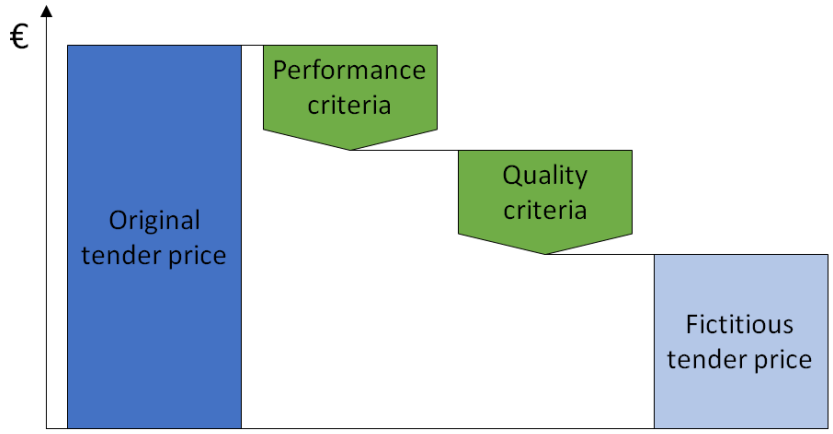

FIGURE 1.2: MEAT: fictitious tender price as the result of performance and quality criteria *[Transumo, nd]*

the last years due to economic growth and it is predicted that in 2021 the overall congestion rate will have increased by 34% (Figure 1.3) *[Francke and Wüst, 2016]*. This growth in traffic intensity will not only cause more congestions but will also cause an increase in relative economic impact.

An indication of this economical impact is given by looking at the numbers from 2014 and 2015. The total economic damage as a result of traffic hindrance in 2015 is estimated to lie between €857 million and €1.114 billion, which is an increase of 30% compared to 2014 (€655 million to €852 million). In Figure 1.3 it can be seen that this period coincides with an increase of travel time loss of more than 20%.

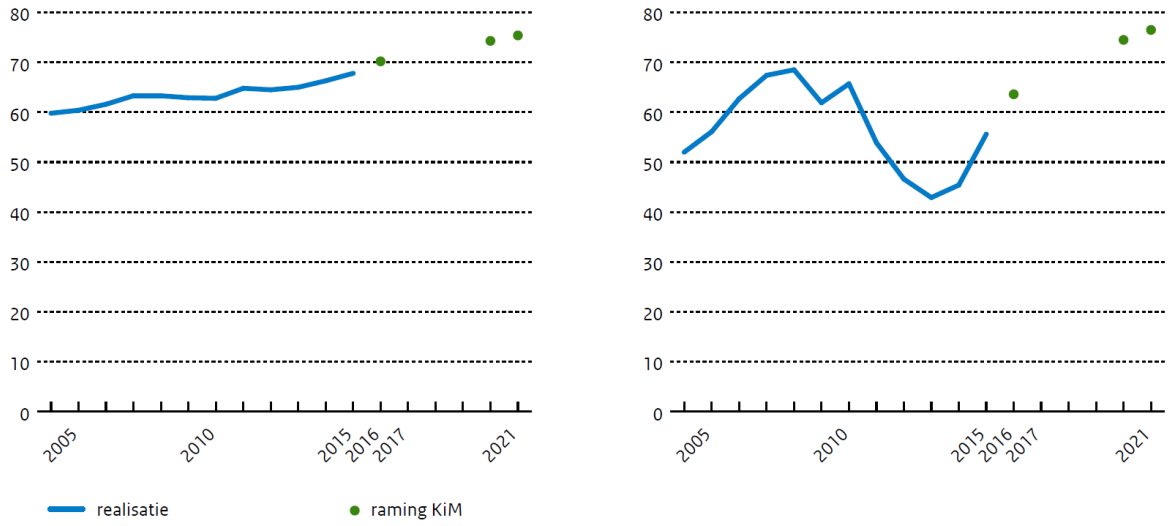

FIGURE 1.3: Predicted increase of traffic (in billion vehicle kilometres: left) and congestion (in million travel time loss hours: right) *[Kennisinstituut voor Mobiliteitsbeleid, 2016]*

Thus it is very beneficial for contractors, the government and product suppliers to invest in design concepts that minimise traffic hindrance during construction. This is especially the case with the large infrastructural replacement task that lies in the near future.

Another important quality criteria for bridge replacement nowadays is the sustainability in design and the incorporation into the circular economy. This not only refers to a structure with high durability characteristics and a long service life time, but it also means that a flexible design is required. To face these challenges smart solutions for limited material use are required, such as the use of high performance materials (like Ultra-High Performance Concrete (UHPC)) or the reuse of structural elements.

1.2. RESEARCH OBJECTIVE

The overall objective of this research is to develop a quick bridge replacement strategy that minimises the traffic hindrance during bridge construction works. It depends on the case-specific characteristics and boundary conditions to which extent on-site time reduction is required and whether this is stimulated by a price reduction in a MEAT procedure.
The on-site construction time can be reduced by limiting the amount of actions required, through quick element erection, reusing as many elements as possible and eliminating work on-site.

In the context of sustainability and the reuse of elements, retaining the existing foundation seems a promising solution. Theory even indicates that a profit in bearing capacity might be obtained, given that the state of the foundations is still adequate.
Also, preliminary research *[Reitsema, 2017]* shows that the majority of the currently existing bridges built before 1980 is constructed as plate bridges with three or four spans. In a new design it would be profitable to avoid the requirement for these intermediate supports, resulting in a longer span. A longer span will however induce higher support reactions on the support and thus the question arises whether retainment of the existing foundation is still an option.

It follows that a solution must thus be sought in an innovative slender and lightweight prefabricated bridge concept. However, to incorporate the strategy just described into project tenders, more insight must be gained in the technical feasibility of the accompanying actions.

1.3. RESEARCH QUESTION

From the problem description and research objective as described in sections 1.1 and 1.2 respectively, the following research question has been formulated:

Can a slender and lightweight UHPC bridge concept be used to enable to structural retainment of existing foundations in a low hindrance replacement strategy?

1.4. RESEARCH SCOPE

Throughout this thesis several principles are used as a basis of design, in order to comprehend the scope and extent of this research. These are:

- Focus is laid on the Dutch infrastructural network only;
- It is assumed that strengthening or maintenance of the existing bridge is found insufficient and thus replacement of the structure is necessary;
- As the Dutch highway network is very dense it is assumed that the new bridge will be located at the same position as the current bridge;
- Speed of construction is governing in all design choices as it is estimated that this has the largest impact on a MEAT-procedure;
- Main focus of the strategy is set on plate bridges with three or four spans, built before 1980;
- UHPC will be used for all structural elements;
- It is assumed that the existing foundation piles have not experienced any detrimental effects during their lifetime.

1.5. GUIDELINE THESIS

The thesis layout has been schematised in Figure 1.4. The fact that a large bridge replacement task awaits in the near future while the economic impact of (traffic) hindrance has increased, means that a solution must be sought in decreasing the on-site building time where possible. In the literature study performed at the start of this research (*[Stap, 2017]*) several requirements regarding time-reduction are identified and transformed into construction methods. This framework - leading to the proposed quick bridge replacement strategy - is elaborated in Chapter 2 and from this the areas for further research are determined.
The results of that research are presented in Chapter 3 for the retainment of existing piled foundations and in Chapter 4 for the design of an innovative UHPC bridge concept. The results of both studies have been combined in Chapter 5 in which the soil-structure interaction of the replacement strategy is considered.

The potential and applicability of the quick bridge replacement strategy will be discussed in Chapter 6. Finally, in Chapter 7, the conclusions are drawn for this graduation research and several recommendations are made for further research into this topic.

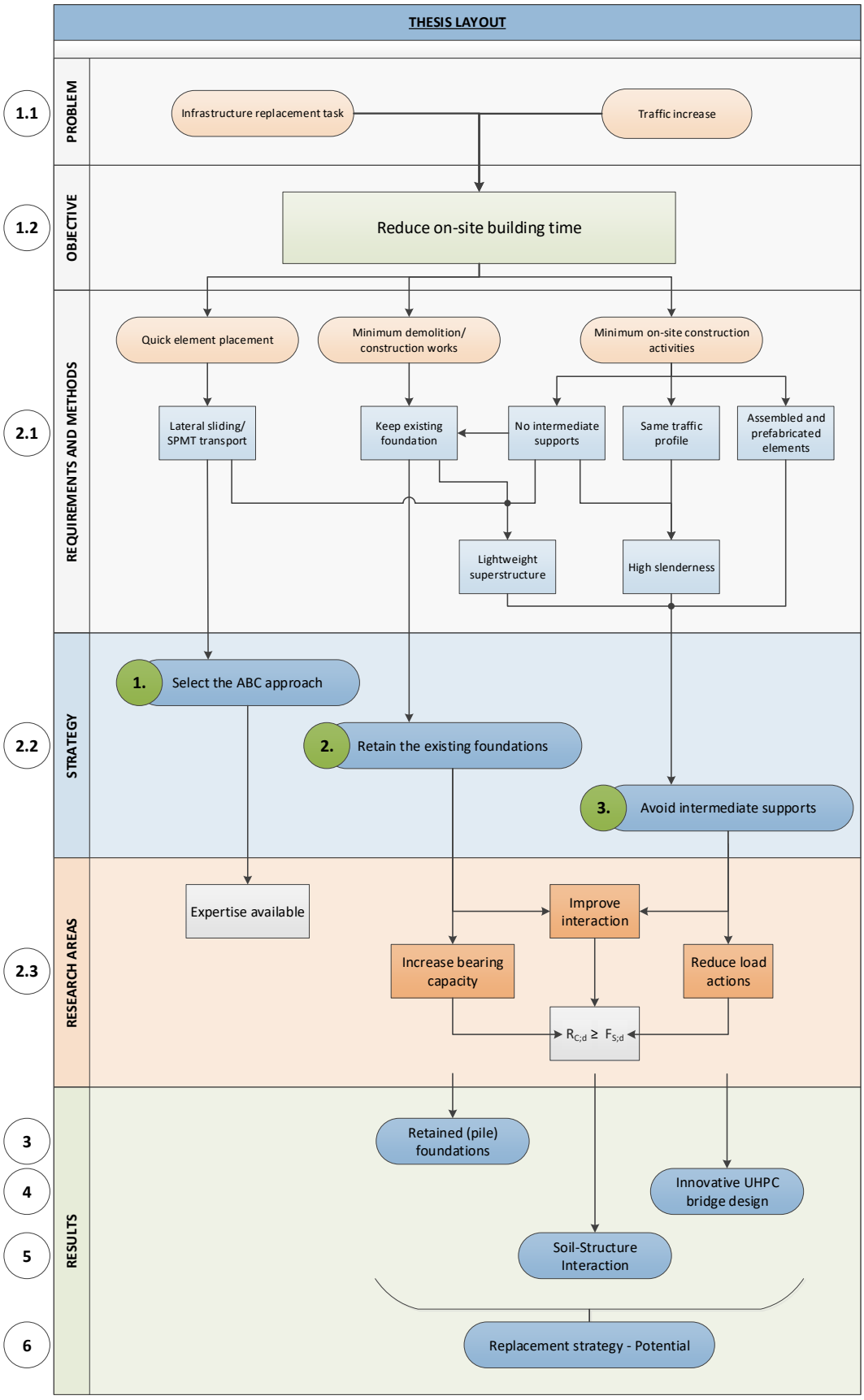

FIGURE 1.4: Schematisation of the thesis layout and different chapters in which each topic is discussed

2

REPLACEMENT STRATEGY - FRAMEWORK

The overall goal of this graduation thesis is to construct a quick replacement strategy that minimises the traffic hindrance during bridge construction works. As multiple bridges will have to be replaced in the near future and every bridge has its own characteristics and boundary conditions, this quick replacement strategy must consist of a generalised action plan. The intention of this action plan is to support decisions that have to be made regarding the execution method and therefore also the design phases, with a focus on the on-site construction time reduction.
In this chapter, the preliminary research conducted in the literature study is summarised in order to formulate a distinctive framework for a quick bridge replacement strategy *[Stap, 2017]*.

2.1. TIME-REDUCING CONSTRUCTION METHODS

When considering a quick bridge replacement strategy in which the on-site construction time is reduced as much as possible, the following requirements apply:

1. **New elements should be placed as quickly as possible:**
   Inevitably, new elements have to be placed in a bridge replacement task, but the goal is to place them as quickly as possible. This asks for prefabricated and lightweight elements to ease transportation and erection.

2. **There should be a minimum of demolition and construction works:**
   As these activities take up time, they should be limited to a minimum. This means that, preferably, elements should be reused and elements that cannot be reused but are not hindering should be left in place. Therefore, the existing foundations and abutments must be retained if possible and otherwise left in the ground.

3. **There should be a minimum of activities on-site:**
   It is favourable to remove as many activities as possible from the construction site. It is therefore desirable to avoid the need for any intermediate supports in the new design.
   In this respect, also groundwork activities should be reduced to a minimum as they require a lot of time. This leads to the requirement of maintaining the same traffic profile while avoiding intermediate supports and thus the need for a high deck slenderness.
   This also entails, that it is favourable to assemble separate elements into modular systems before placement in their final position, to reduce the amount of actions that need to be executed.

It follows from the theoretical background that there are three potential construction methods that can drastically reduce the overall on-site construction time:

- Accelerated Bridge Construction (ABC);
- Retainment of existing foundations;
- Avoid intermediate supports by using Advanced Cementitious Materials (ACM's).

These are also depicted in the thesis layout as given in Figure 1.4, of which the requirements and methods for a minimal hindrance strategy are highlighted in Figure 2.1.

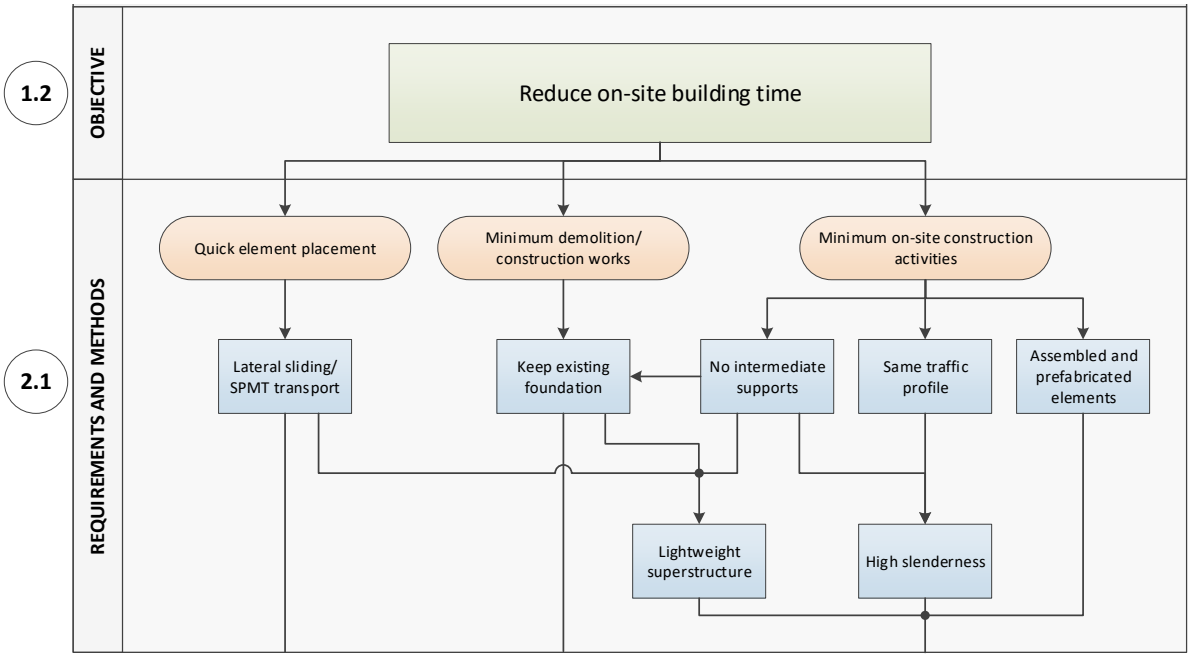

FIGURE 2.1: Schematisation of the methods for a minimal hindrance strategy

The main outcomes of the theoretical background can be judged on their potential in composing a quick replacement strategy. Below, the different methods are discussed by considering the following evaluation criteria:

- Technical feasibility;
- On-site time reduction;
- Ease of application;
- Extent of the theoretical background.

2.1.1. Accelerated Bridge Construction (ABC)

As the term Accelerated Bridge Construction already entails, ABC methods are especially suitable for bridge (replacement) projects. Various techniques of an ABC approach are already common in Dutch building practices, such as the use of prefabricated elements to speed up the process of erection. Therefore, it is not the question whether ABC should be used in a quick bridge replacement strategy, but to which extent it will be applicable. For every project, the targeted time reduction, additional construction costs and boundary conditions such as project site location and available space must be taken into consideration.
From the theoretical background, it follows that four different ABC approaches can be applied, with increasing on-site construction time reduction:

1. Use of prefabricated elements (transported by road) and erection by conventional cranes;
   This approach can be seen as the lower boundary of ABC, since the application of prefabricated elements is a prerequisite. The element dimensions are limited due to road transportation and therefore a minimum amount of elements is required. These elements will be placed one by one on the supports and abutments with the use of conventional cranes, during which the underlying road will have to be closed. Common practice in Dutch regulations is a night-time closure of 15 minutes for each element that has to be placed. After placement of the prefabricated bridge girders (with closed bottom flanges) the construction works can continue without disturbance to the underlying road. The crossing road will however be closed during the entire construction process of demolition, element erection, pouring of the in-situ concrete deck and finishing.
   A case reference, in which two bridges have been replaced within 85 days, speaks of a 40 day closure time *[Dinnissen, 2010]*.

FIGURE 2.2: Erection of prefabricated bridge girders in A9 Badhoevedorp *[Spanbeton, nd]*

2. Use of prefabricated elements (transported by road), construction of modular systems on a location nearby and the erection by conventional cranes;
   If the capacity of conventional cranes allows the erection of modular systems, consisting of several combined prefabricated elements, this approach can reduce the closure time of the underlying road since less elements have to be erected. The elements will still have to be transported by road, though, and therefore their dimensions are limited. Another option is to combine the modular systems at a location next to the project site. The total time reduction of this approach, compared to the lower boundary, is relatively small since the only profit comes from the combination of several elements into one modular system, thereby reducing the number of erection activities.

FIGURE 2.3: Prefabricated modular superstructure element placing *[Roads and Bridges, nd]*

3. Use of prefabricated elements (transported by road), erection by conventional cranes parallel to the existing bridge and placement by lateral sliding;
   If the bridge lies within a highway, the closure time of this road must be minimised. This can be done by building the entire superstructure on a lateral sliding support next to the existing bridge. During the construction period, the highway traffic is undisturbed, while the underlying road only experiences traffic hindrance from the night-time closures needed to erect the prefabricated elements or modules, as explained in the previous two approaches. Also, most of the finishing work can already be performed. If the superstructure is completed, the existing bridge is closed and demolished, after which the new superstructure is slid into place and can be connected to the highway. If necessary, a new foundation can be constructed beneath the existing bridge while it is still being used, otherwise additional closure time is needed in order to install the foundation piles and abutment.
   These activities can take place within a weekend closure of both the highway and the underlying road.

FIGURE 2.4: Lateral slide-in bridge construction *[Technical Services, nd]*

4. Use of prefabricated elements (transported by road), erection by conventional cranes on a nearby location and placement by SPMT (Self-Propelled Modular Transporter) transport;
   This approach can be chosen if the closure time has to be reduced even further, or if the traffic hindrance to the underlying road when using a horizontal launching approach is too high. Instead of constructing the entire superstructure adjacent to the existing bridge, this construction will take place on a separate project site, thus causing no traffic hindrance during erection of the prefabricated elements and other activities.
   Upon completion, both roads will be closed for demolition and placement of the superstructure by means of SPMTs, during a period of several hours to 1 day.

FIGURE 2.5: Superstructure movement by SPMT to the bridge location *[Federal Highway Administration, 2015]*

In general, it can be concluded that the best approach depends on the configuration of the road network, since the main decision parameter is the highway traffic hindrance. If a local road crosses over a highway, approaches one or two have the highest potential, since these lead to short-time closures during the night, when traffic is light. If, however, the bridge lies within a highway, either approach three or four will be chosen, as this limits the closure period of the highway traffic to several days. Furthermore, investment costs, heavy equipment costs and the available space near the project site are governing aspects in choosing the best ABC approach.

2.1.2. Retainment of existing foundations

The retainment of existing foundations is a time-reducing action as less demolition work and less installation activities are required, especially since piled foundations are not easily accessible.
As the foundation has already proven its capability of bearing the current load situation over the last 50 or

more years, this load is assumed to be the lower boundary of the pile bearing capacity in the new design. Therefore it can be assumed that, as long as the new loading situation does not constitute higher loads than before, the existing foundation can be retained without further investigation, provided that the integrity of the pile foundations is still sufficient.

However, when redesigning this bridge the current codes have to be applied, giving rise to an increase in traffic load compared to the old load configuration. Furthermore, the avoidance of intermediate supports will result in a substantial increase of dead load on the end supports and thus on the foundations. It therefore seems unlikely that the new load situation is favourable or equal to the old load situation and thus the bearing capacity of the existing foundation might not be sufficient. A logical conclusion would be to strengthen the existing foundations by adding extra piles, but the accompanying increase of on-site construction time asks for a different solution.

	Effect
Bearing capacity of pile foundations	
Decrease of α_p by 30%	-
Decrease of overall safety	+
Include positive shaft friction	+
Numerical modelling pile spring constant	+
Densification from group effects	+
Lower uncertainties (γ_M and ξ)	+
Superstructure loading	
Increase of traffic load	-
Increase of overall load due to removal of supports	-
Include negative shaft friction	-
Decrease of self-weight from UHPC	+
Change static scheme of supports	+
Make use of the soil-structure interaction:	
Use numerical modelling	+
Allow higher differential settlements	+
Increase stiffness pile cap for larger pile group	+
Allow higher settlements	+
Time-effects	
Include set-up of soil over time	+
Include material time-effects:	+
Strength improvement from ongoing hydration	+
Strength decrease from degredation mechanisms	-
Take into account creep, shrinkage and relaxation	+

TABLE 2.1: Potential influences on the pile bearing capacity of existing foundations *[Stap, 2017]*

The amount of additional piles needed can be reduced or even diminished by including several aspects regarding bearing capacity and load distribution in the design considerations. These aspects have been listed in Table 2.1 and will increase or decrease the amount of additional piles needed to a certain extent. Also, it depends on the depth of the design analysis which aspects will be taken into account. Although less piles will result in a larger reduction of on-site construction time, it must be considered to which extent the pile bearing capacity or load configuration is analysed in the design phase. If additional piles are needed anyway, due to the large increase of load on the existing piles, it might be beneficial to reduce the design activities and accept the relatively small increase in construction time. In this consideration, the construction costs, design costs, time reduction and possibilities in regulations must be taken into account. Therefore, more information is required on the sensitivity of the aspects listed in Table 2.1 with regards to pile bearing capacity and load configuration. This would enable a quick but plausible decision in an early design stage on the feasibility of the existing foundation.

2.1.3. Avoid intermediate supports by using Advanced Cementitious Materials (ACM's)

Advanced Cementitious Material, in short ACM, is a general name for concrete types that are not defined as Normal Strength Concrete (NSC) in the Eurocode (maximum concrete strength class is C50/60 *[Betonlexicon, nd]*) or contains fibres *[NEN-EN 1992-1-1, 2005]*. Overall, there is large amount of ACM's that can be distinguished, each with their own concrete mixture and accompanying advantage in comparison to NSC. From the ACM's considered in *[Stap, 2017]* it follows that, in terms of mechanical optimisation, Ultra-High Performance Fibre-Reinforced Concrete (UHPFRC) has the highest strength and durability properties. Therefore, when looking for a prefabricated, slender and lightweight structure, it can be concluded that UHPFRC has the highest potential.

Throughout the rest of this thesis the term UHPC will be used instead of UHPFRC, because in practice all UHPCs contain fibres.

The application of UHPC for the prefabricated bridge girders does not lead to on-site time reduction directly, but it does increase the technical feasibility of other time-reducing methods.

The enhanced strength and durability properties of UHPC compared to NSC result in a cross-section with less material and thus an overall weight reduction. This weight reduction is not only beneficial for the erection of the elements and the placement of entire superstructures, but also increases the chance that the bearing capacity of the existing foundations is sufficient for the new bridge. The production costs of UHPC are however substantially higher than for NSC and thus a design consideration must be executed based on reduced construction time and increased material costs. In that respect, taking into account the entire life-cycle costs of the structure might be decisive, since UHPC has a high durability and therefore requires little to no maintenance during its lifetime.

Furthermore, it turns out that the most common bridge type applied in the Netherlands is the in-situ concrete plate bridge with 3 or 4 spans, accounting for about 20% of all current bridges *[Reitsema et al., 2015]*. By using UHPC for the girders, a higher slenderness can be obtained, thus possibly enabling the avoidance of the intermediate supports while the traffic profile is kept constant. Whether it is possible to avoid all intermediate supports in the new design depends on the original deck height, the total length of the bridge and the new bridge design.

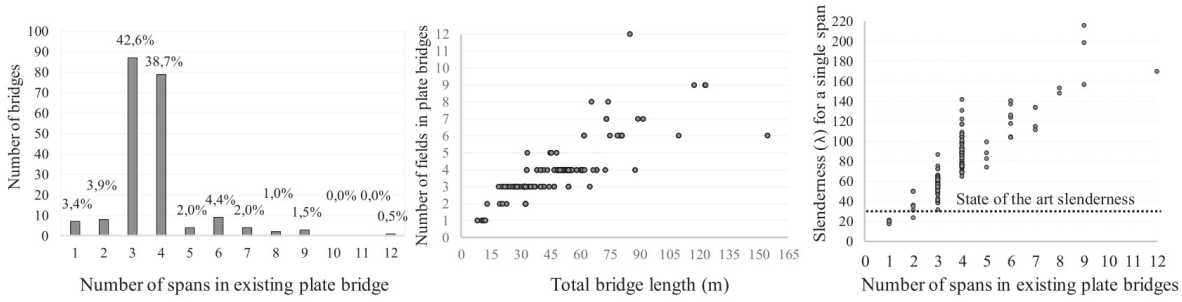

(a) Existing plate bridges (n=204) and the number of spans.

(b) Total length of existing plate bridges with the number of bridge fields.

(c) Slenderness required to replace existing plate bridges with a single span bridge.

FIGURE 2.6: Identification of plate bridges within the Dutch main road network *[Reitsema et al., 2015]*

On the other hand, not rebuilding the intermediate supports will result in an increase of dead load on the end supports, since the span length has increased. Although UHPC girders will have an overall lower weight than NSC girders, due to a cross-section with less material, the increase at the end supports will be substantial, thus increasing the need for additional foundation piles to support the existing foundation.

Therefore, it must be considered whether avoiding the intermediate supports is beneficial for the overall reduction of construction time. This decision must be based on the technical feasibility of a single span bridge, the design requirements from the client, the costs and the profit in construction time.

2.2. QUICK BRIDGE REPLACEMENT STRATEGY

These considerations lead to a general bridge replacement strategy, in which three time-reducing actions can be distinguished. For each specific project the design principles and boundary conditions result in the extent of the time-reducing actions taken into account in the design phase. These actions are, sorted according to their impact on construction time:

1. **Select the ABC approach:**
   The already commonly applied lower bound ABC approach consists of a quick construction process by making use of prefabricated elements and night-time closures. An increasing reduction of highway closure time can be obtained by placing modular systems or even entire superstructures at once, through lateral sliding or transportation by SPMT. This can ultimately result in a total closure time of only several hours to several days.
   The best approach is case-specific and depends on the boundary conditions such as road configuration, investment cost, MEAT price reductions and available construction space at a nearby location.

2. **Retain the existing foundations:**
   By retaining the existing foundations, less demolition work and less installation activities have to take place. The question is, however, whether the old pile foundation is capable of bearing the new loading situation. The lower bound bearing capacity is based on the current loading situation and an increase of load can be taken up by additional piles. This is to be expected, since the traffic load has increased and additionally a larger part of the superstructure loads will be transferred to the end supports if the intermediate supports are avoided (see action 3).
   The amount of additional piles needed can be reduced or even diminished by recalculating the pile bearing capacity, improving the soil-structure interaction and including time-effects. If possible, the exact bearing capacity of the pile foundation can be measured, provided that this does not result in additional traffic hindrance.

3. **Avoid intermediate supports:**
   The avoidance of intermediate supports in the new design reduces the on-site construction time, since less elements have to be erected. Furthermore, the presence of these supports is undesirable due to the freedom of underlying road configuration and safety issues like vehicle collisions.
   By executing this action, however, the design will also become substantially more complicated. Especially the increase of dead weight on the end supports might result in additional foundation piles needed, thus reversing the profit gained by retaining the existing foundation (see action 2). Also, in order to avoid extensive groundwork activities the traffic profile should remain intact, which demands the application of slender and lightweight UHPC bridge concepts.
   The choice whether or not to avoid intermediate supports in the new design must be based on an overall consideration of time reduction, design costs, construction costs and technical feasibility.

It must be stated that the decisions regarding a quick bridge replacement do not depend solely on the reduction of on-site construction time, but also includes the price reduction obtainable from a MEAT-procedure, the total project costs and the technical feasibility of these strategy actions.

2.3. RESEARCH AREAS FOR TECHNICAL FEASIBILITY

The actions proposed for a substantial on-site construction time reduction in a quick bridge replacement strategy will have major impacts on the design of both superstructure and foundations.
Besides the development of a minimal hindrance strategy for bridge replacement, this graduation thesis aims to demonstrate the technical feasibility of this proposed strategy. It must therefore be investigated what the impact of each separate action is on the load distribution or bearing capacity, but also on the overall project design.

1. **Select the ABC approach:**
   Although sliding in bridge constructions are not commonly applied in Holland, Heijmans has a division specialised in moving or sliding large infrastructural works. It is therefore assumed that all technical knowledge required for an ABC approach is already present within the company and within the Dutch market. Therefore this action does not require further research.

FIGURE 2.7: Lateral slide-in tunnel part in A12 Ede before movement *[Heijmans, 2016]*

FIGURE 2.8: Railway bridge Muiderberg during movement by SPMTs *[Rijkswaterstaat, ndb]*

For every structural design, an element must be able to resist the applied loads with inclusion of an adequate safety level:

$R_{C;d} > F_{S;d}$

Profit can thus be gained in increasing the resistance ($R_{C;d}$) of an element, reducing the loads ($F_{S;d}$) acting on the element or by improving the structural interaction between both elements. Therefore, with respect to the proposed strategy, it is the question whether the accompanying time-reducing actions will also turn out beneficial for the overall structural behaviour.

The technical feasibility of this strategy is investigated by looking at the following aspects:

2. **Retain the existing foundations:**
   In the field of foundation retainment there is a lot of potential but almost no practical experience. Due to the statistical nature of the soil characteristics and the many uncertainties in design, RWS and most contractors are hesitant in applying less conservative foundations. However, especially in the interaction with the superstructure, a large profit can be gained.
   From the theoretical background it follows that profit from the existing foundations can be obtained by looking at either the soil-structure interaction between soil, foundation piles and superstructure, or the bearing capacity of the foundation piles.

3. **Avoid intermediate supports:**
   In order to avoid intermediate supports in the new design the slenderness of the deck must be increased quite substantially. This profit can potentially be achieved by applying UHPC in an innovative bridge design.
   An additional benefit of slender UHPC structures is that material will be omitted to a minimum which results in light-weight elements. This in turn can be beneficial for retaining the foundation, since the overall loads acting on the foundation will be reduced. Additional load reduction can be achieved by incorporating orthotropy, which means that the loads will be distributed more evenly over both longitudinal and transversal direction of the deck.
   Also, by avoiding intermediate supports, the static scheme of the superstructure will change, which can be used in advantage but can also lead to disadvantages regarding the load distribution.

These considerations regarding strategy actions 2 and 3 have led to the research areas as presented in Figure 1.4 and which are highlighted in Figure 2.9. It follows that there are three areas of interest for further research, namely:

1. Increasing the bearing capacity of the existing foundation in order to reduce or completely eliminate the need for additional foundation piles. This is further elaborated in Chapter 3.
2. Reduce the loads of the superstructure acting on the foundation by designing an innovative UHPC bridge concept that also allows for the avoidance of intermediate supports. This is further elaborated in Chapter 4.

3. Improving the soil structure interaction between soil, foundation and superstructure to increase the possibilities for a quick bridge replacement. This is addressed in Chapter 5.

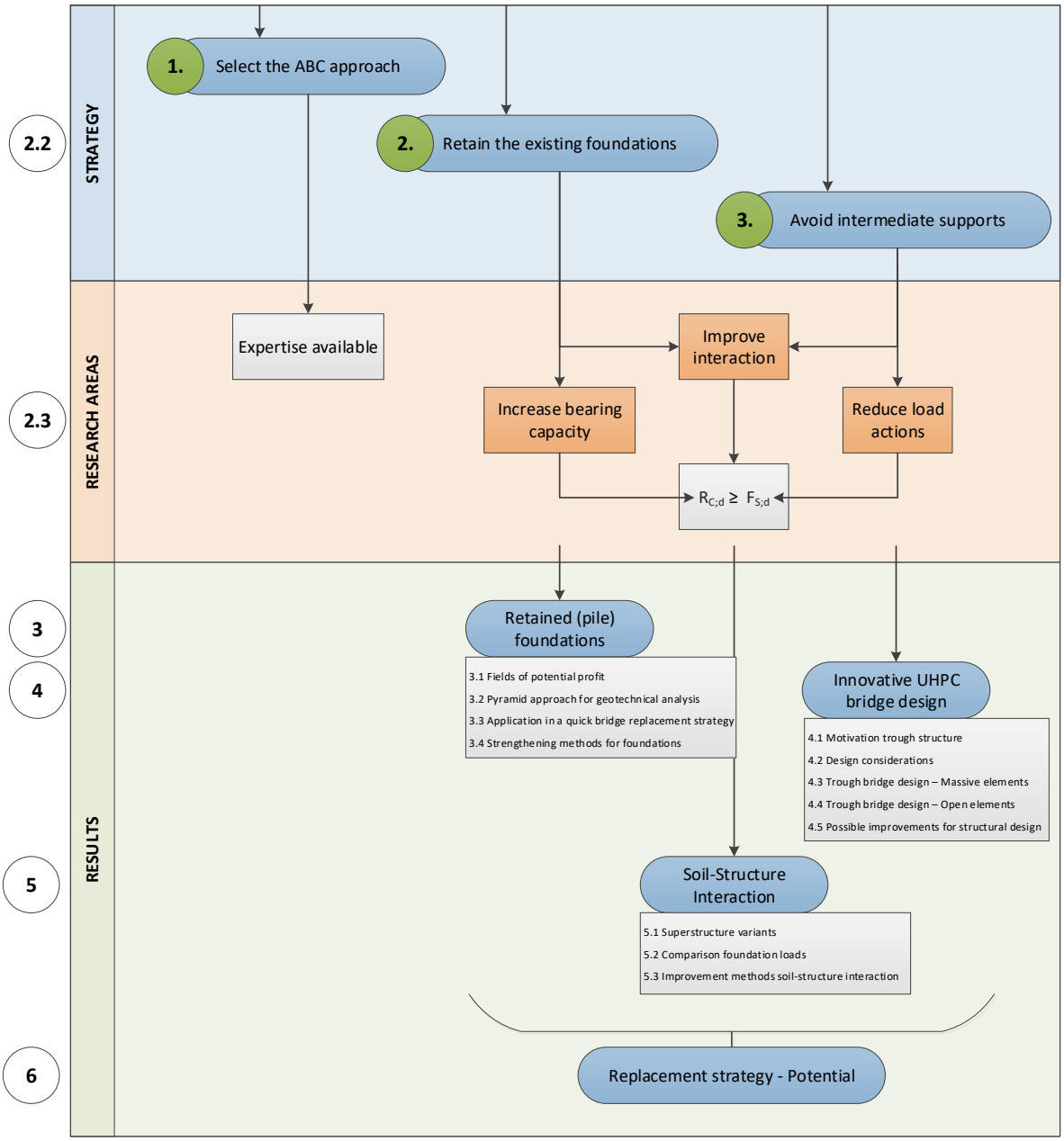

FIGURE 2.9: Schematisation of the research areas in this graduation thesis

3

RETAINED (PILE) FOUNDATIONS

In this chapter, the technical feasibility of retaining existing pile foundations is further investigated. The focus lies on enhancing the bearing capacity of the existing piles and, if required, additional strengthening methods for the foundation. In this the ultimate goal is to increase the bearing capacity in such extent that no additional strengthening is needed in the bridge replacement project. The possible increase of bearing capacity is investigated through:

- Fields of potential profit (section 3.1);
- Bearing capacity calculations through a pyramid approach (section B.2);
- Geotechnical analysis of case study A9 Gaasperdammerweg (section 3.3);
- Possible strengthening methods (section 3.4).

3.1. FIELDS OF POTENTIAL PROFIT

When looking at the potential influences that were defined in *[Stap, 2017]* (Table 2.1) and only taking the increase in bearing capacity into account, the following fields of potential profit are defined:

- Decrease of overall safety in design codes and regulations;
- Decrease of α_p by 30%, since January 2017;
- Densification of soil as a result of pile group effects;
- Long-term set-up of soil over time.

These influences will be further elaborated below.

Safety in design

TGB 1990 was introduced in 1990 as the first geotechnical design regulation based on the safety concept of probabilistic analysis. Safety factors were calculated by taking all uncertainties into account and it turned out that by implementing these safety factors the overall design safety would be much larger than before the TGB 1990. Since there was no reason to doubt the former applied design safety levels, it was decided to reduce the safety factors in such a way that the overall design safety would remain equal.
Nevertheless, a potential profit in overall design safety might be present in existing piled foundations, as it was common practice in those days to apply a somewhat conservative design.

Pile tip resistance factor α_p

In the method of Koppejan, which is used to determine the pile bearing capacity of a foundation pile, the cone resistance q_c obtained from a Cone Penetration Test (CPT) is multiplied by the factors α_p and α_s to obtain the pile tip bearing resistance and pile shaft bearing resistance, respectively. Following the introduction of the first design regulations (TGB 1990), multiple studies have been performed into the pile bearing capacity of prefabricated concrete piles by means of proof loading tests. From the comparison between the measured and calculated pile tip and shaft bearing capacity, it follows that the Dutch code overestimates the pile tip resistance by 30%, while the shaft resistance is slightly underestimated by 6%. Furthermore, a clear dependency was distinguished between the ratio of measured and calculated pile tip bearing resistance and the depth to which the pile has been driven into the sand.

Although the reduced pile factors are in theory only based on soil displacement piles, a lack of further research into the reduction for different pile types has led to a general adaptation of the Dutch code on January 1st 2017. In the new code, the pile tip resistance factor α_p has been reduced by 30% for all pile types and shaft resistance factor α_s is kept unaltered *[van Tol, 2015]*.

Potentially, an increase in bearing capacity can be obtained if further research proves that the α_p-factor for prefabricated piles can be increased for certain boundary conditions. This can especially be interesting in the case of other pile types, since their α_p reduction is also based on the proof loading tests for prefabricated piles.

Densification from group effects

The current regulations for determining the bearing capacity of piles is based on the installation of a single pile. Research has shown however, that there are two positive effects on the bearing capacity of piles installed in a pile group:

- Installation effects increase the bearing capacity of driven piles in groups:
  When driven piles are installed, the soil displacement causes compaction of the soil by reducing the volume of the soil skeleton around the pile shaft. This implies a reduction of pore volume and thus an increase of relative density, which is directly related to an increase in cone resistance. This direct relation is defined as the compaction factor f_1, which is based on the soil composition within an arbitrary influence zone of $6 \cdot D_{eq}$. For tension piles, the factor f_1 has already been included in the regulations, in which the effect depends on the initial relative density of the soil. Although this has not yet been incorporated in the regulations for compression piles, based on practical experiences it seems justified to apply the compaction factor f_1 as calculated in *[NEN-EN 1997-1, 2016]* to compression piles as well *[CUR-commissie C193, 2012]*.
- Increase of vertical effective stress from superstructure load:
  A part of the superstructure load that is present on compression piles is transferred to the subsoil layers through shaft friction. This leads to an increase of vertical stress on the bearing layer, defined as the factor f_2, which is not taken into account explicitly in the determination of bearing capacity. Again, it is already incorporated in the regulations for tension piles, but in this case it can not be used in a similar way for compression piles. In order to apply it to compression piles, further analyses is needed of the behaviour of compression piles in a pile group *[CUR-commissie C193, 2012]*.

Set-up of soil

Multiple studies have been performed on the increase of bearing capacity over time of driven pile foundations in sand, the so-called set-up of soil. The mechanism behind set-up is illustrated in Figure 3.1 and can be described as follows *[Axelsson, 2000]*:

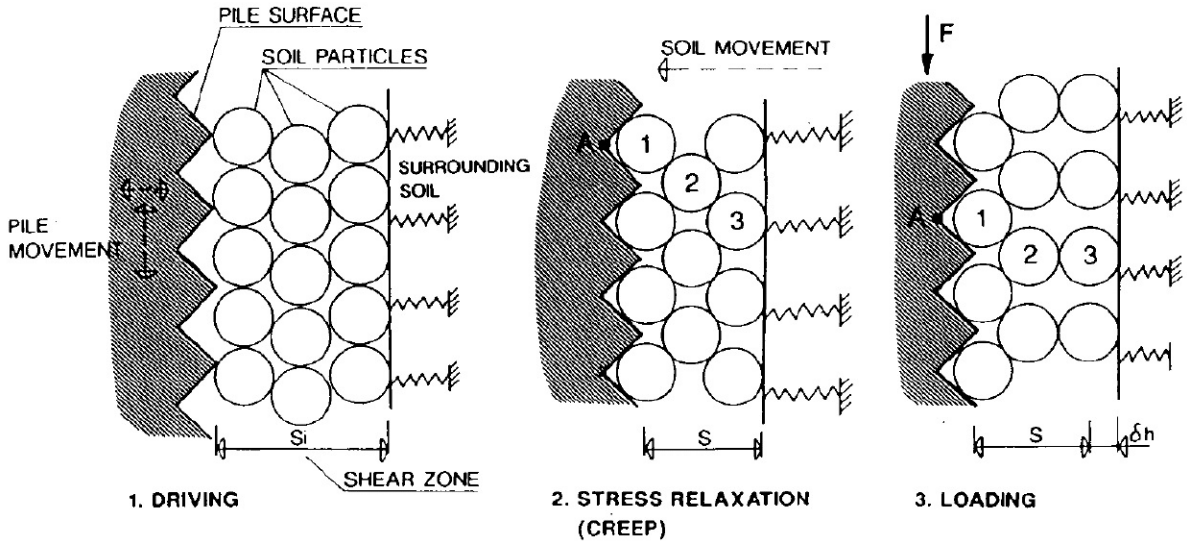

FIGURE 3.1: Conceptual model of the mechanism behind the set-up of soil *[Axelsson, 2000]*

1. Due to the surface roughness of a pile, installation of a pile causes the soil particles around the shaft to be pushed outwards, creating a highly stressed soil arch around the pile.
2. Over time, the stressed soil arch experiences relaxation, resulting in creep of the soil particles in the direction of the pile shaft. This causes an increase in normal stress and thus an increase in shaft bearing capacity of the pile.
3. The movement of particles due to creep leads to an improved interlocking of soil particles with the rough edges of the pile shaft, thus increasing the stiffness of the soil.
4. When loading, the increased interlocking of the soil particles with the roughness of the pile shaft will result in a higher shear capacity of the soil, thus resulting in a higher normal stresses on the pile shaft.

Another effect that positively influences the pile bearing capacity over time is the mechanism of ageing, in which particles in disturbed soil have the tendency to rearrange themselves according to the direction of the major principal effective stress. This will lead to a more stable soil structure and an improved interlocking at microlevel at the contact surface of the particles *[de Lange, 2013]*.

Overall, it can be seen that the set-up behaviour of soil is very complex and depends on many different parameters. Examples are the initial soil stress state, the roughness of the shaft surface and the moment of loading after installation. Nevertheless, multiple studies have demonstrated the positive effect of set-up on the bearing capacity of piled foundations over time, with values found of up to 65% increase in shaft bearing capacity per decade.

3.2. PYRAMID APPROACH FOR GEOTECHNICAL ANALYSIS

Regarding the current practice for foundation retainment and the fields of potential profit as described before, a pyramid approach is proposed (Figure 3.2).

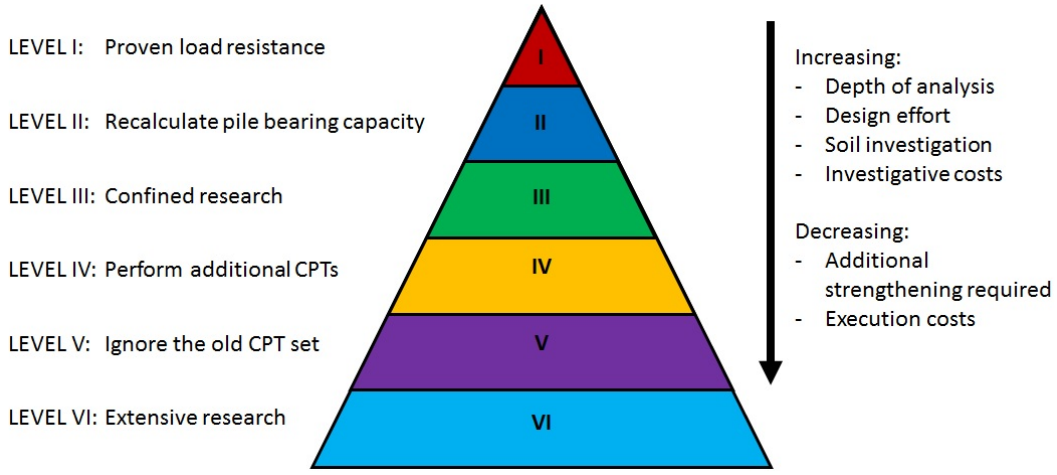

FIGURE 3.2: Schematical representation of the geotechnical analysis for retained (pile) foundations

This strategy for retaining existing pile foundations consists of six levels and each level is further elaborated below. It can be seen that for every higher level an increase in design effort, soil investigation and design costs is required. This is compensated by the fact that each level results in an increased bearing capacity and thus a decrease of additional strengthening required, therefore leading to a reduction of execution costs.
With the exception of Levels I and II, which have to be performed in all cases if the bearing capacity is being investigated, all levels can be applied separately or sequentially. Before starting a new level, the expected effort and potential profit must be considered for each case specifically, in order to make an economically supported decision.
It must be stated that in this analysis the only strengthening method included is the application of additional piles, although other methods are also available (see section 3.4).

LEVEL I: Proven load resistance (current practice)
In current practice it is common to leave the existing piles in place when an old structure supported by foundation piles is replaced, since it is a time-consuming and costly activity to remove them. In this they are

however hardly taken into account when calculating the bearing capacity required for the new structure. Instead, it is common to assume their bearing capacity to be equal to the already proven load resistance.
In other words: the existing pile foundation has proven its ability to resist the loads from the old superstructure for over its previous lifetime. After this period, the piles will have settled into their final position and the soil around and underneath the piles will be in equilibrium. It can therefore be assumed that it will be able to resist these same loads for the lifetime of the new structure without any additional settlements. Any increase of load compared to the old situation, will have to be resisted by extra piles in the new situation *[van Tol, 2017]*.

Therefore, the Level I calculation consists of comparing the old and new load situations to each other, in order to determine whether extra piles are needed.

For that, the difference in working loads must be resisted by the bearing capacity of the new piles, calculated according to the Eurocode. In formula:

Working load difference:	$\Delta F_{S;ki} = F_{S;k;2i} - F_{S;k;1i}$
Unity Check:	$\Delta F_{S;ki} \cdot \gamma_{Fi} \leq n_i \cdot \frac{R_{C;k}}{\gamma_R}$
Safety factors:	$\gamma_{Fi} = \frac{F_{S;d;2i}}{F_{S;k;2i}}$
	$\gamma_R = \frac{R_{C;d}}{R_{C;k}}$
Amount of piles:	$n_{min;i} = \gamma_{Fi} \cdot \gamma_R \cdot \frac{\Delta F_{S;ki}}{R_{C;k}}$

These formulas state the same as Figure 1.4 in Chapter 1: namely that in order to optimize a design, in this case to minimise the amount of piles needed, one can either increase the bearing capacity ($R_{C;d}$) or decrease the loads acting on the foundation ($F_{S;d2}$). The latter can be achieved by both a reduction of governing loads on the superstructure and improvement of the soil structure interaction. In this geotechnical analysis, however, emphasis is laid on increasing the bearing capacity of the foundation. Reduction of governing loads or improvement of the interaction with the superstructure will be dealt with in Chapters 4 and 5 respectively.

LEVEL II: Recalculate pile bearing capacity
The next step is to recalculate the bearing capacity of the existing pile foundation according to the current design codes and to compare this to the required bearing capacity of the new superstructure. Since the α_p factor is reduced by 30% and the safety level is more or less equal to the old regulations, it is expected that this step will not show any profit in the amount of piles needed but will in fact result in an overall loss of bearing capacity.

The required bearing capacity is given by the design load of the new superstructure. The difference between the required design bearing capacity and the design bearing capacity given by the existing foundations, must be taken up by new piles. In formula:

Unity Check:	$R_{C;d;2i} \geq F_{S;d;2i}$
Design capacity difference:	$\Delta R_{C;di} = R_{C;d;2i} - R_{C;d1}$
Unity Check:	$n_i \cdot R_{C;d1} \geq \Delta R_{C;di}$
Amount of piles:	$n_{min;i} = \frac{\Delta R_{C;di}}{R_{C;d2}} = \frac{(F_{S;d;2i} - R_{C;d1})}{R_{C;d2}}$

With $R_{C;d1}$ the bearing capacity of the old piles and $R_{C;d2}$ the bearing capacity of the new piles.

From these formulas it can be seen that the increase of bearing capacity can be obtained in both the old piles ($R_{C;d1}$) and the new piles ($R_{C;d2}$). All following levels of this pyramid approach are aimed at increasing either one of these design resistances, both simultaneously and separately.

LEVEL III: Confined research
This level consists of a desk study on the influence of different parameters that may increase the bearing capacity of both old and new piles, if approved by Rijkswaterstaat. It is expected that the necessary research and documentation for approval can be obtained within the coming years, through relatively simple research. Once approved, these adapted parameters can be applied for every case study using the right type of piles and displaying more or less the same spatial soil variation as the test locations.

- Densification factor f_1:
  It is interesting to investigate the influence of the densification factor f_1 since it increases the shaft bearing resistance. As stated in section 3.1, the CUR-committee that investigated the possible hidden safeties in the bearing capacity of piled foundations recommends the factor f_1 to be taken directly from the regulations for tension piles.
  For each axis it must be determined how many piles there are within the influence zone of a new pile ($r \leq 6 \cdot D_{eq}$) and what the relative distance is of each existing pile to the new pile. This analysis is not only valid for the newly placed piles, but also for the existing piles, since the pile group densification effect was not taken into account in the original capacity calculation.

- Influence of governing CPT:
  In current practice, mostly the governing CPT for one pile group or for the entire pile plan is taken into account for the calculation of the pile bearing capacity. Therefore, it is interesting to alter the method used to determine the governing CPT for a certain pile, for example by taking the average CPT values for one pile group or for the entire pile foundation, or by taking the nearest CPT for each pile into account. In practice, the statistical distribution of a CPT set will be of major importance in selecting the most optimal method for choosing a governing CPT for each pile. If the choice is too conservative, the amount of piles installed will be excessive, while being too optimistic will result in a lower safety level.

For the influence of the α_p-factor on the bearing capacity of the piles, more on-site research is required. Therefore, the acceptance of this influence will require more effort than the desk studies mentioned above.

- The α_p-factor reduction:
  The reduction of the α_p-factor since January 2017 has caused an extensive discussion within the geotechnical market. This reduction is based on proof loading tests performed on prefabricated concrete piles and the results were extended to other pile types, since their original α-factors were mostly based on those of the prefabricated concrete pile. The regulations state that, if it can be proven for a certain pile type that the α_p-factor does not have to be reduced, or at least not with 30%, this may be used in calculations.
  The responsibility for determining the exact values of α_p for the different pile types was placed within the market, since every manufacturer uses its own specific pile characteristics and thus a very extensive research would be necessary if all pile types are to be covered. The problem is, however, that no manufacturer is willing to invest in these proof loading tests, as competitors could also benefit from their results without contributing to the research themselves. Therefore no additional proof loading tests have been carried out up to date and thus the conservative α_p factor, reduced by 30%, has to be taken into account for design. However, voices have been going up to establish a national test ground, in which the investment is equally spread between contractors. It is thus likely that an adaptation of regulations is on its way.
  This elaboration is mainly of interest for all other pile types than the prefabricated concrete piles, as the reduction of α_p was based on proof loading tests performed on the latter. Therefore the α_p-factor for prefabricated concrete piles will probably not increase by a substantial amount. Nevertheless, the influence of a higher α_p-factor is evaluated for this case study, to show the impact of this factor on the total bearing capacity of the foundation.

LEVEL IV: Perform additional CPTs
All relatively simple desk studies have been performed in the previous steps. This next level comprises the execution of additional CPTs in order to decrease the uncertainty in soil characteristics and their spatial distribution.

Although the influence of this calculation step is probably negligible, it is a prerequisite for further the next calculation levels and thus an increase of the pile bearing capacity. Therefore this step should be considered as an easy profit in the case that a Level V or Level VI calculation is proposed.

LEVEL V: Ignore the old CPT set
It is to be expected that, if no large excavations have taken place in the area between the two CPT performances, the cone resistances will be equal or (slightly) better in the new CPT results than in the old CPT results. This is based on the following considerations:

- Difference in CPT methods;
- Settlement of weak layers over time cause an increase of cone resistance;
- Time-effects near the existing piles;
- Densification effects in a certain influence zone around the pile plan.

If this is indeed the case, it would be beneficial to ignore the old CPTs and to take only the new CPTs into account when determining the pile bearing capacity. After all, the bearing capacity is based on the governing CPT, thus by definition this will always be equal to the bearing capacity obtained in Level II when both CPT sets are taken into account. In that case the performance of a new CPT set will have no added value to the dataset.
Thus this level consists of an analysis whether or not the old CPT set may be ignored.

Not all these effects can be easily quantified. There have been various publications on the difference in CPT methods, but the detailed elaboration of this effect lies beyond the scope of this thesis. The settlement of different soil layers is almost impossible to quantify, since it depends on multiple parameters that not only differ in three dimensions but also in time. Furthermore, it is expected to have a negligible effect on the cone resistances obtained in the foundation sand layer. For the effect of densification from pile installation, it holds that the application of f_1 according to the tension pile regulations can be included in the design. For the densification factor f_2 this is however not the case, and further theoretical and practical research is needed before this effect can be quantified.

In theory, however, it is not necessary to quantify all effects mentioned above, as long as it can be proven that the difference in cone resistances as a result of the different CPT methods is lower than the overall increase of cone resistances in the new CPT set. In that case, whatever the influence of the other effects may be, the old CPTs may be ignored.
It must be stated that in case the old CPT set can be ignored, the increase of cone resistance is (partly) due to the densification effect of the existing piles. Since the exact influence of densification factors f_1 and f_2 on this increase is unknown, these factors must be neglected in the other design levels in order to be on the safe side. More research is needed into the overlap of the Level V calculation and the calculations based on f_1 (Level III) and f_2 (Level VI).

LEVEL VI: Extensive research
The last level of this geotechnical analysis consists of quantifying two effects that still require extensive additional research.

- Densification factor f_2:
  It is expected that the densification effect f_2 will result in an increase of cone resistance and thus bearing capacity underneath the pile tip. However, in contradiction to the other densification factor f_1, this factor cannot be taken from the regulations for tension piles since their effect is fundamentally different. More research is needed to quantify f_2 for different pile types and soil conditions. It must also be investigated to which extent the factor f_2 influences the pile tip bearing resistance and pile shaft bearing resistance in order to take it into account in calculations.
  Another aspect that could be very interesting and should be included in this research, is the relation between both densification factors f_1 and f_2. When looking at the theory of Koppejan, the effect of an increased shear capacity in the soil underneath the pile tip (f_2) will in theory cause an increase of the shear capacity along the pile shaft (f_1). It is thus to be expected that the theoretical relationship between q_c and f_1, taken directly from the tension pile regulations, underestimates the densification effect of driven piles on the bearing capacity of pile groups.

- Set-up of soil over time:
  Skov and Denver (1988) have proposed a relation to estimate the increase of bearing capacity over time *[de Lange, 2013]*:

$$Q_t = Q_0 \cdot (1 + A \cdot \log(\tfrac{t}{t_0})$$

  With: t the time after the end of initial driving
  t_0 the initial reference time elapsed since end of driving (= 0.5 days)
  Q_0 the pile capacity at time t_0
  Q_t the pile capacity at time t

In his research *[Axelsson, 2000]* has investigated the results from different studies and by applying above formula he defined a lower and upper boundary value for the parameter A (Figure 3.1). However, it can be seen that not all results lie within these boundaries and therefore there is no consensus yet on the value of A and further research into this area must be performed in order to get more insight. Bullock et al. (2005) states that the increase of pile shaft resistance is proven to such an extent that it can be applied in practice. Without further information conservative values for A and t_0 are proposed, namely $A = 0.1$ for cohesionless soils and $t_0 = 1$ day *[CUR-commissie C193, 2012]*.

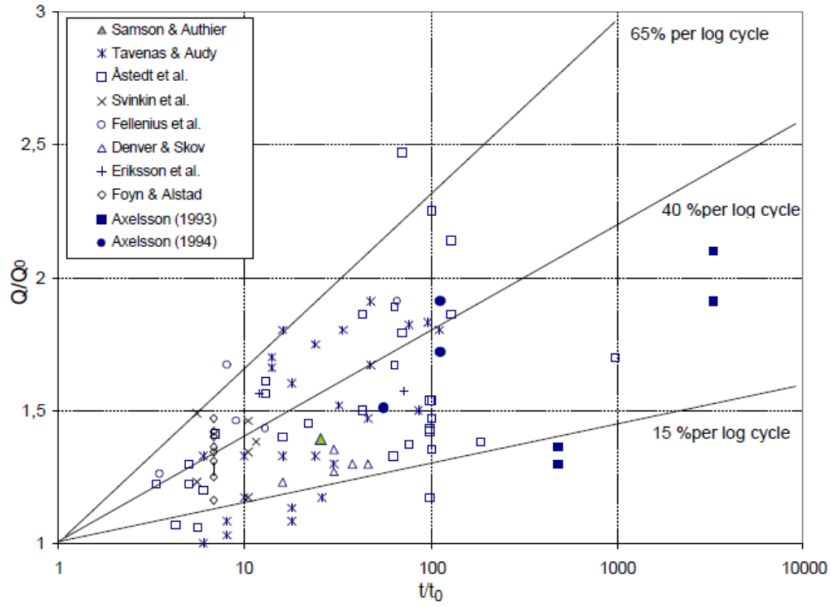

FIGURE 3.3: Case histories of long-term pile set-up *[Axelsson, 2000]*

3.3. APPLICATION IN A QUICK BRIDGE REPLACEMENT STRATEGY

The proposed pyramid approach for the increase of bearing capacity has been tested through a geotechnical analysis on a case study, the A9 Gaasperdammerweg. An introduction to this case study, relevant information and the extensive geotechnical calculations can be found in Appendix B.

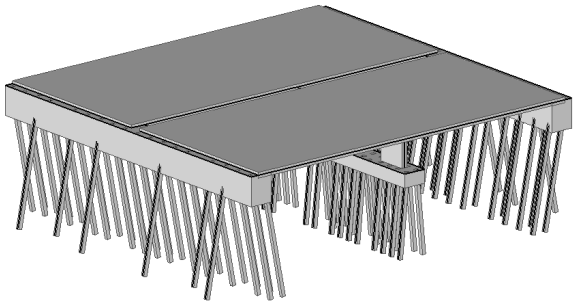

FIGURE 3.4: Finite element model of the case study A9 Gaasperdammerweg with corresponding pile plan

3.3.1. Scenarios of potential profit

In the geotechnical analysis the calculations result in the amount of additional piles needed in order to resist the increased load actions on the foundations (n_1). For that, different scenarios have been determined (see Tables 3.1 to 3.6) according to the levels with the highest potential, not only in bearing capacity profit but also in application:

Scenario 1: Current practice
This scenario contains only Level I, II and IV, which is according to the current code and current practice. The additional parameters are given in Table 3.1.

Scenario 2: Realistic profit
For the second scenario all level calculations are incorporated that will probably be approved in present projects, although they are not regulated yet. This includes the densification factor f_1, a CPT method based on the governing CPT for one pile group, additional CPTs within the vicinity of the existing foundation and a conservative set-up of 10%. All other scenarios are based on these realistic values.

Scenario 3: Lower boundary set-up
If additional research shows that indeed the lower boundary of set-up as determined by *[Axelsson, 2000]*, in which the shaft resistance increases 15% per log cycle, this can be incorporated in the analysis.

Scenario 4: Upper boundary set-up
The same is done for the upper boundary of set-up as determined by *[Axelsson, 2000]*, in which the shaft resistance increases 65% per log cycle. However, it is not considered very likely that research will indeed proof the applicability of this upper boundary.

Scenario 5: Unreduced pile tip bearing factor α_p
The discussion on the reduction of the pile tip bearing factor α_p is not concluded yet. Additional research could result in an increase of this factor. However, an increase of 30%, to the original value again, is considered very unlikely, especially for driven piles. Nevertheless, this scenario is included in the analysis, with parameters as presented in Table 3.5.

Scenario 6: Average CPT for entire pile plan
Another parameter that is considered interesting is the method to determine the governing CPT for calculation. CPT method 3, in which the average is taken of all CPTs, gives the highest profit in bearing capacity and will thus be taken into account in this analysis.

1 - Current practice		
Level	**Parameter**	
III	α_p [-]	0.70
	f_1 taken into account?	No
	CPT method	1
IV	n [-]	9
V	Old CPT set ignored?	No
	f1 taken into account?	No
VI	A [-]	0.10

TABLE 3.1: Specific parameters for scenario 1: Current practice

2 - Realistic profit		
Level	**Parameter**	
III	α_p [-]	0.70
	f_1 taken into account?	Yes
	CPT method	2
IV	n [-]	18
V	Old CPT set ignored?	Yes
	f1 taken into account?	No
VI	A [-]	0.10

TABLE 3.2: Specific parameters for scenario 2: Realistic profit

3 - Lower boundary set-up		
Level	**Parameter**	
III	α_p [-]	0.70
	f_1 taken into account?	Yes
	CPT method	2
IV	n [-]	18
V	Old CPT set ignored?	Yes
	f1 taken into account?	No
VI	A [-]	0.15

TABLE 3.3: Specific parameters for scenario 3: Lower boundary set-up

4 - Upper boundary set-up		
Level	**Parameter**	
III	α_p [-]	0.70
	f_1 taken into account?	Yes
	CPT method	2
IV	n [-]	18
V	Old CPT set ignored?	Yes
	f1 taken into account?	No
VI	A [-]	0.65

TABLE 3.4: Specific parameters for scenario 4: Upper boundary set-up

5 - Unreduced α_p		
Level	**Parameter**	
III	α_p [-]	1.00
	f_1 taken into account?	Yes
	CPT method	2
IV	n [-]	18
V	Old CPT set ignored?	Yes
	f1 taken into account?	No
VI	A [-]	0.10

TABLE 3.5: Specific parameters for scenario 5: Unreduced pile tip bearing capacity α_p

6 - Average CPT		
Level	**Parameter**	
III	α_p [-]	0.70
	f_1 taken into account?	Yes
	CPT method	3
IV	n [-]	18
V	Old CPT set ignored?	Yes
	f1 taken into account?	No
VI	A [-]	0.10

TABLE 3.6: Specific parameters for scenario 6: Average CPT for entire pile plan

3.3.2. Case study results

The results of analysis are presented for both the individual levels as for the scenarios depicted in section 3.3.1.

Individual level results

In Figure 3.5, a summary of all obtained results in Appendix B is given. Although these results are based on one case study only, and thus statistically have no significant value, they give a good indication of the possibilities of the pyramid approach in retaining existing foundations.

It can be seen that the impact of every individual level is, in general, quite small. As expected, the Level II calculation even results in an increase of additional piles needed, with regards to the Level I calculation, due to the large reduction of the α_p-factor. The calculation applied in Level IV also results in an increase of piles, since there can only be a minimal reduction in scatter factors ξ_3 and ξ_4 in this case study. All other levels result in a decrease of additional piles needed.
Especially the increase of α_p and a different choice for governing CPT (both Level III calculations) are interesting to investigate further. Furthermore, the influence of long-term set-up on the bearing capacity of the existing piles is an interesting investigation, since the possible profit can be very substantial, depending on the obtained value for set-up.

Scenario results

Overall it can be concluded that applying any level individually – with the exception of Level VI with a set-up of 65% - will not be sufficient to compensate entirely for the increase of design loads on the foundation. However, if multiple levels of the pyramid approach are combined the obtainable profit is rather significant.
In section 3.3.1 several scenarios have been formulated that consider a different depth of analysis. The results are shown in Figure 3.6. These scenarios are based on the findings of the individual levels and the potential profit.

It can be concluded that the increase of bearing capacity that follows from all scenarios but the current practice is substantial.
Although scenario 2 – which includes the realistic profit obtainable with the current knowledge – constitutes a large profit in bearing capacity, it is not enough for full retainment of the existing foundation in this case study. This is mainly caused by the limited increase of pile bearing capacity in foundation axis 2 as a result of the short piles and by the simultaneous relatively large increase of load actions on this same axis.
Thus in order to completely retain the existing foundation without additional strengthening required, more research is needed into either the set-up of soil, the α_p-factor or the CPT method in order to eliminate the need for additional piles completely.

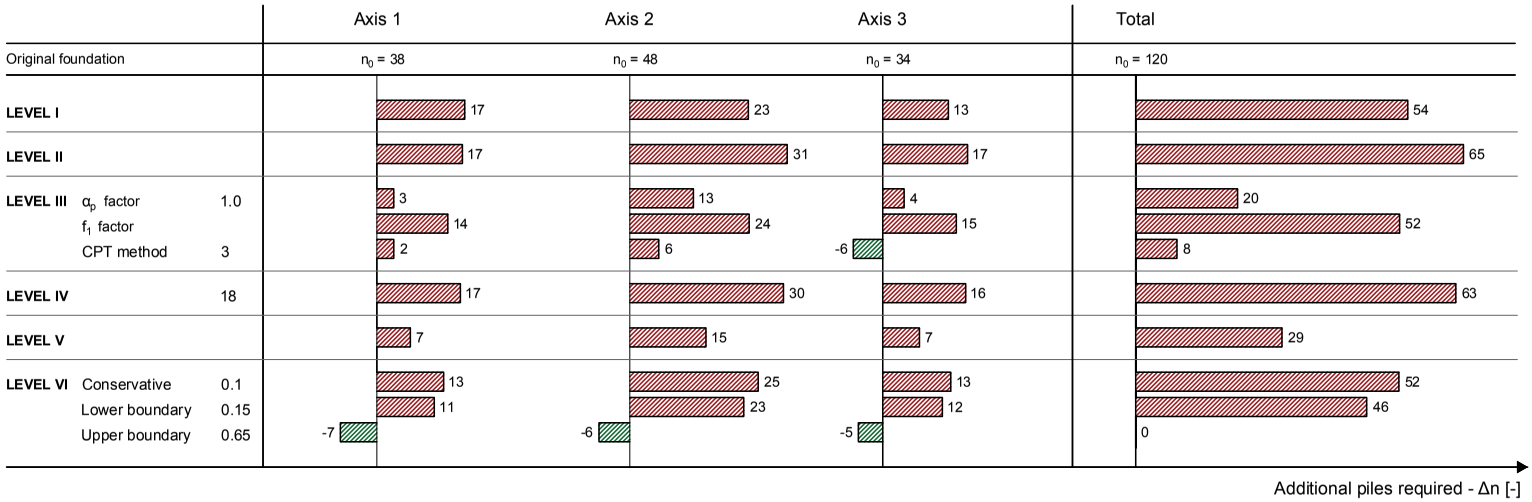

FIGURE 3.5: Amount of foundation piles required in every pyramid level separately, for both the foundation axes and the total foundation

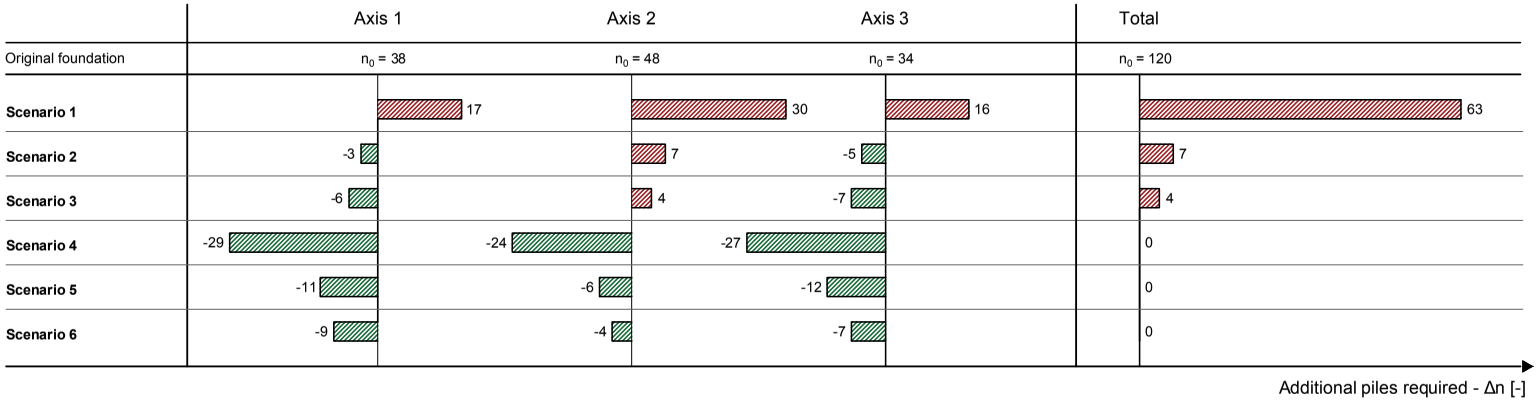

FIGURE 3.6: Amount of foundation piles required for every profit scenario separately, for both the foundation axes and the total foundation

3.3.3. General remarks

Following the results of the geotechnical analysis for the case study A9 Gaasperdammerweg, it can be concluded that the pyramid approach as proposed in this chapter is very promising. Further research is definitely required in order to utilize these profits and also the results of more case studies must be analysed, but nevertheless this study is a clear indication of the possibilities and future application of retained pile foundations.
In this geotechnical analysis several assumptions have been made that might influence the applicability of the calculations presented in Appendix B. The possible implications of these assumptions have been elaborated below. As already mentioned, further research will be needed in order to implement these assumptions into the geotechnical design for practical purposes.

Overall design safety

In *[Stap, 2017]* an extensive background is given on the reliability of a foundation and the overall design safety taken into account by the current codes and regulations. Regarding the discussion on the reliability of pile bearing capacity, *[van Tol, 1994]* states that the safety margin already applied in Dutch practice before introduction of the TGB1990, the first geotechnical design regulation that made use of probabilistic analysis, was sufficient. Although the safety factors obtained from the probabilistic approach resulted in a larger safety margin, it was decided to adapt these safety factors in such a way that the overall design safety would remain even. From this it can be concluded that either the uncertainties taken into account in the probabilistic analysis are smaller than expected or that there are some hidden safeties present in the system.

In this geotechnical analysis, research has been done into these hidden safeties and their application in practice. However, *[van Tol, 1994]* clearly states that when using these hidden safeties in design this must be accompanied by a reduction of uncertainties, otherwise the overall safety of the system might be diminished. Thus, in order to obtain a more economical design and to apply the use of this pyramid approach in practice, more research must be conducted into the overall design safety and the reduction of uncertainties.

Available case study information

The applied case study on the A9 Gaasperdammerweg was chosen because it comprises a plate bridge built before 1980 for which both original and new CPTs were available. These new CPTs were however not executed for examination of the existing foundation put for the purpose of a new temporary structure to the south of the bridge. It is expected that, when new CPTs are performed in the direct vicinity of the existing foundation, either in-between or directly next to the already present piles, the positive influences as mentioned in Level V will be increased.
Also, little information on the original foundation design was present. Therefore all calculations performed in this analysis were based on the maximum working load per meter of abutment length as prescribed by the structural engineer. It is also uncertain to what degree several mechanisms have been taken into account, such as positive and negative shaft friction, settlement of the piles and redistribution of the loads.

Quality of the existing foundation

In this analysis it is assumed that the existing foundations are still in perfect state and have not experienced any detrimental effects on their bearing capacity during their lifetime. This assumption should be checked in practice and an adequate control system should be developed. The largest challenge in this respect is to determine the quality of the existing foundation without causing hindrance to the highway traffic.
In this respect also the determination of the exact pile locations and their respective settlements is of interest for the applicability of this geotechnical approach.

Influence of inclined piles

In this analysis, the inclination of the piles has been neglected in obtaining the bearing capacities. If this analysis is to be applied in practice, the influence of this inclination must be further investigated.

Influence of PTL new piles

In Level II in Appendix B the influence of the PTL of the newly installed piles has been investigated and it can be seen that much higher bearing capacities can be obtained. It is however unknown what the influence of a different PTL is on the calculations performed in the other levels, such as the group effect on the existing piles or the pile spring stiffness of the new piles.

Load distribution
In this geotechnical analysis it is assumed that all additional load in the new design will be carried by the newly placed piles. In reality, however, the old piles will behave stiffer than the new piles since the former have already settled into an equilibrium with the surrounding soil. The consequence is that the load action of the new bridge will redistribute itself according to the relative stiffness of the different piles and thus the old foundation will carry part of the additional load.

Horizontal loads
The horizontal loads following from earth pressures on the abutments are neglected in design but will have a large influence on the horizontal loads on the foundation piles. This influence is especially interesting in combination with inclined piles.

Different foundation piles
In this geotechnical analysis only driven prefabricated concrete piles are investigated. There are however many different pile types and also shallow foundations are often applied in bridge foundations located in the eastern part of the Netherlands. Therefore this analysis should be extended for the use of other foundation types.

3.4. STRENGTHENING METHODS FOR FOUNDATIONS

In case the existing foundations are not capable of resisting the increased load from the superstructure, they must be strengthened in order to increase the overall bearing capacity. For this, several methods can be distinguished, of which the most common will be briefly discussed below:

- **Additional piles**
  The shortage on foundation bearing capacity can be solved by installing additional piles next to or in-between the existing piles. These additional piles will have to be dimensioned according to the present design codes and will therefore have to take the reduction in pile tip bearing resistance into account. On the other hand, if the new piles are installed in the influenced zone of the existing foundation, use can be made of an increased cone resistance from group effects that is measured in new CPTs.

  The location of the new piles depends on the available on-site construction time and the spacing between the existing piles. If time is stringent, the choice can be made to install the piles next to the existing foundation without hindrance to the traffic, however, the increased cone resistance will be lower due to a smaller influence from adjacent piles. To increase this influence, the new piles can be installed in-between the existing piles, provided that these piles are not too close to each other. In both cases, however, it must be examined how the new piles can be coupled to the existing piles through the existing pile cap or through a new pile cap, again depending on the available on-site construction time.

  Another question is whether it is possible to perform CPTs within the influence zone of the existing foundation, regarding the existing pile cap and the unhindered traffic flow.

- **Densification of soil**
  The pile bearing capacity of the existing pile foundation could In theory also be increased by further densification of the soil in the influence zone of the pile tip and shaft.

  This is automatically achieved when driving additional piles into the influence zone, but can also be obtained by vibrations or dynamic methods. The densification is the result of a decrease in pore volume from the dissipation of pore water and is thus a function of the permeability of the soil. During densification the soil particles must shift relatively to each other, thereby breaking contact and thus a temporary relaxation of effective stress will take place. This means an increase in water pore pressure, thereby instigating a pressure gradient that pushes the pore water away to a low pressure zone.

  However, since the effective stress (temporarily) decreases during densification, this method might have an undesirable influence on the bearing capacity of the existing foundation. As the magnitude and long-term effect of this relaxation is unknown, it is not recommended to apply vibration or dynamic densification as a strengthening method. Nevertheless, the densification as a result of additional pile driving is of course still an option.

- **Grouting**
  Another method to increase the soil bearing capacity is grouting, through reduction of soil permeability and an increased shear strength or stiffness. Different types can be distinguished:
  - Permeation grouting;
    Here the pore water is replaced by a fluid that hardens after injection, but the soil structure itself is left intact. This method decreases the permeability of the soil but also increases the shear strength and stiffness of the soil. It is mainly suitable for strengthening and supporting foundations on sand, creating horizontal or vertical water barriers and limiting settlements as a result of tunnelling.
  - Displacement grouting and jet grouting;
    These are grouting methods that do affect the soil structure. In jet grouting, the soil is cut up and mixed with a hardening injection fluid, often cement. As this method does not depend on the permeability of the soil, the application is much more widespread. It is mainly used to strengthen and support shallow foundations, creating water retaining layers and strengthening the soil when excavating underneath an existing building. Displacement grouting is also called fracture grouting, which displaces the soil somewhat. A distinction is made between compaction grouting, in which the soil is stressed and densified, mainly to restore an unwanted relaxation of the soil, and compensation grouting that compensates or prevent settlements to occur.

  In general, however, all these grouting methods disturb the soil to a certain extent before increasing the bearing capacity. The magnitude and effect on the already present piles is unknown and thus this method is not suitable as a strengthening measure for the existing foundation. Furthermore, the initial stress level will be rather high from the thick piles that have been present and loaded for over 50 years and it is expected that this high initial stress level can never be reached again, let alone be improved, after grouting.

From these considerations it can be concluded that the highest potential in strengthening of the existing foundation must be sought in the installation of additional piles.

4

INNOVATIVE UHPC BRIDGE DESIGN

From Chapter 2 it follows that an innovative slender and lightweight structure is needed to allow for the avoidance of intermediate supports. Of all ACM's considered, UHPC has the highest strength and durability properties and thus it has the highest potential for application in a prefabricated slender and lightweight structure. The resulting weight reduction compared to a NSC structure is not only beneficial for the erection of the elements and the placement of entire superstructures, but it also increases the chance that the bearing capacity of the existing foundation is sufficient for the new bridge.

This chapter will discuss the design of a suitable UHPC bridge structure. All calculations and verifications can be found in Appendices E to I, but this chapter aims to give an adequate summary of the obtained results and implications. This is done by addressing the following points:

- Motivation for a trough bridge design (section 4.1);
- General design considerations (section 4.2);
- Massive element trough bridge design (section 4.3): dimensions and Unity Checks;
- Open structure element trough bridge design (section 4.4): dimensions and Unity Checks;
- Possible improvements for structural design (section 4.5).

4.1. MOTIVATION TROUGH STRUCTURE

The goal of this innovative bridge design in UHPC is to improve the slenderness of the concrete deck compared to the original plate structure with multiple spans present in the case study A9.
Avoiding the intermediate supports in a new design and thereby increasing the span length will lead to higher cross-sectional loads. In general it holds that the higher these cross-sectional loads are, the more construction height is needed to generate an adequate bearing capacity.

Box girders in NSC

According to the design graphs given by *[Spanbeton, 2017]* box girders with concrete class C60/70 can be used to span a length of 40 m in a single go. For that, a construction height of 1200 mm is needed as illustrated in Figures 4.1 and 4.2, which requires a heightening of the original alignment.

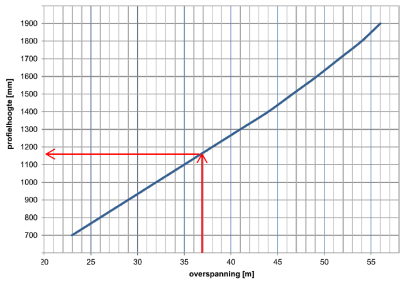

FIGURE 4.1: Maximum slenderness achievable for prefabricated box girders in NSC *[Spanbeton, 2017]*

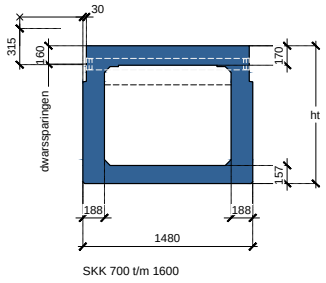

FIGURE 4.2: Cross-sectional dimensions for prefabricated box girders with h = 1200 mm in NSC *[Spanbeton, 2017]*

However, in a quick bridge replacement strategy where groundwork activities must be avoided as much as possible, an increase of deck height is not desired. When looking at the maximum slenderness for box girder in NSC according to *[Spanbeton, 2017]*, the limit in current practice is reached at $\lambda = 35$.

A possible solution for this slenderness problem lies in the application of UHPC, as already discussed in subsection 2.1.3. UHPC has an enhanced compressive strength compared to NSC and can therefore resist much higher prestress forces. The increased bending resistance that is thus obtained can result in a higher slenderness of the bridge deck.
Furthermore, UHPC has high durability characteristics which are beneficial for the life-cycle costs of the structure, since less to no maintenance is required throughout its lifetime.

Box girders in UHPC

In his PhD research, *[Reitsema, 2017]* has developed a calculation program to design box girders in UHPC with concrete strength class C170/200. By applying UHPC, a slenderness of $\lambda = 40$ - 60 can be reached, depending on the span length and construction height (see Figure 4.3).

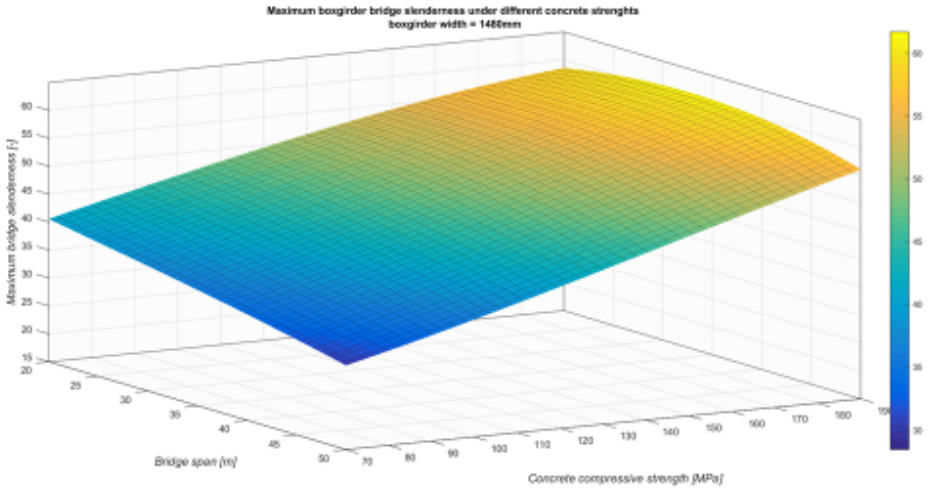

FIGURE 4.3: Maximum slenderness achievable for prefabricated box girders in UHPC as given by *[Reitsema, 2017]*

For this case study design a slenderness $\lambda = 60$ is required, which is close to the limit of the theoretical possibility. In order to be sufficient for design, the depth of the asphalt layer is taken at a lower value than prescribed by current practice so that the construction height can be increased from 610 mm to 670 mm. Due to the enhanced structural characteristics of UHPC this decrease in asphalt layer is not considered to cause any problems. The resulting dimensions are given in Figure 4.4 with the accompanying Unity Checks presented in Figure 4.5.

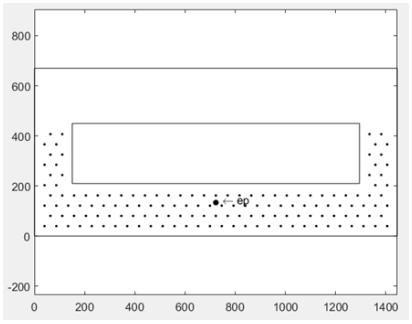

FIGURE 4.4: Cross-sectional dimensions for a box girder in UHPC with a length of l = 36.8 m and a height of 0.67 m *[Reitsema, 2017]*

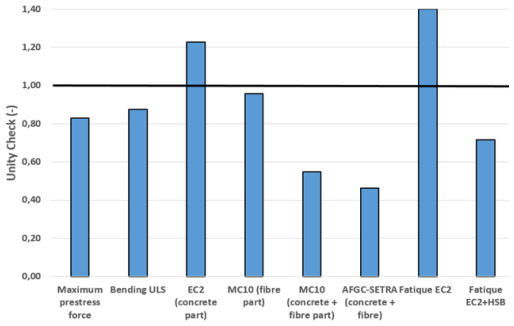

FIGURE 4.5: Unity Checks for the UHPC box girder design by *[Reitsema, 2017]*

Another possible solution lies in the application of a trough bridge (Figure 4.6). With this design it is possible to keep the current deck height fixed while also creating sufficient structural height within the raised sides of the trough.

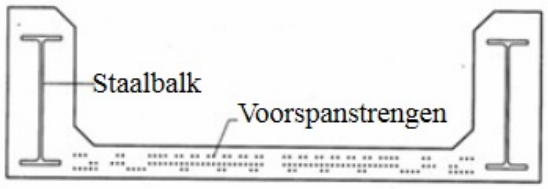

FIGURE 4.6: Cross-sectional view of a typical trough girder *[FEBE, 2013]*

Trough structures are mainly applied in railway bridges as prefabricated monolithic elements integrated with considerate steel profiles to guarantee its structural behaviour (Figure 4.7). The main challenges in designing a trough structure lie in the connection of the bottom plate and side elements - to withstand large shear forces - and the containment of cracks that have a detrimental effect on the prestressing *[Dienst Expertise Beton en Staal, 2012]*.

FIGURE 4.7: Prefabricated trough girder *[Dienst Expertise Beton en Staal, 2012]*

For application in a traffic bridge this structural concept must be adapted. After all, the significant width of a highway is not suitable for prefabrication and transportation as one element. Deck and side elements must therefore be divided into elements of limited dimensions and this means that the deck will no longer consist of one plate element but of multiple floor girders, as illustrated in Figure 4.8.

The advantage of this construction is that the deck will no longer be spanning from abutment to abutment but from side to side, thereby lowering the cross-sectional loads within the deck. Furthermore, the majority of the weight from the superstructure will be led into the foundation through the side girders. This means that any strengthening activities needed for the existing foundation can be performed next to the existing road without causing hindrance to the traffic flow.

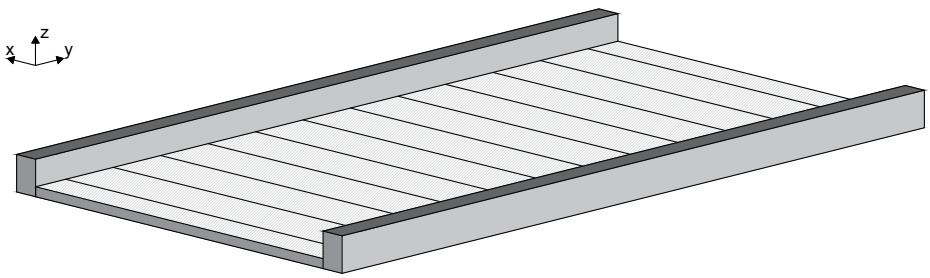

FIGURE 4.8: Trough structure design for normal traffic bridges with separate elements

However, the application of massive elements are undesired in both floor and side girders, for several reasons that are listed below:

1. **Lightweight structure**
   - To decrease the load reactions on the existing foundations:
     With the application of a trough bridge most loads will be drawn towards the outer sides of the foundation, thus giving rise to very high point loads. This will increase the chance of requiring foundation improvement (see Chapter 3) and therefore the loads on the foundation must be reduced as much as possible.
   - To increase ease of transportation:
     The lower the weight of the separate elements, the easier they can be transported and the more elements can be transported in one go.
   - Reduce the material costs:
     Less material means less initial material costs. This is especially interesting with UHPC, since the production costs of one cubic meter are much higher than for NSC (€1000 compared to €100 per cubic meter).
   - To increase the speed of erection:
     A lower weight of the separate elements also increases the speed of erection.
2. **Tunnel effect**
   Drivers can experience a so-called tunnel effect when approaching a passage with high walls which will cause them to slow down unknowingly. This behaviour can be subdued by opening up the side girder as much as possible.
3. **Ice formation**
   In winter, bridge decks are prone to ice formation as a result of the low insulation capacity of the confined construction height. Therefore shaded areas should be avoided as much as possible to not increase the ice-formation any further and thus an open side structure must be applied.

From these considerations it follows that a trough bridge design with open structural elements is required.

In the following sections a conceptual design is made for application of a trough structure in the traffic bridge of case study A9. In this, two different variants are elaborated. First a structure consisting of massive elements will be considered to determine the challenges in design. This is followed by a design consisting of open floor and side elements to reduce the weight of the superstructure as much as possible and to fulfil the practical requirements as discussed above.

4.2. DESIGN CONSIDERATIONS

The conceptual design for both massive and open elements will be bound by several design considerations. Below, a selection is presented from all requirements considered in Appendix E.

Considerations regarding material characteristics:

- The material characteristics are:
  - Concrete: UHPC, strength class C170/200;
  - Prestressing steel: Y1860S7;
  - Reinforcement steel: B500B;

Considerations regarding geometry:

- Weight reduction is governing for the design of open element structures;
- For the side girders the openings are governing for design;
- To allow for transportation the deck will consist of multiple floor girders with a width of 3.0 m;
- The width of the side girder is chosen at b_t = 1.2 m, according to safety requirements stated in the design regulations for railway bridges;
- Both floor -to- floor and floor-to-side connections are assumed fixed through prestressing;

Considerations regarding load actions taken into account:

- The governing load combination consists of permanent loads from self-weight from concrete and asphalt and a variable load from traffic according to Load Model 1;

- Time-dependent behaviour, construction phase loading and fatigue loads are not considered;
- The side girders will be post-tensioned and the floor girders will be pre-tensioned. Both elements will be partially prestressed;

Considerations regarding the structural capacity:

- The calculations and design checks are based on *[NEN-EN 1992-1-1, 2005]* and *[AFGC, 2013]*;
- The elements are checked for moment capacity, shear capacity and deformation capacity both globally and internal. The torsional capacity of the side girder will be checked globally.
- The following boundary conditions are valid:
  - The requirement for minimum concrete cover is met;
  - The maximum compressive stress after prestress release is smaller than $0.6 \cdot f_{ck}(t)$;
  - The maximum tensile stress in the cross-section due to prestressing at t = 0 must be lower than the tensile strength f_{ctd1} to prevent cracking;
  - In SLS, no tensile stresses may occur in the cross-section;
  - To provide sufficient ductility, cracking should occur in ULS;
  - The shear capacity and torsion capacity are limited by the ultimate strength of the compressive struts;
- Crack widths are assumed sufficiently small to fulfil durability requirements.
- Although the structure is designed to crack in ULS, the reduced modulus of elasticity due to this crack formation is not taken into account for simplicity reasons.

4.3. TROUGH BRIDGE DESIGN - MASSIVE ELEMENTS

The elaborate calculations of the massive element trough bridge can be found in Appendix F, here only a brief summary of the obtained results is given.

4.3.1. Design results

The design is based mainly on fulfilment of the boundary conditions as given in section 4.2. The resulting geometric parameters and prestress areas required are given in Table 4.1 and supported by Figures 4.9 and 4.10 for the floor girders and in Table 4.2 and Figures 4.11 to 4.13 for the side girders respectively.

Floor girder - massive			
Parameter		**Value**	**Unit**
Dimensions			
Height floor girder	h_f	0.61	*m*
Width floor girder	b_f	3.00	*m*
Length floor girder	l_f	18.17	*m*
Height top connection	h_{c1}	0.11	*m*
Height bottom connection	h_{c2}	0.11	*m*
Prestress			
Bottom; x-direction	$A_{p;x1}$	10700	mm^2
Eccentricity	$e_{p;x1}$	0.25	*m*
Top; x-direction	$A_{p;x2}$	13500	mm^2
Eccentricity	$e_{p;x2}$	0.25	*m*
Bottom; y-direction	$A_{p;y1}$	2600	mm^2
Eccentricity	$e_{p;y1}$	0.25	*m*
Bottom; y-direction	$A_{p;y2}$	2700	mm^2
Eccentricity	$e_{p;y2}$	0.25	*m*

TABLE 4.1: Cross-sectional dimensions and prestress areas for the massive floor girders

FIGURE 4.9: Cross section for the massive floor girder in x-direction

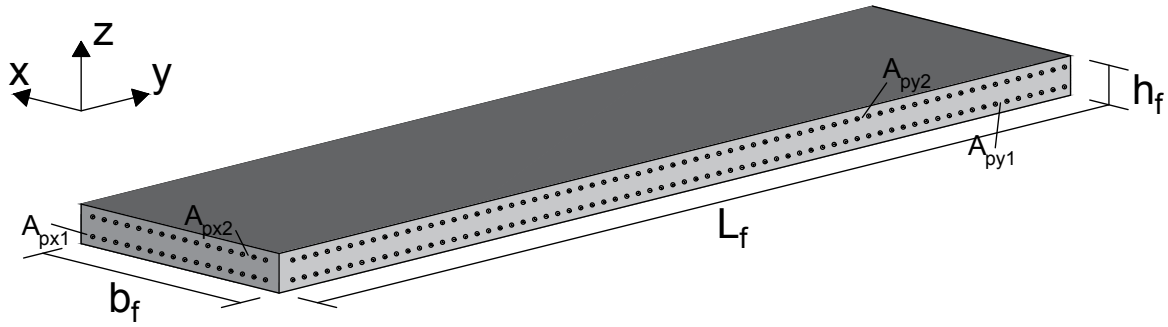

FIGURE 4.10: Massive floor girder design with directions and indicated prestress cables

Side girder - massive			
Parameter		**Value**	**Unit**
Dimensions			
Height side girder	h_t	2.30	*m*
Width side girder	b_t	1.20	*m*
Length side girder	l_t	36.80	*m*
Prestress			
Bottom; y-direction - phase 1	$A_{p;y1}$	31000	mm^2
Bottom; y-direction - phase 2	$A_{p;y1}$	40600	mm^2
Eccentricity	$e_{p;y1}$	0.55	*m*
Drag	f_p	0.35	*m*
Top; y-direction - phase 1	$A_{p;y2}$	2600	mm^2
Top; y-direction - phase 2	$A_{p;y2}$	2600	mm^2
Eccentricity	$e_{p;y1}$	1.03	*m*
Drag	f_p	0.00	*m*

TABLE 4.2: Cross-sectional dimensions and prestress areas for the massive side girders

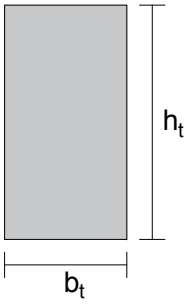

FIGURE 4.11: Cross section for the massive side girder in y-direction

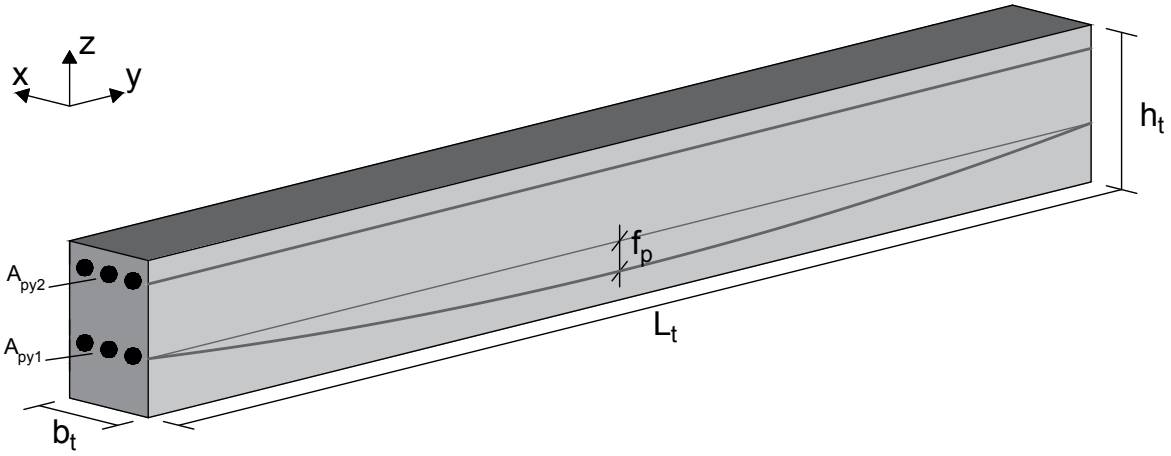

FIGURE 4.12: Massive side girder design with directions and indicated prestress cables

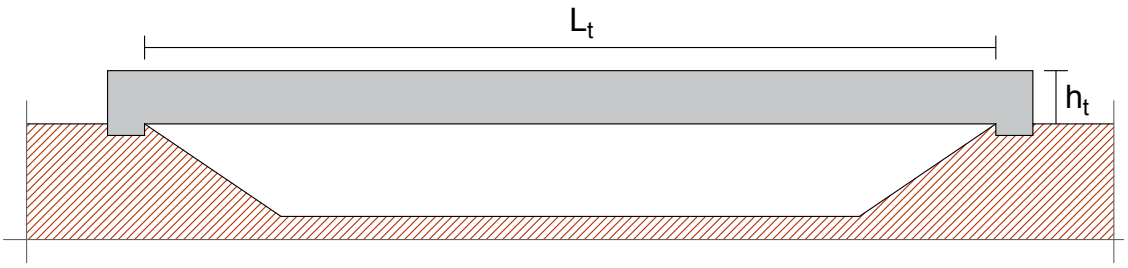

FIGURE 4.13: Side view of the massive side girder design

4.3.2. Unity Checks

The accompanying unity checks for both floor and side girder are presented in Tables 4.3 and 4.4 respectively.

Floor girder - massive			
			UC
Global			
	Moment	M_y^+	0.33
		M_y^-	0.46
		M_x^+	0.40
		M_x^-	0.33
	Shear	V_z	0.72
	Deformation	w_z	0.37

TABLE 4.3: Unity Checks performed for the massive floor girders

Side girder - massive			
			UC
Global			
	Moment	M_x^+ - phase 1	0.63
		M_x^+ - phase 2	0.71
	Shear	V_z	3.71
	Torsion	M_y	0.62
	Combined shear and torsion		3.91
	Deformation	w_z	0.14

TABLE 4.4: Unity Checks performed for the massive side girders

It can be seen that for the floor girders all bending, shear and deformation checks are sufficient (Table 4.3) and from Appendix F it follows that all boundary conditions are met. Due to these boundary conditions the Unity Checks are rather conservative, implying that a smaller construction height or longer floor span would also suffice.
For the side girders, however, Table 4.4 shows that although the bending and deformation requirements are met, this cannot be said for the shear capacity and for the combination of shear and torsion.

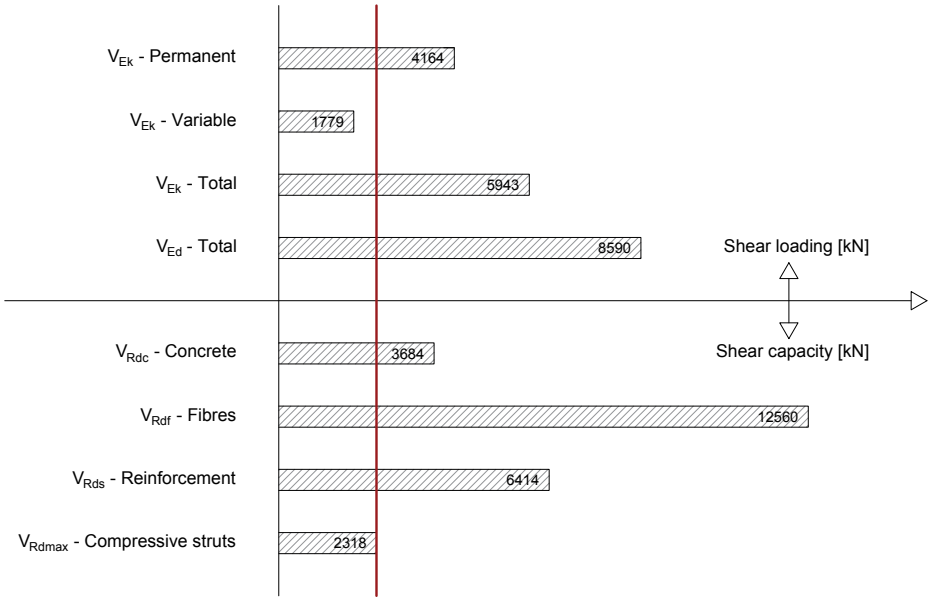

FIGURE 4.14: Comparison of the shear force following from different load actions to the shear capacity of the massive side girders

In Figure 4.14 the shear load action in the side girder is compared to the different shear capacities and from this it follows that the ultimate strength of the compressive struts ($V_{Rd;max}$) is insufficient for only the permanent load actions already. When looking at the formula for calculation of $V_{Rd;max}$ two options are identified that might lead to a higher capacity, namely the concrete compressive strength f_{ck} and the concrete cross-section given by $b_w \cdot z$.

$$V_{Rd;max} = \frac{2 \cdot 1.14 \cdot \frac{\alpha_{cc}}{\gamma_c} \cdot b_w \cdot z \cdot {f_{ck}}^{\frac{2}{3}}}{\cot(\theta) + \tan(\theta)}$$

Since UHPC concrete class C170/200 is already one of the highest concrete classes available, f_{ck} cannot be increased and thus the only option for increase of shear capacity lies in a larger cross-section.

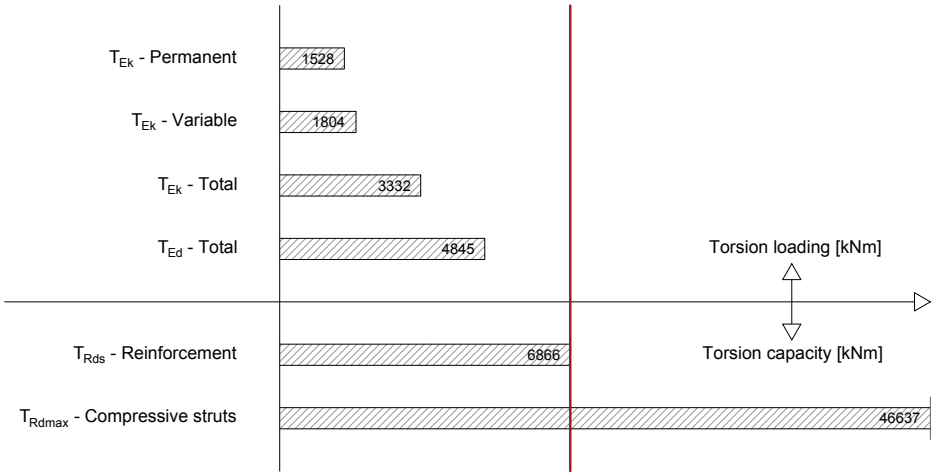

FIGURE 4.15: Comparison of the torsion moment following from different load actions to the torsion capacity of the massive side girders

The same comparison is made for torsion, as presented in Figure 4.15. Although the torsional capacity is sufficient it can be seen that the amount of reinforcement possible is governing for the overall torsion capacity, instead of the ultimate strength of the compressive struts.

Since the Unity Check for combined shear and torsion is based on the ultimate strength of the compressive struts in the concrete, improvement of the Unity Check is mainly governed by the maximum shear capacity.

$$T_{Rd;max} = 2 \cdot 1.14 \cdot \frac{\alpha_{cc}}{\gamma_c} \cdot f_{ck} \cdot 2 \cdot A_k \cdot t_{eff} \cdot \sin(\theta) \cdot \cos(\theta)$$

$$\frac{V_{Ed}}{V_{Rd;max}} + \frac{T_{Ed}}{T_{Rd;max}} \leq 1.0$$

By increasing the cross-sectional area to account for a higher shear capacity the torsion capacity will also increase, thereby improving the Unity Check for combined loading even further. Other possible improvements for the combined shear and torsion capacity of a trough structure are further elaborated in section 4.5.

Overall it can be concluded that with applying a trough bridge design to obtain a slender and light-weight structure, the challenge is no longer focussed on the required slenderness but it has shifted towards a shear and torsion capacity problem.

4.4. TROUGH BRIDGE DESIGN - OPEN ELEMENTS

As considered in section 4.1, the side girders of the trough bridge need to be open to reduce the tunnel effect and to avoid ice formation in winter. Also, a low-weight structure is desired for retainment of the existing foundations, ease of transportation and speed of erection. Therefore a design in open structure elements is considered.

The elaborate analysis is performed in Appendix G, but in this section a brief summary of the obtained results is given.

4.4.1. Design results

The design is based mainly on fulfilment of the boundary conditions as given in section 4.2. The resulting geometric parameters and prestress areas required are given in Table 4.5 and supported by Figures 4.16 and 4.17 for the floor girders and in Table 4.6 and Figures 4.18 to 4.22 for the side girders respectively. For the floor girders a design consisting of multicell box girders is chosen, while the side girder will be constructed as a truss structure.

Floor girder - open			
Parameter		**Value**	**Unit**
Dimensions			
Height floor girder	h_f	0.61	*m*
Width floor girder	b_f	3.00	*m*
Length floor girder	l_f	18.17	*m*
Height top flange	t_{ft}	0.13	*m*
Height bottom flange	t_{fb}	0.12	*m*
Thickness webs	t_w	0.09	*m*
Number of box cells	n_b	3	-
Height top connection	h_{c1}	0.13	*m*
Height bottom connection	h_{c2}	0.12	*m*
Prestress			
Bottom; x-direction	$A_{p;x1}$	5500	mm^2
Eccentricity	$e_{p;x1}$	0.24	*m*
Top; x-direction	$A_{p;x2}$	7600	mm^2
Eccentricity	$e_{p;x2}$	0.25	*m*
Bottom; y-direction	$A_{p;y1}$	1300	mm^2
Eccentricity	$e_{p;y1}$	0.24	*m*
Bottom; y-direction	$A_{p;y2}$	1600	mm^2
Eccentricity	$e_{p;y2}$	0.25	*m*

TABLE 4.5: Cross-sectional dimensions and prestress areas for the open floor girders

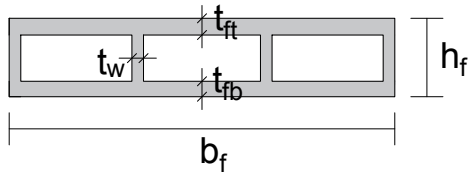

FIGURE 4.16: Cross section for the open floor girder in x-direction

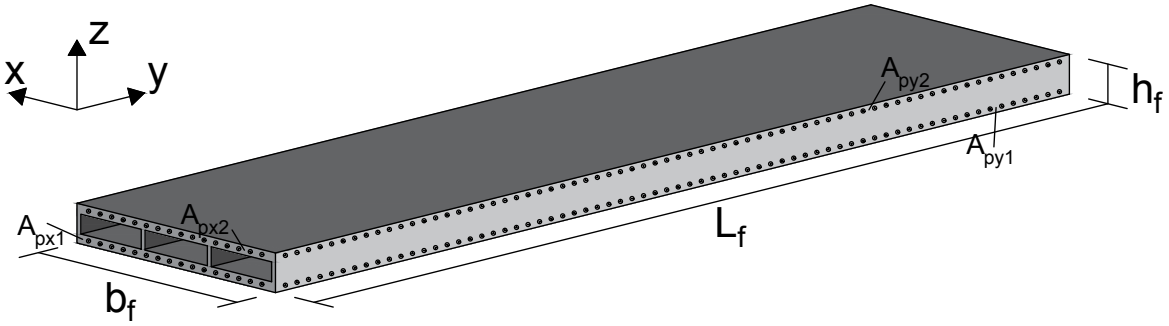

FIGURE 4.17: Open floor girder design with directions and indicated prestress cables

Side girder - open			
Parameter		**Value**	**Unit**
Dimensions			
Height side girder	h_t	2.30	*m*
Width side girder	b_t	1.20	*m*
Span side girder	l_t	36.80	*m*
Length side girder	l_{tot}	40.00	*m*
Height top beam	h_{tt}	0.40	*m*
Height lower beam	h_{tb}	0.80	*m*
Thickness verticals	d_{tv}	0.30	*m*
Thickness diagonals	d_{td}	0.30	*m*
Length segment	l_{ts}	2.50	*m*
Number of segments	n_{ts}	14	-
Length end segment	l_{tse}	2.50	*m*
Prestress			
Bottom; y-direction	$A_{p;y1}$	20000	mm^2
Eccentricity	$e_{p;y1}$	0.57	*m*
Drag	f_p	0.00	*m*
Top; y-direction	$A_{p;y2}$	8000	mm^2
Eccentricity	$e_{p;y1}$	1.13	*m*
Drag	f_p	0.00	*m*

TABLE 4.6: Cross-sectional dimensions and prestress areas for the open truss girders

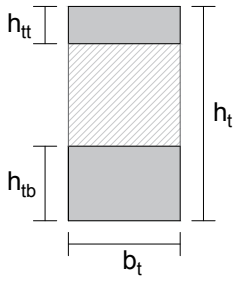

FIGURE 4.18: Cross section for the open truss girder in y-direction

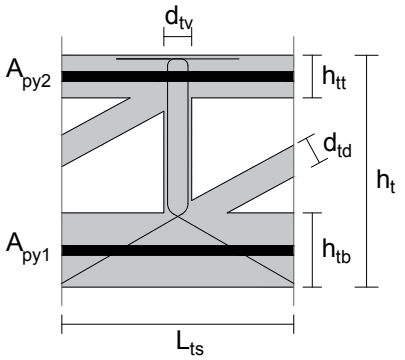

FIGURE 4.19: Detailed view of the open truss girder with indicated prestress and suspension reinforcement

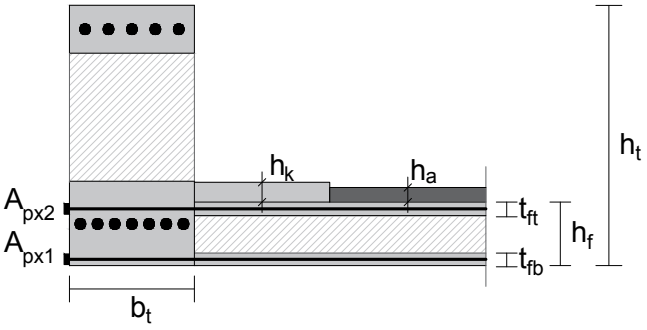

FIGURE 4.20: Detailed view of the floor-to-side connection in the open structure design with indicated prestressing

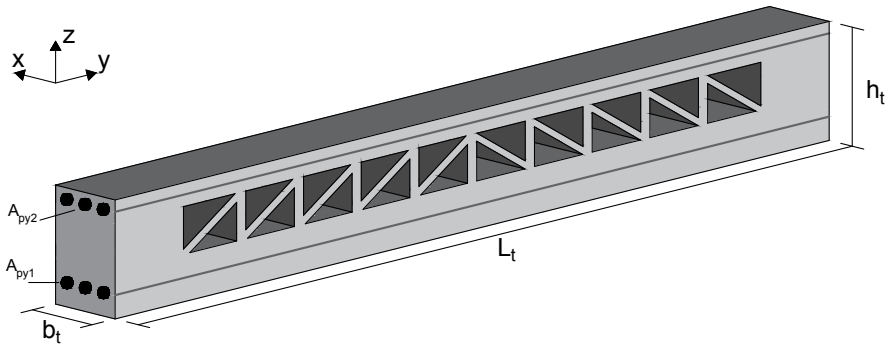

FIGURE 4.21: Open truss girder design with directions and indicated prestress cables

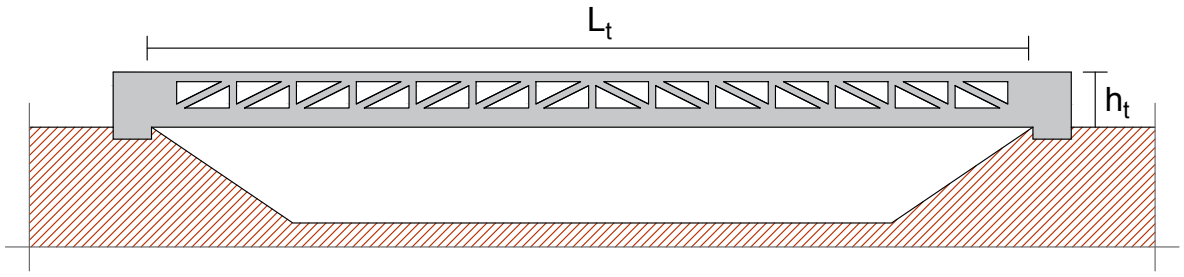

FIGURE 4.22: Side view of the open truss girder design

4.4.2. Unity Checks

The accompanying unity checks for both floor and side girder are presented in Table 4.7 and 4.8 respectively.

With the multicell box girders a weight reduction of 52% is obtained compared to the massive floor girders. The dimensions are based on the boundary conditions and internal Unity Checks, in which the bottom flange and web dimensions are based on the minimum concrete cover and the top flange is based on the Unity Check for positive bending moments.

Floor girder - open			
			UC
Global			
	Moment	M_y^+	0.60
		M_y^-	0.75
		M_x^+	0.66
		M_x^-	0.44
	Shear	V_z	4.95
	Deformation	w_z	0.36
Internal			
Upper flange	Moment	M_x^+	0.96
		M_x^-	0.84
	Shear	V_z	0.48
	Normal	N^-	0.25
		λ_{buc}	0.00
	Deformation	w_z	0.07
Lower flange	Shear	V_z	0.02
	Normal	N^+	0.16
Webs	Normal	N^-	0.05
		λ_{buc}	0.25

TABLE 4.7: Unity Checks performed for the open floor girders

Side girder - open			
			UC
Global			
	Moment	M_x^+	0.88
	Deformation	w_z	0.70
Internal			
Upper beam	Normal	N^-	0.25
		λ_{buc}	0.97
Lower beam	Moment	M_x^+	0.03
		M_x^-	0.07
	Shear	V_z	2.02
	Torsion	M_y	0.49
	Combined shear and torsion		2.51
	Deformation	w_z	0.01
Verticals	Normal	N^+	0.65
Diagonals	Normal	N^-	0.10
		λ_{buc}	0.86
End segment	Shear	V_z	1.19
	Combined shear and torsion		2.37

TABLE 4.8: Unity Checks performed for the open truss girders

All requirements are met, with the exception of the Unity Check for global shear. Since the shear load is taken up by the webs only, the width of these webs must be widened towards the end of the floor girder. At the end, a web width of t_w = 0.5 m will lead to a Unity Check of 0.89.

By applying a truss girder instead of a massive side girder, a weight reduction of 37% is obtained. Again, the dimensions are based on the boundary conditions and Unity Checks in the following design order:

1. The height of the lower beam is based on the total height of the floor girders and concrete kerbs;
2. The segment length is based on the maximum angle of the suspension reinforcement that transfers the load from the lower beam to the top of the truss;
3. The height of the truss is based on the moment arm for the global bending moments;
4. The height of the upper arm is based on the buckling capacity due to the normal compression load

from bending and prestressing;
5. The thickness of the verticals is based on the minimum concrete cover needed for the suspension and shear reinforcement;
6. The thickness of the diagonals is based on the buckling capacity due to the normal compression load.

In the internal Unity Checks it can be seen that the lower beam – although sufficient for torsion loading separately – is not capable of resisting the shear load or the combined load from shear and torsion in the compressive struts, again mainly due to the maximum shear capacity.
The global shear force has to be resisted by the cross-sectional area of the end segments but the Unity Check for shear is not met. On top of that, an additional load component has to be taken into account that deals with unaccounted fatigue loads and torsional load actions, even though the torsion is assumed to be taken up by the lower beam only. To obtain a conservative result the acting shear force is therefore assumed to be twice as much and thus also the combination of shear and torsion cannot be adequately resisted by the end segment.

It must thus be concluded that despite the weight reduction of both floor and side girders in the open structure design, the shear and torsion capacities are still insufficient.

4.5. POSSIBLE IMPROVEMENTS FOR STRUCTURAL DESIGN

From sections 4.3 and 4.4 it follows that due to the high compressive strength of the UHPC, high prestress forces can be applied and thus a high slenderness of the side girders can be obtained. However, the small cross-sectional area that follows from this slenderness is not sufficient to withstand the shear and torsional load actions with respect to the ultimate compressive strut strength. Although the open structure design has an overall weight reduction of 47% compared to the massive element design, this still leads to problems in shear and torsion.

Several possible improvements have been identified that could help in reducing this shear and torsional challenge:

1. **Weight reduction**
   In the open structure design it could be seen that weight reduction has a positive influence on the shear force, but the acquired reduction of 47% is not sufficient to fulfil the boundary conditions for shear and torsion. The question is therefore if further weight reduction might solve this problem.

   A quick analysis shows that the variable bridge loading alone constitutes a shear force higher than the maximum shear capacity. Thus it can be concluded that the even maximum weight reduction will never lead to a sufficient shear capacity, let alone for combined shear and torsion actions, and thus other solutions must be sought.

2. **Increase cross-sectional area**
   The boundary condition for shear and torsion is based on the ultimate strength of the compressive struts, which is described by the following formulas:

$$V_{Rd;max} = \frac{2 \cdot 1.14 \cdot \frac{\alpha_{cc}}{\gamma_c} \cdot b_w \cdot z \cdot {f_{ck}}^{\frac{2}{3}}}{\cot(\theta) + \tan(\theta)}$$

$$T_{Rd;max} = 2 \cdot 1.14 \cdot \frac{\alpha_{cc}}{\gamma_c} \cdot f_{ck} \cdot 2 \cdot A_k \cdot t_{eff} \cdot \sin(\theta) \cdot \cos(\theta)$$

   Since the concrete class C170/200 is already one of the highest possible, no profit can be gained in the concrete compressive strength f_{ck} and the only option left is to increase the cross-sectional area ($b_w \cdot z$). For the massive element design this would lead to a required cross-section of $A_c = 10.8$ m^2 and for the open structure design this would lead to $A_c = 4.8$ m^2. The currently applied cross-section in both cases is $b_t \cdot h_t = 1.2 \cdot 2.3 = 2.76$ m^2, which is significantly lower. If only the height were to be increased, a height of $h_t = 9.0$ m and $h_t = 4.0$ m would be required, respectively.

3. **Plate model analysis**
   In the analytical analysis the floor girders are modelled as beams in which the loads are reduced due to the plate behaviour of the combined girders. A possible improvement of the shear problem can be sought in the adaptation of this model into a plate model, where part of the load will be transferred to the abutments instead of the side girders (see Figure 4.23). In an isotropic plate the spread angle is equal to 45 degrees, resulting in a force reduction of almost 25% on the side girders (see Figure 4.24) and thus also a total shear force reduction of almost 25%.
   In an orthotropic plate this profit will be lower since more load will be drawn towards the side girder, in the stiff direction of the floor girders.

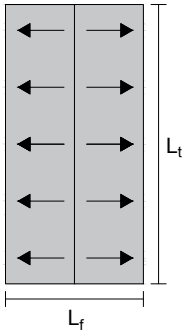

FIGURE 4.23: Load distribution to the sides in a beam model spanned in one direction

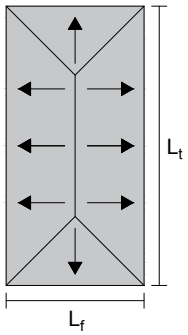

FIGURE 4.24: Load distribution to the sides in a plate model spanned in two directions

4. **Box structure**
   As already mentioned above, the only way to increase the shear and torsion capacity is by increasing the cross-sectional area. It was also shown that a height of h_t = 4.0 m would be required to solve this problem in an open structure design (Figure 4.25) and from this the possibility arises for a new kind of structural design. In this design the side girders are also connected at the top, forming a box structure through which the traffic moves (see Figure 4.26).

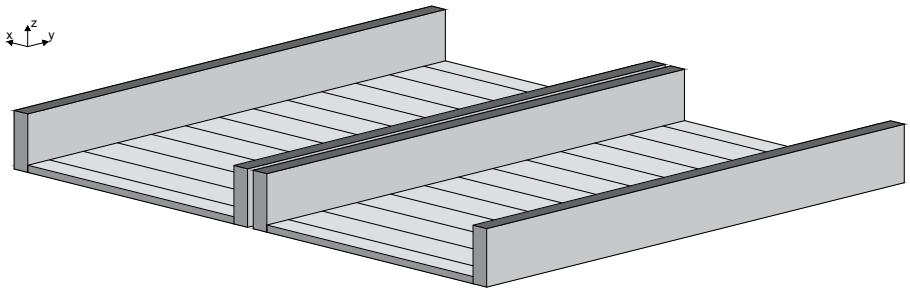

FIGURE 4.25: Dimensions for a double trough bridge design with a side girder height of h_t = 4.0 m

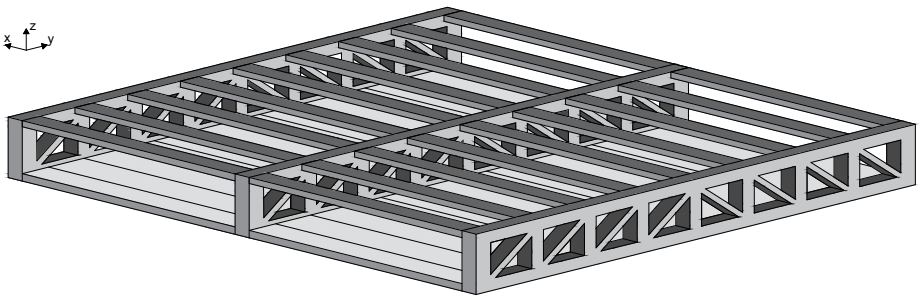

FIGURE 4.26: Indication of a box bridge structure in which the high side girders are connected at the top

The possible advantages of this system are very promising. Not only is the height of the side girder sufficient for the shear force, this structure has a significantly higher torsion capacity since the entire structure now forms a closed section. In the current design the torsional capacity is limited by the width of the side girder (see Figure 4.27) while in the box structure the width is increased significantly (see Figure 4.28).

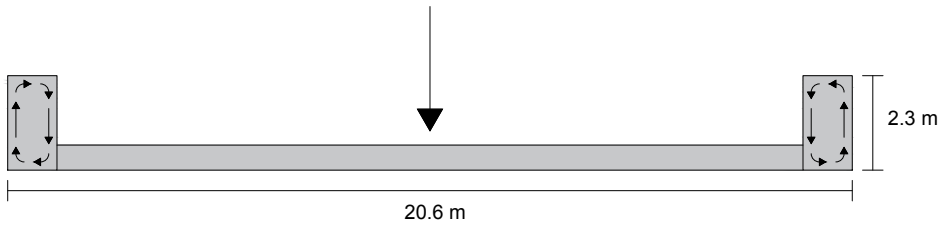

FIGURE 4.27: Shear loading from torsion in the side girders of a trough bridge

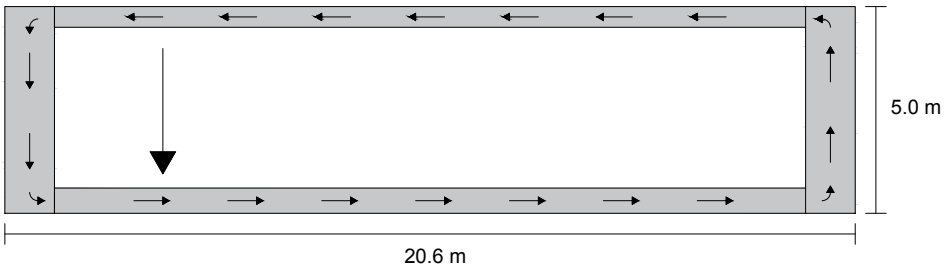

FIGURE 4.28: Shear loading from torsion in an indicated closed section formed by floor girders, side girders an top connections

By applying this box structure it seems plausible that not only the shear and torsion problem is solved, but also that much larger spans can be reached without the need for intermediate supports.

5. **End segments**
   At the moment, closed end segments are assumed in the open structure design, mainly for the introduction of the high prestress forces in the upper and lower beam of the truss girder. It would be interesting to investigate the possibility of replacing these end segments by a vertical beam, so that only normal forces arise near the supports. In that case, no shear force arises and the maximum capacity is given by:

$$N_{Rd;max} = A_c \cdot f_{cd} = A_c \cdot \frac{\alpha_{cc}}{\gamma_c} \cdot f_{ck}$$

   In this case, with verticals of d_{tv} = 0.3 m wide, this would lead to $N_{Rd;max}$ = 57800 kN while the shear capacity in the end segments is limited to $V_{Rd;max}$ = 2318 kN.

6. **Composite structure**
   In this analysis only concrete is applied in both floor and side girders, but the incorporation of other materials might be beneficial. The application of composite floors has been very successful in buildings and might also be applicable in traffic bridges. Also, the side girders could be (partly) composed out of steel to increase the tensile capacity of the verticals and to reduce the self-weight of the structure even further.

7. **Width reduction**
   In railway trough bridges a rule of thumb states that for sufficient structural behaviour the bridge should have a slenderness of λ = 14. This means that for a length of 36.8 m a height of 2.63 m is required. The main difference is however that in railway bridges the typical width is only 5 m – just a quarter of the required width in this traffic bridge design. With the shear force in the side girders being linearly proportional to the width of the bridge, it can easily be seen that this increased width will lead to a much larger required cross-section.
   Therefore it will be beneficial for structural design if the traffic bridge is divided into two parts with

smaller widths (Figure 4.29. For practical reasons this solutions is however not as adequate, since the division of traffic lanes will lead to higher safety issues (chance of collision with the intermediate side girder) and a higher congestion rate.

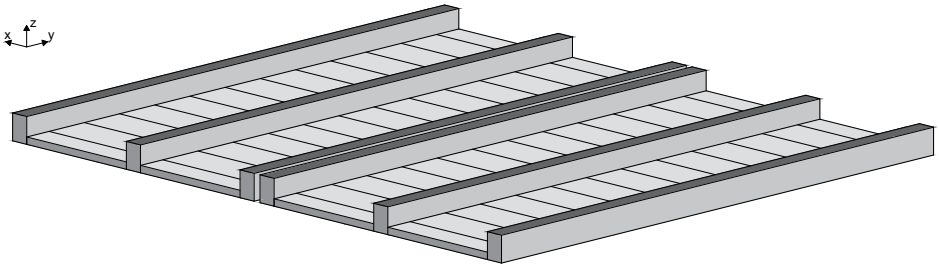

FIGURE 4.29: Indication of a trough bridge structure with width reduction through extra side girders

With these improvements it is expected that the problems in shear and torsion can be overcome, thereby introducing the trough or box structure bridge design as a very promising structural solutions for a quick bridge replacement strategy.

5

SOIL-STRUCTURE INTERACTION

The quick bridge replacement strategy as proposed in Chapter 2 consists of three time-reducing actions:

1. Select the ABC approach
2. Retain the existing foundation
3. Avoid intermediate supports

In Chapter 3 the possible increase in bearing capacity for existing foundations is discussed while in Chapter 4 structural concepts are given for a slender and lightweight superstructure as to make the avoidance of intermediate supports possible.
The latter not only reduces construction time, since less elements have to be placed, but it is also beneficial for the traffic safety and for the flexibility of the underlying road layout. On the other hand, avoiding the intermediate supports results in an increase of dead load on the end supports, since the span length has increased. Although UHPC girders will have an overall lower weight than NSC girders, due to a cross-section with less material, the increase of loading at the end supports will be substantial, thereby increasing the need for additional foundation piles to support the existing foundation.

Thus in order for the avoidance of intermediate supports to be beneficial with regards to reducing the construction time on-site, the soil-structure interaction of the existing foundation and lightweight superstructure must be sufficient.

This chapter will investigate this interaction by comparing the increase of foundation loads from the different superstructure variants to the increase of foundation bearing capacity according to different scenarios. This is done by discussing:

- The different superstructure variants in brief (section 5.1)
- The results of the comparison in foundation loads and foundation capacity (section 5.2)
- Several improvement methods for the soil-structure interaction (section 5.3)

5.1. SUPERSTRUCTURE VARIANTS

In total five different superstructure variants for case study A9 have been discussed already in this thesis:

1. **Two-span plate bridge in NSC:**
   The currently existing plate bridge is replaced by an equal design, with unaltered outer dimensions and cross-sections. The difference is constituted by the current design codes for traffic loading, which has increased since the original bridge was constructed.

2. **Single span box girder bridge in NSC:**
   To avoid intermediate supports a box girder design in NSC is investigated. According to *[Spanbeton, 2017]* a total girder height of 1200 mm is required for a span length of 36.8 m. The acquired slenderness of this bridge design is then $\lambda = 31$ and as a result additional groundwork will have to be executed to connect the bridge deck to the road alignment.

3. **Single span box girder bridge in UHPC:**
   In order to avoid these additional groundwork activities a slenderness of $\lambda = 60$ is needed in the new design. In his PhD research *[Reitsema, 2017]* has developed a calculation program for box girders in UHPC that allows for slenderness ratios of up to $\lambda = 60$. Therefore the application of box girders in UHPC has already reached its limit in this case study.

4. **Single span trough bridge with massive elements in UHPC:**
   As a new structural concept a trough bridge design is considered for normal traffic bridges. By spanning the floor girders between the two side girders, the span length is decreased and thus a slenderness of only $\lambda = 30$ is required. Furthermore, the height of the side girders is not restricted which makes longer spans possible, especially when combined with the enhanced structural behaviour of UHPC.

5. **Single span trough bridge with open elements in UHPC:**
   An open element trough bridge is desired to avoid ice formation and to reduce the overall weight of the structure. For this, the floor girders are designed as multicell box girders and for the side girders a truss is considered. Overall, a weight reduction of 47% is obtained.

These superstructure variants are incorporated with the existing foundation of the A9 Gaasperdammerweg case study through FEM models in SCIA Engineer, as presented in Figures 5.1 to 5.3.

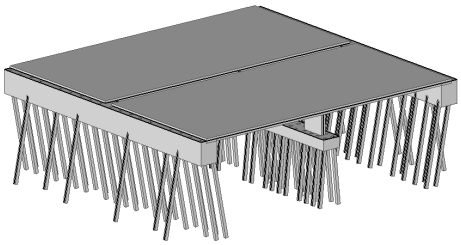

FIGURE 5.1: Finite element model of the case study A9 Gaasperdammerweg with corresponding pile plan

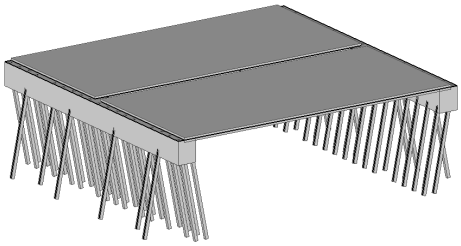

FIGURE 5.2: Finite element model of the case study A9 Gaasperdammerweg with corresponding pile plan

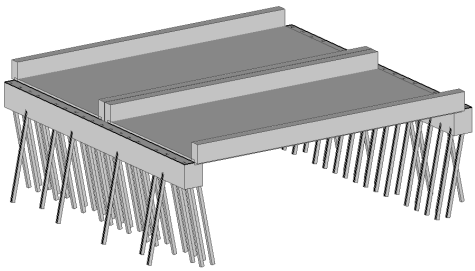

FIGURE 5.3: Finite element model of the case study A9 Gaasperdammerweg with corresponding pile plan

5.2. COMPARISON FOUNDATIONS LOADS

The amount of additional foundation piles required for each superstructure variant is calculated in analogy to the geotechnical analysis performed in Appendix B for the two-span plate bridge. This is done for all six scenarios introduced in section 3.3.1:

Scenario 1: Current practice
Scenario 2: Realistic profit
Scenario 3: Lower boundary set-up
Scenario 4: Upper boundary set-up
Scenario 5: Unreduced pile tip bearing factor α_p
Scenario 6: Average CPT for entire pile plan

For the increase of bearing capacity obtained in each of these scenarios a comparison is made to the increase of foundation loads for each of the superstructure variants. The results are shown in Figure 5.4.

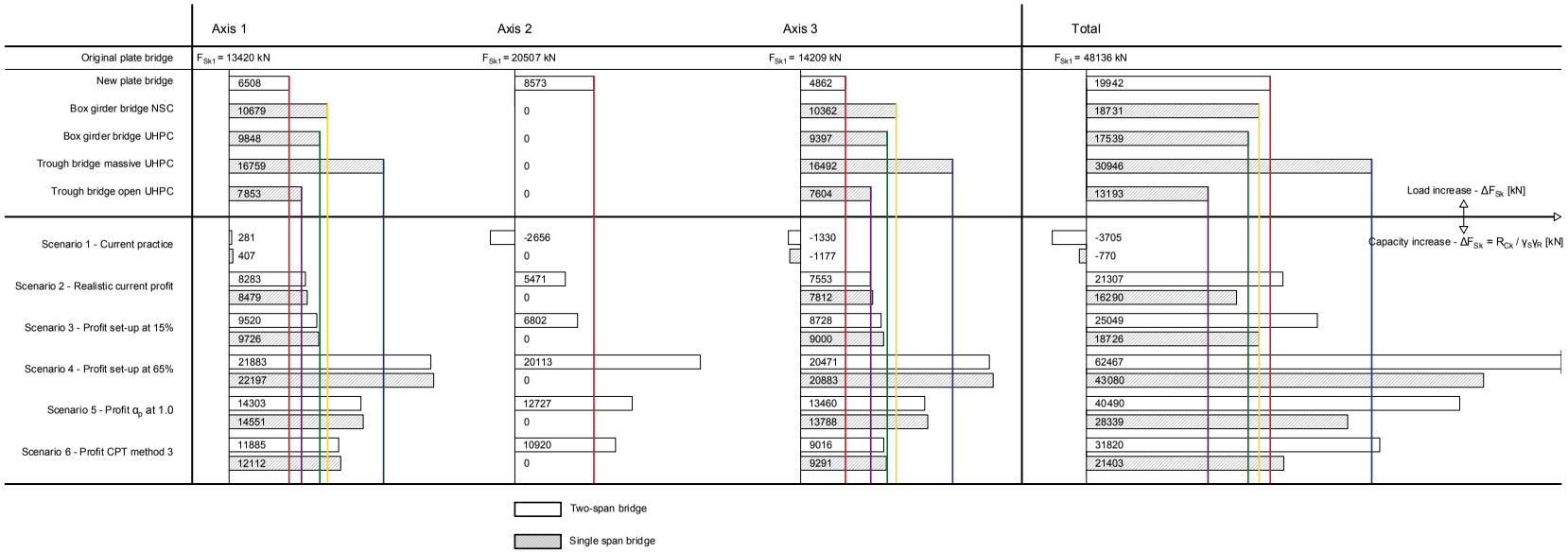

FIGURE 5.4: Comparison between the load increase on the foundations from each superstructure variant ($\Delta F_{S;k}$) and the increase in bearing capacity following from each profit scenario ($\Delta F_{S;k} = \Delta R_{C;k} / \gamma_S \gamma_R$)

Scenario	Plate (NSC)				Box girders (NSC)				Box girders (UHPC)				Massive trough (UHPC)				Open trough (UHPC)			
	Axis 1	Axis 2	Axis 3	Total	Axis 1	Axis 2	Axis 3	Total	Axis 1	Axis 2	Axis 3	Total	Axis 1	Axis 2	Axis 3	Total	Axis 1	Axis 2	Axis 3	Total
1	-	-	-	-	-	X	-	-	-	X	-	-	-	X	-	-	-	X	-	-
2	+	-	+	+	-	X	-	-	-	X	-	-	-	X	-	-	+	X	+	+
3	+	-	+	+	-	X	-	-	-	X	-	+	-	X	-	-	+	X	+	+
4	+	+	+	+	+	X	+	+	+	X	+	+	+	X	+	+	+	X	+	+
5	+	+	+	+	-	X	+	+	+	X	+	+	-	X	-	-	+	X	+	+
6	+	+	+	+	+	X	-	+	+	X	-	+	-	X	-	-	+	X	+	+

TABLE 5.1: Overview of which profit scenarios for bearing capacity increase are sufficient for application of the different superstructure variants

In these results, the increase of loads and bearing capacities are presented as bars, with a length according to their absolute value in kNs. The increase of load on the foundation of each superstructure variant can be compared to the increase of bearing capacity for each scenario. The comparison includes all three foundation axes separately, since the governing load situation differs for each foundation axis. Also, a comparison of total bridge loading and total bearing capacity is given.
For the bearing capacities a differentiation is made between the two-span plate bridge and the single span variants, since the distribution of loads over three supports gives rise to different foundation loads than in the case of two supports. This difference in foundation loads has in turn influence on the possible increase of bearing capacities of each foundation pile and therefore different values are obtained for the two-span and single span bridges.
Figure 5.4 is supported by Table 5.1 in which for each bridge type and each axis the possibility for foundation retainment is given. This is either denoted as a minus, indicating that the bearing capacity is not sufficient for the load action, or as a plus, indicating that it is sufficient. For every bridge the scenarios which make foundation retainment possible are highlighted in green.

Interpretation of results
These results lead to several interesting observations:

- **In no case is the current practice for retainment of foundation sufficient for the replacement of a bridge on both three and two supports.**
- **The increase of bearing capacity of the existing foundations, by applying a realistic profit scenario, is sufficient to carry the load increase as a result of the open element trough structure.**
- At first sight the same holds for the two-span plate bridge, where the total increase of bearing capacity is enough for the increase of loads, however foundation axis 2 would require additional strengthening of the foundation.
- The set-up of soil that was taken into account in the realistic profit scenario is very conservative and below the proposed lower-boundary by *[Axelsson, 2000]*. When taken this lower boundary into account instead of the conservative assumption in scenario 2, it can be seen that scenario 3 is still not sufficient for the two-span plate bridge but it would be sufficient for the open element trough bridge.
- The influence of the set-up of soil on retaining the existing foundations becomes clear when looking at scenario 4, in which the upper boundary of set-up is taken into account. In that case all superstructure variants can be applied without requiring additional strengthening measures for the existing foundations. It is however very unlikely that this upper boundary will indeed be proven in further research.
- The influence of the pile tip bearing factor α_p on retaining the foundations is also significant, as for nearly all superstructure variants the unreduced factor (α_p = 1.0) would suffice, with the exception of the massive element trough bridge. Since however the reduction of the α_p-factor is mainly based on driven prefabricated concrete piles, the same that are used in this case study, it is not expected that this factor can be increased back to the original value.
- Scenario 6 considers the choice for the governing CPT and it can be seen that this also has a significant influence on the bearing capacity of the existing foundation. By reconsidering the governing CPT, in this case by taking the average of the entire pile plan, both the two-span plate bridge and the open element trough bridge can be applied. Additional CPTs and practical experience could support this choice for the governing CPT although it is not expected that the average of all CPTs will constitute the required safety level in design.

- **Of all superstructure variants the open element trough bridge has the highest potential for foundation retainment, followed by the two-span plate bridge in NSC. This shows that overall weight reduction has a very large contribution to the potential of retaining existing foundations.**
- Since the difference in traffic load between the original bridge and the new bridge is equal for all superstructure variants, the difference in load action comes entirely from the differences in concrete self-weight. From this it can be concluded that the weight reduction of a slender UHC box girder is quite small compared to that of the NSC box girder with increased height.
- It would be expected that the high concentrated loads underneath the point supports of the trough bridge side girders will lead to problems when retaining the foundations, but apparently this influence can be compensated by the weight reduction. Another explanation for this small difference is that the governing load situation is load situation 4 (Figure E.5) where the traffic load is situated at the outer

beams above the considered foundation axis. Therefore in all cases the load action will be highest towards the end of the abutments and thus the difference with the concentrated supports from the trough bridge side girders is quite small.

- In this overview of results, the bearing capacity is divided into the results for a two-span bridge and a single span bridge. In reality, however, the bearing capacities of the different single span superstructure variants differ slightly and it appears that the higher the load on the foundations, the higher the increase of bearing capacity that can be obtained. Since this difference is rather small for the different variants it is chosen to only incorporate the most governing into these results. As the open element trough bridge has the lowest load action on the foundation it follows that this is the governing superstructure variant for bearing capacity of the existing foundation.

So overall it can be concluded that the combination of retained existing foundations and the avoidance of intermediate supports is possible for the open trough superstructure. The safety margin is however quite small and furthermore all other superstructure variants will require additional research. In this, the influence of set-up, governing CPT method and influence of the α_p-factor are most interesting to further investigate.

5.3. IMPROVEMENT METHODS SOIL-STRUCTURE INTERACTION

If the combination of foundation retainment and lightweight superstructure turn out to be insufficient, different improvement methods can be applied. Several strengthening methods for existing foundations have been discussed in section 3.4 already and in section 4.5 improvements were presented for the load distribution. There are however also possibilities in the enhancement of the overall soil-structure interaction.

- **Improve abutment stiffness**
  The stiffness of the abutment determines the distribution of the loads over the separate foundation piles. By creating a higher stiffness of the pile cap a more favourable load distribution among the separate piles is obtained. The result is that the low bearing capacity of weaker piles can be compensated by the stronger piles, thereby increasing the overall bearing capacity of the existing foundation.

  For all superstructure variants considered it holds that the largest foundation loads occur for traffic loading at the outer side of the deck, since most loads are then concentrated at the ends of the abutments and the distribution is limited. This is illustrated in Figures 5.5 and 5.6 for a plate bridge on two supports, in Figures 5.7 and 5.8 for a box girder bridge and in Figures 5.9 and 5.10 for a trough bridge.

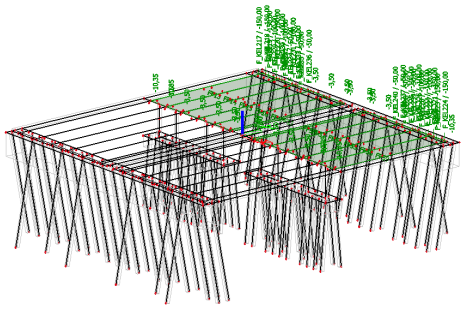

FIGURE 5.5: Governing load situation (load situation 4) for traffic loading on the FEM model for a two-span plate bridge

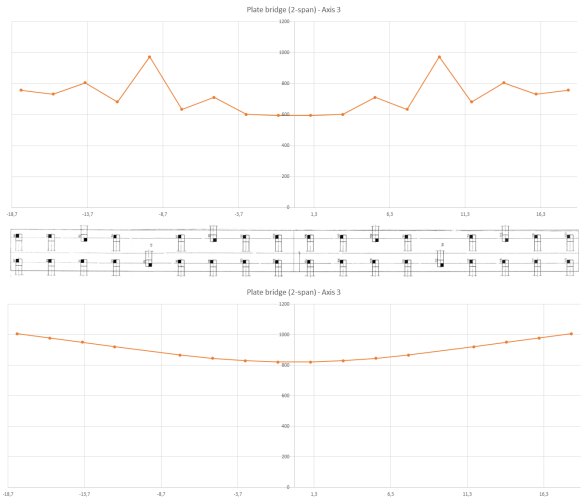

FIGURE 5.6: Resulting reaction forces on the foundations in axis 3 for the two-span plate bridge in the governing load situation

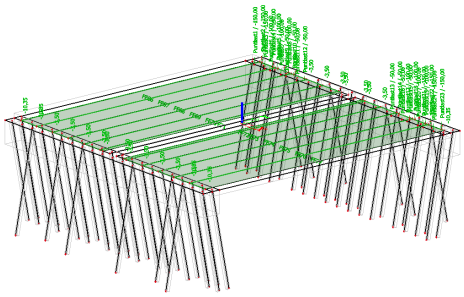

FIGURE 5.7: Governing load situation (load situation 4) for traffic loading on the FEM model for a single span box girder bridge

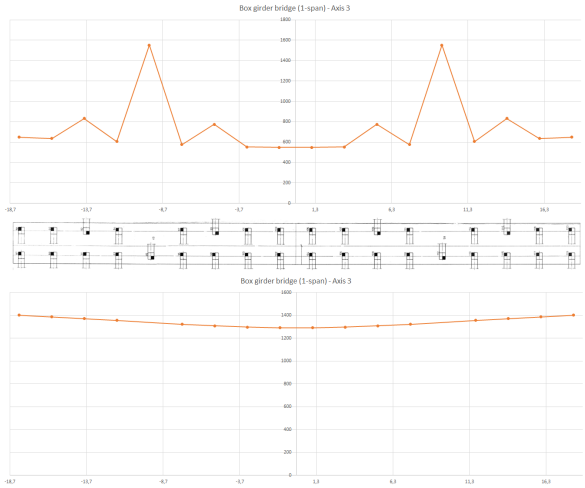

FIGURE 5.8: Resulting reaction forces on the foundations in axis 3 for the single span box girder bridge in the governing load situation

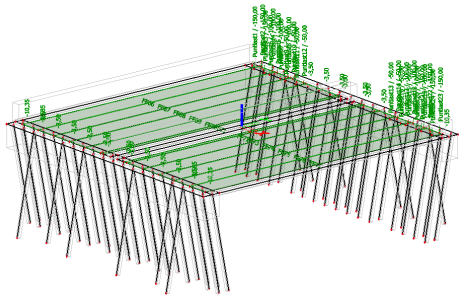

FIGURE 5.9: Governing load situation (load situation 4) for traffic loading on the FEM model for a single span trough bridge

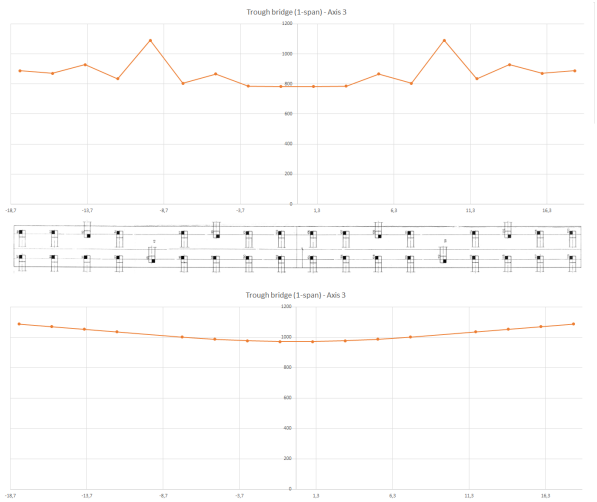

FIGURE 5.10: Resulting reaction forces on the foundations in axis 3 for the single span trough bridge in the governing load situation

It can be seen in all cases that the outer foundation piles experience a higher load action than the middle piles. By increasing the stiffness of the abutment these loads will be distributed more evenly which is beneficial for retainment of the existing foundation piles, but it can also be seen that this profit is quite small. A stiffer pile cap can be obtained by applying a concrete type with a higher modulus of elasticity or by increasing the concrete cross-section dimensions. In the latter case it must however be considered that the increase of weight will have a negative effect on the retainability of the existing foundations.

Although stiffening of the pile cap can increase the overall bearing capacity of the foundation, the execution aspect of stiffening a pile cap in combination with a minimised on-site construction time decreases the potential of this strengthening method substantially.

- **Improve support layout**
  There are two ways in which the supports can be altered in favour of the soil-structure interaction. The first is based on the geometry of the abutment itself, the second is based on the global configuration of the different (intermediate) supports.

1. In this case study, but also in many other cases, the bridge deck is eccentrically positioned on the end abutments, as can be seen in Figure 5.11. This eccentricity generates a moment in the support that gives rise to both compression and tension in the foundation piles. Therefore the outer foundation piles will only be partly loaded in compression while the inner piles have already reached their limit. This can also be seen in Figure 5.8, where the lower graph represents the inner foundation pile row while the upper graph represents the outer foundation pile row of axis 3.
   A more sufficient load distribution could be achieved in the layout of the support is changed so that the bridge deck is positioned in the centre of gravity of the abutment (see Figure 5.12).

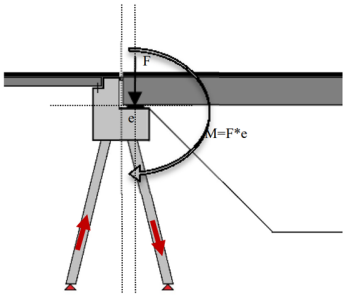

FIGURE 5.11: Eccentrically loaded support system

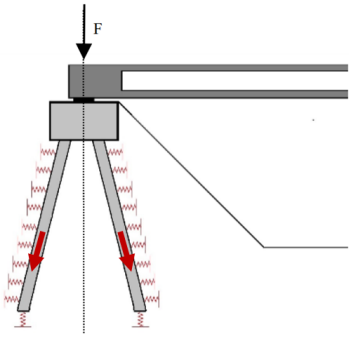

FIGURE 5.12: Centrically loaded support system

2. If multiple intermediate supports are present in the original bridge structure, there is a high possibility that not every support can be avoided in design as the required slenderness is just too high. In that case, the amount and position of the remaining intermediate supports are important to the design as they govern the moment and shear force distribution over the length of the bridge. Therefore the most optimal force distribution must be chosen, within the possibilities of support position, transportation limits and speed of erection.

- **Increase of pile spring stiffness in calculation**
  The bearing capacity of a foundation pile depends on its total deformation and therefore on its spring stiffness (see also Figure 5.13). In this it holds that the higher the spring stiffness of the foundation piles, the higher the allowed bearing capacity before ultimate deformation is reached.

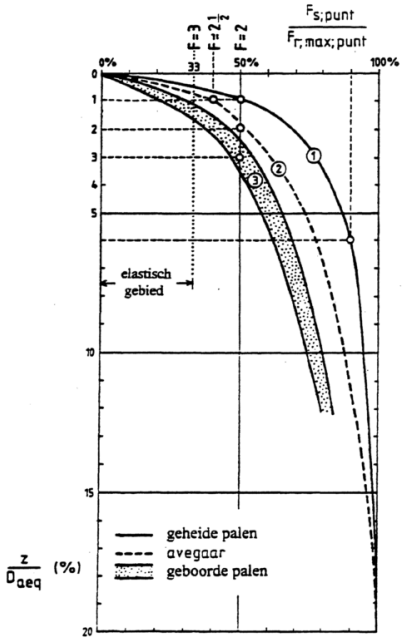

FIGURE 5.13: Load settlement diagram for different pile types *[van Tol, 2006]*

This spring stiffness considers the elastic deformation of the pile itself and the settlement of the soil beneath the pile tip. Soil settlement is a mechanism which is governed by the dissipation of pore water so that the soil particles can redistribute themselves in an increased packing density. Since the dissipation of pore water requires time, the pile spring stiffness is also time-dependent. Therefore, a higher pile spring stiffness can be taken into account for short-term dynamic loading than for long-term static loading.
This can be used as an advantage when considering retainment of existing foundations for bridge replacement. If the intermediate supports are not avoided, the only increase in load actions comes from an increased traffic load, which can be classified as dynamic short-term loading and thus a higher spring stiffness can be taken into account. Furthermore, since the foundation has proven over time to be able to bear the static load and also the accompanying settlements have already occurred, it could be concluded that the same static load can be carried without recalculation.

In case intermediate supports are avoided in design, there is also an increase in static load on the existing foundations and thus new calculations must be performed on the load deformation behaviour of the existing piles. However, the increased spring stiffness for variable traffic loads can still be beneficial and should therefore be considered in design.

- **Allow for higher (differential) settlements**
  As explained in the previous improvement method, a foundation pile obtains its bearing capacity through settlement of the pile. This means that the higher the settlement, the higher the load resisting capacity of the pile is, as depicted in Figure 5.13. Pile failure is defined at a total settlement w equal to 10% of the pile diameter: $w = 0.1 \cdot D_p$. Increasing this limit would lead to an additional profit in pile bearing capacity but in *[Stap, 2017]* it was determined that this limit already gives a good representation of practice.

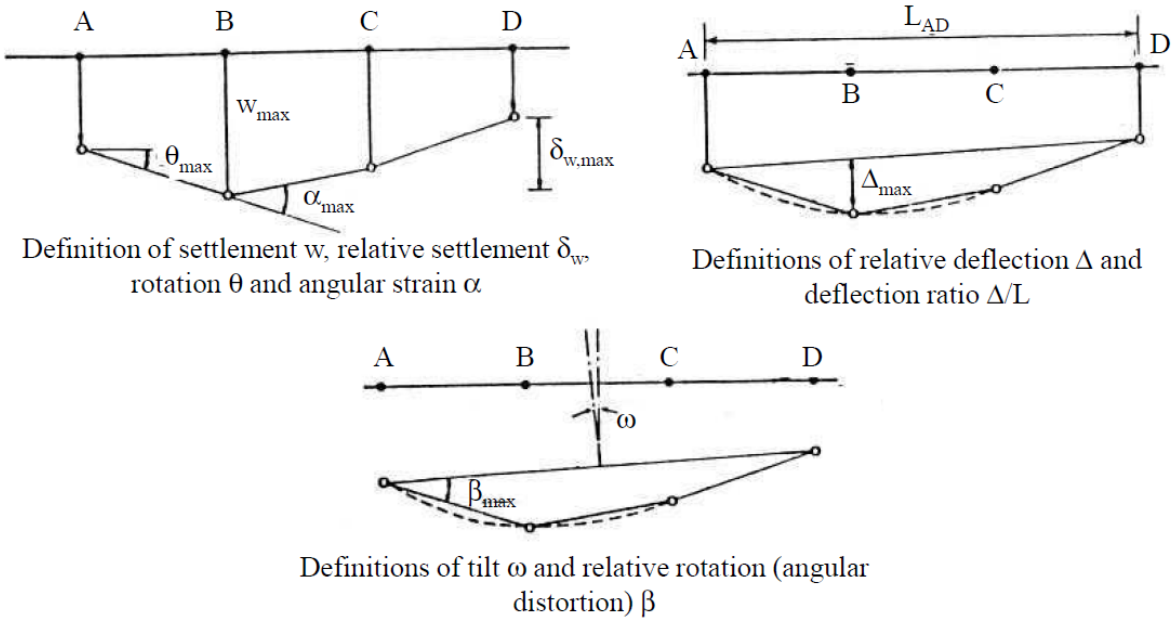

FIGURE 5.14: Definition of settlement and (relative) rotation according to *[Everts, 2015]*

The requirement for maximum settlement is however not always met as other requirements such as the maximum allowable rotation θ or the maximum allowable relative rotation β of the superstructure is governing (Figure 5.14). Especially in older structures these requirements for superstructure loading were very conservative. It could thus be beneficial for design if the maximum allowable (relative) rotation is increased.
With the incorporation of numerical models in superstructure designs, the redistribution of loads according to the relative element stiffness can be taken into account more adequately. This allows for sufficient detailing and thus for higher (differential) settlements.

6

REPLACEMENT STRATEGY - POTENTIAL

The former chapters show that the feasibility of the different time-reducing actions is very promising, also when all actions are combined.

The full potential of the proposed quick bridge replacement strategy is best demonstrated by comparing it to the current practice for bridge replacement construction. For that purpose a case study by Heijmans is investigated, in which two bridges were replaced within 85 days – a schedule that is considered very quick in current practice.

6.1. QUICK BRIDGE REPLACEMENT STRATEGY

The quick bridge replacement strategy as proposed in Chapter 2 consists of three time-reducing actions. These are, listed according to their respective time reduction:

1. Select the ABC approach
2. Retain the existing foundation
3. Avoid intermediate supports

If all actions are to be applied, certain design choices are required with respect to the existing foundation and the slender superstructure. For the case study considered throughout this thesis, regarding the A9 Gaasperdammerweg, this leads to:

1. Since the highway crosses over the local road it is chosen to transport the superstructure by means of SPMTs from the off-site construction location to its final position within the highway.

   The ABC approach can be incorporated in different ways. For a highway crossing over a local road both a lateral slide-in and transportation by SPMTs can be considered. The lateral slide-in will cause additional hindrance to the underlying local road but for the highway the total hindrance for bridge replacement in both directions is limited to only 20 hours *[Raglow, 2013]*. If SPMTs are used to transport the two bridges to its final location the underlying road will only experience 15 hours of hindrance according to *[Federal Highway Administration, 2015]*, but the highway requires additional activities - like coupling of the bridge to the road and finishing works – that will require a total closure of 31 hours *[Raglow, 2013]*.

   In case a highway crosses underneath a local road transportation by SPMT will give the lowest hindrance to both highway and local road with a total closure time of 15 hours and 31 hours respectively *[Federal Highway Administration, 2015]*.
2. The existing foundation is kept in place and the theoretical bearing capacity is increased in calculations according to the realistic profit scenario.
3. The superstructure deck will consist of single span, open element trough bridge so that the intermediate support is avoided from design but the weight of the superstructure will be as low as possible.
4. This low weight is beneficial for multiple reasons:
   - The increase of support reactions on the foundations is reduced to a minimum;
   - More prefabricated elements can be transported in one go from the prefabrication site to the construction site, thus reducing traffic hindrance during construction;

- Erection of the separate elements can be done by conventional cranes since the elements are light and also because there is no time limitation for erection.
- Transportation of the superstructure by SPMTs will require less effort since less weight will have to be transported.
- The temporary scaffolding can consist of smaller elements, thereby saving material costs.

5. Additional prestressed concrete piles are installed next to the existing foundation underneath the side girders. The new abutment will be cast in-situ against the existing abutment to ensure correct bonding and compatibility of the two structural elements.

   Although in theory the increase of bearing capacity is sufficient for the replacement by an open structure trough bridge, it is assumed here that additional foundation piles are needed. This is done for two reasons:

   – If the realistic profit scenario for foundation retainment is to be applied in practice the risks for both contractor and RWS increase since there is no practical experience yet. This will probably result into the requirement that the assumed increase of bearing capacity must be demonstrated and proved in practice, which is a process that will induce additional construction time and thus traffic hindrance. Also, if it turns out that the increase of bearing capacity is insufficient the delay in construction will cancel out all positive effects of the quick bridge replacement strategy.

   – In the case study the side girders would be positioned just on top of the existing abutment, but only partially. It could be beneficial for structural design if the width of the bridge is increased slightly so that the side girder will be positioned entirely next to the existing abutments. In that case additional foundation piles will be needed underneath the side girder supports. Additionally, another benefit of the trough bridge structure is demonstrated. Since the largest support reactions will occur underneath the side girder supports the most sufficient way of increasing the overall bearing capacity will be to apply additional piles underneath those supports. As they are situated outside the current highway alignment these groundwork activities will not result in any traffic hindrance.

6. Most finishing work is already done at the off-site construction location thus only coupling of the bridge to the existing highway alignment will have to be executed on site.

6.2. CASE STUDY A50 - BRIDGE REPLACEMENT IN 85 DAYS

For a bridge replacement project according to conventional construction methods, the case study A50 is chosen *[Dinnissen, 2010]*. This project was finished in 2010 but still counts as one of the quickest executions in current practice.

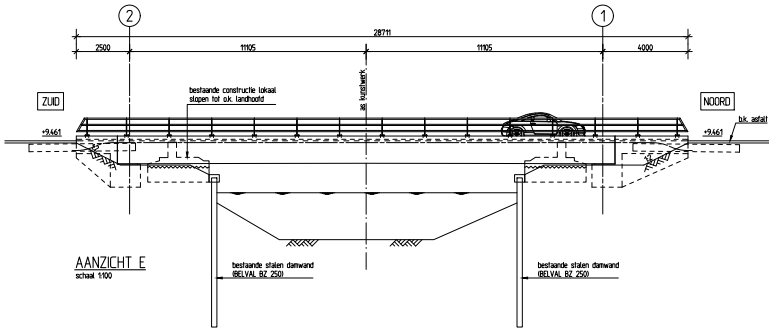

FIGURE 6.1: Sideview of the bridge over the Linge *[Dinnissen, 2010]*

The project considers a widening of the A50 between junctions Valburg and Grijsoord and for this two bridges will have to be replaced. One crosses the river Linge (Figure 6.1) and the other crosses the river Eldensche Zeeg and both bridges consist of two separate decks for each traffic direction. Their spans are somewhat short compared to the case study A9, just 20.0 m and 16.0 m respectively.
This project was appointed through a MEAT-procedure in which the amount of traffic hindrance was governing and therefore the allowed time span for on-site construction was set at 85 days for both bridges. Therefore, all design choices were firstly based on the resulting time reduction before a cost comparison was made.

The construction consisted of two phases in which a single traffic direction of both bridges was to be replaced while the other bridge deck was used for traffic in two directions (see Figure 6.2). Thus both traffic directions (the right side bridge (RSB) and left side bridge (LSB)) were replaced within 40 days. In that time span the existing bridge deck and foundation had to be removed, new foundation piles had to be installed, a new abutment had to be reinforced and cast in-situ, the prefabricated deck girders had to be placed and the compressive concrete layer had to be reinforced and cast before finishing of the new bridge.

FIGURE 6.2: Picture of the traffic detour during construction *[Dinnissen, 2010]*

The accompanying construction sequence is further elaborated in section 6.3 and the time schedule is given in section 6.4.

6.3. CONSTRUCTION SEQUENCE

For a comparison of the quick replacement strategy to conventional building practice the construction sequence has to be considered. This is first done for the conventional construction practice (case study A50, Table 6.1) and followed by the quick bridge replacement strategy (case study A9, Table 6.2). Both sequences are supported by illustrations given in Figures 6.3 and 6.4 respectively.

	Construction activity
1	Preparation activities - Design - Soil investigations - Prefabrication deck girders and falsework
2	On-site preparation - Rerouting of traffic over LSB
3	Closure of the bridge in one traffic direction (RSB)
4	Demolition of existing bridge
5	Groundwork and installation of new foundation piles
6	Placement of prefabricated girders
7	Welding of reinforcement and casting concrete deck
8	Finishing works
9	Opening of RSB and rerouting traffic over RSB
10	Closure of second traffic direction (LSB)
11	Demolition of existing bridge
12	Groundwork and installation of new foundation piles
13	Placement of prefabricated girders
14	Welding of reinforcement and casting concrete deck
15	Finishing works
16	Opening of second direction (LSB)

TABLE 6.1: Conventional practice construction sequence for bridge replacement in 85 days *[Dinnissen, 2010]*

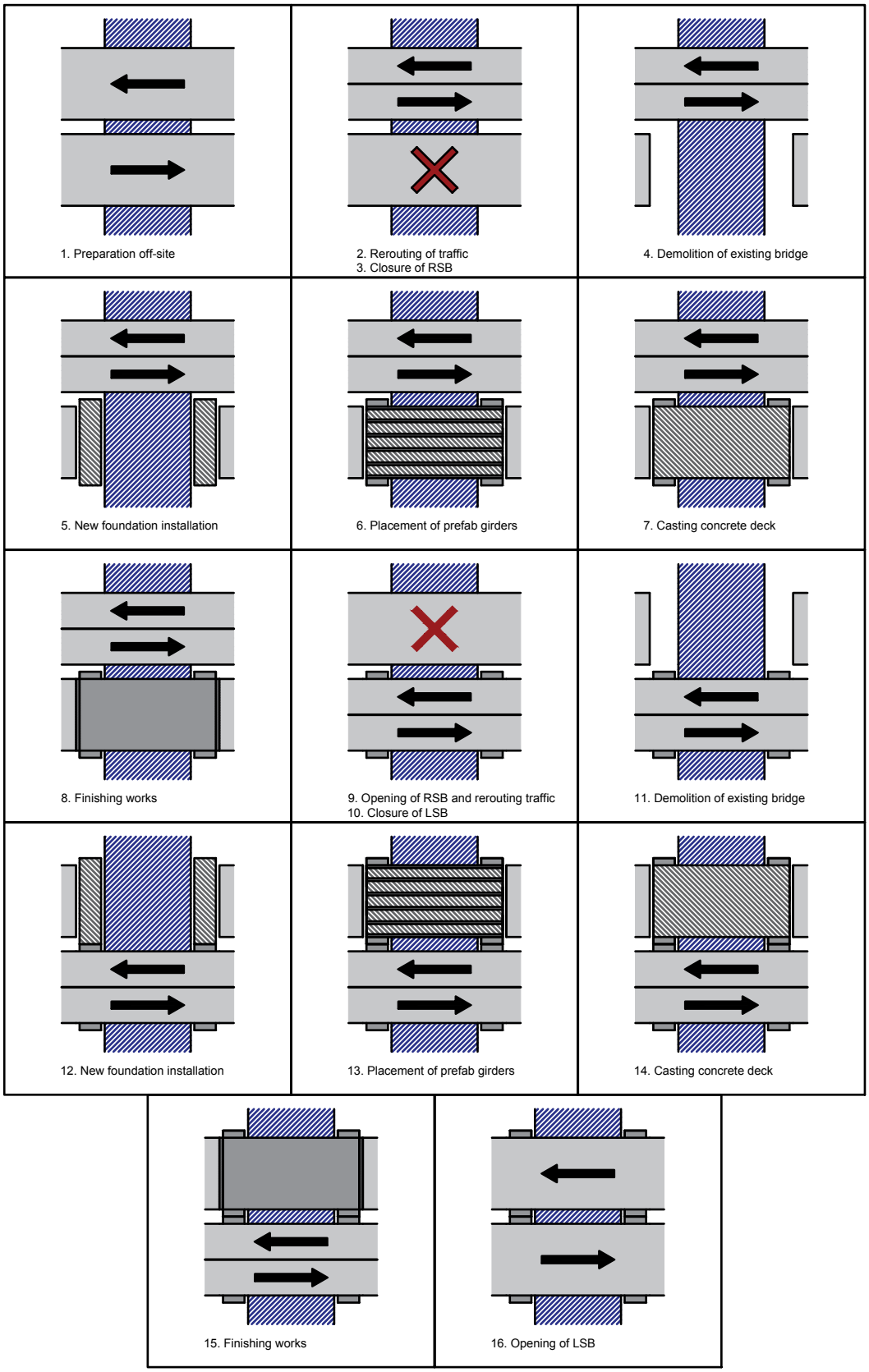

FIGURE 6.3: Illustrated construction sequence for a double bridge replacement as conducted in *[Dinnissen, 2010]*

	Construction activity
1	Preparation activities - Design - Additional CPTS next to existing abutments - Prefabrication of elements
2	Construction site preparations - Groundwork for heavy transport equipment and temporary falsework - Temporary falsework for superstructure - Erection of elements by conventional cranes - Finishing works
3	On-site preparations - Installation of foundation piles next to highway abutment - Welding of reinforcement and casting of new abutments
4	Closure of both highway and local road
5	Demolition of existing bridge
6	Transportation of new bridge to site by SPMTs
7	Installation of new bridge and coupling to existing highway
8	End of highway and local road closure

TABLE 6.2: Quick bridge replacement construction sequence according to the proposed strategy

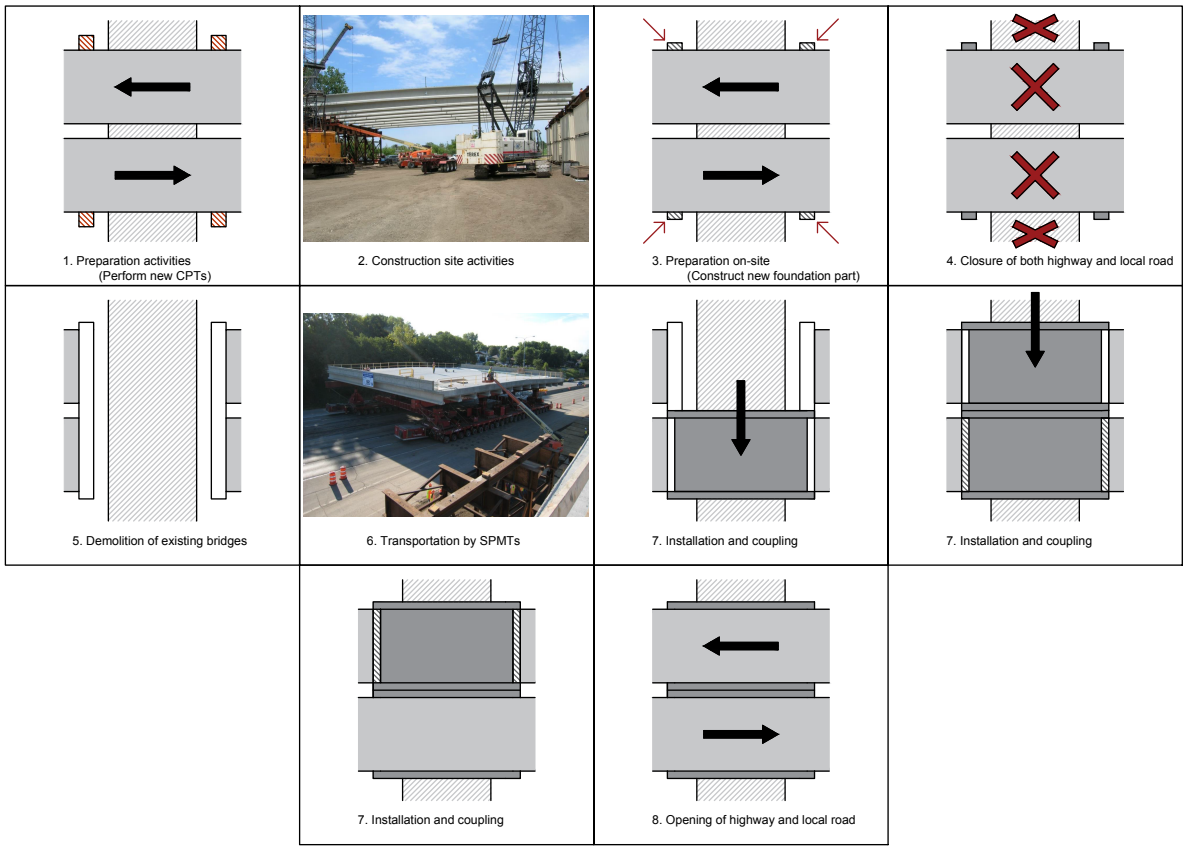

FIGURE 6.4: Illustrated construction sequence for a quick bridge replacement strategy *[Federal Highway Administration, 2015]*

6.4. REDUCTION OF ON-SITE CONSTRUCTION TIME

Both construction sequences have been compared in required construction time and induced traffic hindrance. The results are given in Figure 6.5 in which the red shaded area shows the period in which traffic hindrance occurs. The time indications are taken from *[Dinnissen, 2010]* and to reference projects in the USA *[Raglow, 2013][Federal Highway Administration, 2015]*.

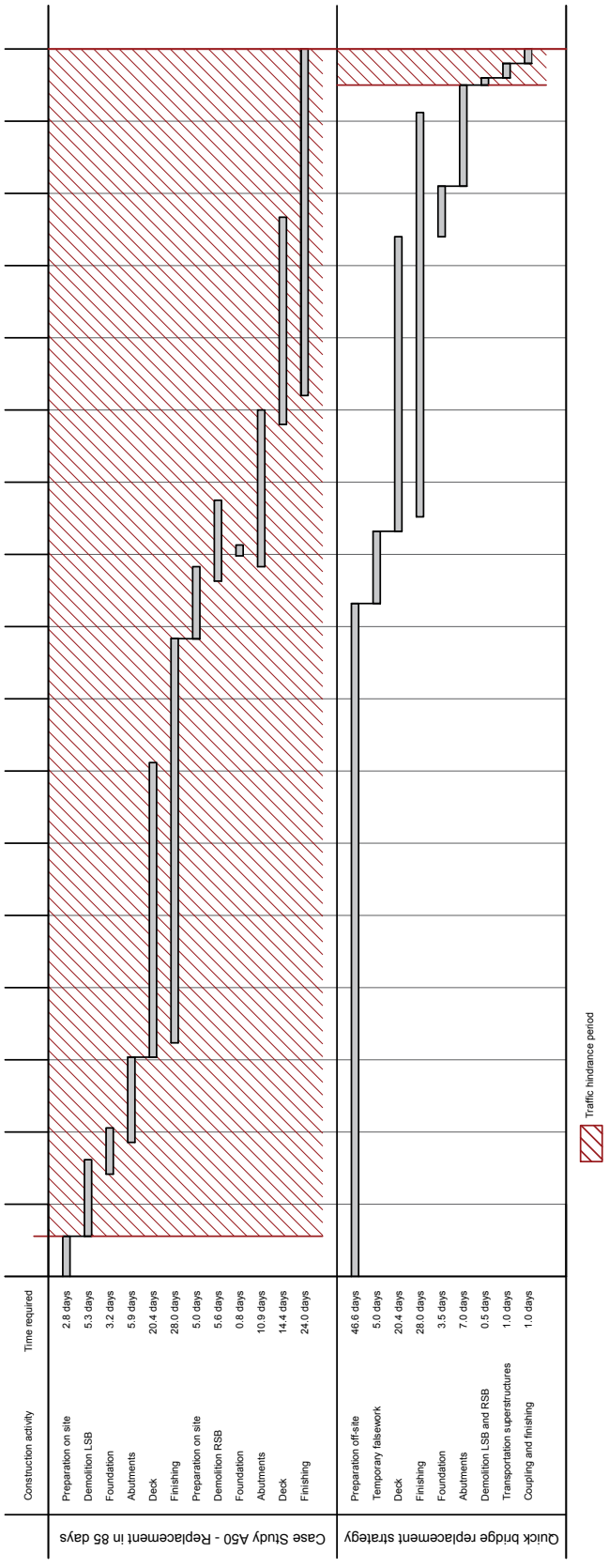

FIGURE 6.5: Comparison in construction sequences and planning of the case study A50 to the replacement strategy applied on case study A9, with indicated period of traffic hindrance in red

It can immediately be seen that the period of traffic hindrance is reduced from more than 80 days to merely 60 hours which is equal to a weekend closure.
This large benefit is caused by the extraction of almost all construction activities from the bridge location to a more remote building site. Also, the installation of additional foundation piles does not cause any traffic hindrance since they are located outside the current alignment of the highway.

The small time frame for on-site construction activities in the quick bridge replacement strategy does result in a very strict activity sequence and therefore delays can have very large consequences. On the other hand, erection of the superstructure off-site is not influenced by many factors and thus planning should not be a problem.

6.5. POTENTIAL FOR GENERAL APPLICATION

In Chapter 5 it was shown that the combination of foundation retainment and slender single span structures is indeed possible for a two-span plate bridge as considered in the case study. However, section 2.1.3 states that the majority of all bridges in the current highway network are plate bridges with 3 or 4 spans. Replacing those in accordance to the proposed strategy will require a larger increase of bearing capacity and also a larger reduction of superstructure load actions. Otherwise, the existing foundation will require additional strengthening, or not every intermediate support can be avoided.

In Figure 2.6 an overview is given of the existing plate bridges, their span length and the required slenderness for a single span.
This same dataset has been used to obtain a rough indication of the general applicability of the strategy for current plate bridges in the Dutch highway network. This is done by estimating the increase in foundations loads as a result of the removal of all intermediate supports in a new design. It is assumed that the new superstructure design will consist of an open trough bridge structure with a weight reduction relative to that found in the A9 case study. Besides the self-weight of the concrete also the traffic load has been taken into account by assuming a conservative distributed load of q_{UDL1} = 10.35 kN/m^2 over a width of 1 meter. The KEL loading is considered by taking an additional load of $F_{KEL1} \cdot \frac{2}{3.0}$ = 200 kN/m into account directly on top of the foundation.
The estimated increase in foundation loads has been compared to the increase in bearing capacity from the different scenarios as found in the case study (section 3.3.1). The results are given in Figure 6.6, where for each bridge the required slenderness and resulting increase of foundation loads is depicted.

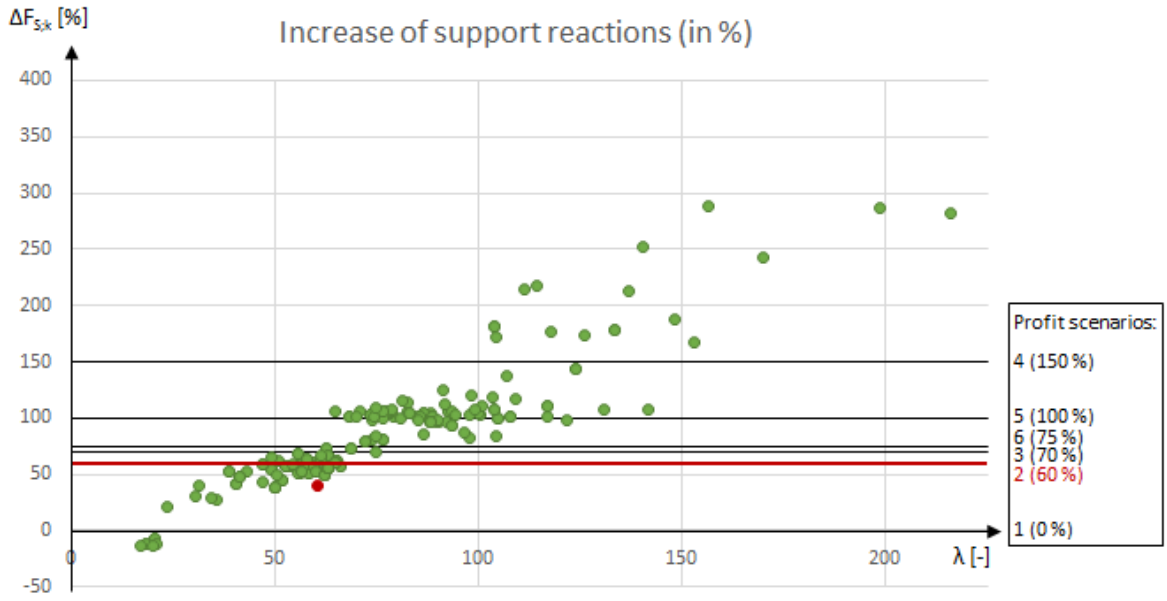

FIGURE 6.6: Comparison of required slenderness and resulting increase of foundation loads for the currently existing plate bridges

Profit scenario 2, which considers the realistic profit for current practice, is indicated by the red line and the results for the other scenarios are indicated by the black lines. The bridge considered in the case study is denoted by the red dot and it can be seen that the increase of foundation loads for this case study is indeed lower than the increase of bearing capacity.
It can however also be seen that for most bridges the obtained profit in bearing capacity is not enough and additional strengthening of the foundations is required. This is even the case for the most optimistic scenario - profit scenario 6 - in which the upper boundary of set-up is taken into account.
Additionally, the initial increase of traffic load following from new design codes compared to the original regulations, has not been taken into account in this analysis. Incorporating this into the estimation would result in even less bridges that can retain the existing foundation while avoiding all intermediate supports in the new design.

It must thus be concluded that for overall applicability of this strategy in the replacement challenge either more research is required, additional strengthening of the foundations must occur or not all intermediate supports can be removed.

7

CONCLUSIONS AND RECOMMENDATIONS

The aim of this research was to develop a quick bridge replacement strategy that minimises traffic hindrance during construction. For this, three actions are proposed that will reduce the on-site construction time drastically:

1. Select the ABC approach
2. Retain the existing foundations
3. Avoid intermediate supports

From preliminary research it followed that more insight was required into the technical feasibility of the proposed strategy, leading to the following research question:

Can a slender and lightweight UHPC bridge concept be used to enable the structural retainment of existing foundations in a low hindrance replacement strategy?

Overall it can be concluded from the research performed, that yes, a slender and lightweight UHPC trough bridge can indeed be used in combination with a retained pile foundation to minimise the on-site construction time and therefore traffic hindrance during a bridge replacement task. It has also been shown that in order to develop a strategy that is generally applicable, additional research is required in the field of bearing capacity of piled foundations and on the shear and torsional capacity of UHPC trough bridges.
With respect to the vision as defined by RWS considering sustainability in design through minimal hindrance, recycling and durability, it can be seen that these are all covered in the time-reducing actions. It can therefore be concluded that the proposed strategy is suitable for a MEAT-procedure according to this vision of RWS.

The elaborate conclusions and recommendations for further research can be found in sections 7.1 and 7.2 respectively.

7.1. CONCLUSIONS

Besides the general conclusion of the research question, several other interesting observations can be made.

Regarding the technical feasibility of the time-reducing actions it can be said that:

- There lies a promising potential in bearing capacity profit as the negative effect of the $alpha_p$ reduction can be compensated by addressing certain hidden safeties in geotechnical design. This profit can mainly be found in the set-up of soil, incorporation of the group effect and determining the governing CPT in a different manner.
- In current practice, without additional research, the largest profit in bearing capacity can be obtained by performing new CPTs as closely to the existing foundation piles as possible. In this manner the group effect will be taken into account directly.
- The set-up of soil is very promising, but without additional research only a conservative value can be applied, leading to a limited increase in bearing capacity.
- Although the group effect f_1 can be taken into account easily from the regulations for tension piles, this results in only a limited increase of bearing capacity.

- From all six profit scenarios considered for the possible increase of bearing capacity, scenario 2 is most promising in current practice. It considers several positive influences on the foundations, such as the densification from pile group effects and a conservative value for set-up, which are thought to be excepted for practical use. It also contains the performance of additional CPTs in the vicinity of the existing pile foundation, thereby decreasing the uncertainty factor ξ but also obtaining a more realistic value for the overall group effects.

- The application of a trough superstructure concept in traffic bridges is a suitable solution to obtain a slender structure, as the floor girders are spanned over the width only and furthermore the side girders are not limited in height.
- Another advantage of the trough superstructure concept is that the largest support forces will lie at the end of the abutments, enabling the possible required strengthening of the existing foundation just outside the current road alignment.
- The trough bridge design must consist of open structural elements, not only to reduce the weight on the foundations as much as possible but also to prevent ice-formation in winter. In this, a variant with multicell box girders for the deck and a truss structure for the side girders is regarded as a viable option.
- The high structural and durability characteristics of UHPC make this material very suitable for application in a slender and lightweight bridge superstructure. Due to the high compressive strength, large prestress forces are possible on a relatively small cross-section. Although this indeed results in a slender and lightweight structure, it has now shifted towards a shear and torsion capacity problem as the reduced cross-sectional area limits the ultimate strength of the compression struts.
- The reduced cross-sectional area not only leads to benefits in slenderness and weight reduction, it also leads to an enhanced sustainability since less cement is required for the production of the UHPC elements.
- A possible solution for the limited shear and torsion capacity can be found in increasing the cross-sectional area, but this is undesirable with respect to weight reduction, dangers of ice-formation and sustainability. Instead, a potentially suitable solution might be found in altering the trough structure into a single box structure through which the traffic moves. The high side girders will be connected at the top, forming a closed cross-section which is very beneficial for the torsion capacity. It is expected that this bridge concept will allow for even longer spans.
- For all structural concepts detailing becomes very important in the reduced cross-sectional areas and elements under high prestressing.

Regarding the on-site time reduction of the three strategy actions:

- Applying an ABC approach can reduce the on-site construction time drastically as in many cases a mere weekend closure will be sufficient.
- In every replacement project the concept of ABC can be applied, to some extent at least, by using prefabricated elements and assembling these off-site. Additional time reduction can be obtained by assembling entire superstructures off-site and transporting them to their final location through lateral sliding or by means of SPMTs.
- Regardless of the requirement for additional strengthening, retaining the existing foundations will always lead to on-site time reduction as less demolition works are required but also less additional piles have to be installed. It is even more beneficial if no additional foundation work is required because the obtained profit in bearing capacity can adequately resist the increased support reactions from the superstructure.
- Avoiding intermediate supports has a positive effect on the reduction of on-site construction time, but this effect is rather small compared to the other strategy actions. It does, however, result in a design with a much higher complexity, especially if it is to be combined with retainment of the existing foundations. It must therefore be considered for every case specifically whether the benefits outweigh the consequences. An additional advantage of avoiding intermediate supports in the new design can be found in enhanced safety of the underlying road and full flexibility of the underlying road layout.

Regarding the potential of the quick bridge replacement strategy:

- By applying the proposed replacement strategy a drastic reduction of traffic hindrance is obtained. Furthermore, sustainability of a replacement project is enhanced through recycling of elements, the high durability of UHPC and the reduced material production required.

- All strategy actions are designed to be implemented in the tender phase of a project. Together with the achieved quality criteria for traffic hindrance and sustainability this makes the strategy particularly suitable for a MEAT-procedure within a tender assignment.

7.2. RECOMMENDATIONS FOR FURTHER RESEARCH

From these conclusions it follows that the proposed quick bridge replacement strategy has a high potential, but to incorporate this into practice more research is required. Some recommendations for the further development of a suitable tender strategy are given below.

Regarding the technical feasibility of the time-reducing actions:

1. Statistical reliability of foundations
   A potential profit in bearing capacity is obtained by addressing hidden safeties in design. If, however, this is not accompanied by a simultaneous reduction of uncertainties it might to lead to an inadequate statistical reliability. This insinuates that if these hidden safeties are indeed to be applied in practice, research on the effects on parameter uncertainties and overall design safety is essential.

2. Research on the pile tip bearing factor α_p
   The reduction of the pile tip bearing factor α_p in 2017 was accompanied by an extensive discussion within the geotechnical market. The introduced reduction is based on limited research and only on driven prefabricated piles, and thus the effect on most geotechnical foundations is not quantified yet. The regulations state that if a supplier or contractor can prove the reduction of α_p to be too high for a certain pile type, it is allowed to incorporate the newly found value into design. The responsibility for this research is attributed to the market but the problem is that no manufacturer is willing to invest in these proof loading tests as competitors could also benefit from this. Nevertheless, this research can in theory provide a substantial profit in bearing capacity and therefore it is recommended to be executed within the coming few years.

3. Research on the set-up of soil and a quantification of the mechanisms and parameters
   Multiple studies on this mechanism have already been performed with very divergent, but also very promising results. Getting more insight into these parameters will most likely lead to an increase in bearing capacity profit. For practical purposes it might however be more profitable to execute a research based on certain design considerations regarding the retained foundations, instead of focusing on the theory behind it.

4. Research on the group effect factor f_2
   The positive influence of group effects in a pile foundation under compression is generally accepted, but only the factor f_1 can be taken into account in current calculations. It is however expected that factor f_2 can potentially lead to a large profit in bearing capacity, especially for existing foundations that have been loaded over decades already. For quantification of f_2 and its influence on f_1 and the overall pile bearing capacity both theoretical and practical research must be done.
   For current practice it could be beneficial to compose a database of strategically executed CPTs in the vicinity of the existing foundations at ongoing projects. This can give insight into the magnitude and spread of the densification effect and will require little additional actions.

5. Insight into the approval regulations from RWS or other institutions
   Before most hidden safeties can be applied in practice, approval is required by RWS or other regulatory institutions. By investigating the required proof or persuasion it is possible to aim further research more towards a decisive result.

6. Further development of the trough bridge concept
   The UHPC trough bridge concept with open structural elements shows a high potential for slender and lightweight superstructures. There is however a problem in shear and torsional capacity that has to be solved before application. A possible solution can be found in the development of a box structure, which will require additional research. Also, the connections and reinforcement configuration of the

different slender elements has to be elaborated in more detail.

7. Investigation of the possibilities of SPMTs or lateral sliding
   Although the expertise regarding lateral sliding and transport by SPMTs is already available within the market, it is interesting to investigate the possibilities of those systems and their limitations.

Regarding the application of the replacement strategy in tender designs:

1. General applicability in bridge replacement
   This thesis has focussed on the technical feasibility of one particular case study. It was however also shown that the majority of plate bridges built before 1980 will require a higher slenderness and that this will constitute higher support reactions on the existing foundations. Extended research into the feasibility for a wider range of slenderness and span lengths should be conducted in order to make this strategy suitable for general application.

2. Insight into the achievable on-site time reduction and costs
   In order to make adequate design choices in the tender phase regarding the replacement strategy, more insight must be gained in the achievable on-site construction time reduction of different actions, together with their expected additional costs. It is also beneficial to look at the predefined award criteria incorporated in a MEAT procedure to fully benefit from the sustainable design with minimal traffic hindrance. If these can be combined to the achievable on-site time reduction and expected costs for certain actions a tool for efficient decision making can be developed.

REFERENCES

3Angle (2016a). Engineeringspecificatie Bestaande Kunstwerken.

3Angle (2016b). Engineeringspecificatie Nieuwe Kunstwerken.

AFGC (2013). Ultra High Performance Fibre-Reinforced - Recommendations. *Française de Génie Civil*.

Allaart, A. (1994). Uitgangspunten voor het ontwerp van trogbruggen. *N.V. Nederlandse Spoorwegen*.

Axelsson, G. (2000). Long-term set-up of driven piles in sand.

Betonlexicon (n.d.). Hogesterktebeton. http://betonlexicon.nl/H/Hogesterktebeton/ [Accessed: January 5 2017].

Blauwendraad, J. (2006). Plate analysis,theory and application - Volume 1 Theory. *Delft University of Technology*.

Braam, C. (2010). Rekenvoorbeelden bij Eurocode 2 (12) - Stabiliteit. *Cement*, (No. 3).

CUR-commissie C193 (2012). Werkdocument Verborgen Veiligheden.

de Lange, D. A. (2013). On the possibility of simulating pile set-up in sand by means of centrifuge model testing. *Delft University of Technology*.

Dienst Expertise Beton en Staal (2012). Cursus bruginspecteur - Hoofdstuk 2.1: Brugtypes. *Vlaams Ministerie van Mobiliteit en Openbare Werken*.

Dinnissen, M. (2010). Kennisdossier vervangen twee kunstwerken in 85 dagen. *Heijmans*.

Everts, H. (2015). CIE4362 Soil Structure Interaction - Lecture Slides. *Delft University of Technology*.

FEBE (2013). Cursus Ontwerpen van constructies in prefab beton - Les 11: Geprefabriceerde betonnen bruggen. http://slideplayer.nl/slide/2080871/ [Accessed: October 25 2017].

Federal Highway Administration (2015). Minnesota Demonstration Projects: Rapid Replacement of the Maryland Ave. Bridge over I-35E in St. Paul. *Highways for Life*.

Francke, J. and Wüst, H. (2016). Trendprognose wegverkeer 2016-2021 voor RWS. *Kennisinstituut voor Mobiliteitsbeleid*.

Fugro (2011). Sondering met plaatselijke kleefmeting - DKMP2003.

Heijmans (2016). Schuiven en belijnen bij A12 Veenendaal - Grijsoord. https://www.heijmans.nl/nl/nieuws/schuiven-en-belijnen-bij-a12-veenendaal-grijsoord/ [Accessed: March 1 2017].

Hoogenboom, P. (2014). Aantekeningen over wringing. *Delft University of Technology*.

IXAS (2015). Berekeningsnota UO KW 150 Huntumdreef.

Kennisinstituut voor Mobiliteitsbeleid (2016). Mobiliteitsbeeld 2016. *Ministerie van Infrastructuur en Milieu*.

Ketel, H., Willemse, R., van Rijen, P., and Koolen, E. (2011). Rekenmodel vvUHSB. *Cement*, (No. 3).

Laboratorium voor grondmechanica (1975). Rapport grondonderzoek ten behoeve van de bouw van kunstwerken E, F en G in de Gaasperdammerweg te Amsterdam-Bijlmer.

Mos Grondmechanica (2015). Sonderingen Gaasperdammerweg.

NEN-EN 1990 (2011). Eurocode: Basis of structural design. *Normcommissie 351 001 "Technische Grondslagen voor Bouwconstructies"*.

NEN-EN 1990-NB (2011). National Annex for Eurocode: Basis of structural design. *Normcommissie 351 001 "Technische Grondslagen voor Bouwconstructies"*.

NEN-EN 1991-1-1 (2011). Eurocode 1: Actions on structures - Part 1-1: General actions - Densities, self-weight, imposed loads for buildings. *Normcommissie 351 001 "Technische Grondslagen voor Bouwconstructies"*.

NEN-EN 1991-1-2 (2011). Eurocode 1: Actions on structures - Part 1-2: General actions - Actions on structures exposed to fire. *Normcommissie 351 001 "Technische Grondslagen voor Bouwconstructies"*.

NEN-EN 1991-1-3 (2003). Eurocode 1: Actions on structures - Part 1-3: General actions - Snow loads. *Normcommissie 351 001 "Technische Grondslagen voor Bouwconstructies"*.

NEN-EN 1991-1-4 (2005). Eurocode 1: Actions on structures - Part 1-4: General actions - Wind actions. *Normcommissie 351 001 "Technische Grondslagen voor Bouwconstructies"*.

NEN-EN 1991-1-4-NB (2005). National Annex for Eurocode 1: Actions on structures - Part 1-4: General actions - Wind actions. *Normcommissie 351 001 "Technische Grondslagen voor Bouwconstructies"*.

NEN-EN 1991-1-6 (2005). Eurocode 1: Actions on structures - Part 1-6: General actions - Actions during execution. *Normcommissie 351 001 "Technische Grondslagen voor Bouwconstructies"*.

NEN-EN 1991-1-7 (2015). Eurocode 1: Actions on structures - Part 1-7: General actions - Accidental actions. *Normcommissie 351 001 "Technische Grondslagen voor Bouwconstructies"*.

NEN-EN 1991-1-7-NB (2015). National Annex for Eurocode 1: Actions on structures - Part 1-7: General actions - Accidental actions. *Normcommissie 351 001 "Technische Grondslagen voor Bouwconstructies"*.

NEN-EN 1991-2 (2015). Eurocode 1: Actions on structures - Part 2: Traffic loads on bridges. *Normcommissie 351 001 "Technische Grondslagen voor Bouwconstructies"*.

NEN-EN 1991-2-NB (2015). National Annex for Eurocode 1: Actions on structures - Part 2: Traffic loads on bridges. *Normcommissie 351 001 "Technische Grondslagen voor Bouwconstructies"*.

NEN-EN 1992-1-1 (2005). Eurocode 2: Design of concrete structures – Part 1-1: General rules and rules for buildings. *Normcommissie 351 001 "Technische Grondslagen voor Bouwconstructies"*.

NEN-EN 1997-1 (2016). Eurocode 7: Geotechnical design of structures - Part 1: General rules. *Normcommissie 351 006 "Geotechniek"*.

NEN-EN 1997-2 (2007). Eurocode 7: Geotechnical design of structures - Part 2: Ground investigation and testing. *Normcommissie 351 006 "Geotechniek"*.

NEN-EN 1998-1-1 (2005). Eurocode 8: Design of structures for earthquake resistance - Part 1: General rules, seismic actions and rules for buildings. *Normcommissie 351 006 "Geotechniek"*.

Raglow, R. (2013). I-84 at Dingle Ridge Road in Brewster, NY - Bridge Slide Shot from Underneath Bridge. https://vimeo.com/76763826 [Accessed: February 28 2017].

Reitsema, A. (2017). *Delft University of Technology*.

Reitsema, A., Lukovic, M., and Hordijk, D. (2015). Towards Slender, Innovative Concrete Structures for Replacement of Existing Viaducts.

Rijkswaterstaat (1975). Bestektekening - Overzicht. *Verbinding R.W.1-RW.2 Gaasperdammerweg - Viaduct over de Huntumdreef nabij KM 4.623 K.W.E.*

Rijkswaterstaat (1977a). Maten STP.1. *Verbinding R.W.1-RW.2 Gaasperdammerweg - Viaduct over de Huntumdreef nabij KM 4.623 K.W.E.*

Rijkswaterstaat (1977b). Palenplan. *Verbinding R.W.1-RW.2 Gaasperdammerweg - Viaduct over de Huntumdreef nabij KM 4.623 K.W.E.*

Rijkswaterstaat (n.d.a). A9 Holendrecht - Diemen (Gaasperdammerweg). https://bezoekerscentrum.rijkswaterstaat.nl/SchipholAmsterdamAlmere/?project=a9-gaasperdammerweg#.WWR6AYjyhPZ [Accessed: July 11 2017].

Rijkswaterstaat (n.d.b). Verplaatsing spoorbrug in beeld. https://bezoekerscentrum.rijkswaterstaat.nl/SchipholAmsterdamAlmere/?gallery=verplaatsing-spoorbrug-beeld#.WLaoUPnhBPY [Accessed: March 1 2017].

Roads and Bridges (n.d.). A travelling relief. https://www.roadsbridges.com/traveling-relief [Accessed: February 24 2017].

SCIA Engineer (2015). Topic Training - Finite Element Model.

Spanbeton (2017). Kokerbalkoplossingen SKK.

Spanbeton (n.d.). Krachtsverdelingsberekening.

Spanbeton (n.d.). Spanbeton ontwerpt en monteert grootste viaduct in traject omlegging A9 Badhoevedorp. http://www.spanbeton.nl/be/references/item/omlegging-a9-badhoevedorp/ [Accessed: March 1 2017].

Spencer, P. (2009). Standaarddetails voor betonnen bruggen. *Rijkswaterstaat Dienst Infrastructuur*.

Stap, M. A. G. (2017). Technical feasibility of a quick bridge replacement strategy that minimises traffic hindrance - Literature Study. *Delft University of Technology*.

Steele, C. and Balch, C. (2009). Introduction to the Theory of Plates. *Stanford University*.

Technical Services, E. (n.d.). Hartford slide bridge. http://www.eivtech.com/hartford-slide-bridge/ [Accessed: July 16 2017].

Transumo (n.d.). Gunnen op Doorstroming.

van Breugel, K., Braam, C. R., and Koenders, E. A. B. (2013). Concrete Structures under Imposed Thermal and Shrinkage Deformations - Theory and Practice. *Delft University of Technology*.

van Tol, A. (1994). Regelgeving in de Funderingstechniek. *Cement*, (No. 4).

van Tol, A. (2006). Funderingstechnieken. *Delft University of Technology*.

van Tol, A. (2015). Veranderende regelgeving paal- draagvermogen. *Cement*, (No. 5).

van Tol, A. (2017). Interview - March 2 2017 - TU Delft.

Verruijt, A. (2012). Soil Mechanics. *Delft University of Technology*.

Walraven, J. (2010). Gewapend Beton. *Delft University of Technology*.

Walraven, J. and Braam, C. (2015). Prestressed concrete. *Delft University of Technology*.

Part II

Appendices

General information

A

GENERAL BRIDGE LOAD CALCULATION

Eurocodes NEN-EN 1990: Basis of structural design *[NEN-EN 1990, 2011]*, NEN-EN 1991-1: Actions on structures *[NEN-EN 1991-1-1, 2011] to [NEN-EN 1991-1-7, 2015]* and NEN-EN 1991-2: Traffic load on bridges *[NEN-EN 1991-2, 2015]* prescribe the load actions that have to be taken into account when designing a traffic bridge. This appendix will treat these load actions together with the load combinations, in sections A.1 and A.2 respectively.

A.1. LOAD ACTIONS

In Table A.1, all possible load actions for a traffic bridge are listed. Not all loads will be taken into account in this thesis, due to varying reasons. In the following subsections, all loads will be further elaborated.

Load actions	Duration	Origin	Spatial variation	Nature and/or structural response	In project scope?
Self-weight	Permanent	Direct	Fixed	Static	Yes
Imposed loads					
Asphalt layer	Permanent	Direct	Fixed	Static	Yes
(Non-)structural elements	Permanent	Direct	Fixed	Static	No
Traffic loads					
LM1	Variable	Direct	Free	Static/dynamic	Yes
LM2	Variable	Direct	Free	Static/dynamic	No
LM3	Variable	Direct	Free	Static/dynamic	No
LM4	Variable	Direct	Free	Static/dynamic	No
Brake and acceleration forces	Variable	Direct	Free	Static/dynamic	Yes
Centrifugal forces	Variable	Direct	Free	Static/dynamic	No
Collision force	Accidental	Direct	Fixed/free	Static/dynamic	Yes
Soil pressure	Permanent/variable	Direct	Fixed/free	Static	Yes
Water pressure	Permanent/variable	Direct	Fixed/free	Static	Yes
Wind load	Variable/accidental	Direct	Fixed/free	Static/dynamic	Yes
Snow load	Variable/accidental	Direct	Fixed/free	Static/dynamic	Yes
Imposed deformations					
Thermal loading	Variable	Indirect	Free	Static	Yes
Shrinkage/hydration effects	Permanent/variable	Indirect	Free	Static	Yes
Excessive settlements	Permanent/variable	Indirect	Free	Static	Yes
Fire load	Accidental	Indirect	Free	Static	No
Execution loads					
Non-permanent storage of materials/equipment	Variable	Direct	Fixed/free	Static	No
Movable heavy machinery/equipment	Variable	Direct	Free	Static/dynamic	No
Loads from structural elements in temporary state	Variable	Direct	Free	Static	Yes
Accidental actions	Accidental	Direct	Free	Static/dynamic	No
Extraordinary loads					
Collission (see also traffic load)	Accidental	Direct	Free	Static/dynamic	Yes
Explosion	Accidental	Indirect	Free	Static/dynamic	No
Seismic loads	Variable/accidental	Indirect	Free	Dynamic	No

TABLE A.1: Load action overview

A.1.1. Self-weight

The self-weight of the prefabricated or in-situ poured concrete girder depends on the type of concrete applied, but can generally be taken as *[NEN-EN 1991-1-1, 2011]*:

$$q_{ck} = \rho_c \cdot A_c \text{ [kN/m]}$$

With: $\rho_c = 2500$ kg/m^3 for NSC
$\rho_c = 2500$-2800 kg/m^3 for UHPC
$g = 10$ m/s^2

A.1.2. Imposed loads

Imposed loads are caused by the self-weight of resting elements on the concrete deck, such as the asphalt layer or other non-structural elements. In this thesis, no detailed design steps will be executed and thus the non-structural elements are not considered. However, as the thickness of the asphalt layer determines the maximum possible construction height of the concrete deck, the self-weight of asphalt will be taken into account:

$$Q_{ak} = \rho_a \cdot d_a \text{ [kN/m}^2\text{]}$$

With: $\rho_a = 23$ kN/m^3 for hot-rolled asphalt *[3Angle, 2016a]*
d_a is the depth of the asphalt layer

According to *[3Angle, 2016b]*, the minimum asphalt depth for new viaducts is given by:

$$d_a = 130 + \text{a [mm]}$$

With: $a = 0.25 \cdot (\text{L}-30)$ [mm]
$0 \leq a \leq 30$ mm
L is the longest span in [m]

A.1.3. Traffic loads

Traffic loads are variable, static and dynamic loads that can be described by so-called load models. Eurocode NEN-EN 1991-2 defines four load models *[NEN-EN 1991-2-NB, 2015]*:

- Load model 1 (LM1)
  A combination of concentrated and uniformly distributed loads describe most effects of freight and passenger traffic.
- Load model 2 (LM2)
  A singular axle load with a surface equal to that of the tires is used to determine the dynamic effects of normal traffic on compact elements.
- Load model 3 (LM3)
  A combination of axle loads is used to model exceptional transport vehicles that move along specially determined routes.
- Load model 4 (LM4)
  A uniformly distributed load is taken into account to model a crowd.

In most cases, LM1 is governing for traffic bridges and therefore it is assumed that only LM1 has to be considered within the scope of this thesis.

Breedte van de rijweg w	Aantal theoretische rijstroken	Breedte van een theoretische rijstrook w_l	Breedte van het resterende oppervlak
$w < 5{,}4$ m	$n_l = 1$	3 m	$w - 3$ m
$5{,}4$ m $\leq w < 6$ m	$n_l = 2$	$\frac{w}{2}$	0
6 m $\leq w$	$n_l = Int\left(\frac{w}{3}\right)$	3 m	$w - 3 \times n_l$
OPMERKING Bijvoorbeeld geldt voor een breedte van de rijweg gelijk aan 11 m, dat: $n_l = Int\left(\frac{w}{3}\right) = 3$ *) en dat de breedte van het resterende oppervlakte gelijk is aan: $11 - 3\times3 = 2$m.			

TABLE A.2: Classification of theoretical traffic lanes *[NEN-EN 1991-2, 2015]*

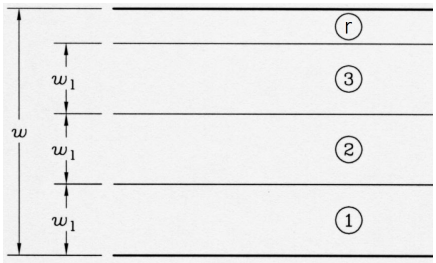

FIGURE A.1: Top view of theoretical traffic lanes *[NEN-EN 1991-2, 2015]*

In all load models, the bridge width that is used for traffic (w), is divided into traffic lanes with widths as given in Table A.2 (w_1). The width of the remaining area (r) is also included as a traffic lane in the model calculations.

For each case, the traffic lane with the most unfavourable effect must be taken as traffic lane 1, followed by traffic lane 2 and the rest.

Load model 1 (LM1)
As described above, LM1 consists of a combination of concentrated Knife Edge Loads (KEL) and uniformly distributed vertical loads (UDL).

KEL: A single, concentrated double-axle system (see Figure A.2) for every theoretical traffic lane, with a load per axle according to:
$\alpha_Q \cdot Q_k$ with α_Q correction factors
The contact area for every tire is taken as 0.4x0.4 m. The double-axle system can occur at every position along the axis of the theoretical traffic lane.

UDL: A uniformly distributed load for every theoretical traffic lane, with a load per meter squared of:
$\alpha_q \cdot q_k$ with α_q correction factors
These loads must only be taken into account on the unfavourable parts of the traffic zone in both longitudinal as transversal direction.

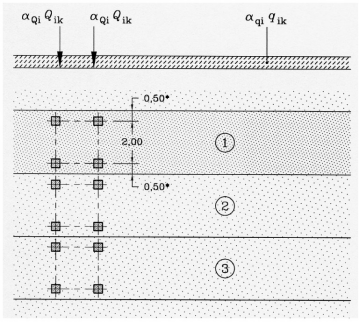

FIGURE A.2: Axle distribution over the theoretical traffic lanes in LM1 *[NEN-EN 1991-2, 2015]*

	KEL [kN/m²]	UDL [kN/m²]			KEL [kN/m²]	UDL [kN/m²]
Lane nr.	$Q_{i;k}$	$q_{i;k}$	$\alpha_{Q;i}$	$\alpha_{q;i}$	$\alpha_{Q;i}Q_{i;k}$	$\alpha_{q;i}q_{i;k}$
1	300	9.0	1.0	1.15	300	10.35
2	200	2.5	1.0	1.4	200	3.5
3	100	2.5	1.0	1.4	100	3.5
> 3	0	2.5	1.0	1.4	0	3.5
r	0	2.5	1.0	1.4	0	3.5

TABLE A.3: Characteristic KEL and UDL loads for LM1 *[NEN-EN 1991-2-NB, 2015]*

The correction factors for a Dutch highway with more than 3 traffic lanes, according to *[NEN-EN 1991-2-NB, 2015]*, are given in Table A.3, together with the characteristic values for KEL and UDL loads.

Horizontal loads
As a result of break and acceleration forces, horizontal loads can occur at the asphalt surface. In longitudinal direction, Q_{lk} is taken as a percentage of the maximum vertical load from LM1:

$$Q_{lk} = 0.6 \cdot \alpha_{Q;1} \cdot 2 \cdot Q_{1k} + 0.1 \cdot \alpha_{q;1} \cdot q_{1k} \cdot w_1 \cdot L = 360 + 0.115 \cdot w_1 \cdot L \text{ [kN]}$$

With: $180 \cdot \alpha_{Q;1} \leq Q_{lk} \leq 900$

A transversal component Q_{trk} must also be taken into account, with a value equal to 25% of the longitudinal horizontal force Q_{lk}.

If a viaduct is curved horizontally with a radius r, centrifugal forces Q_{tk} occur which are radially directed at the asphalt surface. Q_{tk} depends on the radius r, according to Table A.4.

$Q_{tk} = 0{,}2Q_v$ (kN)	voor $r < 200$ m
$Q_{tk} = 40Q_v / r$ (kN)	voor $200 \leq r \leq 1500$ m
$Q_{tk} = 0$	voor $r > 1500$ m

TABLE A.4: Centrifugal forces Q_{tk} as a relation of the radius r of a curved viaduct *[NEN-EN 1991-2, 2015]*

Traffic load groups

The simultaneity of the traffic loads that can occur is included by traffic load groups, as presented in Table A.5. Since the scope of this thesis is restricted to road bridges and LM1, only traffic load groups gr1a and gr2 are considered.

		RIJWEG						VOET- EN FIETSPADEN
Belastingtype		**Verticale krachten**				**Horizontale krachten**		**Alleen verticale krachten**
Verwijzing		4.3.2	4.3.3	4.3.4	4.3.5	4.4.1	4.4.2	5.3.2-(1)
Belastingssysteem		BM1 (TS en UDL)	BM2 (enkele as)	BM3 (bijzondere voertuigen)	BM4 (mensen-menigte)	Rem- en versnellings-krachten [a]	Centrifugaal-krachten en krachten in dwarsrichting [a]	Gelijkmatig verdeelde belastingen
Groepen van belastingen	gr1a	Karakteristieke waarde						Combinatiewaarde [b]
	gr1b		Karakteristieke waarde					
	gr2	Frequente waarde				Karakteristieke waarde	Karakteristieke waarde	
	gr3 [d]							Karakteristieke waarde [c]
	Gr4				Karakteristieke waarde			Karakteristieke waarde
	Gr5	Zie bijlage A		Karakteristieke waarde				
	Overheersende belastingscomponent (aangeduid als component behorend bij de groep)							

[a] Kan zijn vastgesteld in de nationale bijlage (voor de genoemde gevallen).
[b] Kan zijn vastgesteld in de nationale bijlage. De aanbevolen waarde is 3 kN/m^2.
[c] Zie 5.3.2.1-(2). Er behoort slechts één voetpad als belast te zijn beschouwd, indien het effect hiervan ongunstiger is dan bij belasting op twee voetpaden.
[d] Deze groep is niet van belang als gr4 wordt beschouwd.

TABLE A.5: Classification of traffic load groups *[NEN-EN 1991-2, 2015]*

Load configuration

A traffic load is a free load, which means that in theory it can occur anywhere on the viaduct surface. The transversal spatial distribution has been covered by the load models, but in longitudinal direction the KEL loads can still occur anywhere along the span. This means that for each case, the most governing load configuration must be chosen.

For a single span case, the KEL is situated at mid-span for the governing cross-section, while for the maximum reaction forces the KEL loads must be situated on top of the supports (Figure A.3). All governing load situations can be obtained from these schemes.

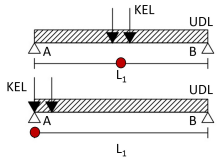

FIGURE A.3: Governing traffic load configuration for a statically determinate structure

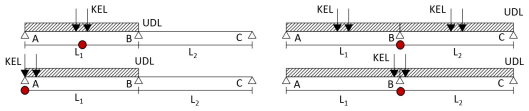

FIGURE A.4: Governing traffic load configuration for a 2-span statically indeterminate structure

For cases with multiple spans, the most governing situation must be sought for both the governing cross-section at mid-span as the reaction forces at the support. This has been illustrated for 2-, 3- and 4-span structures in Figures A.4 to A.11. Again, the most governing load situations can be obtained from these schemes given.

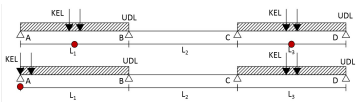

FIGURE A.5: Governing traffic load configuration for a 3-span statically indeterminate structure

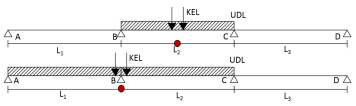

FIGURE A.6: Governing traffic load configuration for a 3-span statically indeterminate structure

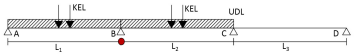

FIGURE A.7: Governing traffic load configuration for a 3-span statically indeterminate structure

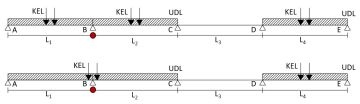

FIGURE A.8: Governing traffic load configuration for a 3-span statically indeterminate structure

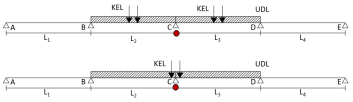

FIGURE A.9: Governing traffic load configuration for a 3-span statically indeterminate structure

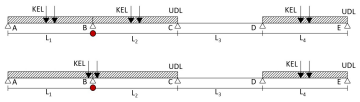

FIGURE A.10: Governing traffic load configuration for a 3-span statically indeterminate structure

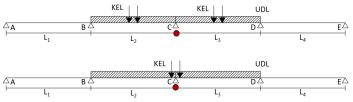

FIGURE A.11: Governing traffic load configuration for a 3-span statically indeterminate structure

Collision load

A viaduct is also prone to collision forces from traffic passing underneath, either acting on the deck or acting on the intermediate supports.

On the substructure (i.e. the intermediate supports) this accidental load may be taken as equivalent static forces. The design values are given in Table A.6, where x is taken parallel to the traffic direction and y is perpendicular to the traffic direction.

	Flexible		Stiff	
	Fdx [kN]	Fdy [kN]	Fdx [kN]	Fdy [kN]
Highways	1000	500	2000	1000
Local roads	750	375	1500	750

TABLE A.6: Design values for the collision loads on the substructure *[NEN-EN 1991-1-7, 2015]*

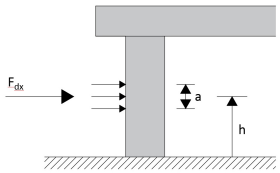

FIGURE A.12: Geometry of the impact force following a collision *[NEN-EN 1991-1-7, 2015]*

It is assumed that F_{dx} and F_{dy} do not work simultaneously. Figure A.12 illustrates the geometry of the impact force in which it holds:

For trucks: $a = 0.5$ m $h = 1.5$ m
For cars: $a = 0.25$ m $h = 0.5$ m

On the superstructure (i.e. the deck) the accidental collision load can also be taken as an equivalent static force, with the design values given in Table A.7. These design values must be multiplied by a reduction factor r_F, that takes into account the relative height of the viaduct compared to the recommended values (Figure A.13).

	Fdy [kN]
Highways	500
Local roads	375

TABLE A.7: Design values for the collision loads on the superstructure *[NEN-EN 1991-1-7, 2015]*

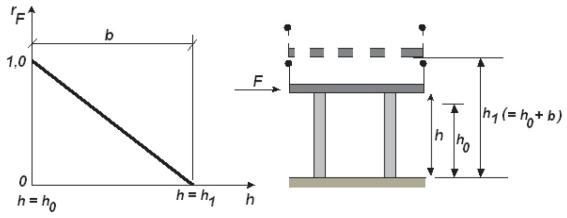

FIGURE A.13: Geometry of the impact force following a collision *[NEN-EN 1991-1-7, 2015]*

The recommended value for $h_0 = 4.8$ m, for $h_1 = 7.0$ m and thus for $b = 2.2$ m. The recommended area of impact is given as 0.25x0.25 m.

A.1.4. Soil pressure

In case structural elements are situated (partly) under ground level, the soil pressure on this element must be taken into account. For the vertical pressure it holds *[Verruijt, 2012]*:

$$Q_{sp;v;k} = \Sigma \sigma_{zz;i} \text{ [kN/m}^2\text{]}$$

With: $\sigma_{zz;i} = \gamma_{sat;i} \cdot z_i$ for saturated soil layers
$\sigma_{zz;i} = (\gamma_{unsat;i} + \gamma_w) \cdot z_i$ for unsaturated soil layers
γ the specific soil weight [kN/m^3]
z_i the layer depth [m]
γ_w the water pressure (γ_w = 10 kN/m^3)

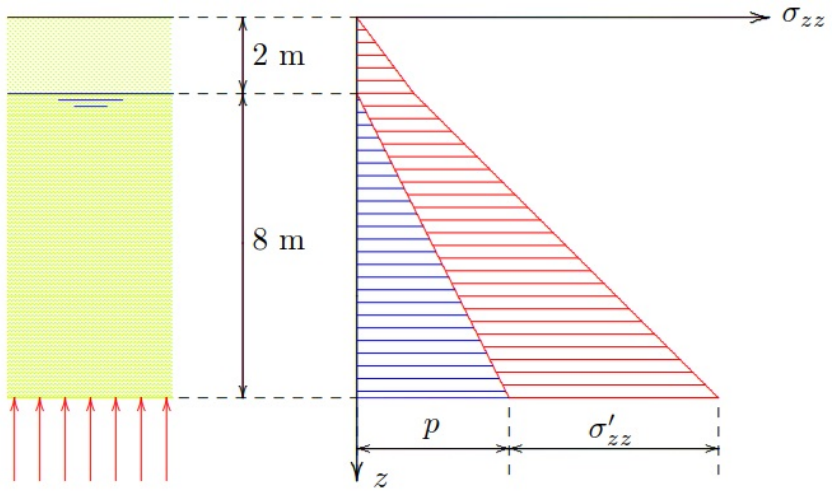

FIGURE A.14: Vertical soil pressure, divided into effective soil pressure and water pressure *[Verruijt, 2012]*

For the horizontal pressure, the vertical stress component must be multiplied by K, the factor of lateral earth pressure. When the earth is at rest, the factor K is equal to K_0, which is given by:

$$K_0 = (1 - sin(\phi')) \cdot \sqrt{OCR}$$

With: ϕ' the angle of shearing resistance
OCR the over-consolidation ratio

If the ground level is not horizontal but inclined over an angle β, the factor K becomes:

$$K_{0;\beta} = K_0 \cdot (1 + sin(\beta))$$

$$Q_{sp;h;k} = \Sigma K_{0;\beta;i} \cdot \sigma_{zz;i} \text{ [kN/m}^2\text{]}$$

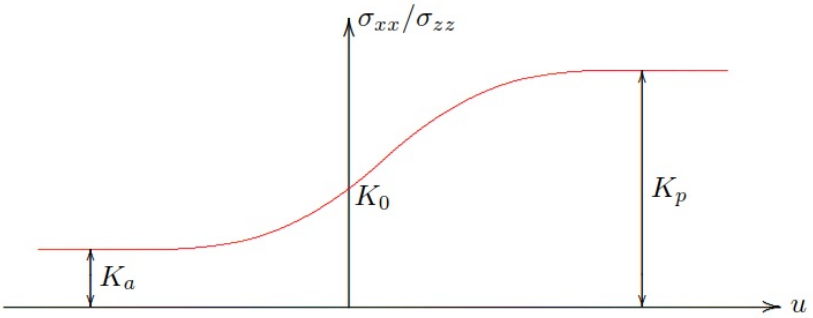

FIGURE A.15: Factor K for horizontal soil pressure as a relation of the displacement u *[Verruijt, 2012]*

A.1.5. Water pressure

If structural elements are in contact with water permanently during a certain design phase, the water pressure must be taken into account. As the water pressure is hydrostatic, it is equal in all directions *[Verruijt, 2012]*:

$$Q_{wp;k} = \gamma_w \cdot z \text{ [kN/m}^2\text{]}$$

A.1.6. Wind load

From Eurocode NEN-EN 1991-1-4 *[NEN-EN 1991-1-4, 2005]* it follows that wind forces in horizontal (x- or y-)direction on a bridge should be taken into account separately. Unfavourable wind forces in z-direction, however, will have to be combined with the x- or y-direction forces. The same formula for wind loads on buildings may be applied on bridges:

$$F_{w;i} = c_s c_d \cdot C_{f;i} \cdot q_p(z_e) \cdot A_{ref} \text{ [kN]}$$

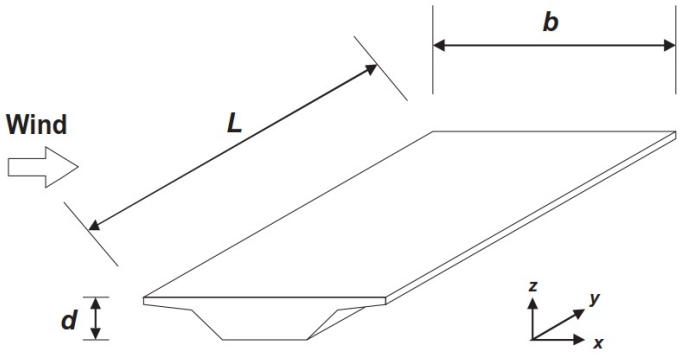

FIGURE A.16: Directions of the wind force on a bridge girder *[NEN-EN 1991-1-4, 2005]*

For spans smaller than 40 m, $c_s c_d = 1.0$ as dynamical response calculations are unnecessary.

- x-direction:

  $$F_{wxk} = 0.5 \cdot \rho \cdot {v_b}^2 \cdot C_x \cdot A_{ref;x}$$

  with: $C_x = c_e(z_e) \cdot c_{fx}$

  Since it holds that: $c_e(z_e) = \frac{q_p(z_e)}{q_b(z_e)}$

  $$q_p(z_e) = (1 = 7 \cdot I_v(z)) \cdot 0.5 \cdot \rho \cdot {v_m}^2(z)$$
  $$q_b(z_e) = 0.5 \cdot \rho \cdot {v_b}^2$$
  $$v_m = c_r(z) \cdot c_0(z) \cdot v_b$$

  It follows that:

  $$F_{wxk} = q_b(z_e) \cdot c_e(z_e) \cdot c_{fx} \cdot A_{ref;x} = q_p(z_e) \cdot c_{fx} \cdot A_{ref;x}$$

  This corresponds to F_{wi} for buildings, provided that $c_s c_d = 1.0$.

  As $B/d_{tot} \geq 5$: $c_{fx} = c_{fx0} = 1.3$ in construction
  $= 1.0$ in use

  The reference area $A_{ref;x}$ is taken as the sum of:
  - The projected area towards the wind of the first girder;
  - The projected area towards the wind of protruding following girders;
  - The projected area towards the wind of protruding structural elements on top;
  - The projected area towards the wind of protruding obstacles or 0.3 m for open railings.

- y-direction:

  For girder bridges, it is given that:

  $$F_{wyk} = 0.25 \cdot F_{wxk}$$

- z-direction:

With the same analogy as was performed in x-direction, it holds that:

$$F_{wzk} = q_p(z_e) \cdot c_{fz} \cdot A_{ref;z}$$

with: $c_{fz} = \pm 0.9$ for horizontal bridges

$A_{ref;z} = B \cdot L$

The extreme wind pressure $q_p(z_e)$ depends on the wind area, the building density and the reference height z_e, which can be taken from Figures A.17 and A.18.

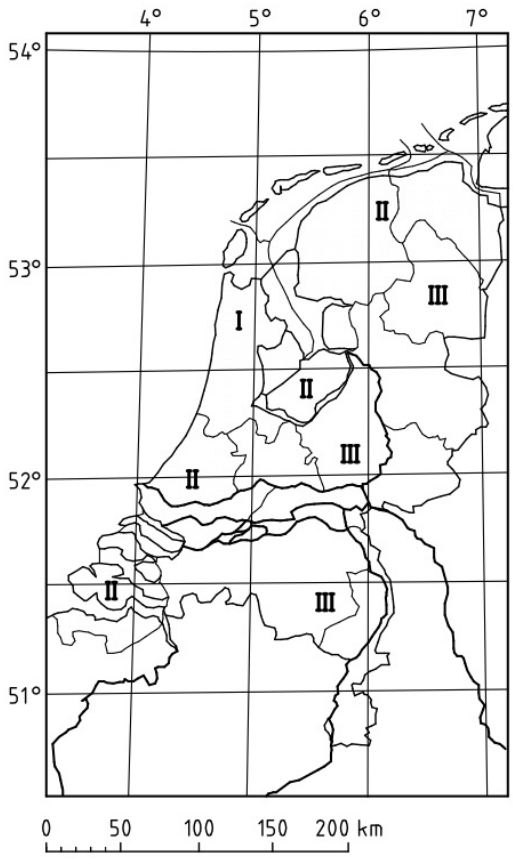

Windgebied	I	II	III
$v_{b,0}$ [m/s]	29,5	27,0	24,5

FIGURE A.17: Classification of wind areas in the Netherlands *[NEN-EN 1991-1-4-NB, 2005]*

Hoogte	Gebied I			Gebied II			Gebied III	
m	kust	onbebouwd	bebouwd	kust	onbebouwd	bebouwd	onbebouwd	bebouwd
1	0,93	0,71	0,69	0,78	0,60	0,58	0,49	0,48
2	1,11	0,71	0,69	0,93	0,60	0,58	0,49	0,48
3	1,22	0,71	0,69	1,02	0,60	0,58	0,49	0,48
4	1,30	0,71	0,69	1,09	0,60	0,58	0,49	0,48
5	1,37	0,78	0,69	1,14	0,66	0,58	0,54	0,48
6	1,42	0,84	0,69	1,19	0,71	0,58	0,58	0,48
7	1,47	0,89	0,69	1,23	0,75	0,58	0,62	0,48
8	1,51	0,94	0,73	1,26	0,79	0,62	0,65	0,51
9	1,55	0,98	0,77	1,29	0,82	0,65	0,68	0,53
10	1,58	1,02	0,81	1,32	0,85	0,68	0,70	0,56
15	1,71	1,16	0,96	1,43	0,98	0,80	0,80	0,66
20	1,80	1,27	1,07	1,51	1,07	0,90	0,88	0,74
25	1,88	1,36	1,16	1,57	1,14	0,97	0,94	0,80
30	1,94	1,43	1,23	1,63	1,20	1,03	0,99	0,85
35	2,00	1,50	1,30	1,67	1,25	1,09	1,03	0,89
40	2,04	1,55	1,35	1,71	1,30	1,13	1,07	0,93
45	2,09	1,60	1,40	1,75	1,34	1,17	1,11	0,97
50	2,12	1,65	1,45	1,78	1,38	1,21	1,14	1,00
55	2,16	1,69	1,49	1,81	1,42	1,25	1,17	1,03
60	2,19	1,73	1,53	1,83	1,45	1,28	1,19	1,05
65	2,22	1,76	1,57	1,86	1,48	1,31	1,22	1,08
70	2,25	1,80	1,60	1,88	1,50	1,34	1,24	1,10
75	2,27	1,83	1,63	1,90	1,53	1,37	1,26	1,13
80	2,30	1,86	1,66	1,92	1,55	1,39	1,28	1,15
85	2,32	1,88	1,69	1,94	1,58	1,42	1,30	1,17
90	2,34	1,91	1,72	1,96	1,60	1,44	1,32	1,18
95	2,36	1,93	1,74	1,98	1,62	1,46	1,33	1,20
100	2,38	1,96	1,77	1,99	1,64	1,48	1,35	1,22
110	2,42	2,00	1,81	2,03	1,68	1,52	1,38	1,25
120	2,45	2,04	1,85	2,05	1,71	1,55	1,41	1,28
130	2,48	2,08	1,89	2,08	1,74	1,59	1,44	1,31
140	2,51	2,12	1,93	2,10	1,77	1,62	1,46	1,33
150	2,54	2,15	1,96	2,13	1,80	1,65	1,48	1,35
160	2,56	2,18	2,00	2,15	1,83	1,67	1,50	1,38
170	2,59	2,21	2,03	2,17	1,85	1,70	1,52	1,40
180	2,61	2,24	2,06	2,19	1,88	1,72	1,54	1,42
190	2,63	2,27	2,08	2,20	1,90	1,75	1,56	1,44
200	2,65	2,29	2,11	2,22	1,92	1,77	1,58	1,46

FIGURE A.18: Extreme wind pressure for a certain wind area and a reference height z_e *[NEN-EN 1991-1-4-NB, 2005]*

In case the wind load and traffic load are combined, the highest value of $\psi_0 \cdot F_{wk}$ or F'_{wk} must be taken, where F'_{wk} is based on $v'_{b0} = 23$ m/s. In formula:

$$F'_{wk} = F_{wk} \cdot \frac{{v'_{b0}}^2}{{v_{b0}}^2}$$

A.1.7. Snow load

For the application of snow loads on bridge decks, it is assumed that it can be takes as equal to the snow load on roof tops. It then holds *[NEN-EN 1991-1-3, 2003]*:

$$Q_{sk} = \mu_i \cdot C_e \cdot C_t \cdot s_k$$

where: C_e depends on the topography: Windswept: $C_e = 0.8$

Normal: $C_e = 1.0$

Sheltered: $C_e = 1.2$

C_t depends on the thermal transmittance

μ_i depends on the angle of the roof (α)
In Holland, it holds for all cases: $C_e = 1.0$ [-]
$C_t = 1.0$ [-]
$s_k = 0.7$ [kN/m^2]
$\mu_1 = 0.8$ [-] (for all bridges, since $\alpha < 30°$)
$\mu_2 = 0$ [-]

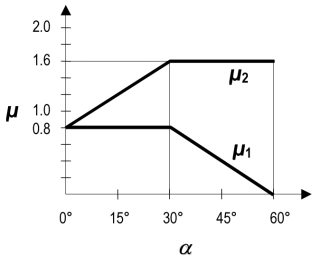

FIGURE A.19: Relation between the roof angle α and coefficients μ_1 and μ_2 *[NEN-EN 1991-1-3, 2003]*

Angle of pitch of roof α	$0° \leq \alpha \leq 30°$	$30° < \alpha < 60°$	$\alpha \geq 60°$
μ_1	0,8	0,8(60 - α)/30	0,0
μ_2	0,8 + 0,8 α/30	1,6	--

TABLE A.8: Relation between the roof angle α and coefficients μ_1 and μ_2 *[NEN-EN 1991-1-3, 2003]*

Thus the snow load is given by:

$$Q_{sk} = 0.8 \cdot 1.0 \cdot 1.0 \cdot 0.7 = 0.56 \text{ kN/m}^2$$

A.1.8. Imposed deformations

Indirect load actions can occur on the structural elements as imposed deformations *[van Breugel et al., 2013]*, such as:

- Thermal loading;
  A variation in temperature over time or over space, will give rise to thermal expansion of a structural element. The value of the loads that have to be taken into account depends on the temperature distribution, the coefficient of thermal expansion and the degree of restraint.
- Excessive settlements;
  When excessive differential settlements occur, load actions within the structural element will be redistributed, leading to a change in stresses in the material.
- Shrinkage/hydration effects
  During the ageing process of concrete, ongoing hydration and various forms of shrinkage cause imposed deformations within the element. Depending on the degree of restraint, this will lead to internal forces that will have to be taken into account.

For ease of calculation, loads following from imposed deformations are not included in the scope of this thesis.

A.1.9. Fire load

Structures must be able to withstand fire loads, according to the choice of design fire scenario and the temperature development within the elements. This calculation takes both loads for a thermal and loads for a mechanical analysis into account *[NEN-EN 1991-1-2, 2011]*.

For ease of calculation, the fire load is not included in the scope of this thesis.

A.1.10. Execution loads

During construction, different load actions may occur for which the structure must be designed adequately *[NEN-EN 1991-1-6, 2005]*. This includes as a result of loads the following:

- Non-permanent storage of materials/equipment
- Movable heavy machinery/equipment
- Loads from structural elements in temporary state
- Accidental actions

For ease of calculation, it is assumed that loads during the construction phase will not exceed the loads taken into account for the usage phase. Therefore, execution loads are not included in the scope of this thesis.

A.1.11. Extraordinary loads

In Eurocode NEN-EN 1991-1-7: General actions – Accidental actions *[NEN-EN 1991-1-7, 2015]* the extraordinary loads following from collisions or explosions are considered. The collision loads from traffic are already considered in subsection A.1.3.
For loads following from an explosion, it holds that the structure must be designed in such a way that progressive collapse is prevented. For ease of calculation, designing for explosions is not included in the scope of this thesis.

A.1.12. Seismic loads

Eurocode NEN-EN 1998-1-1 *[NEN-EN 1998-1-1, 2005]* states that structures that are located in seismic regions must be designed and constructed to prevent collapse or excessive damage as a result of seismic actions.
For ease of calculation, it is assumed that all considered projects do not lie within a seismic region and thus the seismic action is not included in the scope of this thesis.

A.2. LOAD COMBINATIONS

NEN-EN 1990-1 states that for every governing load situation, the design value of the load effects must be determined by combining the loads that are expected to occur simultaneously. For both the Ultimate Limit State (ULS) and Serviceability Limit State (SLS), multiple load combinations can be distinguished.

Within the scope of this thesis, the following is considered *[NEN-EN 1990, 2011]*:

- With respect to the design situations, only the user phase is taken into account.
- The limit states under consideration are:
  - ULS: Strength – Bending and shear
  - SLS: Deformation
- The loads taken into account are discussed in section A.1;
- Thus the load combinations applied are:
  - ULS: 6.10a - Fundamental combination for permanent or variable loads

$$E_d = E\left\{\sum_{j\geq 1} \gamma_{G,j} \cdot G_{k,j} \text{ " + " } \gamma_P \cdot P \text{ " + " } \gamma_{Q,1} \cdot \psi_{0,1} \cdot Q_{k,1} \text{ " + " } \sum_{i>1} \gamma_{Q,i} \cdot \psi_{0,i} \cdot Q_{k,i}\right\}$$

6.10b - Fundamental combination for permanent or variable loads

$$E_d = E\left\{\sum_{j\geq 1} \xi_j \cdot \gamma_{G,j} \cdot G_{k,j} \text{ " + " } \gamma_P \cdot P \text{ " + " } \gamma_{Q,1} \cdot Q_{k,1} \text{ " + " } \sum_{i>1} \gamma_{Q,i} \cdot \psi_{0,i} \cdot Q_{k,i}\right\}$$

6.11a - Combination for accidental loads

$$E_d = E\left\{\sum_{j\geq 1} G_{k,j} \text{ " + " } P \text{ " + " } A_d \text{ " + " } (\psi_{1,1}; \psi_{2,1}) \cdot Q_{k,1} \text{ " + " } \sum_{i>1} \psi_{2,i} \cdot Q_{k,i}\right\}$$

SLS: 6.15a - Frequent combination for reversible loads

$$E_d = E\left\{\sum_{j\geq 1} G_{k,j} \text{ " + " } P \text{ " + " } \psi_{1,1} \cdot Q_{k,1} \text{ " + " } \sum_{i>1} \psi_{2,i} \cdot Q_{k,i}\right\}$$

The partial safety factors γ are given in Table E.3 and the transient load factors ψ in Table A.10, of which ψ_0 is the characteristic, ψ_1 is the frequent and ψ_2 is the quasi-permanent factor. For the non-dominant traffic loads, an additional group factor equal to $f = 0.8$ must be taken into account.

		Unfavourable				Favourable	
		6.10a	6.10b	6.11a	6.15a	6.10a	6.10b
G	Permanent load	1.40	1.25*	1.00	1.00	0.90	0.90
Q	Variable traffic load	1.50	1.50	1.00	1.00	0.00	0.00
	Variable load	1.65	1.65	1.00	1.00	0.00	0.00
P	Prestressing	1.00	1.00	1.00	1.00	1.20	1.20

* Includes the factor ξ

TABLE A.9: Safety factors γ to be taken into account in the different load combinations *[NEN-EN 1990-NB, 2011]*

	Ψ_0	Ψ_1	Ψ_2
gr1a	0.8	0.8	0.4
gr2	0.8	0.8	0.0
Wind	0.3*	0.6	0.0
Snow	0.0	0.0	0.0
Collision		0.0	

* Choose max[$\Psi_0 \cdot F_{wk}$;F^*_{wk}]

TABLE A.10: Transient load factors ψ to be taken into account in the different load combinations *[NEN-EN 1990-NB, 2011]*

Geotechnical analysis

B

RETAINED (PILE) FOUNDATIONS

In this appendix the application of the proposed pyramid approach for the reuse of existing pile foundations is demonstrated. A single specific case study is considered in order to give an indication of the potential profit in bearing capacity.
First, the case study will be briefly introduced in section B.1, after which the geotechnical analysis is performed in section B.2 for each level separately. The results for this case study are given in section B.3. Additional information is given in Appendices A, C and D.

It must be stated that the outcomes have no statistical value, since they are based on one case study only. Nevertheless, this appendix clearly shows the applicability and potential of this geotechnical analysis.

B.1. INTRODUCTION CASE STUDY A9

The A9 Gaasperdammerweg project is executed by IXAS, a collaboration of Heijmans, Ballast Nedam, Fluor and 3i *[Rijkswaterstaat, nda]*. The current A9 highway between junctions Holendrecht and Diemen divides the eastern part of Amsterdam, as can be seen in Figure B.2. To fulfil the increasing demand for mobility in the future, the A9 has to be widened from 2x3 to 2x5 driving lanes. A large part of the A9 Gaasperdammerweg will be transferred to a 3 km long tunnel, mainly to reduce traffic hindrance to the surrounding districts, but also to establish a green connection between those districts.

FIGURE B.1: Case Study location in the Netherlands

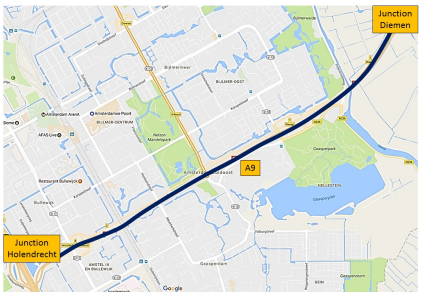

FIGURE B.2: Current location of highway A9 dividing East-Amsterdam

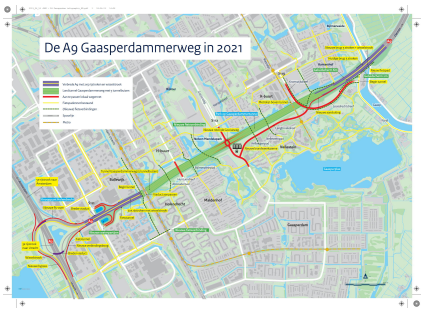

FIGURE B.3: New layout of highway A9 *[Rijkswaterstaat, nda]*

In the current situation, the A9 crosses the Huntumdreef, a local N-road (Figure B.4). This viaduct, also known as KW150, was built in 1980 and will be removed completely, since in the new situation the Huntumdreef will cross the A9 on top of the tunnel. However, during the construction stage of this project, the A9 will have to be shifted to the south and therefore temporary structures are needed to cross the Huntumdreef (Figure B.5). For that reason, additional CPTs have been performed around the existing Huntumdreef viaduct, in order to determine the soil conditions and foundation bearing capacity.
Together with the old CPTs, performed around 1970 for the design of the current viaduct, the new CPTs create a dataset that can be used to demonstrate the application of the strategy as proposed in Chapter 3. This strategy for the reuse of existing piled foundations (Figure B.6) consists of six levels, each with increasing depth

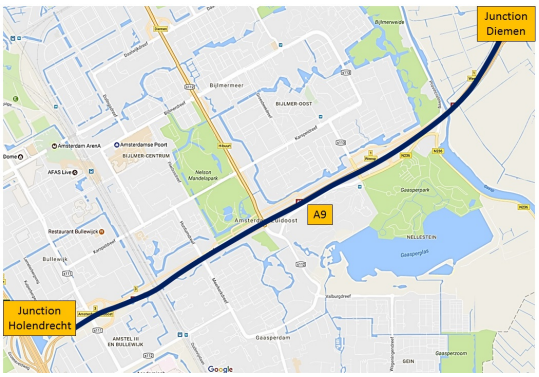

FIGURE B.4: Location of KW150 within highway A9

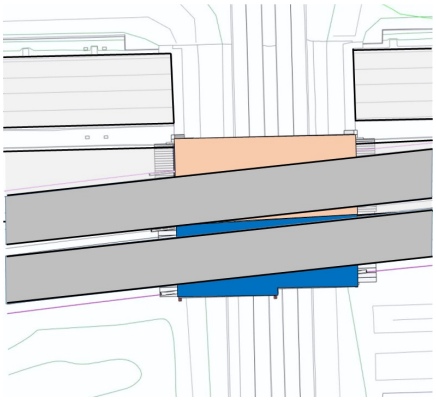

FIGURE B.5: Temporary structure to ensure crossing of the A9 and the Huntumdreef during construction *[IXAS, 2015]*

of calculation and therefore increasing design costs. The application of this strategy will be demonstrated in subsections B.2.1 to B.2.6, for every level.

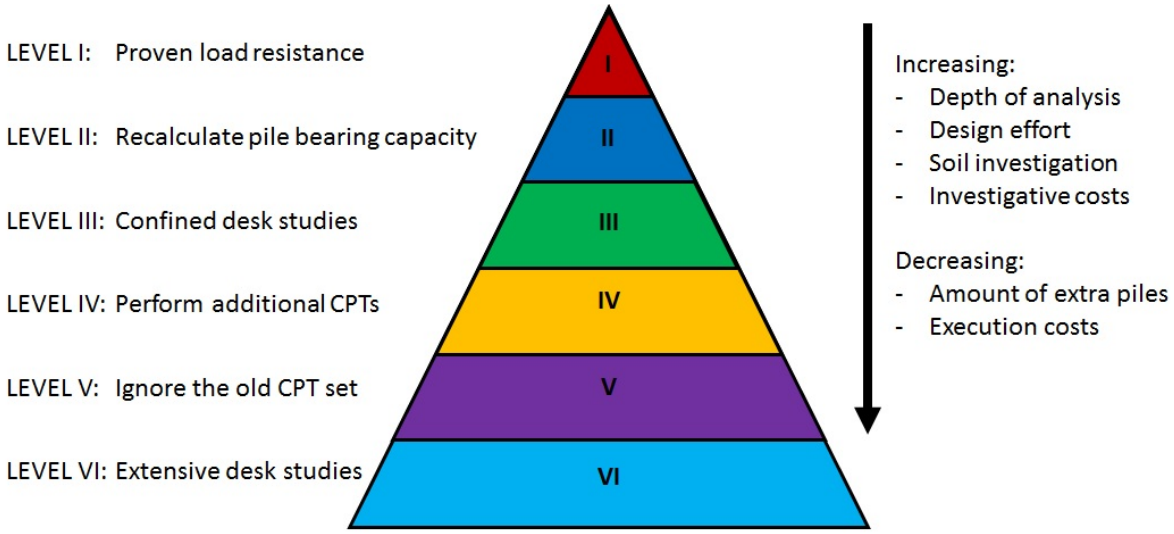

FIGURE B.6: Schematical representation og the geotechnical analysis for the reuse of (piled) foundations

Fictitious superstructure

The planned temporary viaduct is however not suitable for a full analysis of the proposed strategy. Not only is it a temporary structure, with a decreased safety level compared to a permanent viaduct, it is also not located at the same position as the current viaducts and it is supported by sheet piling, not piles.
Therefore, a fictitious superstructure is proposed that will be located at the current viaduct position. This fictitious superstructure will have the same dimensions and the same traffic profile as the existing structure. It is however designed according to the current codes and regulations and will therefore experience higher loads, mainly due to the increased traffic load models.

The fictitious superstructure will be analysed in a SCIA Engineer model, which is a Finite Element Program that can give an adequate indication of the working loads and design loads acting on the foundation. More information on this fictitious superstructure and the SCIA model is given in Appendix C.

Existing superstructure

The existing viaduct KW150 consists of two separate 2-span decks for each traffic direction, both with a width of 18 m. The total length is 36.8 m, with an intermediate support located at 19.9 m from the west abutment.

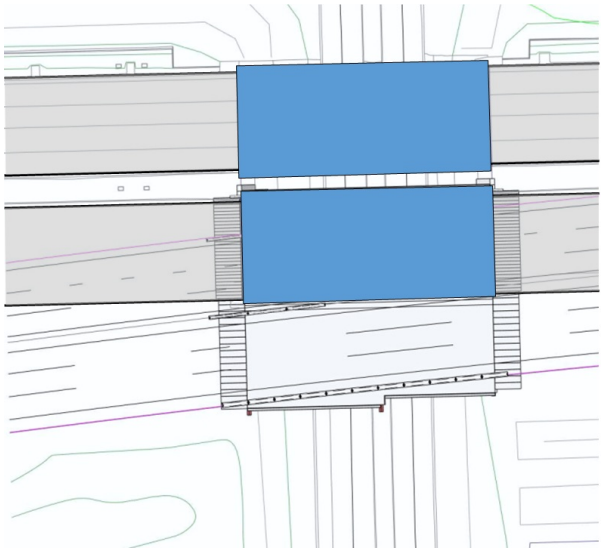

FIGURE B.7: Location of the fictitious superstructure for this geotechnical analysis *[IXAS, 2015]*

The deck is an in-situ concrete plate girder with post-tensioning steel and a height of 650 mm. The asphalt layer on top has a height of 70 mm, bringing the total superstructure height to 720 mm.
Both abutments are highly supported on piles, with their bottom situated at + 1.75 m NAP. The mid support is 4 m high and is founded on a low abutment with the top situated at – 1.0 m NAP, which is also supported by piles.
A top view and cross-section of the existing superstructure are given in Figures B.8 and B.9.

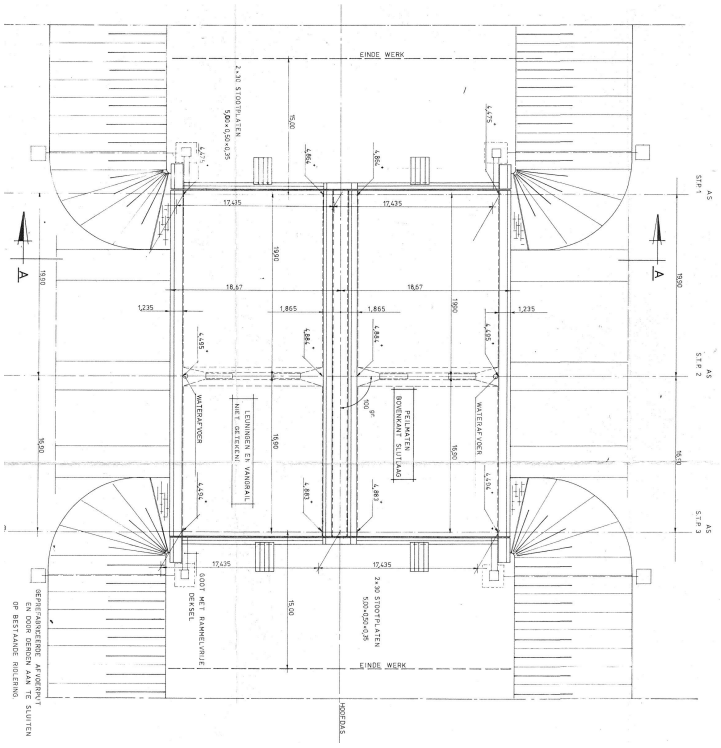

FIGURE B.8: Top view of the existing viaduct KW150 *[Rijkswaterstaat, 1975]*

Existing pile plan
The existing pile plan is presented in Figure B.10. It consists of three axes: axis 1 is the abutment on the west

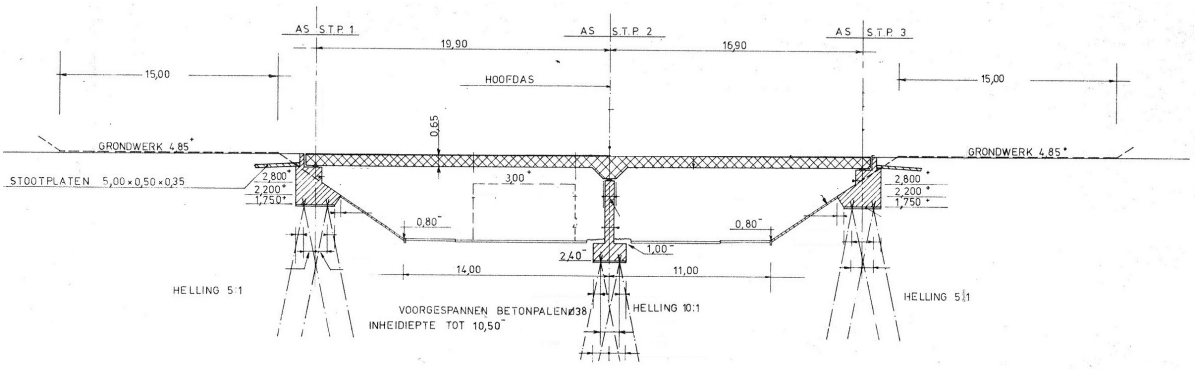

FIGURE B.9: Side view of the existing viaduct KW150 *[Rijkswaterstaat, 1975]*

side, axis 2 is the abutment underneath the mid support and axis 3 is the abutment on the east side. All piles are prestressed concrete piles of 380x380 mm, with a total of 120 piles. The different foundation properties per axis are given below:

	Axis 1	**Axis 2**	**Axis 3**
Abutment level:	+ 1.75 m NAP	- 2.4 m NAP	+ 1.75 m NAP
Pile tip level:	- 10.65 m NAP	- 10.50 m NAP	-10.65 m NAP
Pile length:	13.15 m	8.65 m	13.15 m
Inclination:	1:5	1:10	1:5
Heart-to-heart distance:	1.9 m	1.3 m	2.13 m
Amount of piles:	38	44	34

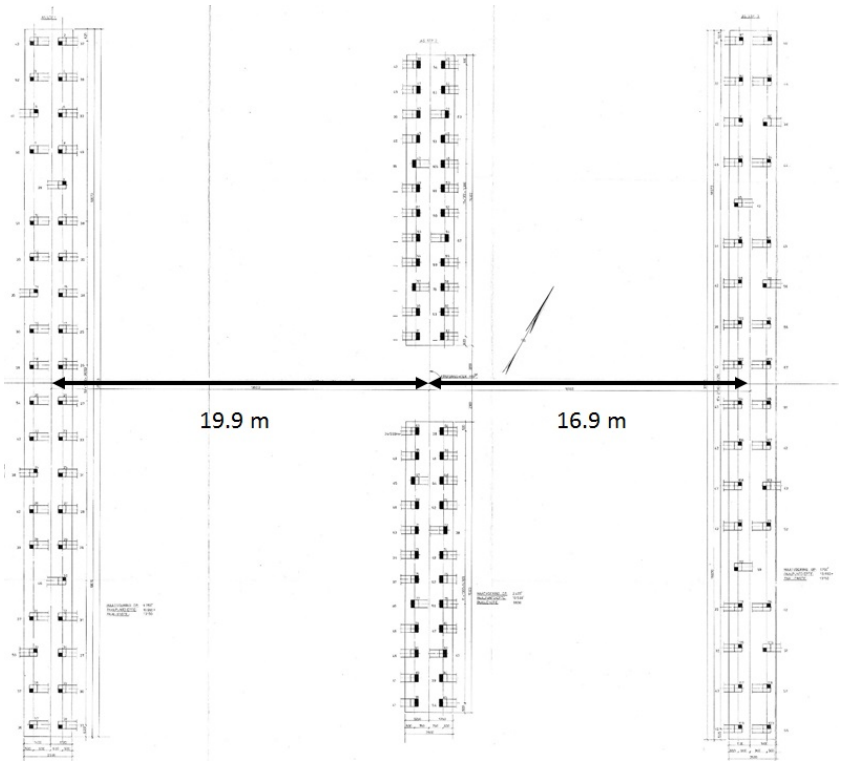

FIGURE B.10: Top view of the existing pile plan of viaduct KW150 *[Rijkswaterstaat, 1977b]*

In 1974, the soil investigation for the original viaduct was carried out, leading to 9 different CPT results. These CPTs are given in Appendix D and their position compared to the original pile plan is presented in Figure B.11.

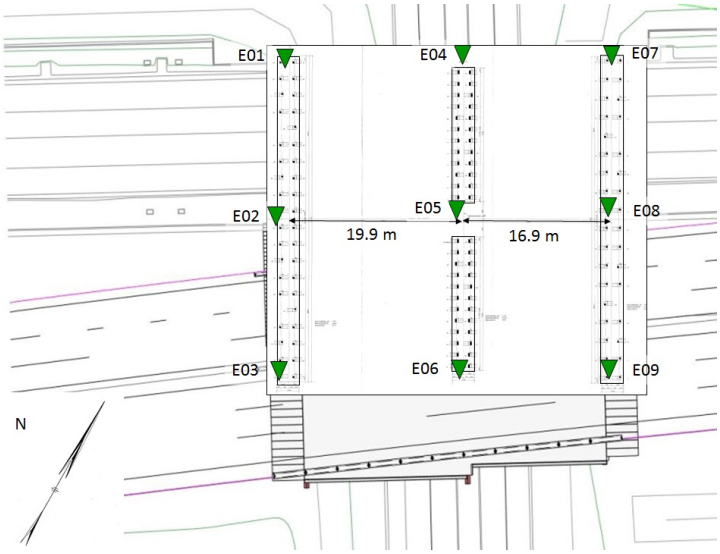

FIGURE B.11: Top view of the existing pile plan of viaduct KW150 and the locations of the old CPT set [bron]

B.2. ANALYSIS ACCORDING TO THE PYRAMID APPROACH

The geotechnical analysis that is used to determine the extent to which the piled foundation can be reused, consists of a pyramid approach with six levels. The pyramid is presented in Figure B.6 and with every level an increase in design effort, soil investigation and design costs can be seen. This is compensated by the fact that each level results in an increased bearing capacity and thus a decrease of additional piles needed and construction costs. Before starting a new level, the expected effort and potential profit must be considered for each case specific, in order to make an economic decision.

In the following subsections, the geotechnical analysis of every level is performed for the case study A9 Gaasperdammerweg.

B.2.1. LEVEL I: Proven load resistance (Current practice)

In current practice, when an old structure supported by foundation piles is replaced, it is common to leave the existing piles in place, since it is a time-consuming and costly activity to remove them. They are, however, hardly taken into account when calculating the bearing capacity required for the new structure. Instead, it is common to assume their bearing capacity to be equal to the already proven load resistance.
In other words: the existing pile foundation has proven its ability to resist the loads from the old superstructure for over the previous lifetime. After this period, the piles will have settled into their final position and the soil around and underneath the piles will be in equilibrium. It can therefore be assumed that it will be able to resist these same loads for the lifetime of the new structure without any additional settlements. Any increase of load compared to the old situation, will have to be resisted by extra piles in the new situation.
Therefore, the Level I calculation consists of comparing the old and new load situations with each other, in order to determine the number of extra piles are needed.

Although the original geotechnical calculation is unknown, some information can be obtained from the geotechnical report *[Laboratorium voor grondmechanica, 1975]*. This document states that the loads given by the structural engineer for each axis are as follows:

Axis 1	Maximum:	35 - 40 tf per meter abutment
	Minimum:	24 tf/m
Axis 2	Maximum:	67 tf/m
	Minimum:	49 tf/m
Axis 3	Maximum:	35 - 40 tf/m
	Minimum:	24 tf/m

In which tf stands for ton force, an old unit that can be converted into kN: 1 tf = 9.81 kN.

As was common in early regulations, it is assumed that the loads given by the structural engineer are working loads, not design loads.

With a heart-to-heart distance of 1.9 m, 1.3 m and 2.13 m for axes 1, 2 and 3, respectively, the force per pile in the old situation amounts:

Axis 1:	40 tf/m = 392.4 kN/m Pile distance: 1.9 m Max. load per pile: 392.4 · 0.5 · 1.9 = 372.78 kN
Axis 2:	67 tf/m = 657.27 kN/m Pile distance: 1.3 m Max. load per pile: 657.27 · 0.5 · 1.3 = 427.23 kN
Axis 3:	40 tf/m = 392.4 kN/m Pile distance: 2.13 m Max. load per pile: 392.4 · 0.5 · 2.13 = 417.91 kN

It is assumed that this maximum force per pile can occur on every pile, thus all piles in the existing pile plan will be designed adequately and are thus able to resist this force.

To determine the maximum pile loads that are governed by the new load situation, the fictitious superstructure and existing pile foundation are modelled in SCIA Engineer, a finite element program (Figure B.12). The model input and applied considerations and assumptions for this case study are given in Appendix C. The maximum working loads per pile following from this model are given in Table B.1.

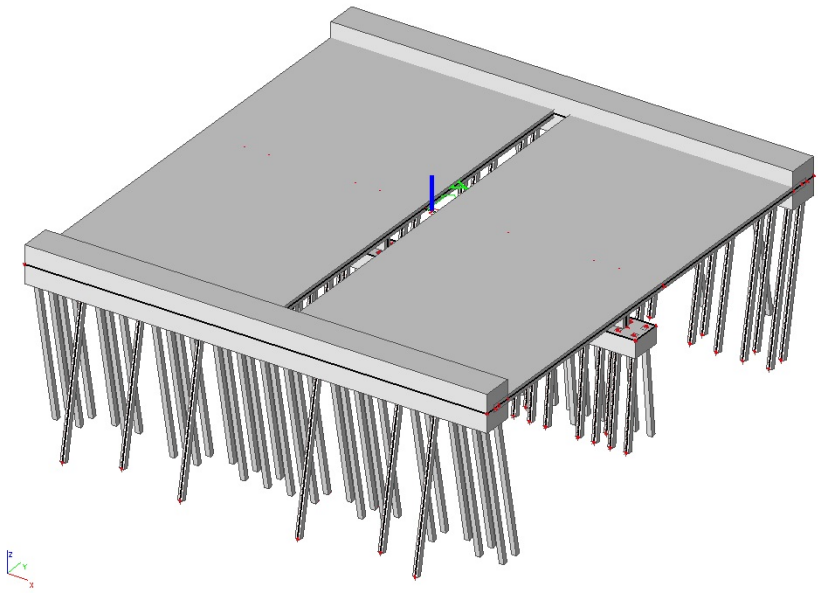

FIGURE B.12: Overview of the fictitious superstructure as a model in SCIA

It can be seen that for almost every pile, the new load situation governs a higher working load than the load that is currently working on the pile. This means that extra piles are needed in addition to the existing pile plan.

The bearing capacity of these extra piles are calculated according to the Eurocode, by using D-Foundations. The model input and applied considerations and assumptions for this case study are given in Appendix D. It is assumed that the new piles will be installed at the same PTL as the existing pile foundation. Then, for the old CPTs, the results as presented in Figures B.13 and B.14 are generated.
In practice, the most governing CPT will be used for the calculation of the characteristic bearing capacity, which in this case is CPT E07, $R_{C;k}$ = 810 kN for piles on axis 1 and 3, and CPT E06, with $R_{C;k}$ = 808 kN for piles on axis 2.

Axis 1			
Pile number		Load action [kN]	
In SCIA	In pile plan	SLS	ULS
Sn1	1	479,89	693,74
Sn2	2	738,88	1078,90
Sn3	3	460,27	663,37
Sn4	4	718,82	1047,88
Sn5	5	512,97	727,51
Sn6	6	698,69	1016,70
Sn8	7	420,54	602,01
Sn7	8	677,47	983,88
Sn10	9	727,04	1043,08
Sn11	10	382,24	544,72
Sn12	11	637,87	922,60
Sn13	12	365,69	520,00
Sn14	13	620,51	895,81
Sn15	14	424,03	590,66
Sn16	15	606,80	874,64
Sn17	16	343,11	486,28
Sn18	17	596,93	859,41
Sn19	18	338,27	479,09
Sn20	19	592,29	852,28
Sn104	20	338,22	479,08
Sn105	21	592,87	853,34
Sn102	22	342,92	486,19
Sn103	23	597,55	860,69
Sn100	24	423,57	589,70
Sn101	25	606,76	875,06
Sn98	26	365,24	519,80
Sn99	27	620,08	895,81
Sn96	28	381,68	544,54
Sn97	29	636,80	921,83
Sn95	30	727,49	1043,29
Sn93	31	419,83	601,98
Sn94	32	676,10	983,04
Sn91	33	511,90	725,39
Sn92	34	696,79	1015,31
Sn89	35	459,47	663,73
Sn90	36	717,29	1047,32
Sn87	37	479,08	694,35
Sn88	38	737,55	1078,97

Axis 2			
Pile number		Load action [kN]	
In SCIA	In pile plan	SLS	ULS
Sn63	39	731,92	1065,70
Sn64	40	758,35	1125,02
Sn65	41	719,75	1046,43
Sn66	42	745,29	1104,48
Sn67	43	698,47	1013,69
Sn68	44	703,53	1038,59
Sn69	45	665,51	963,62
Sn70	46	690,44	1020,63
Sn71	47	638,54	924,97
Sn72	48	646,74	954,20
Sn73	49	580,25	833,88
Sn74	50	604,89	890,12
Sn75	51	551,17	788,45
Sn76	52	575,33	843,94
Sn77	53	535,11	762,11
Sn78	54	544,56	793,11
Sn79	55	524,20	743,65
Sn80	56	548,12	798,90
Sn81	57	519,29	737,46
Sn82	58	531,34	772,46
Sn83	59	483,99	681,33
Sn84	60	508,59	735,96
Sn85	61	456,02	639,13
Sn86	62	482,08	693,34
Sn128	63	477,07	662,62
Sn129	64	497,37	715,77
Sn126	65	503,20	703,95
Sn127	66	524,48	757,57
Sn124	67	534,16	755,59
Sn125	68	546,37	791,96
Sn122	69	538,94	763,29
Sn123	70	560,96	815,78
Sn120	71	547,33	779,26
Sn121	72	556,83	809,96
Sn118	73	560,86	802,67
Sn119	74	583,52	855,54
Sn116	75	587,64	845,36
Sn117	76	610,99	899,28
Sn114	77	642,63	932,34
Sn115	78	650,92	961,29
Sn112	79	668,71	970,96
Sn113	80	692,80	1026,25
Sn110	81	699,58	1019,69
Sn111	82	704,73	1044,27
Sn108	83	718,86	1051,38
Sn109	84	743,90	1108,18
Sn106	85	729,33	1069,96
Sn107	86	755,46	1128,30

Axis 3			
Pile number		Load action [kN]	
In SCIA	In pile plan	SLS	ULS
Sn45	87	685,89	993,81
Sn46	88	527,58	762,98
Sn47	89	701,54	1018,04
Sn49	90	511,13	737,08
Sn48	91	693,76	1006,36
Sn50	92	550,34	807,70
Sn51	93	653,82	944,06
Sn53	94	478,73	686,27
Sn52	95	661,70	966,33
Sn55	96	577,88	827,67
Sn57	97	448,06	639,19
Sn56	98	552,65	790,14
Sn58	99	490,18	713,54
Sn59	100	550,50	785,95
Sn61	101	425,97	606,29
Sn60	102	565,81	807,27
Sn62	103	420,99	599,00
Sn145	104	572,33	817,17
Sn146	105	421,30	599,65
Sn143	106	577,47	825,35
Sn144	107	426,84	608,13
Sn141	108	587,29	840,83
Sn142	109	491,46	716,27
Sn140	110	601,12	862,56
Sn139	111	451,14	644,99
Sn138	112	672,01	981,30
Sn136	113	635,75	917,13
Sn137	114	485,43	698,27
Sn135	115	654,01	946,07
Sn134	116	557,81	819,19
Sn132	117	671,76	974,31
Sn133	118	520,41	753,70
Sn130	119	688,83	1011,55
Sn131	120	537,09	780,30

TABLE B.1: Pile loads following from the governing load situations on the fictitious superstructure, in both SLS and ULS

Results of the option Preliminary Design, Bearing capacity at fixed pile tip levels

Results for pile type :
Rect 380x380

CPT name	Level [m R.L.]	Groundlevel [m R.L.]	Rb;cal;max [kN]	Rs;cal;max [kN]	Rc;cal;max [kN]	Rc;d [kN]	F;nst;rep [kN]	Fnst;d [kN]
E01	-10.65	4,70	840	239	1080	714	513	718
E02	-10.65	4,84	676	299	975	645	483	676
E03	-10.65	4,69	531	296	827	547	463	649
E04	-10.65	-1,13	1035	294	1329	879	121	169
E05	-10.65	-1,11	681	278	959	634	128	179
E06	-10.65	-1,07	572	265	837	554	118	166
E07	-10.65	4,79	628	192	819	542	500	700
E08	-10.65	5,03	1178	337	1515	1002	480	672
E09	-10.65	5,00	1233	443	1676	1108	448	627

FIGURE B.13: Results for the bearing capacities of piles with a PTL at -10.65 m NAP in D-Foundations

Results of the option Preliminary Design, Bearing capacity at fixed pile tip levels

Results for pile type :
Rect 380x380

CPT name	Level [m R.L.]	Groundlevel [m R.L.]	Rb;cal;max [kN]	Rs;cal;max [kN]	Rc;cal;max [kN]	Rc;d [kN]	F;nst;rep [kN]	Fnst;d [kN]
E01	-10.50	4,70	887	205	1092	722	513	718
E02	-10.50	4,84	670	271	941	623	483	676
E03	-10.50	4,69	645	270	915	605	463	649
E04	-10.50	-1,13	1003	241	1244	823	121	169
E05	-10.50	-1,11	673	250	924	611	128	179
E06	-10.50	-1,07	577	231	808	534	118	166
E07	-10.50	4,79	663	164	827	547	500	700
E08	-10.50	5,03	1135	303	1438	951	480	672
E09	-10.50	5,00	1208	409	1617	1069	448	627

FIGURE B.14: Results for the bearing capacities of piles with a PTL at -10.65 m NAP in D-Foundations

It must be stated that the reaction forces taken from the SCIA model are the vertical forces, whilst the piles are actually inclined. In this respect, there is a discrepancy between the SCIA model for reactions loads and the D-foundations model for the bearing capacities, since D-Foundations only considers vertical piles. The question therefore is whether the numbers following from both models are comparable or not. Within the scope of this geotechnical analysis, this discrepancy is ignored for the following reasons:

- The difference between vertical reaction force and absolute reaction force (parallel to the pile) is quite small (0.5% for axes 1 and 3 and 2.0% for axis 2);
- The bearing capacity for inclined piles will most likely decrease slightly:
  - The pile tip capacity remains equal, since the pile tip level is equal;
  - The longer pile length gives an increase in positive skin friction but a decrease in negative skin friction; the exact influence depends on the ratio between both friction components;
  - The inclined pile will probably experience a higher shaft friction at the top side but a lower shaft friction at the bottom side of the pile, compared to a vertical pile. On the other hand, the bottom side might experience more vertical bearing capacity than the top side. The actual difference is unknown and will largely depend on the pile inclination and the relative settlement of the soil layers compared to the pile itself.

Since it is unknown to what extend the pile bearing capacity for inclined piles decreases, it is not taken into account. Furthermore, the exact number of piles needed is less relevant for the purpose of this geotechnical analysis, compared to showing the possibilities of the overall approach. Therefore, it is assumed that neglecting this discrepancy is acceptable.

In order to determine the amount of piles needed, the difference in working loads must be resisted by the bearing capacity of the new piles, calculated according to the Eurocode. In formula:

Working load difference: $\Delta F_{S;ki} = F_{S;k;2i} - F_{S;k;1i}$

Unity Check: $\Delta F_{S;ki} \cdot \gamma_{Fi} \leq n_i \cdot \frac{R_{C;k}}{\gamma_R}$

Safety factors: $\gamma_{Fi} = \frac{F_{S;d;2i}}{F_{S;k;2i}}$

$\gamma_R = \frac{R_{C;d}}{R_{C;k}}$

Amount of piles: $n_{min;i} = \gamma_{Fi} \cdot \gamma_R \cdot \frac{\Delta F_{S;ki}}{R_{C;k}}$

It follows that the amount of extra piles needed to resist the increase of loads on the existing pile foundation is:

$n_1 =$ **54 piles**

These formulas state the same as Figure 1.4 in Chapter 3: namely that in order to optimize a design, in this case to minimise the amount of piles needed, one can either increase the bearing capacity ($R_{C;d}$) or decrease the loads acting on the foundation ($F_{S;d2}$). The latter can be achieved by both a reduction of governing loads on the superstructure and improvement of the soil structure interaction. In this geotechnical analysis, however, emphasis is laid on increasing the bearing capacity of the foundation. Reduction of governing loads or improvement of the interaction with the superstructure will be dealt with in 4 and 5 respectively.

PTL new piles

As stated before, the PTLs of the new piles are taken equal to that of the existing piles, at -10.65 m NAP for axes 1 and 3 and at – 10.50 m NAP for axis 2. However, these new piles can be driven deeper into the sand layer, which would result in a higher pile bearing capacity. To illustrate this influence, a calculation has been performed for pile tip levels at an arbitrary -15.00 m NAP. The increased bearing capacities that follow from D-foundations are given in Figure B.15.

CPT name	Level [m R.L.]	Groundlevel [m R.L.]	Rb;cal;max [kN]	Rs;cal;max [kN]	Rc;cal;max [kN]	Rc;d [kN]	F;nst;rep [kN]	Fnst;d [kN]
E01(1)	-15.00	4,70	523	951	1474	975	439	615
E02(1)	-15.00	4,84	1226	1046	2272	1503	412	577
E03(1)	-15.00	4,69	1113	928	2040	1350	402	563
E04(1)	-15.00	-1,13	1164	1277	2441	1614	86	121
E05(1)	-15.00	-1,11	1619	1059	2678	1771	92	129
E06(1)	-15.00	-1,07	1559	1088	2647	1751	83	116
E07(1)	-15.00	4,79	1091	875	1966	1300	429	601
E08(1)	-15.00	5,03	2143	1316	3459	2288	418	585
E09(1)	-15.00	5,00	1062	1413	2475	1637	378	529

FIGURE B.15: Results for the bearing capacities of piles with a PTL at -15.00 m NAP in D-Foundations

When using the governing value $R_{C;k}$ = 1474 kN (CPT E01), it follows that the amount of piles needed drastically decreases:

n_1 = **24 piles**

In practice, this means that the PTL must be chosen at such a depth that the benefits of increased pile bearing capacity and the drawbacks of installation at a larger depth are most optimal.

B.2.2. LEVEL II: Recalculate bearing capacity

The next step is to recalculate the bearing capacity of the existing pile foundation according to the current design codes and to compare this to the required bearing capacity of the new superstructure. Since the α_p factor is reduced by 30% and the safety level is more or less equal to the old regulations, it is expected that this step will not show any profit in the amount of piles needed but will in fact result in an overall loss of bearing capacity.

The recalculation of bearing capacity has already been executed in Level I, since it is assumed that the existing and new piles have the same properties and PTLs.

The required bearing capacity is given by the design load of the new superstructure. The difference between the required design bearing capacity and the design bearing capacity given by the existing foundations, must be taken up by new piles. In formula:

Unity Check:	$R_{C;d;2i} \geq F_{S;d;2i}$
Design capacity difference:	$\Delta R_{C;di} = R_{C;d;2i} - R_{C;d1}$
Unity Check:	$n_i \cdot R_{C;d1} \geq \Delta R_{C;di}$
Amount of piles:	$n_{min;i} = \frac{\Delta R_{C;di}}{R_{C;d2}} = \frac{(F_{S;d;2i} - R_{C;d1})}{R_{C;d2}}$

In which $R_{C;d1}$ is the bearing capacity of the old piles and $R_{C;d2}$ the bearing capacity of the new piles.

Again, the governing CPT is taken to determine the bearing capacity, resulting in a design bearing capacity per pile of $R_{C;d1} = R_{C;d2}$ = 542 kN for axes 1 and 3 (Figure B.13, CPT E07) and $R_{C;d1} = R_{C;d2}$ = 534 kN for axis 2 (Figure B.14, CPT E06).

It follows that the amount of extra piles needed to resist the increase of loads on the existing pile foundation is:

n_2 = **65 piles**

As expected, this amount is higher than that obtained in the Level I calculation, mainly because the α_p factor has decreased. The fact that the total loss between n_2 and n_1 is less than 30%, can partly be explained by the different safety levels applied in 1980 and in current practice and partly by the inclusion of positive and negative shaft friction in the current codes.

From these formulas it can be seen that the increase of bearing capacity, as discussed at the end of subsection B.2.1, can be obtained in both the old piles ($R_{C;d1}$) and the new piles ($R_{C;d2}$). All following levels of this pyramid approach are aimed at increasing these design resistances, both simultaneously and separately.

B.2.3. LEVEL III: Confined research

This level consists of a desk study on the influence of different parameters that may increase the bearing capacity of both old and new piles, if approved by Rijkswaterstaat. It is expected that the necessary research and documentation for approval can be obtained within the coming years, through relatively simple research. Once approved, these adapted parameters can be applied for every case study using the right type of piles and displaying more or less the same spatial soil variation as the test locations.

The α_p-factor reduction

The reduction of the α_p-factor since January 2017 has caused an extensive discussion within the geotechnical market. This reduction is based on proof loading tests performed on prefabricated concrete piles and the

results were extended to other pile types, since their original α-factors were mostly based on those of the prefabricated concrete pile. The regulations state that, if it can be proven for a certain pile type that the α_p-factor does not have to be reduced, or at least not with 30%, this may be used in calculations.
The responsibility for determining the exact values of α_p for the different pile types was placed within the market, since every manufacturer uses its own specific pile characteristics and thus a very extensive research would be necessary if all pile types are to be covered. The problem is, however, that no manufacturer is willing to invest in these proof loading tests, as competitors could also benefit from their results without contributing to the research themselves. Therefore no additional proof loading tests have been carried out up to date and thus the conservative α_p factor, reduced by 30%, has to be taken into account for design. However, voices have been going up to establish a national test ground, in which the investment is equally spread between contractors. It is thus likely that an adaptation of regulations is on its way.

This elaboration is mainly of interest for all other pile types than the prefabricated concrete piles, as the reduction of α_p was based on proof loading tests performed on the latter. Therefore the α_p-factor for prefabricated concrete piles will probably not increase by a substantial amount. Nevertheless, the influence of a higher α_p-factor is evaluated for this case study, to show the impact of this factor on the total bearing capacity of the foundation.

Using D-foundations, α_p = 1.0 is evaluated, leading to the results as presented in Figures B.16 and B.17 It can indeed be seen in comparison to Figures B.13 and B.14 that the difference in pile tip resistance is 30%. Due to the fact that the α_p-factor only applies on the pile tip bearing capacity and the α_s-factor for shaft resistance remains unaltered, the increase in total bearing capacity will not be linear.

Results of the option Preliminary Design, Bearing capacity at fixed pile tip levels

Results for pile type :
Rect 380x380

CPT name	Level [m R.L.]	Groundlevel [m R.L.]	Rb;cal;max [kN]	Rs;cal;max [kN]	Rc;cal;max [kN]	Rc;d [kN]	F;nst;rep [kN]	Fnst;d [kN]
E01	-10.65	4,70	1200	239	1440	952	513	718
E02	-10.65	4,84	966	299	1265	837	483	676
E03	-10.65	4,69	759	296	1055	698	463	649
E04	-10.65	-1,13	1479	294	1773	1172	121	169
E05	-10.65	-1,11	973	278	1251	827	128	179
E06	-10.65	-1,07	818	265	1082	716	118	166
E07	-10.65	4,79	897	192	1088	720	500	700
E08	-10.65	5,03	1683	337	2020	1336	480	672
E09	-10.65	5,00	1761	443	2204	1458	448	627

FIGURE B.16: Results for the bearing capacities of piles (for $alpha_p$ = 1.0) with a PTL at -10.65 m NAP in D-Foundations

Results of the option Preliminary Design, Bearing capacity at fixed pile tip levels

Results for pile type :
Rect 380x380

CPT name	Level [m R.L.]	Groundlevel [m R.L.]	Rb;cal;max [kN]	Rs;cal;max [kN]	Rc;cal;max [kN]	Rc;d [kN]	F;nst;rep [kN]	Fnst;d [kN]
E01	-10.50	4,70	1267	205	1472	974	513	718
E02	-10.50	4,84	958	271	1229	813	483	676
E03	-10.50	4,69	921	270	1191	788	463	649
E04	-10.50	-1,13	1433	241	1674	1107	121	169
E05	-10.50	-1,11	962	250	1212	802	128	179
E06	-10.50	-1,07	825	231	1055	698	118	166
E07	-10.50	4,79	947	164	1111	735	500	700
E08	-10.50	5,03	1622	303	1925	1273	480	672
E09	-10.50	5,00	1726	409	2135	1412	448	627

FIGURE B.17: Results for the bearing capacities of piles (for $alpha_p$ = 1.0) with a PTL at -10.65 m NAP in D-Foundations

The increase of pile bearing capacity is valid for both old and new piles, thus both $R_{C;d1}$ and $R_{C;d2}$ from the Level II calculation are improved. This would lead to the following amount of piles:

$n_{3(\alpha_p)}$ = **20 piles**

The increased value for α_p, obtained after proof loading, will most likely not be equal to 1.0 for any pile type but will probably lie somewhere between 0.7 and 1.0. However, the linear relationship as shown in Figure B.18 of the pile tip resistance can be used together with the absolute value of the shaft resistance, to construct the new bearing capacity.

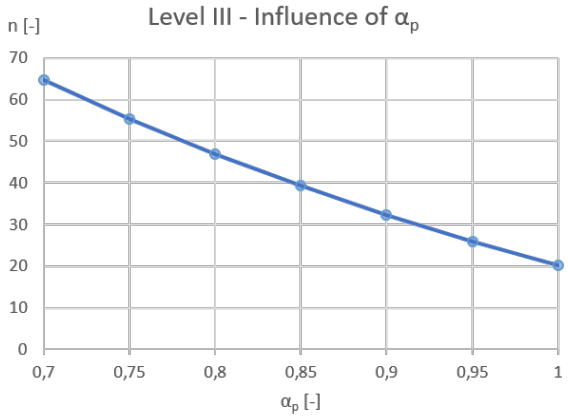

FIGURE B.18: Influence of α_p on the amount of additional piles needed

Densification factor f_1
Another influence that is interesting to investigate, is that of the densification factor f_1. As stated in Chapter 2, the CUR-committee that investigated the possible hidden safeties in the bearing capacity of piled foundations, recommends the factor f_1 to be taken directly from the regulations for tension piles. The formulas are:

$$f_1 = e^{2.93 \cdot \Delta R_e}$$

With:
$$\Delta R_e = \frac{\Sigma \Delta e}{(e_{max} - e_{min})}$$
$$\Sigma \Delta e = \frac{-(r-6)}{5.5} \cdot \frac{(1+e_0)}{50}$$
$$e_0 = -R_e \cdot (e_{max} - e_{min}) + e_{max}$$
$$R_e = 0.24 \cdot \ln\left(\frac{q_{c;z}}{61 \cdot {\sigma'_{v;z;0}}^{0.71}}\right)$$

ΔR_e the increase of relative density from pile installation
e the void ratio
Δe the decrease of void ratio as a result of a ground displacement pile within a distance of $6 \cdot D_{eq}$
e_{max} is the maximum void ratio of the soil. Since the influence is limited, a global estimation is sufficient. In the Netherlands it holds for most cases that $e_{max} = 0.80$
e_{min} is the minimum void ratio of the soil. Since the influence is limited, a global estimation is sufficient. In the Netherlands it holds for most cases that $e_{min} = 0.40$
n is the amount of piles within a distance of $6 \cdot D_{eq}$
r is the heart-to-heart distance expressed in D_{eq} between the two evaluated piles, with a maximum of $r = 6$
e_0 is the initial void ratio of the soil
R_e is the initial relative density of the soil
$q_{c;z}$ is the measured cone resistance at depth z, in kPa
$\sigma'_{v;z;0}$ is the initial effective vertical stress at depth z as present at the moment of the CPT, in kPa

Thus, for each axis it must be determined how many piles there are within the influence zone of a new pile ($r \leq 6 \cdot D_{eq}$) and the relative distance of each existing pile to the new pile. This calculation will be based on the governing CPT from the original CPT set, thus CPT E07. This analysis is not only valid for the newly placed piles, but also for the existing piles, since the pile group densification effect was not taken into account in the original capacity calculation.

For the old piles, the installation sequence is assumed as presented in Figures B.19 to B.21 on the left: first an entire row of piles is installed, before installing the adjacent row of the pile group. For the new piles it is assumed that a new row of piles will be installed at the outer side of the existing pile plan, at the same distance of the existing pile rows (see Figures B.19 to B.21 on the right). For axis 2 this means a symmetric installation of new piles. The exact densification factor that is to be taken into account, is of course dependent of the chosen installation sequence and their mutual distances.

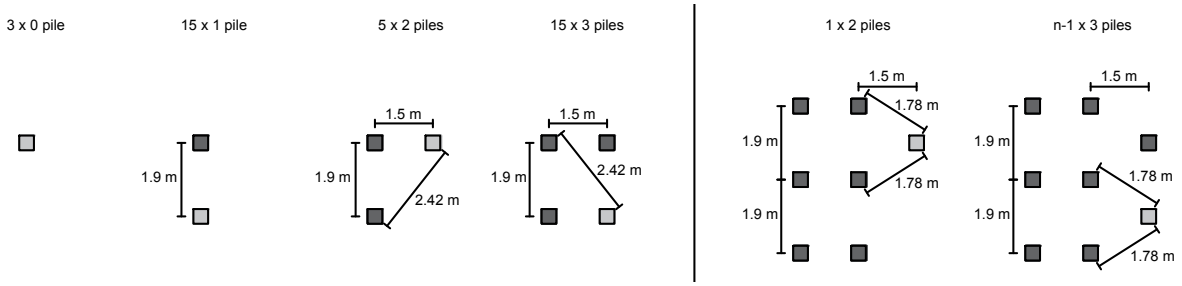

FIGURE B.19: Installation sequence and distances taken into account for the densification effect on axis 1; for the existing piles (left) and new piles (right)

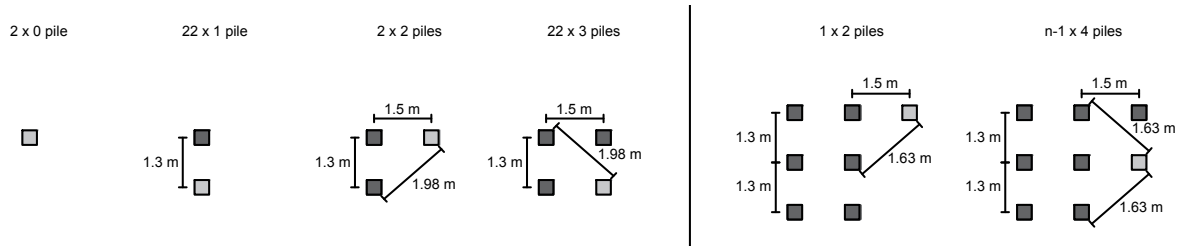

FIGURE B.20: Installation sequence and distances taken into account for the densification effect on axis 2; for the existing piles (left) and new piles (right)

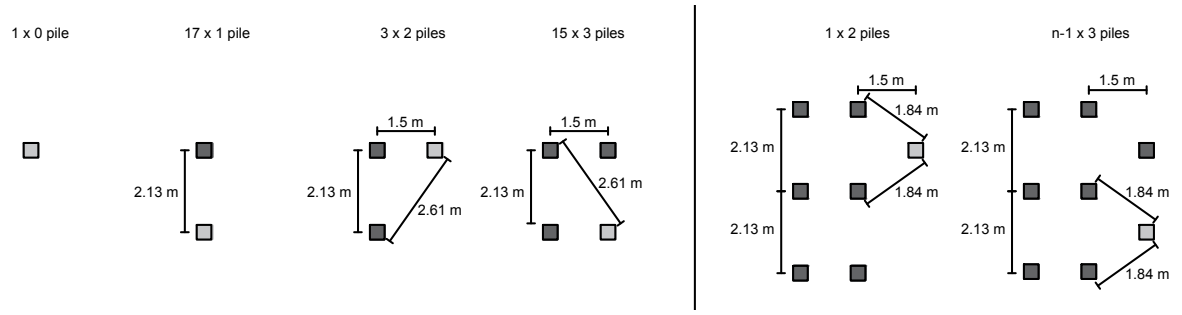

FIGURE B.21: Installation sequence and distances taken into account for the densification effect on axis 3; for the existing piles (left) and new piles (right)

The outcomes of the f_1 densification factor for these configurations are listed in Table B.2. For ease of calculation, it is assumed that the pile shaft bearing capacity for every pile is increased with the average densification factor. For the new piles, the exact average depends on the amount of piles installed, since only the first pile has a lower f_1-factor. This contribution is neglected to allow for a linear calculation instead of an iterative procedure. Overall, it can be seen that the smaller the distance between two piles, the larger the average f_1-factor, which is to be expected.

	Old piles					New piles			
	Nr. of piles in influence zone					Nr. of piles in influence zone			
	0	1	2	3	Average	2	3	4	Average
Axis 1	1.0	1.115	1.219	1.360	**1.216**	1.294	1.443		**1.294**
n_0	3	15	3	15		1	n-1		
Axis 2	1.0	1.228	1.308	1.607	**1.607**	1.308		1.768	**1.308**
n_0	2	22	2	22		1		n-1	
Axis 3	1.0	1.074	1.184	1.272	**1.164**	1.268	1.362		**1.268**
n_0	1	17	3	15		1	n-1		

TABLE B.2: Value of the densification factor f_1 for axes 1 to 3, depending on the amount of piles in the influence zone and the number of piles to which f_1 applies

By using the average f_1-factors as given in Table B.2, the following amount of extra piles is needed to resist the fictitious superstructure loads:

$n_{3(f_1)}$ = **52 piles**

In this calculation, the inclination of the piles have been neglected. However, the factor f_1 does depend on this inclination and large deviations are to be expected when two adjacent piles are inclined in opposite directions. This implies that for each calculation the spatial variation over the height, between two piles, must be taken into account adequately.

Influence of governing CPT

In determining the pile bearing capacity for the piled foundation in the case study, the governing CPT for the entire CPT set has been used. Therefore, the bearing resistance taken into account is very conservative.
An interesting elaboration is thus to alter the method used to determine the governing CPT for a certain pile. In this respect, several methods are proposed and analysed:

1. Governing CPT for entire pile plan
   This is the most conservative method, as used in the case study. When looking at the original CPT set, it can be seen that CPT E07 is governing for piles where PTL = - 10.65 m NAP (thus axes 1 and 3), while CPT E06 is governing for piles where PTL = - 10.50 m NAP (axis 2). Then:

	CPT	$R_{C;d}$ [kN]	n_0 [-]	n_{3i} [-]
Axis 1:	E07	542	38	17
Axis 2:	E06	534	48	31
Axis 3:	E07	542	34	17
			n_0 = 120	$n_{3(CPT1)}$ = 65 piles

2. Governing CPT for one pile group
   Since all pile groups can be assumed to work separately, it is also widely accepted to take the most governing CPT for each pile group into account. In this analysis, it is assumed that since the middle abutment is divided into two parts, the piles underneath each abutment acts as a separate pile group. This implies the consideration of CPT E03 for axis 1, CPTs E05 and E06 for axis 2 and CPT E07 for axis 3. Then:

	CPT	$R_{C;d}$ [kN]	n_0 [-]	n_{3i} [-]
Axis 1:	E03	605	38	16
Axis 2 (N):	E05	611	22	10
Axis 2 (S):	E06	534	22	16
Axis 3:	E07	542	34	17
			n_0 = 120	$n_{3(CPT2)}$ = 59 piles

3. Average CPT values for entire pile plan
   With regards to the statistical value of the bearing capacities it is logical to look at the average CPT values for the entire CPT set. This is done at a fixed PTL, thus for - 10.65 m NAP for axes 1 and 3 and - 10.50 m NAP for axis 2. Then:

	CPT	$R_{C;d}$ [kN]	n_0 [-]	n_{3i} [-]
Axis 1:	All	736	38	2
Axis 2:	All	721	48	6
Axis 3:	All	736	34	-8 = 0
			n_0 = 120	$n_{3(CPT3)}$ = 8 piles

4. Average CPT values for one pile group
   However, as already explained under method 2, it is widely accepted to assume the different pile groups separately. When looking at the average values for the CPT set, this would imply the following:

	CPT	$R_{C;d}$ [kN]	n_0 [-]	n_{3i} [-]
Axis 1:	E01-E03	635	38	9
Axis 2 (N):	E04-E05	717	22	5
Axis 2 (S):	E05-E06	573	22	13
Axis 3:	E07-E09	884	34	-3 = 0
			n_0 = 120	$n_{3(CPT4)}$ = 27 piles

5. Nearest CPT for each pile
When looking at the statistical value of the above mentioned CPT methods, it would be statistically more accurate to take the nearest CPT for each pile as governing. After all, the chance that the soil characteristics at a pile location coincide with a CPT, is larger when the CPT lies closer to the pile position.

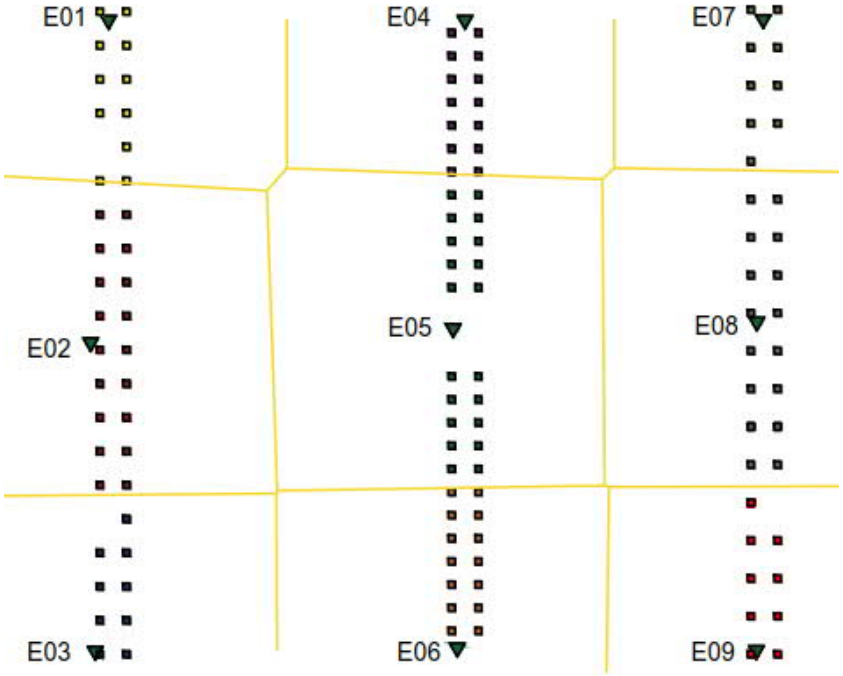

FIGURE B.22: Appointment of each pile to its nearest CPT

In Figure B.22, the pile plan has been divided into 9 zones, according to their nearest CPT. It then follows:

	CPT	$R_{C;d}$ [kN]	n_0 [-]	n_{3i} [-]
Axis 1:	E01	714	11	2
	E02	645	18	2
	E03	547	9	5
Axis 2:	E04	823	14	3
	E05	611	20	4
	E06	534	14	12
Axis 3:	E07	542	9	6
	E08	1002	15	-4 = 0
	E09	1108	8	-2 = 0
			n_0 = 120	$n_{3(CPT5)}$ = 34 piles

6. Interpolation of CPT values for each pile
Method 5 might however give an over- or underestimation for the piles located at a larger distance of the CPT. A more exact approach would be to interpolate the CPT values for piles situated between the CPTs and to extrapolate for the piles situated on the outside of the CPT plan. This has been done for all piles, resulting in the following:

	CPT	$R_{C;d}$ [kN]	n_0 [-]	n_{3i} [-]
Axis 1:	-	546 - 739	38	9
Axis 2:	-	561 - 834	48	16
Axis 3:	-	802 - 1213	34	-2 = 0
			n_0 = 120	$n_{3(CPT6)}$ = 25 piles

All values for pile bearing capacity are obtained from Figures B.13 and B.14 and are valid for the design bearing capacity of both the old and new piles.

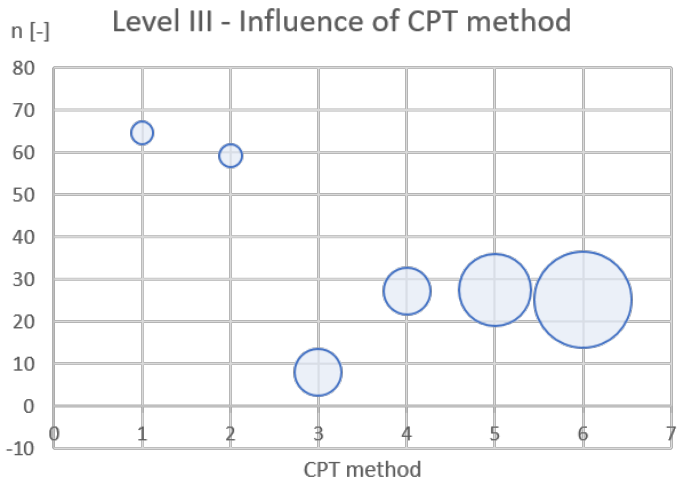

FIGURE B.23: Influence of the choice of CPT in the calculations on the amount of additional piles required, with a classification according to the amount of calculation work

It can thus be seen that the amount of piles needed to resist the additional superstructure load depends largely on the governing CPT taken for each separate pile (Figure B.23). In this case study, using a single governing CPT for the entire pile plan is the most conservative method, resulting in $n_{3(CPT)}$ = 65 piles. On the other hand, the method in which the average CPT value for the entire pile plan is taken, is the most optimistic with a total of $n_{3(CPT)}$ = 8 additional piles needed.
In practice, the statistical distribution of a CPT set will be of major importance in selecting the most optimal method for choosing a governing CPT for each pile. If the choice is too conservative, the amount of piles installed will be excessive, while being too optimistic will result in a lower safety level.

B.2.4. LEVEL IV: Perform additional CPTs

All relatively simple desk studies have been performed in the previous steps. This next level comprises the execution of additional CPTs in order to decrease the uncertainty in soil characteristics and their spatial distribution.

The uncertainty in soil conditions is directly related to the amount of CPTs performed: the more CPT samples are available, the smaller the uncertainty on the scatter of cone resistances. In the calculations, this uncertainty is taken into account through the scatter factors ξ_3 and ξ_4. The characteristic values for shaft and tip resistance are determined by:

$$R_{C;k} = (R_{b;k} + R_{s;k}) = \frac{(R_{b;cal} + R_{s;cal})}{\xi} = \min\left[\frac{(R_{C;cal})_{ave}}{\xi_3}; \frac{(R_{C;cal})_{min}}{\xi_4}\right]$$

With: $(R_{C;cal})_{ave} = (R_{b;cal} + R_{s;cal})_{ave} = (R_{b;cal})_{ave} + (R_{s;cal})_{ave}$

$(R_{C;cal})_{min} = (R_{b;cal} + R_{s;cal})_{min}$

Here factors ξ_3 and ξ_4 are correlation factors that depend on the amount of CPTs performed, as given in Table B.3.

Correlatiefactoren ξ voor de bepaling van karakteristieke waarden uit de resultaten van grondproeven (n is het aantal proeven) voor een niet-stijf bouwwerk

Correlatiefactoren ξ voor een niet-stijf bouwwerk							
ξ voor n =	1	2	3	4	5	7	10
ξ_3	1,39	1,32	1,30	1,28	1,28	1,27	1,25
ξ_4	1,39	1,32	1,30	1,03	1,03	1,01	1,00

Correlatiefactoren ξ voor de bepaling van karakteristieke waarden uit de resultaten van grondproeven (n is het aantal proeven) voor een stijf bouwwerk

Correlatiefactoren ξ voor een stijf bouwwerk							
ξ voor n =	1	2	3	4	5	7	10
ξ_3 [a]	1,26	1,20	1,18	1,17	1,17	1,15	1,14
ξ_4 [a]	1,26	0,96	0,94	0,93	0,93	0,92	0,91
[a] De factor 1,1 volgens NEN-EN 1997-1+C1+A1:2016, 7.6.2.3 (7) is al verwerkt in de factoren van tabel A.10b.							

TABLE B.3: Correlation factors ξ_3 and ξ_4 as a relation of the amount of CPTs n for a non-rigid structure (top) and a rigid structure (bottom) *[NEN-EN 1997-1, 2016]*

It can be seen that the larger the amount of CPTs, the lower these correlation factors are and thus the higher the characteristic bearing capacity is. Therefore, it could be beneficial to perform new CPTs at location to increase n up to a maximum of $n = 10$.
In this respect, it must first be investigated how many CPTs can be regarded as one group. The current codes do not give a decisive statement on the allowable spatial distribution of the different CPTs. It seems that practical experience must be used to determine the amount of CPTs belonging to one group, depending on their spatial distribution and the spatial variation of soil characteristics. The code does recommend two to six CPTs per foundation for bridge structures and, depending on the spatial soil variation, a maximum distance of 25 m between two CPTs *[NEN-EN 1997-2, 2007]*. Based on these regulations, it can be expected that if pile groups are situated at a distance of 25 m or more, the accompanying CPTs for each pile group can be considered as a separate CPT group.
For this case study, however, the three foundation axes lie within 25 m of each other and the original CPT set consists of 9 samples already. Therefore, the benefit of performing additional CPTs in order to decrease the spatial uncertainty is almost negligible. Nevertheless, the impact of this level on the amount of additional piles needed is still analysed.

The new CPTs (in total 9 samples) that were performed at KW150 Huntumdreef in 2011 (DKMP2003) and 2015 (all others) are located as given in Figure B.24.
Applying this level on both the old and new piles in the case study, results in:

n_4 = **63 piles**

It would be interesting to investigate the impact of this level in case less original samples are available. This has been done for the fictitious case that only one original CPT sample is available, thus $n = 1$ (with $\xi_3 = 1.39$ and $\xi_4 = 1.39$). Then, the Level II calculation would result in:

	CPT	$R_{C;d}$ [kN]	n_0 [-]	n_{4i} [-]
Axis 1:	E07	491	38	23
Axis 2:	E06	484	48	39
Axis 3:	E07	491	34	22
			$n_0 = 120$	$n_4 = 84$ piles

The total difference between Level II and Level IV would then become:

$\Delta n = n_2 - n_4 = 84 - 63 = 21$ piles

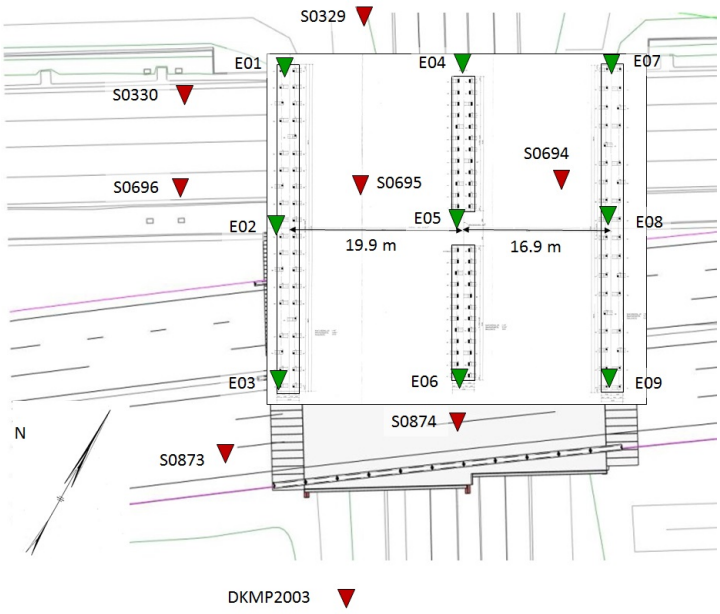

FIGURE B.24: Top view of the existing pile plan of viaduct KW150 and the locations of the old and new CPT set *[IXAS, 2015]*

It thus follows that this step might be beneficial for the amount of piles needed, provided that the original CPT set available consists of just a few samples.

Furthermore, since new CPT samples are needed anyway for the following Level V and Level VI calculations, this step is a prerequisite for further increase of the pile bearing capacity. Therefore this step should be considered as an easy profit in the case that a Level V calculation is proposed.

B.2.5. LEVEL V: Ignore the old CPT set

It is to be expected that, if no large excavations have taken place in the area between the two CPT performances, the cone resistances will be equal or (slightly) better in the new CPT results than in the old CPT results. This is based on the following considerations:

- Difference in CPT methods;
- Settlement of weak layers over time cause an increase of cone resistance;
- Time-effects near the existing piles;
- Densification effects in a certain influence zone around the pile plan.

If this is indeed the case, it would be beneficial to ignore the old CPTs and to take only the new CPTs into account when determining the pile bearing capacity. After all, the bearing capacity is based on the governing CPT, thus by definition this will always be equal to the bearing capacity obtained in Level II, if both CPT sets are taken into account. In that case the performance of a new CPT set will have no added value at all.

Thus, this level consists of an analysis whether or not the old CPT set may be ignored. For this, the considerations mentioned above must be further elaborated.

- Difference in CPT measurements
  There is a discrepancy between the method of Koppejan, based on a mechanical CPT and the current practice in which electrical CPTs are used. Higher cone resistances are obtained when measuring with an electrical CPT, which can get up to 25% higher than the mechanical CPT results, depending on the soil conditions.
  On the other hand, thin layers with low cone resistance are normally not registered in mechanical CPTs, which more or less compensates the difference in measured cone resistance between a mechanical and electrical CPT. This does mean, however, that an overestimation of cone resistance might occur in the case that there are (almost) no setbacks from small layers.

- Settlement of weak layers over time cause an increase of cone resistance

This effect depends on the scatter in soil conditions, the presence of weak soil layers and the different loads at ground level. If no substantial excavation or embankment formation has taken place in the period between the two CPT sets, this effect can be neglected.

- Time-effects near the existing piles
  Due to the disruption of the soil during installation of the piles, time effects will occur in the soil and cause an increase of cone resistance. This effect is however very local, as only the soil directly surrounding the pile shaft will be disturbed. It can therefore not be measured by a CPT, since it would require a test location within the vicinity of an existing pile. Such a CPT would however measure the resistance of the pile, not of the soil and thus the outcomes will have no value.
  It can therefore be concluded that the time-effect will not have an influence on the difference in cone resistances measured between the two CPT sets. This will be further elaborated in Level VI.

- Densification effects in a certain influence zone around the pile plan
  If the new CPT is performed within the influence zone of the existing piles for densification effects ($r \leq 6 \cdot D_{eq}$) this will be visible in an increase of cone resistance along the pile shaft in the sand layer (factor f_1) and below the pile tip level (factor f_2).

Not all these effects can be easily quantified. There have been various publications on the difference in CPT methods, but the detailed elaboration of this effect lies beyond the scope of this thesis. The settlement of different soil layers is almost impossible to quantify, since it depends on multiple parameters that not only differ in three dimensions but also in time. Furthermore, it is expected to have a negligible effect on the cone resistances obtained in the foundation sand layer. For the effect of densification from pile installation, it holds that the application of f_1 according to the tension pile regulations can be included in the design (see subsection B.2.3). For the densification factor f_2 this is however not the case, and further theoretical and practical research is needed before this effect can be quantified.

In theory, however, it is not necessary to quantify all effects mentioned above, as long as it can be proven that the difference in cone resistances as a result of the different CPT methods is lower than the overall increase of cone resistances in the new CPT set. In that case, whatever the influence of the other effects may be, the old CPTs may be ignored.
It must be stated, however, that in case the old CPT set can be ignored, the increase of cone resistance is (partly) due to the densification effect of the existing piles. Since the exact influence of densification factors f_1 and f_2 on this increase is unknown, these factors must be neglected in the other design levels in order to be conservative. More research is needed into the overlap of the Level V calculation and the calculations based on f_1 (Level III) and f_2 (Level VI).

Since the quantification of difference in cone resistances as a result of different CPT methods lies beyond the scope of this thesis, a satisfying conclusion cannot be given on this Level V analysis. Nevertheless, it is interesting to see if the effects mentioned above can be qualitatively demonstrated in the two CPT sets obtained in the case study.
For this, the old and new CPT sets have been analysed statistically along the depth for which every CPT has given values. A comparison in spread and average is given in Figures B.25 to B.28. It can be seen that in general, the average of the new CPT set is higher than the average of the old CPT set. For the spread it holds that the two sets are comparable, in general, with the exception of some larger deviations below PTL. The increase in average cone resistances between the old and the new set ranges from -31% to 154%, with an average of 25%. Whether or not this difference can be ascribed entirely to the difference in CPT methods cannot be concluded yet from these comparisons.
For more insight, every new CPT set is plotted against the statistical distribution of the old CPT set. The results are shown in Figures B.29 to B.37, with the PTL of the nearest pile group indicated by the red horizontal line. Also, the horizontal distance to the PTL of the nearest pile is given in each plot to illustrate the spatial distribution of the new CPT set. Again, only the depth over which all CPT sets have data, are considered. In general no clear conclusions can be drawn from these plots. Natural spread of the soil characteristics will also cause local differences in cone resistances, especially in CPTs obtained at a larger distance from the old CPT set.
There is however one CPT, CPT S0694 (Figure B.32) that requires a closer look. This is the only CPT that lies in the vicinity of the existing pile plan and might therefore expose (part of) the densification effect. When taking

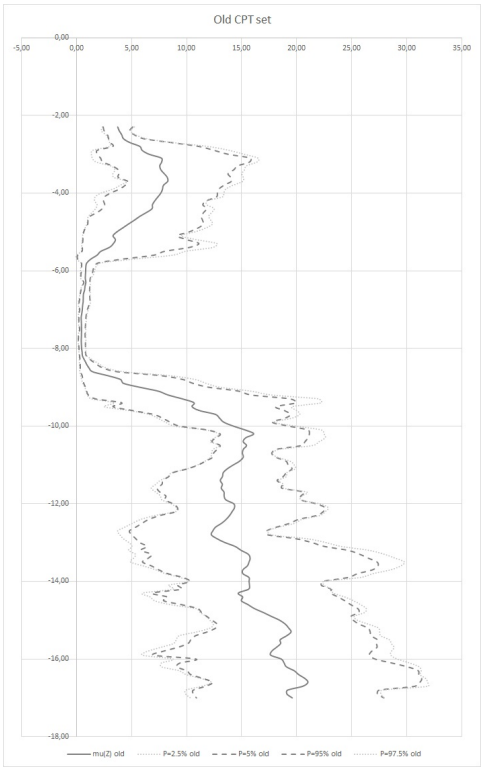

FIGURE B.25: The statistical spread of the old CPT set, with the 2.5-percentile, 5-percentile, $\mu(Z)$, 95-percentile and 97.5-percentile

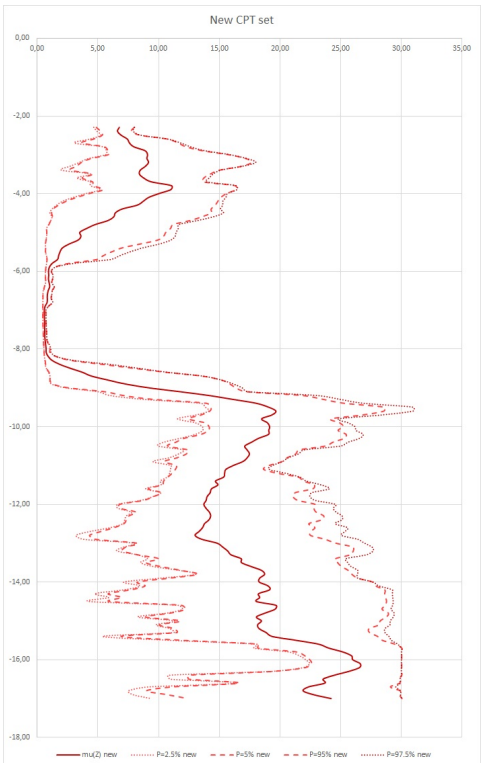

FIGURE B.26: The statistical spread of the new CPT set, with the 2.5-percentile, 5-percentile, $\mu(Z)$, 95-percentile and 97.5-percentile

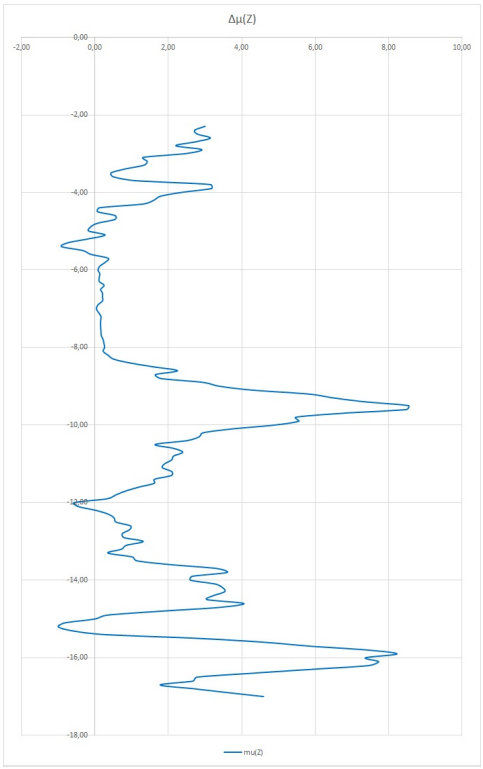

FIGURE B.27: The difference between the average CPT values for the old and new CPT set ($\Delta\mu = \mu(Z)_{new} - \mu(Z)_{old}$)

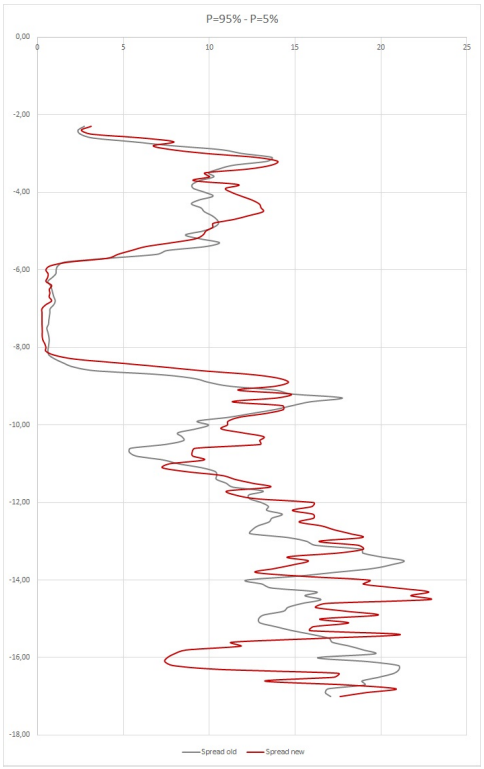

FIGURE B.28: The difference between the 5-percentile and 95-percentile for both the old (grey) and new (red) CPT sets

the pile inclination into account, the horizontal distance between CPT S0694 and the nearest pile tip is 2.46 m, which is equal to 5.7 $\cdot D_{eq}$. Thus the CPT lies just within the influence zone of $r \leq 6 \cdot D_{eq}$ that is considered in the calculation of densification factor f_1. When looking at Figure B.32, however, a very distinctive peak in cone resistance can be distinguished above PTL, along the zone of positive shaft friction. This peak is much larger than is the case in the other plots, thus indicating an influence of the piles located nearby.
Compared to the average cone resistance of the old CPT set, some other CPTs also show an increase of cone resistances along the positive shaft friction zone, but in these cases the increase is less significant and there is no clear correlation with the distance to the nearest piles.

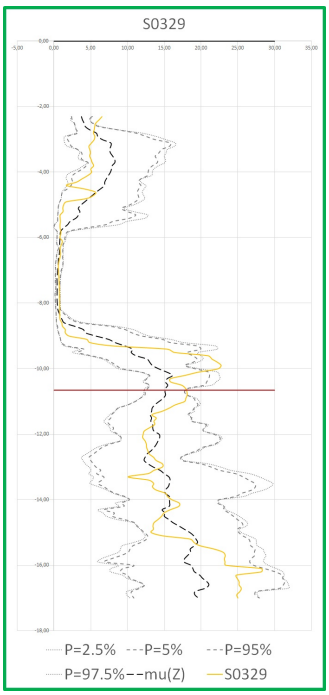

FIGURE B.29: The new CPT S0329 (yellow) plotted against the statistical spread of the old CPT set (grey), with the PTL at -10.65 m NAP (red). Distance to nearest pile at PTL: 17.5 $\cdot D_{eq}$

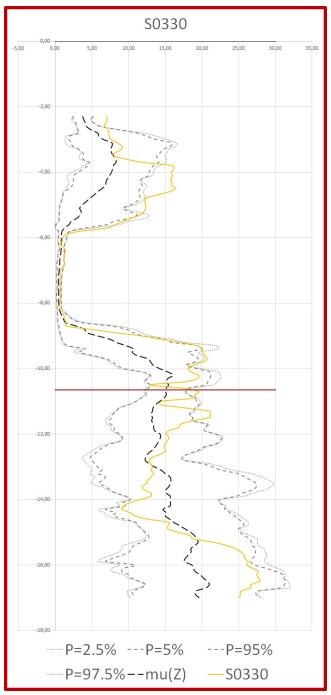

FIGURE B.30: The new CPT S0330 (yellow) plotted against the statistical spread of the old CPT set (grey), with the PTL at -10.65 m NAP (red). Distance to nearest pile at PTL: 19.7 $\cdot D_{eq}$

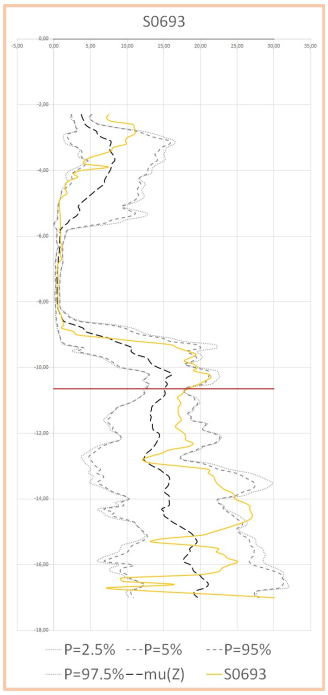

FIGURE B.31: The new CPT S0693 (yellow) plotted against the statistical spread of the old CPT set (grey), with the PTL at -10.65 m NAP (red). Distance to nearest pile at PTL: 35.2 $\cdot D_{eq}$

As the exact influence of the different CPT methods and the densification effect around the existing foundation piles is unknown, a decisive conclusion cannot be drawn on the elaboration presented above. However, Figure B.32 suggests that the actual influence zone of densification factor f_1 might be larger than 6 $\cdot D_{eq}$ as is used in the theoretical calculations. This is to be expected, since theory is generally more conservative than practice.
Another possible explanation can be found in the positive influence of the unknown factor f_2 on the cone resistances above PTL. If the cone resistances beneath PTL are higher, due to the densification effect, this increases the average cone resistances taken into account for section I and II in the method of Koppejan (Figure B.38). Since the value of $q_{c;II}$ at PTL is also the starting value of $q_{c;III}$ along section III, an increased cone resistance below PTL will result in an overall increase of positive shaft friction along section II. This increase will manifest itself within the factor f_1, and thus f_1 is positively influenced by the unknown factor f_2. However, more research into this influence zone of f_1 should be considered to quantify this effect. The same holds for the influence of the different CPT method on the increase of cone resistance and the quantification of factor f_2.

In order to demonstrate the influence of this level on the entire geotechnical analysis, it is assumed for now that the old CPT set may be ignored. Figures B.39 and B.40 show the resulting bearing capacities obtained from the new CPT set in D-foundations. It can be seen that the governing CPT is S0696 for axes 1 and 3, with a bearing capacity of $R_{C;d}$ = 667 kN and CPT S0874 for axis 2, with a bearing capacity of $R_{C;d}$ = 670 kN.

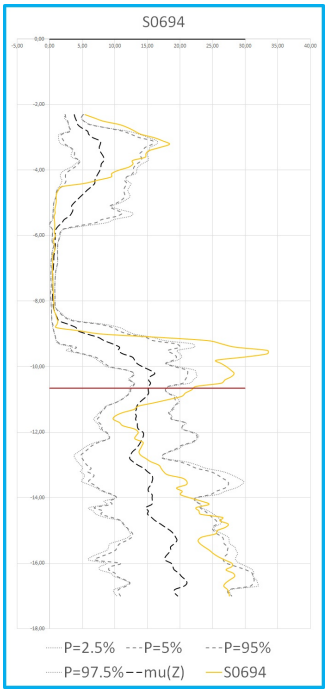

FIGURE B.32: The new CPT S0694 (yellow) plotted against the statistical spread of the old CPT set (grey), with the PTL at -10.65 m NAP (red). Distance to nearest pile at PTL: 5.7 $\cdot D_{eq}$

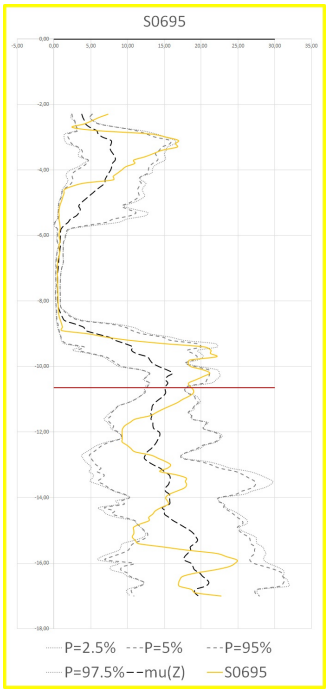

FIGURE B.33: The new CPT S0695 (yellow) plotted against the statistical spread of the old CPT set (grey), with the PTL at -10.65 m NAP (red). Distance to nearest pile at PTL: 11.9 $\cdot D_{eq}$

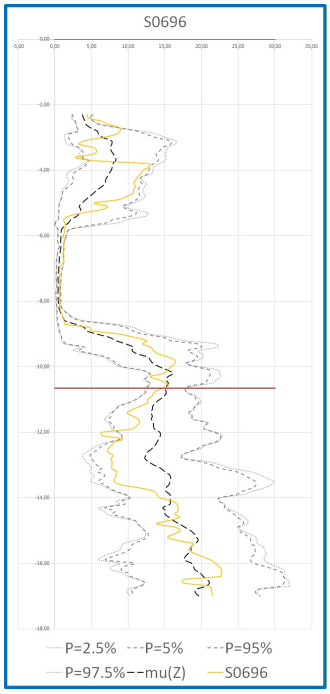

FIGURE B.34: The new CPT S0696 (yellow) plotted against the statistical spread of the old CPT set (grey), with the PTL at -10.65 m NAP (red). Distance to nearest pile at PTL: 20.9 $\cdot D_{eq}$

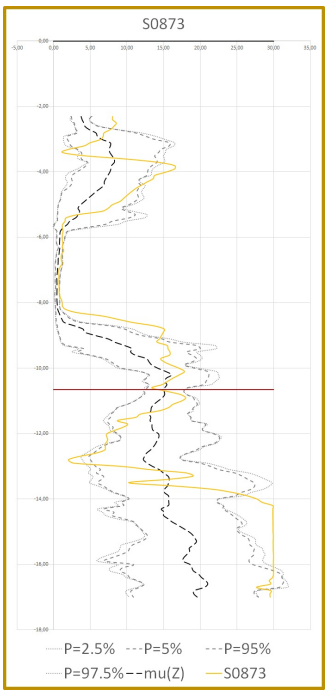

FIGURE B.35: The new CPT S0873 (yellow) plotted against the statistical spread of the old CPT set (grey), with the PTL at -10.65 m NAP (red). Distance to nearest pile at PTL: 27.7 $\cdot D_{eq}$

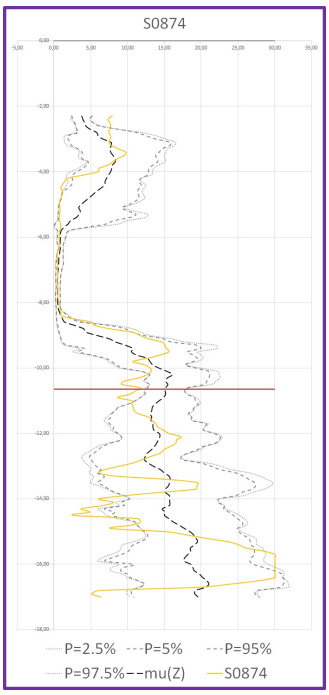

FIGURE B.36: The new CPT S0874 (yellow) plotted against the statistical spread of the old CPT set (grey), with the PTL at -10.50 m NAP (red). Distance to nearest pile at PTL: 13.7 $\cdot D_{eq}$

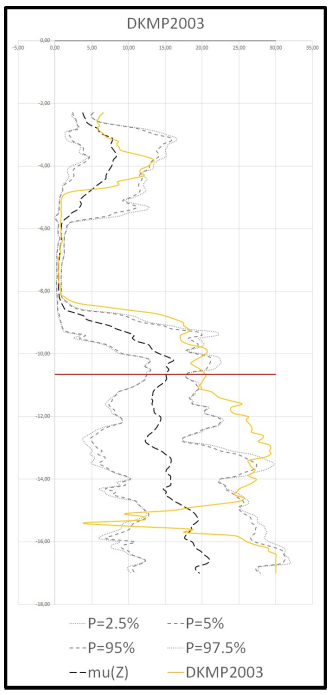

FIGURE B.37: The new CPT DKMP2003 (yellow) plotted against the statistical spread of the old CPT set (grey), with the PTL at -10.65 m NAP (red). Distance to nearest pile at PTL: 58.6 $\cdot D_{eq}$

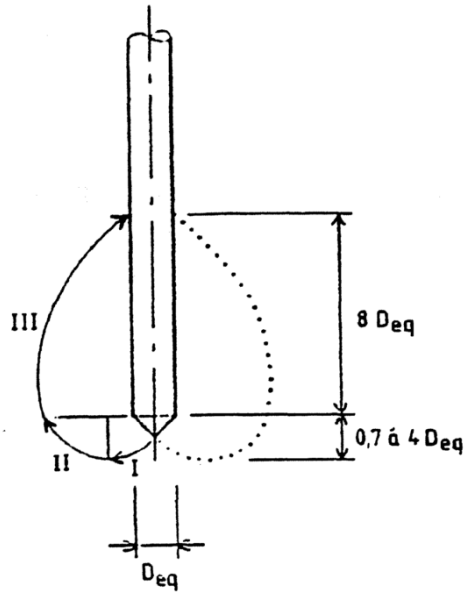

FIGURE B.38: Method of Koppejan with the influence zones from section I (PTL down to -0.7 to -4 $\cdot d_{eq}$), section II (back up to PTL) and section III (PTL up to +8 $\cdot D_{eq}$) *[Verruijt, 2012]*

Results of the option Preliminary Design, Bearing capacity at fixed pile tip levels

Results for pile type :
Rect 380x380

CPT name	Level [m R.L.]	Groundlevel [m R.L.]	Rb;cal;max [kN]	Rs;cal;max [kN]	Rc;cal;max [kN]	Rc;d [kN]	F;nst;rep [kN]	Fnst;d [kN]
DKMP2003	-10.65	-2,27	1571	472	2043	1351	77	107
S0329	-10.65	-0,50	957	305	1262	835	186	261
S0330	-10.65	4,10	1134	378	1512	1000	534	747
S0693	-10.65	4,18	1222	331	1553	1027	518	725
S0694	-10.65	-0,49	876	358	1234	816	183	256
S0695	-10.65	-0,58	796	336	1132	749	180	253
S0696	-10.65	4,19	696	313	1009	667	520	727
S0873	-10.65	1,94	737	405	1142	755	337	471
S0874	-10.65	-1,76	764	303	1067	706	99	139

FIGURE B.39: Results for the bearing capacities of piles based on the new CPT set with a PTL at -10.65 m NAP in D-Foundations

Results of the option Preliminary Design, Bearing capacity at fixed pile tip levels

Results for pile type :
Rect 380x380

CPT name	Level [m R.L.]	Groundlevel [m R.L.]	Rb;cal;max [kN]	Rs;cal;max [kN]	Rc;cal;max [kN]	Rc;d [kN]	F;nst;rep [kN]	Fnst;d [kN]
DKMP2003	-10.50	-2,27	1530	438	1968	1302	77	107
S0329	-10.50	-0,50	942	271	1213	802	186	261
S0330	-10.50	4,10	1099	344	1443	955	534	747
S0693	-10.50	4,18	1191	297	1488	984	518	725
S0694	-10.50	-0,49	881	324	1205	797	183	256
S0695	-10.50	-0,58	797	301	1098	726	180	253
S0696	-10.50	4,19	749	290	1040	688	520	727
S0873	-10.50	1,94	750	376	1125	744	337	471
S0874	-10.50	-1,76	736	277	1013	670	99	139

FIGURE B.40: Results for the bearing capacities of piles based on the new CPT set with a PTL at -10.65 m NAP in D-Foundations

With this bearing capacity taken into account for both old and new piles, the calculation according to Level II can be repeated, resulting in:

$n_5 =$ **29 piles**

B.2.6. LEVEL VI: Extensive research

The last level of this geotechnical analysis consists of quantifying two effects that still require extensive additional research.

Densification factor f_2

First, as already mentioned in 3, it is expected that the densification effect f_2 will result in an increase of

cone resistance and thus bearing capacity underneath the pile tip. However, in contradiction to the other densification factor f_1, this factor cannot be taken from the regulations for tension piles since their effect is fundamentally different. More research is needed to quantify f_2 for different pile types and soil conditions. It must also be investigated to which extent the factor f_2 influences the pile tip bearing resistance and pile shaft bearing resistance in order to take it into account in calculations.
Another aspect that could be very interesting and should be included in this research, is the relation between both densification factors f_1 and f_2. As stated in subsection B.2.5, when looking at the theory of Koppejan, the effect of an increased shear capacity in the soil underneath the pile tip (f_2) will in theory cause an increase of the shear capacity along the pile shaft (f_1). It is thus to be expected that the theoretical relationship between q_c and f_1, taken directly from the tension pile regulations, underestimates the densification effect of driven piles on the bearing capacity of pile groups.

Set-up of soil over time
As mentioned in Chapter 3, the phenomenon of set-up of soil over time causes an increase in bearing resistances of the original piles. Over the years, there have been numerous researches performed to understand the mechanisms behind set-up and to quan.tify the effect.
Skov and Denver (1988) have proposed a relation to estimate the increase of bearing capacity over time *[de Lange, 2013]*:

$$Q_t = Q_0 \cdot (1 + A \cdot \log(\tfrac{t}{t_0}))$$

With: t the time after the end of initial driving
t_0 the initial reference time elapsed since end of driving (= 0.5 days)
Q_0 the pile capacity at time t_0
Q_t the pile capacity at time t

Skov and Denver recommended A to be taken as 0.2 in cohesionless soils, while Chow et al. (1998) reports values between 0.25 and 0.75 *[de Lange, 2013]*. *[Axelsson, 2000]* has gathered several researches and case histories on this topic and compared them to the relation proposed by Skov and Denver (see Figure B.41). Based on these results, he proposes a lower boundary with A = 0.2 and an upper boundary with A = 0.8, obtaining a set-up of 15-65% per log cycle. There are, however, still a lot of uncertainties on the phenomenon of set-up and the value of A. Since there seem to be many influencing factors, Axelsson states that a specific value of A must be determined for each case.

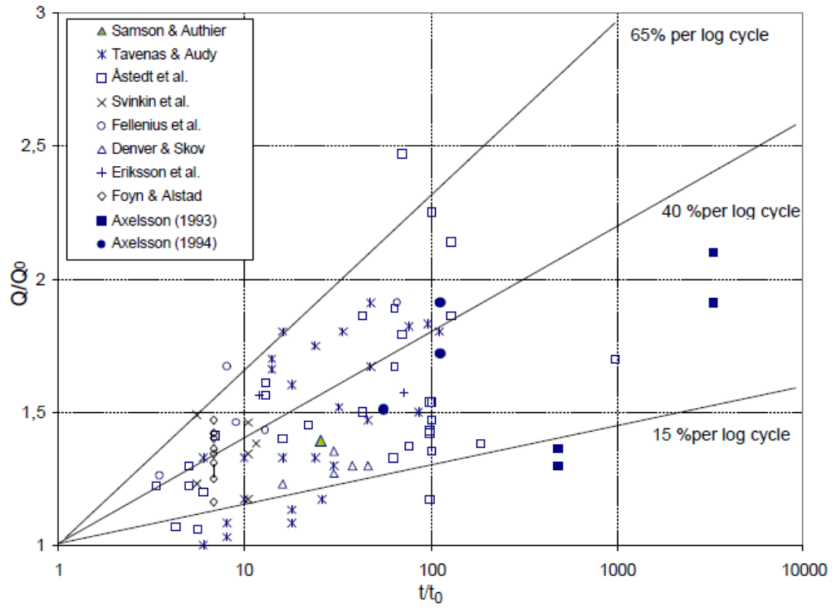

FIGURE B.41: Case histories of long-term pile set-up *[Axelsson, 2000]*

It can thus be said that there is no consensus yet on the value of A and further research into this area must be performed in order to get more insight. Bullock et al. (2005) states that the increase of pile shaft resistance is

proven to such an extent that it can be applied in practice. Without further information conservatives values for A and t_0 are proposed, namely $A = 0.1$ for cohesionless soils and $t_0 = 1$ day *[CUR-commissie C193, 2012]*. This advice has been implemented in the case study. The time difference between the old CPT set and the new set (with the exception of DKMP2003) is taken between August 1974 and February 2015, which equals 40.5 years thus approximately 14800 days. This gives:

$$Q_t = 1.42 \cdot Q_0$$

This increase of bearing capacity is only applicable to the shaft friction of the existing piles. This has been applied to the bearing capacities as given in the Level II calculation in Figures B.13 and B.14, resulting in a bearing capacity of $R_{C;d1} = 595$ kN for axes 1 and 3 (based on CPT E07) and $R_{C;d1} = 598$ kN for axis 2 (based on CPT E06). This leads to the following:

$n_6 =$ **52 piles**

This calculation is however based on the conservative values for A and t_0 as proposed by Burlock et al. It is therefore interesting to investigate the influence of these parameters on the increase of the total bearing capacity over time.
If the lower and upper boundary obtained by Axelsson are taken into account, the following increase can be seen:

Lower boundary: 15% per log cycle, with $t_0 = 1$: $Q_t = 1.63 \cdot Q_0$
Upper boundary: 65% per log cycle, with $t_0 = 1$: $Q_t = 3.91 \cdot Q_0$

This increase is applicable to the total bearing capacity at $t = t_0$, which would result in:

n_6 = -6 = 0 piles (for lower boundary)
n_6 = -70 = 0 piles (for upper boundary)

These results are of course very remarkable and thus it is highly recommended to perform additional research on the applicability of set-up in practice.

B.3. CONCLUSIVE RESULTS CASE STUDY

In the previous section, every individual level of the pyramid approach has been elaborated extensively. In this section these results will be summarised.
In the geotechnical analysis, as performed in section B.2, the calculations resulted in the amount of additional piles needed in order to resist the increased load actions on the foundation (n_i). Another interesting approach is, however, to express the profit of each level in the allowed increase of working load action (ΔF_{Ski}). In the following results, both outcomes have been presented for each level.

Individual level results

In Table B.4, a summary of all obtained results in section B.2 is given. Although these results are based on one case study only, and thus statistically have no significant value, they are a good indicator of the possibilities of the pyramid approach in the reuse of existing foundations.
It can be seen that the impact of every individual level is, in general, quite small. As expected, the Level II calculation even results in an increase of additional piles needed, with regards to the Level I calculation, due to the large reduction of the α_p factor. The calculation applied in Level IV also results in an increase of piles, since there can only be a minimal reduction in scatter factors Ξ_3 and Ξ_4 in this case study. All other levels result in a decrease of additional piles needed. In Figure B.42, the amount of additional piles needed for each level is plotted against the estimated amount of work required for the accompanying calculation. Small circles located higher up in the graph represent calculations with an easy profit. In that regard, especially the increase of α_p and a different choice for governing CPT (both Level III calculations) are interesting to investigate further. This can also be seen in Figure B.43, where the same is done for the increase in working load for each level. Furthermore, the influence of long-term set-up on the bearing capacity of the existing piles is an interesting investigation, since the possible profit can be very substantial, depending on the obtained value for set-up.

Sequential pyramid approach

Overall, it can be concluded that applying any individual level will not be sufficient, in this case study, to compensate entirely for the increase of design loads on the foundation. If the pyramid approach is followed,

SINGULAR - Amount of additional piles (n [-])								
	Level I	Level II	Level III			Level IV	Level V	Level VI
	n_1	n_2	$n_{3(f1)}$	$n_{3(CPT)}$	$n_{3(\alpha p)}$	n_4	n_5	n_6
Axis 1	17,37	16,91	14,02	8,93	3,34	16,51	6,62	13,20
Axis 2	23,43	31,11	23,59	18,63	12,57	30,37	15,05	25,38
Axis 3	12,92	16,72	14,50	-0,61	4,18	16,35	7,21	13,40
	53,72	**64,73**	**52,12**	**26,95**	**20,09**	**63,23**	**28,88**	**51,98**

SINGULAR - Increase in working load (ΔF [%])								
	Level I	Level II	Level III			Level IV	Level V	Level VI
	ΔF_{Sk1}	ΔF_{Sk2}	$\Delta F_{Sk3}a$	$\Delta F_{Sk3}b$	$\Delta F_{Sk3}c$	ΔF_{Sk4}	ΔF_{Sk5}	ΔF_{Sk6}
Axis 1	0,00	1,23	19,88	1,23	34,46	1,98	24,58	11,12
Axis 2	0,00	-13,76	-4,00	4,99	12,63	-12,95	8,20	-3,48
Axis 3	0,00	-10,05	-6,60	50,82	19,48	-9,38	10,70	-1,26
	0,00	**-7,52**	**3,09**	**19,01**	**22,19**	**-6,78**	**14,50**	**2,13**

TABLE B.4: Amount of additional piles required (top) and possible increase in working load (bottom) for each level individually, based on the case study A9 Gaasperdammerweg

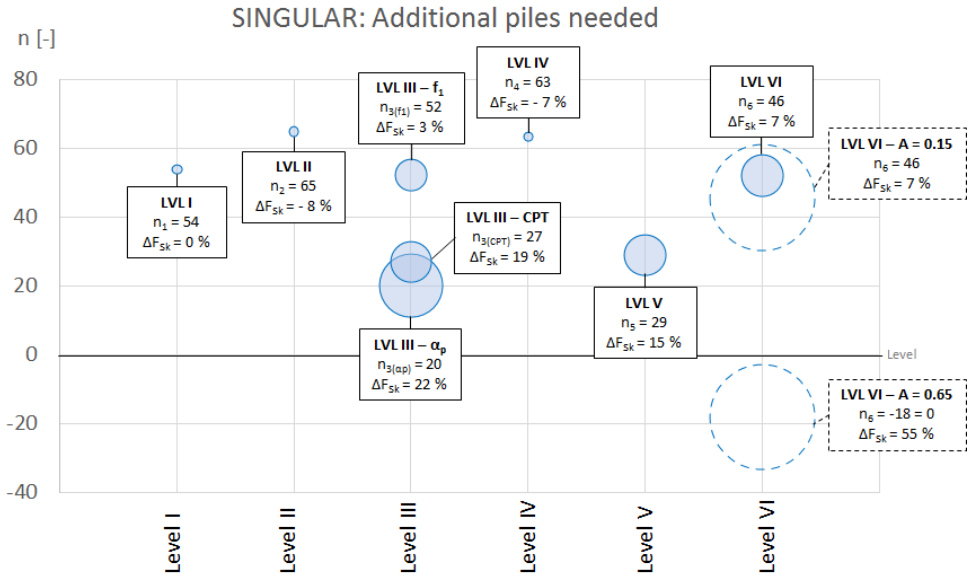

FIGURE B.42: The amount of additional piles needed for each level plotted against the estimated amount of work required for the accompanying calculation

however, in which each level is applied in sequence, the obtainable profit is rather significant. If all adaptations, as proposed for this case study, are taken into account, it can be seen in Figure B.44 and Table B.5 that the increase in loads on the foundation is already compensated in Level III.
Various sequential approaches have been presented in Figures B.45 to B.48 and Tables B.6 to B.9. The first approach corresponds to current practice, in which only Level I and II are applied. The second approach is based on values that have a large possibility of being approved by RWS without any additional research. The profit in this approach is almost negligible, thus further research will be necessary to enhance this profit. In approach 3, the values incorporated are based on relatively easy researches or analyses. If all these values can be proven, it is shown that no additional piles are needed after the Level VI calculations. Finally, in the fourth approach, the possibilities of foundation reuse are presented in case extensive research is performed and very optimistic values can be proven.

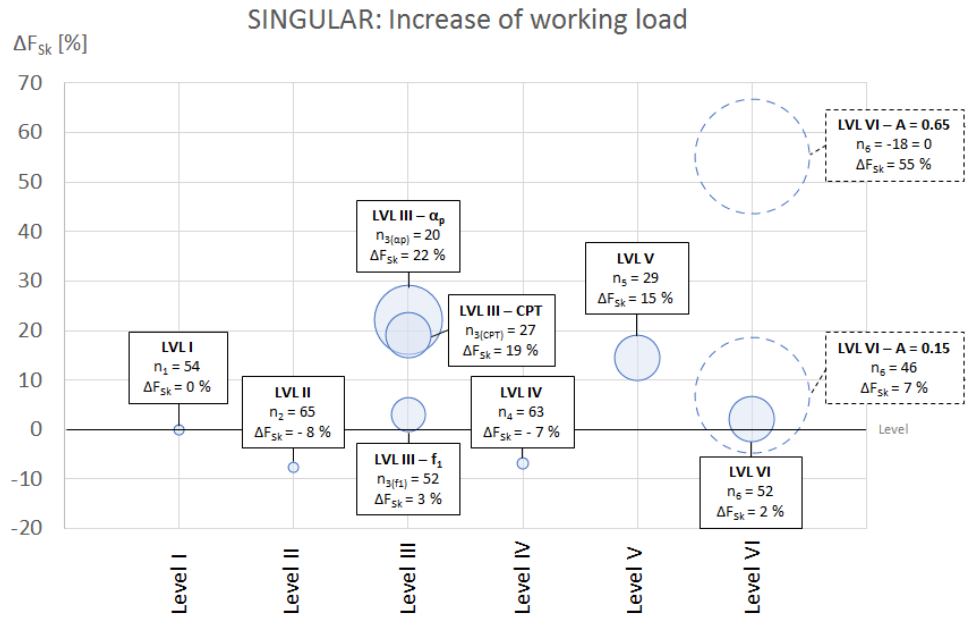

FIGURE B.43: The possible increase in working load for each level plotted against the estimated amount of work required for the accompanying calculation

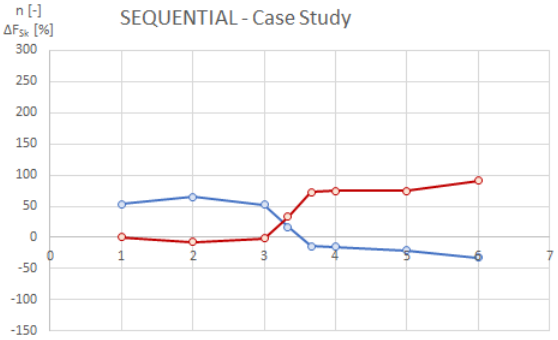

FIGURE B.44: Results of the sequential approach applied to the case study, with the amount of additional piles in blue and the possible increase in working load in red

Case Study		
Level	**Parameter**	
III	α_p [-]	1.0
	f_1 taken into account?	Yes
	CPT method	5
IV	n [-]	18
V	Old CPT set ignored?	Yes
	f1 taken into account?	No
VI	A [-]	0.1

TABLE B.5: Applied parameters in the sequential approach applied to the case study

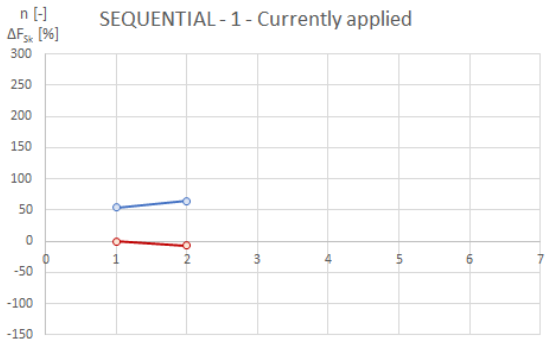

FIGURE B.45: Results of the sequential approach "Currently applied", with the amount of additional piles in blue and the possible increase in working load in red

1 - Currently applied		
Level	**Parameter**	
III	α_p [-]	0.7
	f_1 taken into account?	No
	CPT method	1
IV	n [-]	9
V	Old CPT set ignored?	No
	f1 taken into account?	
VI	A [-]	0.0

TABLE B.6: Applied parameters in the sequential approach "Currently applied"

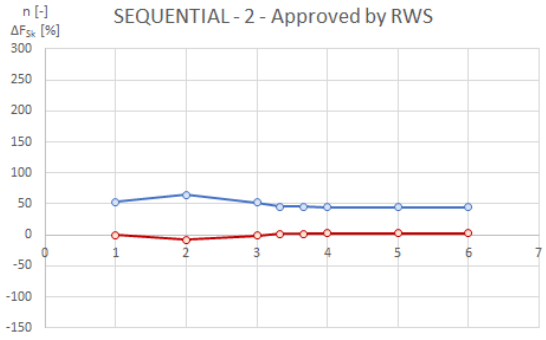

FIGURE B.46: Results of the sequential approach "Approved by RWS", with the amount of additional piles in blue and the possible increase in working load in red

2 - Approved by RWS		
Level	**Parameter**	
III	α_p [-]	0.7
	f_1 taken into account?	Yes
	CPT method	2
IV	n [-]	18
V	Old CPT set ignored?	No
	f1 taken into account?	
VI	A [-]	0.0

TABLE B.7: Applied parameters in the sequential approach "Approved by RWS"

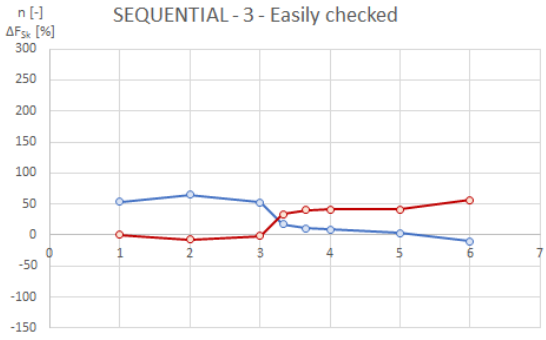

FIGURE B.47: Results of the sequential approach "Easily checked", with the amount of additional piles in blue and the possible increase in working load in red

3 - Easily checked		
Level	**Parameter**	
III	α_p [-]	0.75
	f_1 taken into account?	Yes
	CPT method	5
IV	n [-]	18
V	Old CPT set ignored?	Yes
	f1 taken into account?	No
VI	A [-]	0.1

TABLE B.8: Applied parameters in the sequential approach "Easily checked"

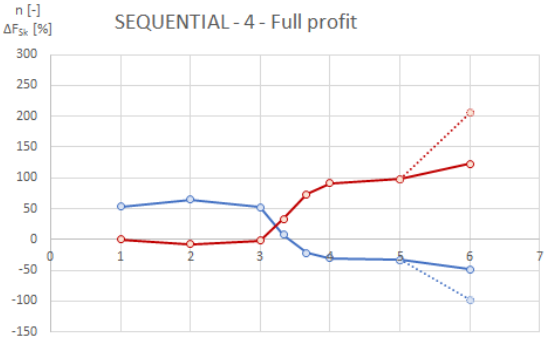

FIGURE B.48: Results of the sequential approach "Full profit", with the amount of additional piles in blue and the possible increase in working load in red

4 - Full profit		
Level	**Parameter**	
III	α_p [-]	1.0
	f_1 taken into account?	Yes
	CPT method	3
IV	n [-]	18
V	Old CPT set ignored?	Yes
	f1 taken into account?	Yes
VI	A [-]	0.15
	A [-]	0.65

TABLE B.9: Applied parameters in the sequential approach "Full profit"

C

CASE A9: INPUT SCIA ENGINEER

SCIA Engineer is a Finite Element Program that enables the modelling of complex structures. For the Case Study KW150 Huntumdreef in the project A9 Gaasperdammerweg, a new fictitious superstructure has been modelled in SCIA in order to obtain the reaction forces on the foundation piles. In this appendix, the model input, applied assumptions and design considerations are presented, as an explanation for the calculations performed in Appendix B.

C.1. GEOMETRY

For the fictitious superstructure that will replace the existing viaduct KW150 over the Huntumdreef, it is assumed that the geometry will remain almost equal to the existing structure. This assumption removes the need for extensive calculations whether or not the superstructure is adequately designed to withstand all acting loads. Since this analysis is about possible geotechnical profits, the output of this model is merely to demonstrate the impact of an increased loading situation on the amount of extra piles needed. The actual reaction forces on the foundation will off course be higher when the intermediate support is removed, which will decrease the chance that no extra piles are needed in a bridge replacement. All dimensions are obtained from the original drawings of the viaduct.

Concrete deck:

The deck is modelled as a 2D plate element with a thickness of 580 mm.

> This is smaller than the deck height of the original structure, which was 650 mm high. However, originally the asphalt layer was 70 mm high, but current regulations prescribe a minimum height of 140 mm *[3Angle, 2016b]*. In order to prevent additional groundwork or a lowered traffic profile, the concrete deck height must thus be decreased to 580 mm in order to maintain the same overall deck height. Quick hand calculations have shown that this is sufficient in HPC for a span of 19.9 m and it is assumed that this deck can indeed resist all loads acting on it during its lifetime.

The length of the deck is 36.8 m, plus an additional assumed extension of 0.5 m at each end support. The width is equal to 18.04 m and the horizontal gap between both separate decks is 1.26 m.

The concrete strength class applied is C90/105, a HPC.

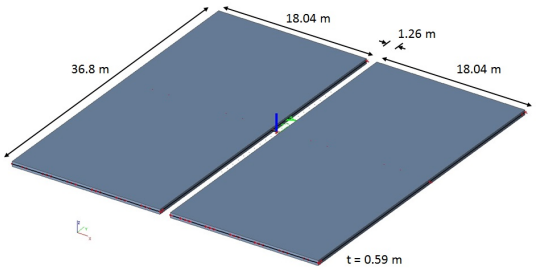

FIGURE C.1: Concrete deck elements in SCIA

Intermediate supports:
The intermediate supports are modelled as a 2D wall, with a thickness of 650 mm. Their length is equal to 3.2 and their height is 4.052 m.

The concrete strength class applied in the original structure is unknown, in the model it is assumed to be C35/45.

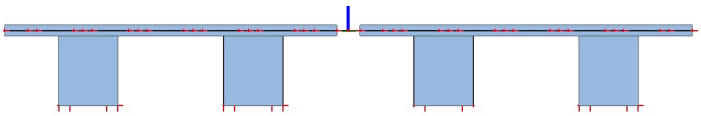

FIGURE C.2: Cross-sectional view of the intermediate supports in SCIA

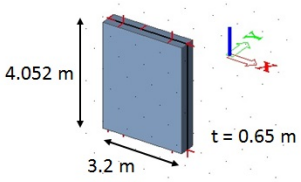

FIGURE C.3: Intermediate support dimensions

Concrete abutments:
The concrete abutments are modelled as a 2D plate element with a thickness of 3000 mm for the end abutments and a thickness of 1400 mm for the intermediate abutment.

The original end abutments have a rather complex shape, as can be seen in Figure C.4. To model an adequate stiffness, the moment of inertia of the original abutment must be equal to that of the 2D element model with a certain thickness. As it turns out that these dimensions are almost equal to the total height and bottom width of the complex geometry, it is chosen to take those dimensions. Furthermore, as is the case in the original abutment, the deck will be supported at half the height of the end abutments.

The length of the end abutments is 37.34 m and both intermediate abutments are 15.3 m long. All abutments have an equal width of 2.5 m.

The concrete strength class applied in the original structure is unknown, in the model it is assumed to be C35/45.

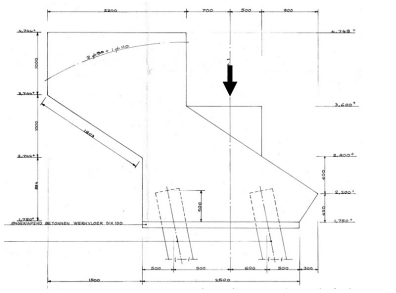

FIGURE C.4: Original layout and dimensions of the end abutments *[Rijkswaterstaat, 1977a]*

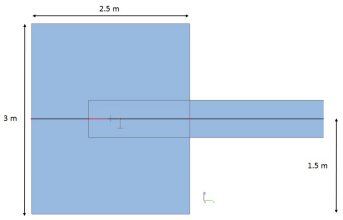

FIGURE C.5: Connection between end abutment and concrete deck in SCIA

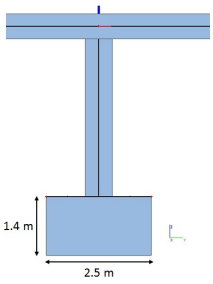

FIGURE C.6: Connection between intermediate abutments, concrete piers and concrete deck in SCIA

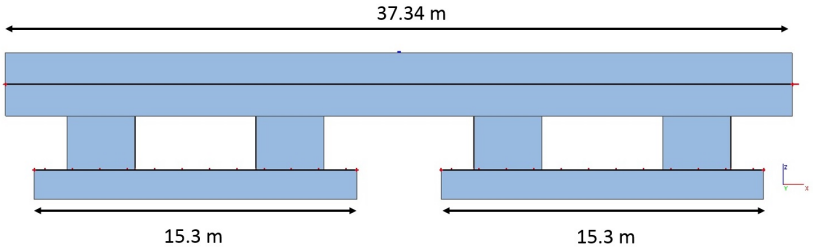

FIGURE C.7: Cross-sectional view of the end and intermediate abutments in SCIA

Foundation piles:
The foundation piles are modelled as 1D column elements with a cross-section of 380x380 mm.

> In the original structure, the pile heads are embedded 500 mm into the abutments. In this model, however, they coincide with the central axis of the abutment, which is a 1500 mm embedding. Since the pile reaction force depends more on the total length of the pile than on the length of the pile surrounded by the soil, it is chosen to maintain the total pile lengths of the original structure. This means that the interaction between pile head and abutment is stronger than the actual interaction, but this difference is expected to be small and will thus be neglected.

The pile axes are located at a distance of 0.9 m and 0.6 m from the end supports, and 0.5 m from the mid supports (see Figures C.8 and C.9).
The pile lengths for axis 1 piles (beneath the west abutment) and axis 3 piles (beneath the east abutment) are 13.15 m and for axis 2 piles (beneath the intermediate abutments) are 8.65 m. Their respective inclinations are 1:5 and 1:10.

The concrete strength class applied in the original structure is unknown, in the model it is assumed to be C35/45.

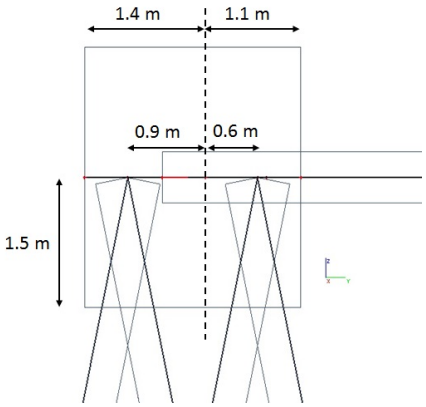

FIGURE C.8: Connection between west abutment and axis 1 piles in SCIA

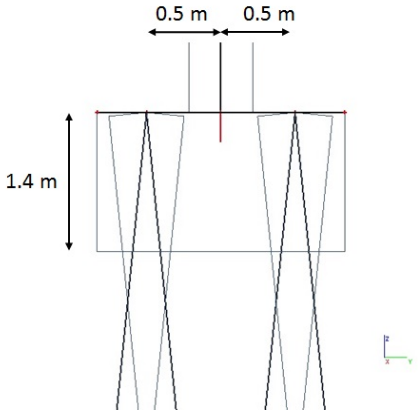

FIGURE C.9: Connection between intermediate abutment and axis 2 piles in SCIA

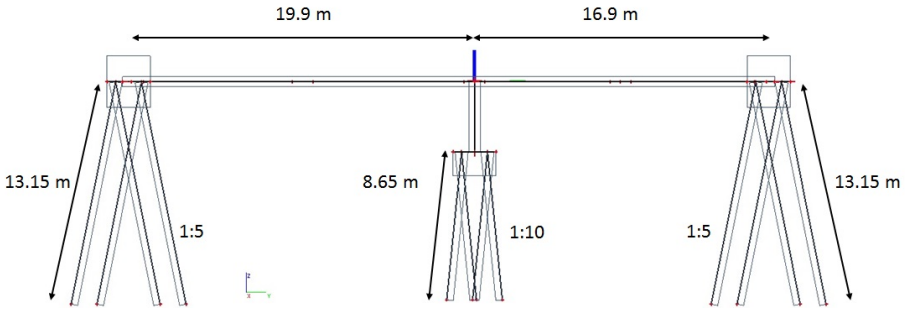

FIGURE C.10: Side view of the pile plan and respective dimensions in SCIA

C.2. SUPPORTS

The deck is statically indeterminate, thus it can rotate freely over the x-axis at all three supports. The intermediate supports have a fixed connection at the bottom to the intermediate abutments.

The pile heads are also modelled as fixed to the abutment, as they are embedded up to 500 mm.
All pile tips are supported by a spring support in z-direction with a stiffness of 100 MN/m, which is an estimation based on common practice. Movement is fixed in all other directions, but the pile tip is able to rotate freely (see Figure C.11).

The piles are also laterally supported by springs over their entire length, to simulate the soil stiffness around the embedded piles. Normally, this horizontal spring stiffness is taken as increasing over the depth, but for ease of calculation in this case study, it is modelled as 5 MN/m^2 over the entire length, in both x and y-direction (see Figure C.12).

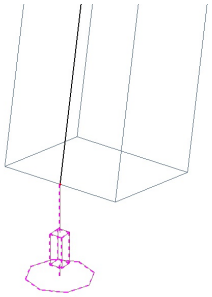

FIGURE C.11: Pile tip support in SCIA

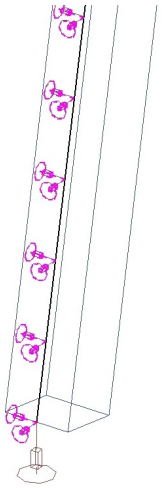

FIGURE C.12: Lateral support piles in SCIA

C.3. LOADS

The loads that act on a highway viaduct in general are elaborated in Appendix A. For this case specific, the values are listed in this section.

C.3.1. Self-weight

With a height of h_c = 0.58 m and the density of UHPC taken as ρ_c = 2500 kg/m^3, the load from self-weight becomes:

$$Q_{ck} = \rho_c \cdot h_c = 2500 \cdot 10 \cdot 10^{-3} \cdot 0.58 = 14.75 \text{ kN/m}^2$$

SCIA generates the self-weight from the inserted geometry and material. When looking at Figure C.13, which depicts the displacement as a result of self-weight, it can be concluded that the model takes this load into account correctly.

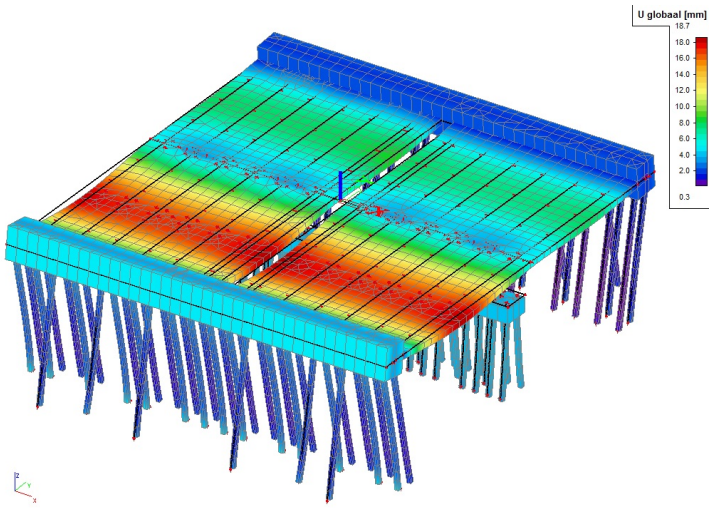

FIGURE C.13: Vertical displacement as a result of self-weight in SCIA

C.3.2. Imposed loads

The asphalt has a minimum height of:

$$d_a = 140 + a \text{ [mm]}$$

With: $a = 0.25 \cdot (\text{L-}30)$ [mm]
$0 \leq a \leq 30$ mm
$L = 19.9$ m

Thus the imposed load is equal to:

$$Q_{ak} = \rho_c \cdot d_a = 23 \cdot 0.14 = 3.22 \text{ kN/m}^2$$

This is shown in Figure C.14.

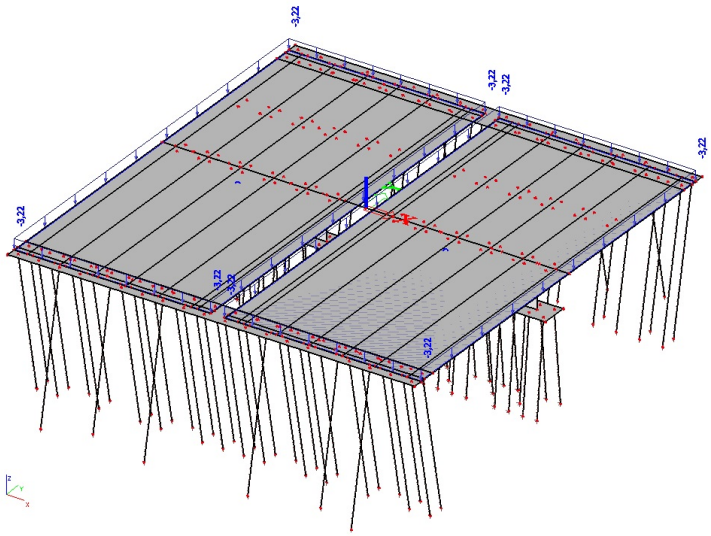

FIGURE C.14: Imposed load from asphalt on the concrete deck in SCIA

C.3.3. Prestressing

Since this SCIA model is used to determine the maximum reaction forces on the foundation piles, the amount of prestressing applied is superfluous information. The prestressing load will not have any influence on the reaction forces, only on the cross-sectional force equilibrium, therefore it has not been determined.

C.3.4. Traffic loads

The total traffic width of the viaduct is equal to the viaduct width minus the two curbs, which have a width of 1.235 m. Thus:

$$w = 18.04 - 2 \cdot 1.235 = 15.57 \text{ m}$$

From Table A.2 in Appendix A it follows that the width of a theoretical traffic lane w_1 is therefore 3.0 m. Thus there are 5 theoretical traffic lanes and the remaining area has a width of 0.57 m.

It is assumed that the most unfavourable effect is obtained if traffic lane 1 is the outer traffic lane. Although this indeed gives the highest absolute reaction forces in the foundation piles, not all foundation piles will be loaded to their maximum. For these values to be known, all possible combinations for traffic lane distribution should be considered, after which the highest load per foundation pile is selected. For reasons of simplicity this difference is neglected.

Two traffic load groups have to be taken into account, namely gr1a and gr2. For gr1a the vertical traffic loads from Table A.3 in Appendix A are valid, whilst for gr2 these vertical loads will have to be multiplied by the frequent transient load factor $\psi_1 = 0.8$ and these are combined with the horizontal load factors:

$Q_{lk1} = 0.6 \cdot \alpha_{Q;1} \cdot 2 \cdot Q_{1k} + 0.1 \cdot \alpha_{q;1} \cdot q_{1k} \cdot w_1 \cdot L_1 = 360 + 1.035 \cdot 3 \cdot 19.9 = 421.79$ kN
$Q_{lk2} = 0.6 \cdot \alpha_{Q;1} \cdot 2 \cdot Q_{1k} + 0.1 \cdot \alpha_{q;1} \cdot q_{1k} \cdot w_1 \cdot L_2 = 360 + 1.035 \cdot 3 \cdot 16.9 = 412.48$ kN
$Q_{lk1+2} = 0.6 \cdot \alpha_{Q;1} \cdot 2 \cdot Q_{1k} + 0.1 \cdot \alpha_{q;1} \cdot q_{1k} \cdot w_1 \cdot L = 360 + 1.035 \cdot 3 \cdot 36.8 = 474.26$ kN

$Q_{trk1} = 0.25 \cdot Q_{lk1} = 105.45$ kN
$Q_{trk2} = 0.25 \cdot Q_{lk2} = 103.12$ kN
$Q_{trk1+2} = 0.25 \cdot Q_{lk1+2} = 118.57$ kN

The two traffic load groups are summarised in Tables C.1, C.2 and C.3.

	gr1a	
	KEL [kN/m²]	UDL [kN/m²]
Lane nr.	$\alpha_{Q;i}Q_{i;k}$	$\alpha_{q;i}q_{i;k}$
1	300	10.35
2	200	3.5
3	100	3.5
> 3	0	3.5
r	0	3.5

TABLE C.1: Vertical traffic loads to be taken into account in load group gr1a

	gr2	
	KEL [kN/m²]	UDL [kN/m²]
Lane nr.	$\alpha_{Q;i}Q_{i;k}$	$\alpha_{q;i}q_{i;k}$
1	240	8.28
2	120	2.8
3	80	2.8
> 3	0	2.8
r	0	2.8

TABLE C.2: Vertical traffic loads to be taken into account in load group gr2

	gr2		
	L_1	L_2	$L = L_1 + L_2$
Q_{lk} [kN]	421.79	412.48	474.26
Q_{trk} [kN]	105.45	103.12	118.57

TABLE C.3: Horizontal traffic loads to be taken into account in load group gr2

Since the purpose of this SCIA model is to determine the maximum reaction forces in the foundation piles, there are three load configurations applied (see Figure C.15).

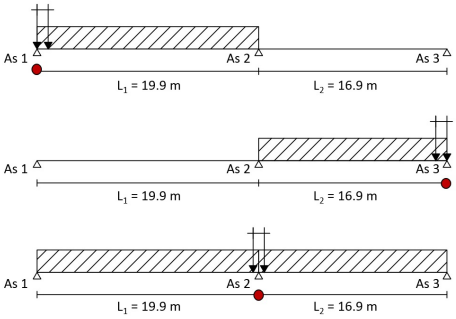

FIGURE C.15: Governing load configuration for the foundation reaction forces in axis 1, 3 and 2 respectively

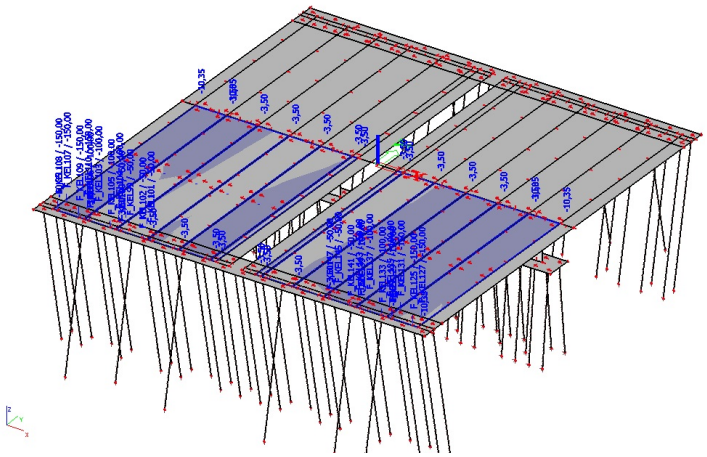

FIGURE C.16: Vertical traffic load from load group gr1a in SCIA

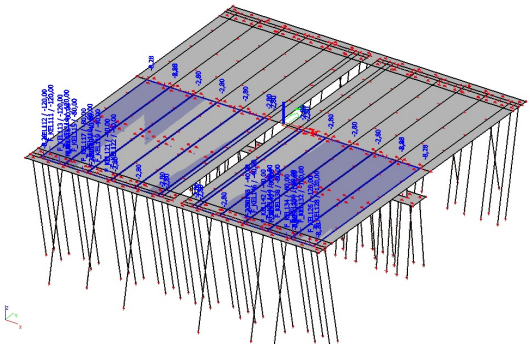

FIGURE C.17: Vertical traffic load from load group gr2 in SCIA

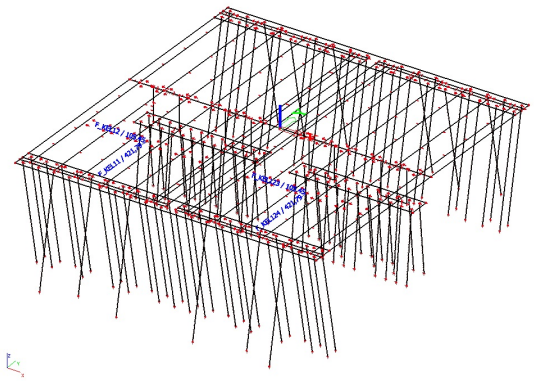

FIGURE C.18: Horizontal traffic load from load group gr2 in SCIA

C.3.5. Earth pressure

Although the abutments are situated below ground level, the influence of horizontal earth pressure is not taken into account for reasons of simplicity.

In reality, however, the horizontal earth pressure can have rather high values, since an extra vertical surface load from traffic on the approach slab has to be considered, leading to an increased horizontal soil stress. This horizontal pressure leads to horizontal forces in the abutment, which will be taken up by the inclined piles. Due to this inclination, the horizontal force will be decomposed into a horizontal and vertical component and thus the overall vertical support reaction of the foundation piles will increase due to the horizontal earth pressure.

C.3.6. Water pressure

There are no significant water pressures acting on the viaduct and thus this is not considered.

C.3.7. Wind load

The A9 Gaasperdammerweg project lies in Wind Area I (see Figure A.17 in Appendix A), in between buildings. The structural deck lies at a height of + 4.85 m NAP, which is taken as the reference height z_e. It then follows from Figure A.18 in Appendix A that the extreme wind pressure is given by:

$$q_p(z_e) = 0.69 \text{ kN/m}^2$$

Furthermore, since the only design situation considered is the user phase (see Appendix A, subsection A.1.6), $c_{fx} = 1.0$. Then:

$$F_{wxk1} = q_p(z_e) \cdot c_{fx} \cdot A_{ref;x1} = 0.69 \cdot 1.0 \cdot 0.58 \cdot 19.9 = 7.96 \text{ kN}$$
$$F_{wxk2} = q_p(z_e) \cdot c_{fx} \cdot A_{ref;x2} = 0.69 \cdot 1.0 \cdot 0.58 \cdot 16.9 = 6.76 \text{ kN}$$

$$F_{wzk1} = q_p(z_e) \cdot c_{fz} \cdot A_{ref;z1} = 0.69 \cdot 0.9 \cdot 18.04 \cdot 19.9 = 222.94 \text{ kN}$$
$$F_{wzk2} = q_p(z_e) \cdot c_{fz} \cdot A_{ref;z2} = 0.69 \cdot 0.9 \cdot 18.04 \cdot 16.9 = 189.33 \text{ kN}$$

If combined with traffic load, the maximum of $\psi_1 \cdot F_{wk}$ or F'_{wk} must be taken, in which:

$$F'_{wk} = F_{wk} \cdot \frac{{v'_{b0}}^2}{{v_{b0}}^2}$$

With: $v_{b0} = 29.5$ m/s (Figure A.17 in Appendix A)
$v'_{b0} = 23.0$ m/s

$$F'_{wk} = 0.61 \cdot F_{wk}$$

The wind loads are summarised in Table C.4.

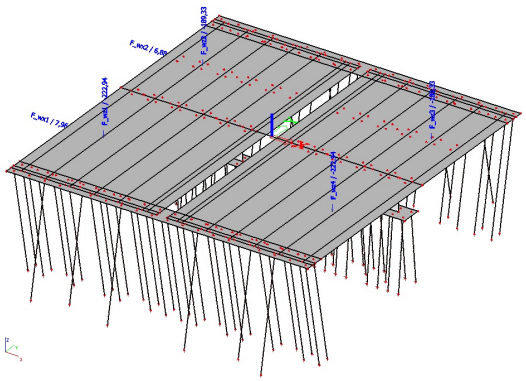

FIGURE C.19: Wind loads acting in horizontal and vertical direction on the concrete deck in SCIA

		L_1	L_2
Fwk [kN]	x-direction	7.96	6.76
F*wk [kN]		4.36	4.12
Fwk [kN]	z-direction	222.94	189.33
F*wk [kN]		135.99	115.49

TABLE C.4: Horizontal and vertical wind loads

C.3.8. Snow load

The fictitious superstructure deck is assumed to be horizontal, although the original structure has a small inclination. Nevertheless, the inclination of the superstructure deck is less than 30° and therefore the snow load can be taken as:

$$Q_{sk} = 0.8 \cdot 1.0 \cdot 1.0 \cdot 0.7 = 0.56 \text{ kN/m}^2$$

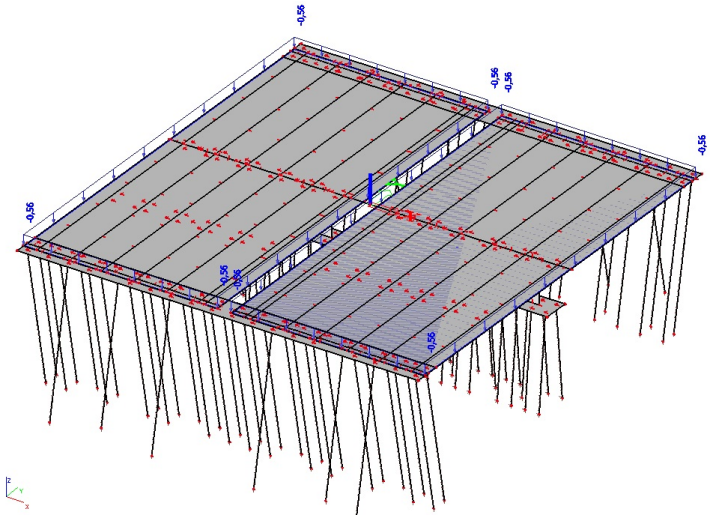

FIGURE C.20: Snow load acting on the concrete deck in SCIA

C.3.9. Collision load

From Appendix A it follows that collision loads can act on either the intermediate support or the superstructure. These loads only have to be taken into account separately, with the following design values:

- Substructure:
  It is assumed that the structure is stiff, giving a maximum collision force of: F_{dx} = 1500 kN and F_{dy} = 750 kN for local roads. The most governing location of impact is given by trucks, with a spread of a = 0.5 m and a height of h = 1.5 m.
- Superstructure:
  As h = 5.0 m, which is higher than h_0 = 4.8 m but lower than h_1 = 7.0 m, F_{dx} must be reduced by a factor r_F *[NEN-EN 1991-1-7-NB, 2015]*:
  $r_F = 1 - \frac{1}{b} \cdot (h - h_0) = 1 - \frac{1}{2.2} \cdot 0.2 = 0.91$
  Thus $F_{dx} = 0.91 \cdot 375 = 341.25$ kN for local roads.

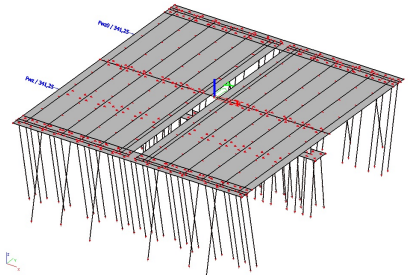

FIGURE C.21: Collision load from traffic acting on the superstructure in SCIA

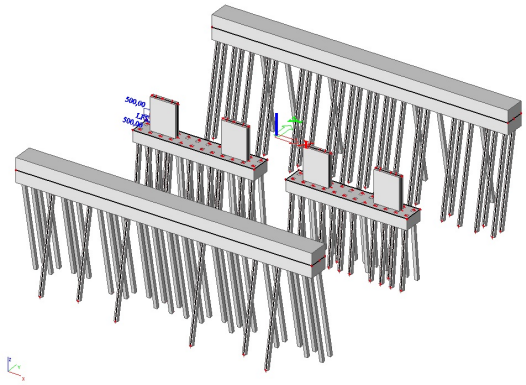

FIGURE C.22: Collision load from traffic acting on the substructure in SCIA

C.4. LOAD COMBINATIONS

The load combinations that that have to be taken into account for a highway viaduct in general are elaborated in Appendix A. All mentioned load combinations are inserted into SCIA Engineer for both the SLS as the ULS.

C.5. RESULTS

In total, three different models were constructed, one for every axis. The resulting maximum displacement and rotation, together with the vertical reaction forces in both SLS and ULS, are given in Figures C.23 to C.28 and Table C.5 for axes 1, 2 and 3.

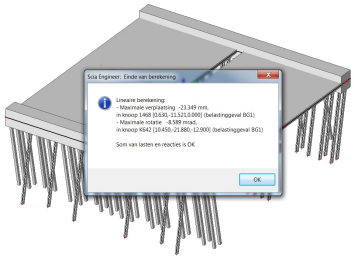

FIGURE C.23: Maximal displacement and rotation for governing load on axis 1

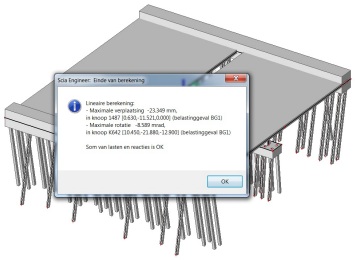

FIGURE C.24: Maximal displacement and rotation for governing load on axis 2

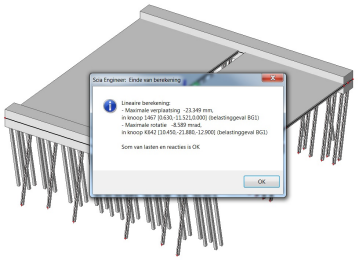

FIGURE C.25: Maximal displacement and rotation for governing load on axis 3

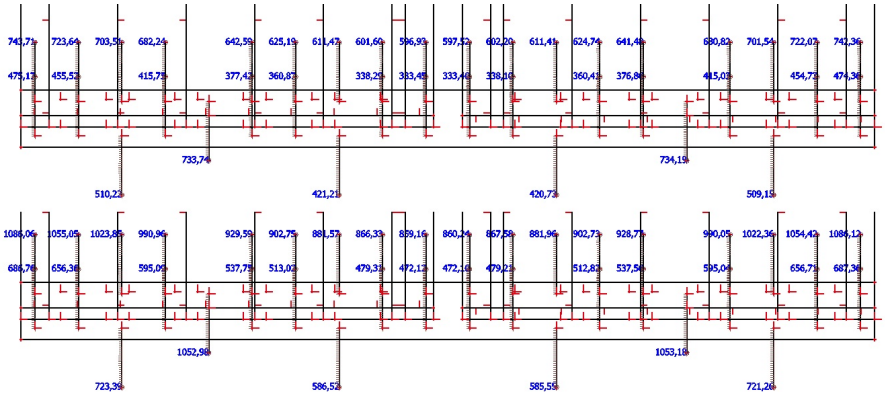

FIGURE C.26: Vertical reaction forces on the piles in axis 1 in SLS (top) and ULS (bottom)

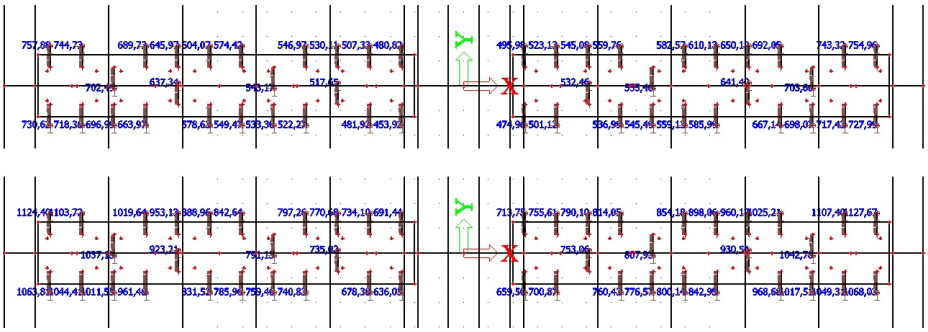

FIGURE C.27: Vertical reaction forces on the piles in axis 2 in SLS (top) and ULS (bottom)

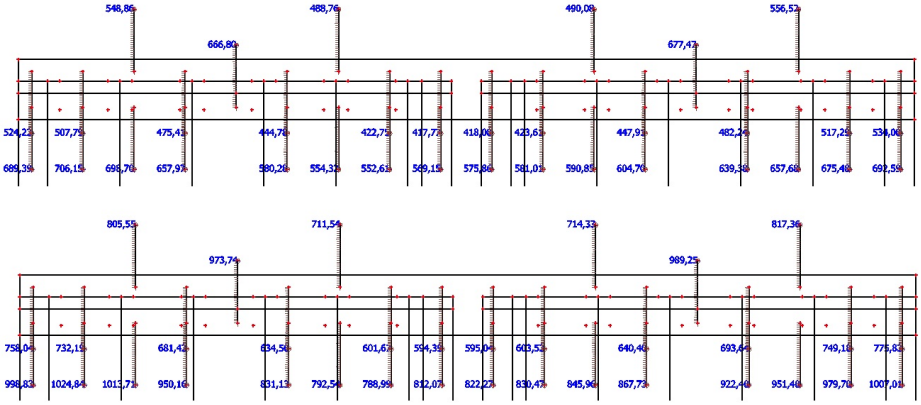

FIGURE C.28: Vertical reaction forces on the piles in axis 3 in SLS (top) and ULS (bottom)

Axis 1			
Pile number		Load action [kN]	
In SCIA	In pile plan	SLS	ULS
Sn1	1	479,89	693,74
Sn2	2	738,88	1078,90
Sn3	3	460,27	663,37
Sn4	4	718,82	1047,88
Sn5	5	512,97	727,51
Sn6	6	698,69	1016,70
Sn8	7	420,54	602,01
Sn7	8	677,47	983,88
Sn10	9	727,04	1043,08
Sn11	10	382,24	544,72
Sn12	11	637,87	922,60
Sn13	12	365,69	520,00
Sn14	13	620,51	895,81
Sn15	14	424,03	590,66
Sn16	15	606,80	874,64
Sn17	16	343,11	486,28
Sn18	17	596,93	859,41
Sn19	18	338,27	479,09
Sn20	19	592,29	852,28
Sn104	20	338,22	479,08
Sn105	21	592,87	853,34
Sn102	22	342,92	486,19
Sn103	23	597,55	860,69
Sn100	24	423,57	589,70
Sn101	25	606,76	875,06
Sn98	26	365,24	519,80
Sn99	27	620,08	895,81
Sn96	28	381,68	544,54
Sn97	29	636,80	921,83
Sn95	30	727,49	1043,29
Sn93	31	419,83	601,98
Sn94	32	676,10	983,04
Sn91	33	511,90	725,39
Sn92	34	696,79	1015,31
Sn89	35	459,47	663,73
Sn90	36	717,29	1047,32
Sn87	37	479,08	694,35
Sn88	38	737,55	1078,97

Axis 2			
Pile number		Load action [kN]	
In SCIA	In pile plan	SLS	ULS
Sn63	39	731,92	1065,70
Sn64	40	758,35	1125,02
Sn65	41	719,75	1046,43
Sn66	42	745,29	1104,48
Sn67	43	698,47	1013,69
Sn68	44	703,53	1038,59
Sn69	45	665,51	963,62
Sn70	46	690,44	1020,63
Sn71	47	638,54	924,97
Sn72	48	646,74	954,20
Sn73	49	580,25	833,88
Sn74	50	604,89	890,12
Sn75	51	551,17	788,45
Sn76	52	575,33	843,94
Sn77	53	535,11	762,11
Sn78	54	544,56	793,11
Sn79	55	524,20	743,65
Sn80	56	548,12	798,90
Sn81	57	519,29	737,46
Sn82	58	531,34	772,46
Sn83	59	483,99	681,33
Sn84	60	508,59	735,96
Sn85	61	456,02	639,13
Sn86	62	482,08	693,34
Sn128	63	477,07	662,62
Sn129	64	497,37	715,77
Sn126	65	503,20	703,95
Sn127	66	524,48	757,57
Sn124	67	534,16	755,59
Sn125	68	546,37	791,96
Sn122	69	538,94	763,29
Sn123	70	560,96	815,78
Sn120	71	547,33	779,26
Sn121	72	556,83	809,96
Sn118	73	560,86	802,67
Sn119	74	583,52	855,54
Sn116	75	587,64	845,36
Sn117	76	610,99	899,28
Sn114	77	642,63	932,34
Sn115	78	650,92	961,29
Sn112	79	668,71	970,96
Sn113	80	692,80	1026,25
Sn110	81	699,58	1019,69
Sn111	82	704,73	1044,27
Sn108	83	718,86	1051,38
Sn109	84	743,90	1108,18
Sn106	85	729,33	1069,96
Sn107	86	755,46	1128,30

Axis 3			
Pile number		Load action [kN]	
In SCIA	In pile plan	SLS	ULS
Sn45	87	685,89	993,81
Sn46	88	527,58	762,98
Sn47	89	701,54	1018,04
Sn49	90	511,13	737,08
Sn48	91	693,76	1006,36
Sn50	92	550,34	807,70
Sn51	93	653,82	944,06
Sn53	94	478,73	686,27
Sn52	95	661,70	966,33
Sn55	96	577,88	827,67
Sn57	97	448,06	639,19
Sn56	98	552,65	790,14
Sn58	99	490,18	713,54
Sn59	100	550,50	785,95
Sn61	101	425,97	606,29
Sn60	102	565,81	807,27
Sn62	103	420,99	599,00
Sn145	104	572,33	817,17
Sn146	105	421,30	599,65
Sn143	106	577,47	825,35
Sn144	107	426,84	608,13
Sn141	108	587,29	840,83
Sn142	109	491,46	716,27
Sn140	110	601,12	862,56
Sn139	111	451,14	644,99
Sn138	112	672,01	981,30
Sn136	113	635,75	917,13
Sn137	114	485,43	698,27
Sn135	115	654,01	946,07
Sn134	116	557,81	819,19
Sn132	117	671,76	974,31
Sn133	118	520,41	753,70
Sn130	119	688,83	1011,55
Sn131	120	537,09	780,30

TABLE C.5: Vertical reaction forces on the piles in axis 1, 2 and 3 for both SLS and ULS, following from SCIA

D

CASE A9: INPUT D-FOUNDATIONS

D-Foundations is a program written by Deltares that allows for 'CPT based foundation engineering'. It enables the design of piled and shallow foundations, according to the current Eurocode NEN-EN 1997-1 *[NEN-EN 1997-1, 2016]* and both the Dutch and Belgium National Annex. It has a simple layout, which is shown in Figure D.1 and by moving along the options in sequence, a foundation can be easily designed.
In section D.1, this will be done for the case study A9 Gaasperdammerweg. Adaptations needed for the several calculation levels as discussed in Appendix B are mentioned in section D.2 and in section D.3 all results will be assembled. Finally, in section D.4 the CPT sets are presented.

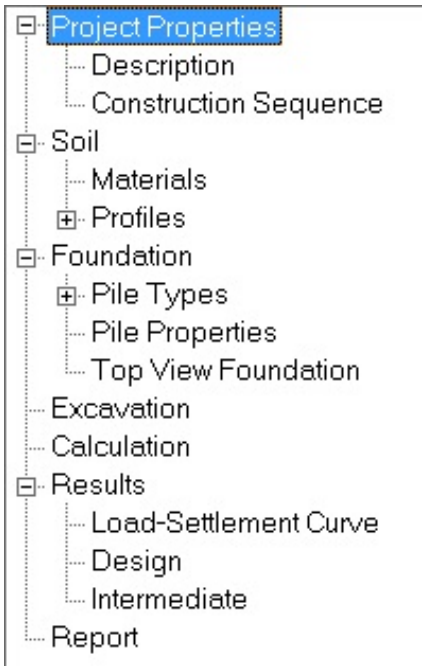

FIGURE D.1: Tree view of model input D-Foundations

D.1. INPUT D-FOUNDATIONS MODEL

D.1.1. Project properties

Description:
In this window, a description can be added regarding the project, such as a Title and a Project ID. This is merely meant for documentation and will not be further discussed.

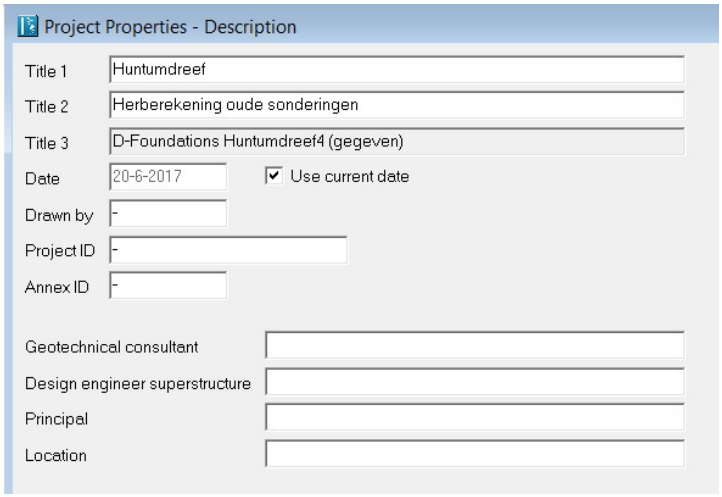

FIGURE D.2: Description window in D-Foundations

Construction sequence:
The construction sequence might lead to certain exceptions in Eurocode 7, therefore it must be given as input. Since in this case study no preliminary excavations have taken place before performing the CPTs, the following option is chosen:

- CPT – Excavation – Install

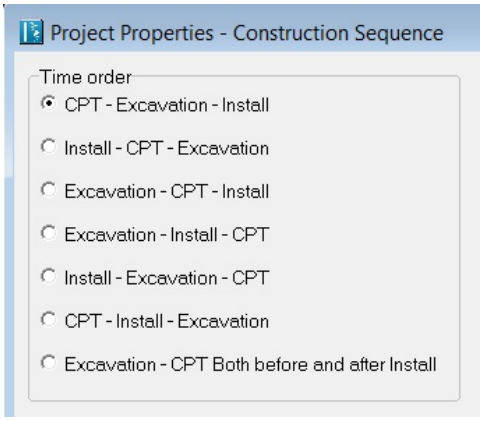

FIGURE D.3: Construction sequence in D-Foundations

D.1.2. Soil

Materials:
A table containing the possible soil materials and their corresponding parameters is given as a default from the Dutch National Annex. Since there is no reason to expect large differences in soil materials in this specific case study, no additional materials have been added.

Profiles:
In this option, CPT profiles are added, in this case from GEF files provided by the project (see section D.4). For the bearing capacity of the old CPT set, CPTs E01 to E09 are added and E01 is presented as an example in Figures D.5 to D.7.
Since these are mechanical CPTs, only the cone resistance is measured and thus the CPT rule used to determine the soil layers is: 'q_c only Rule'. This however generates soil materials according to the Belgium Annex, and thus these materials have to be transferred into Dutch materials. For this conversion the soil densities are the main parameter, since this gives the horizontal soil stress and thus the positive and negative shaft friction.

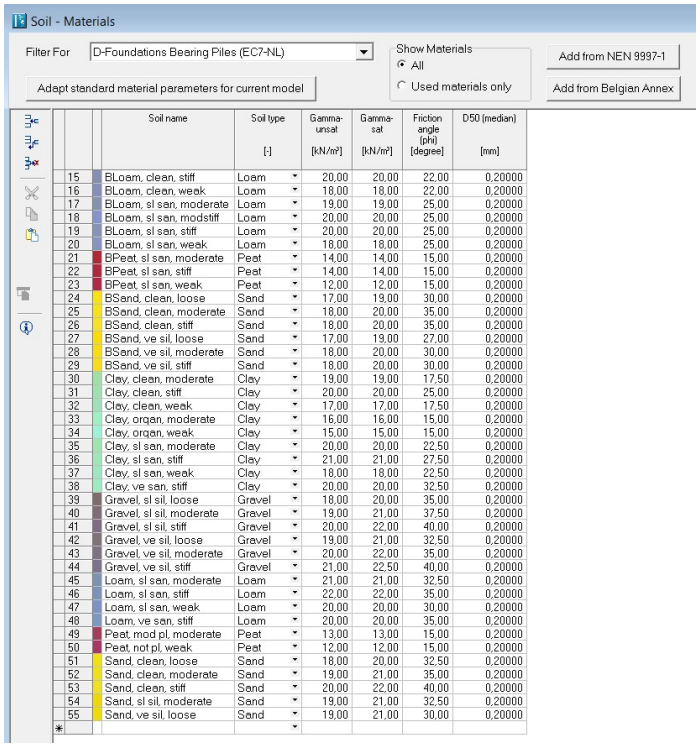

		Soil name	Soil type [-]	Gamma-unsat [kN/m³]	Gamma-sat [kN/m³]	Friction angle (phi) [degree]	D50 (median) [mm]
15		BLoam, clean, stiff	Loam	20,00	20,00	22,00	0,20000
16		BLoam, clean, weak	Loam	18,00	18,00	22,00	0,20000
17		BLoam, sl san, moderate	Loam	19,00	19,00	25,00	0,20000
18		BLoam, sl san, modstiff	Loam	20,00	20,00	25,00	0,20000
19		BLoam, sl san, stiff	Loam	20,00	20,00	25,00	0,20000
20		BLoam, sl san, weak	Loam	18,00	18,00	25,00	0,20000
21		BPeat, sl san, moderate	Peat	14,00	14,00	15,00	0,20000
22		BPeat, sl san, stiff	Peat	14,00	14,00	15,00	0,20000
23		BPeat, sl san, weak	Peat	12,00	12,00	15,00	0,20000
24		BSand, clean, loose	Sand	17,00	19,00	30,00	0,20000
25		BSand, clean, moderate	Sand	18,00	20,00	35,00	0,20000
26		BSand, clean, stiff	Sand	18,00	20,00	35,00	0,20000
27		BSand, ve sil, loose	Sand	17,00	19,00	27,00	0,20000
28		BSand, ve sil, moderate	Sand	18,00	20,00	30,00	0,20000
29		BSand, ve sil, stiff	Sand	18,00	20,00	30,00	0,20000
30		Clay, clean, moderate	Clay	19,00	19,00	17,50	0,20000
31		Clay, clean, stiff	Clay	20,00	20,00	25,00	0,20000
32		Clay, clean, weak	Clay	17,00	17,00	17,50	0,20000
33		Clay, organ, moderate	Clay	16,00	16,00	15,00	0,20000
34		Clay, organ, weak	Clay	15,00	15,00	15,00	0,20000
35		Clay, sl san, moderate	Clay	20,00	20,00	22,50	0,20000
36		Clay, sl san, stiff	Clay	21,00	21,00	27,50	0,20000
37		Clay, sl san, weak	Clay	18,00	18,00	22,50	0,20000
38		Clay, ve san, stiff	Clay	20,00	20,00	32,50	0,20000
39		Gravel, sl sil, loose	Gravel	18,00	20,00	35,00	0,20000
40		Gravel, sl sil, moderate	Gravel	19,00	21,00	37,50	0,20000
41		Gravel, sl sil, stiff	Gravel	20,00	22,00	40,00	0,20000
42		Gravel, ve sil, loose	Gravel	19,00	21,00	32,50	0,20000
43		Gravel, ve sil, moderate	Gravel	20,00	22,00	35,00	0,20000
44		Gravel, ve sil, stiff	Gravel	21,00	22,50	40,00	0,20000
45		Loam, sl san, moderate	Loam	21,00	21,00	32,50	0,20000
46		Loam, sl san, stiff	Loam	22,00	22,00	35,00	0,20000
47		Loam, sl san, weak	Loam	20,00	20,00	30,00	0,20000
48		Loam, ve san, stiff	Loam	20,00	20,00	35,00	0,20000
49		Peat, mod pl, moderate	Peat	13,00	13,00	15,00	0,20000
50		Peat, not pl, weak	Peat	12,00	12,00	15,00	0,20000
51		Sand, clean, loose	Sand	18,00	20,00	32,50	0,20000
52		Sand, clean, moderate	Sand	19,00	21,00	35,00	0,20000
53		Sand, clean, stiff	Sand	20,00	22,00	40,00	0,20000
54		Sand, sl sil, moderate	Sand	19,00	21,00	32,50	0,20000
55		Sand, ve sil, loose	Sand	19,00	21,00	30,00	0,20000

FIGURE D.4: List of materials in D-Foundations

The default minimum layer thickness is kept at 0.10 m. Furthermore, the coordinates of the CPT are inserted. These coordinates are based on the centre of the existing pile plan, which is located at x, y = 0,0 [m]. An overview of all old CPT set coordinates is given in Table D.1.

CPT	x [m]	y [m]
E01	-19.59	17.00
E02	-20.59	-0.84
E03	-20.34	-18.18
E04	0.43	17.53
E05	-0.24	-0.44
E06	0.00	-18.00
E07	17.16	17.32
E08	16.80	0.32
E09	16.78	-18.12

TABLE D.1: Coordinates of all CPT samples from the old CPT set, with the centre of the existing pile plan at x, y = 0,0 [m]

There is also some additional data required, as can be seen in Figure D.6:

- The phreatic level is taken from *[IXAS, 2015]*, as -2.70 [m];
- The pile tip level must be taken at -10.65 m for axes 1 and 3, and at -10.50 m for axis 2;
- The over-consolidation ratio of the bearing layer is kept at 1.00 [-];
- The top of the positive skin friction zone is taken at the top of the bearing sand layer. This is conservative, since higher positioned sand layers may also have a positive effect on the skin friction, but this depends on the settlement of weak layers that are positioned in between;
- The bottom of the negative skin friction zone is taken at the same level as the top of the positive skin friction zone. This is thus a conservative assumption as well;
- The expected ground level settlement is kept at 0.11 [m], the recommended value from D-foundations.

At last, a summary of the pressures over the height is given for each CPT (Figure D.7).

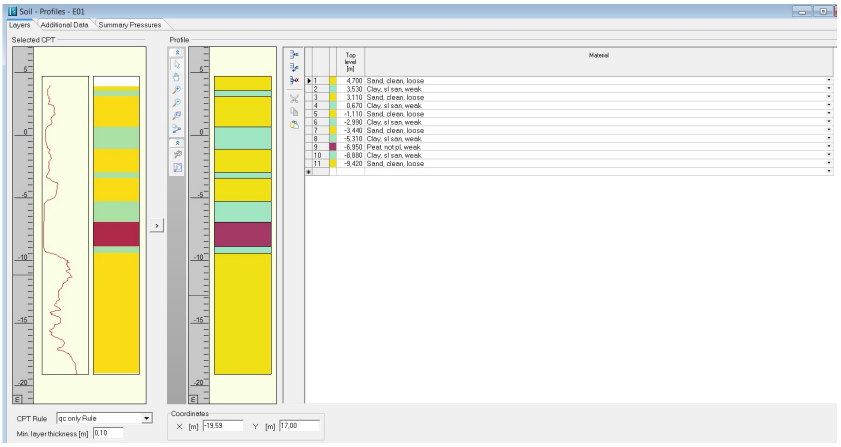

FIGURE D.5: Profile layer of CPT E01 in D-Foundations

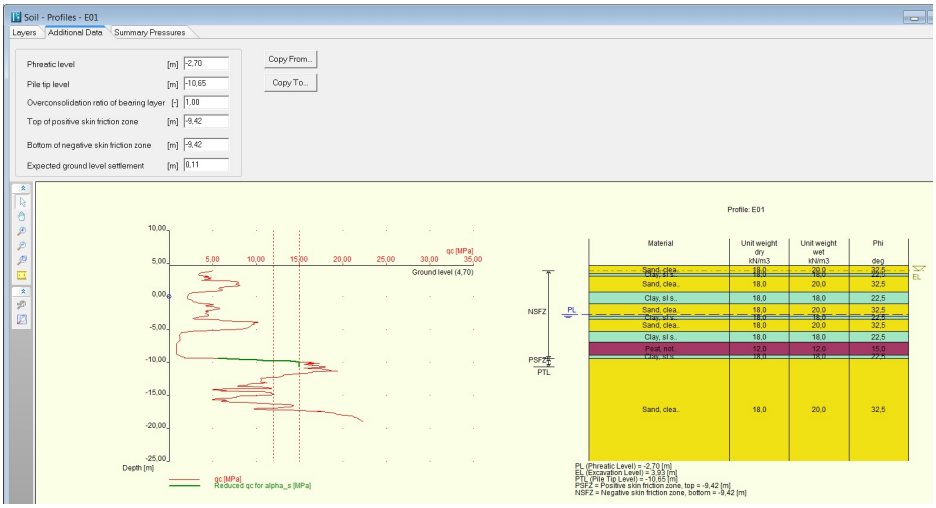

FIGURE D.6: Additional information required for CPT E01 in D-Foundations

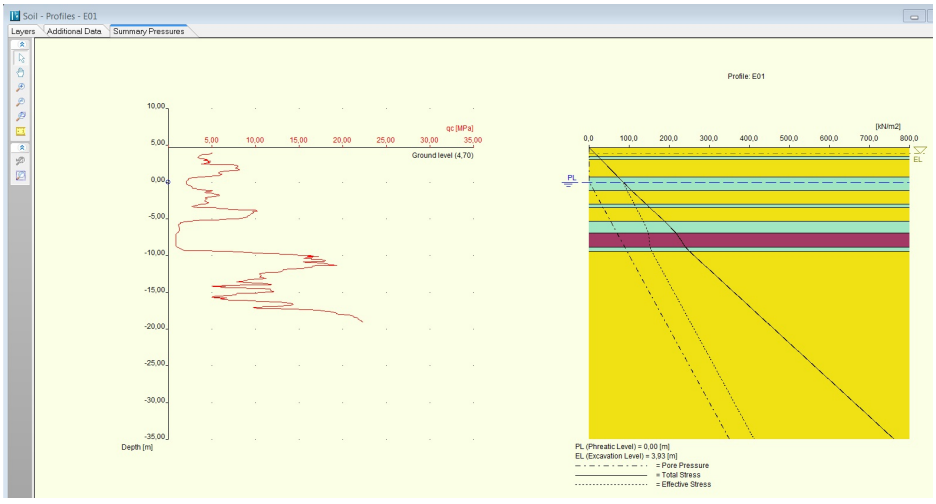

FIGURE D.7: Pressure distribution profile of CPT E01 in D-Foundations

D.1.3. Foundation

Pile types:

From the possible pile types, a rectangular straight pile is chosen with a base width a = 0.380 m and a base

length b = 0.380 m. By selecting a prefabricated concrete pile as pile type, the accompanying α-factors for shaft and pile tip resistance are automatically generated. In the current Eurocode, the α_p factor is reduced to 0.7 for prefabricated concrete piles.
No further adaptations are needed to the default settings.

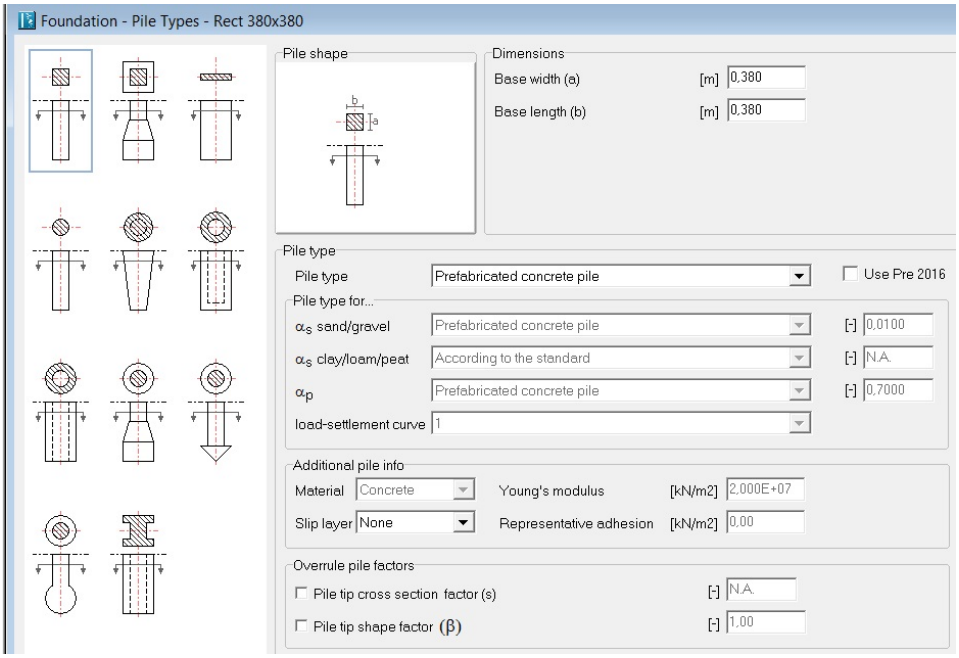

FIGURE D.8: Pile types in D-Foundations

Pile properties:
In this window, all piles can be defined by coordinates and their PTL. Again, the coordinates are based on the centre of the existing pile plan, which is located at x, y = 0,0 [m]. A summary of all piles is given in Table D.2. For the calculation of the bearing capacity of the existing pile plan, based on the CPTs, the load action on each pile is superfluous information and therefore not included.

Top view foundation:
The CPTs and pile plan have been inserted. To check whether this has been done correctly, the top view can be consulted.

D.1.4. Excavation
In this case study, no excavation is performed. Therefore this window is skipped.

D.1.5. Calculation
The calculation window is used to determine additional data required for calculation and the type of calculation (Figure D.11).

- It is assumed that the fictitious superstructure behaves as a non-rigid structure.
- The maximum allowed settlement and relative rotation for both ULS and SLS are taken directly from Eurocode 7 by D-Foundations and there is no reason to change these values:

	ULS	**SLS**
Maximum settlement [mm]	150	150
Maximum relative rotation [-]	1:100	1:300

- In the overrule parameters some changes are made based on the Eurocode 7 and the amount of CPTs performed. The γ_b and γ_s factors are obtained from Table D.3, $\gamma_{f;nk}$ is obtained from article 7.3.2.2 and the ξ-factors from Table D.4. Since there are 9 CPTs in the old CPT set, ξ_3 = 1.255 and ξ_4 = 1.0025.

	Name	X [m]	Y [m]	Pile head level [m R.L.]	Surcharge [kN/m2]	Limit state STR/GEO [kN]	Serviceability Limit state [kN]
▶	1	-20,50	-18,11	2,00	0,00	0,00	0,00
	2	-20,50	-16,21	2,00	0,00	0,00	0,00
	3	-20,50	-14,31	2,00	0,00	0,00	0,00
	4	-20,50	-12,41	2,00	0,00	0,00	0,00
	6	-20,50	-8,61	2,00	0,00	0,00	0,00
	7	-20,50	-6,71	2,00	0,00	0,00	0,00
	8	-20,50	-4,81	2,00	0,00	0,00	0,00
	9	-20,50	-2,91	2,00	0,00	0,00	0,00
	10	-20,50	-1,01	2,00	0,00	0,00	0,00
	11	-20,50	0,89	2,00	0,00	0,00	0,00
	12	-20,50	2,79	2,00	0,00	0,00	0,00
	13	-20,50	4,69	2,00	0,00	0,00	0,00
	14	-20,50	6,59	2,00	0,00	0,00	0,00
	15	-20,50	8,49	2,00	0,00	0,00	0,00
	17	-20,50	12,29	2,00	0,00	0,00	0,00
	18	-20,50	14,19	2,00	0,00	0,00	0,00
	19	-20,50	16,09	2,00	0,00	0,00	0,00
	20	-20,50	17,99	2,00	0,00	0,00	0,00
	21	-19,00	-18,11	2,00	0,00	0,00	0,00
	22	-19,00	-16,21	2,00	0,00	0,00	0,00
	23	-19,00	-14,31	2,00	0,00	0,00	0,00
	24	-19,00	-12,41	2,00	0,00	0,00	0,00
	25	-19,00	-10,51	2,00	0,00	0,00	0,00
	26	-19,00	-8,61	2,00	0,00	0,00	0,00
	27	-19,00	-6,71	2,00	0,00	0,00	0,00
	28	-19,00	-4,81	2,00	0,00	0,00	0,00
	29	-19,00	-2,91	2,00	0,00	0,00	0,00
	30	-19,00	-1,01	2,00	0,00	0,00	0,00
	31	-19,00	0,89	2,00	0,00	0,00	0,00
	32	-19,00	2,79	2,00	0,00	0,00	0,00
	33	-19,00	4,69	2,00	0,00	0,00	0,00
	34	-19,00	6,59	2,00	0,00	0,00	0,00
	35	-19,00	8,49	2,00	0,00	0,00	0,00
	36	-19,00	10,39	2,00	0,00	0,00	0,00
	37	-19,00	12,29	2,00	0,00	0,00	0,00
	38	-19,00	14,19	2,00	0,00	0,00	0,00
	39	-19,00	16,09	2,00	0,00	0,00	0,00
	40	-19,00	17,99	2,00	0,00	0,00	0,00
	41	-0,75	2,50	2,00	0,00	0,00	0,00
	42	-0,75	3,80	2,00	0,00	0,00	0,00
	43	-0,75	5,10	2,00	0,00	0,00	0,00
	44	-0,75	6,40	2,00	0,00	0,00	0,00
	45	-0,75	7,70	2,00	0,00	0,00	0,00
	46	-0,75	9,00	2,00	0,00	0,00	0,00
	47	-0,75	10,30	2,00	0,00	0,00	0,00
	48	-0,75	11,60	2,00	0,00	0,00	0,00
	49	-0,75	12,90	2,00	0,00	0,00	0,00
	50	-0,75	14,20	2,00	0,00	0,00	0,00
	51	-0,75	15,50	2,00	0,00	0,00	0,00
	52	-0,75	16,80	2,00	0,00	0,00	0,00
	53	0,75	2,50	2,00	0,00	0,00	0,00
	54	0,75	3,80	2,00	0,00	0,00	0,00
	55	0,75	5,10	2,00	0,00	0,00	0,00
	56	0,75	6,40	2,00	0,00	0,00	0,00
	57	0,75	7,70	2,00	0,00	0,00	0,00
	58	0,75	9,00	2,00	0,00	0,00	0,00
	59	0,75	10,30	2,00	0,00	0,00	0,00

- In order to obtain the bearing capacity of a pile based on the different CPTs, a preliminary design calculation must be performed, with the bearing capacity at fixed pile tip levels as a result.

D.1.6. Results

In this window the results are presented from the calculation performed above. In case of a preliminary design, only the 'Design' option generates output. For this case study, the result is given in Figures D.12 and D.13 for PTLs -10.65 m and -10.50 m NAP respectively.

D.2. ADAPTATIONS GEOTECHNICAL ANALYSIS

In Appendix B, a geotechnical analysis is performed on the reuse of existing foundations, by considering six different calculation levels. For almost each level, adaptations have to be made to the D-Foundations model:

- Level I:
  No adaptations, the model input described in section D.1 is valid for this level.
- Level II:
  No adaptations, the model input described in section D.1 is valid for this level.
- Level III:
  To determine the influence of α_p on the overall bearing capacity of the foundation, a comparison is made with the previous value of α_p = 1.0. This is done by checking the box 'Use Pre 2016' in the window Foundation – Pile Types. The value of α_p now changes automatically to 1.0.
  To determine the influence of the densification factor f_1, the bearing capacity at fixed pile tip levels must be taken from the model results. There are however no changes to the model input.
  It is also interesting to look at the governing CPT taken into account. This has no influence how-

60	0,75	11,60	2,00	0,00	0,00	0,00
61	0,75	12,90	2,00	0,00	0,00	0,00
62	0,75	14,20	2,00	0,00	0,00	0,00
63	0,75	15,50	2,00	0,00	0,00	0,00
64	0,75	16,80	2,00	0,00	0,00	0,00
65	-0,75	-16,80	2,00	0,00	0,00	0,00
66	-0,75	-15,50	2,00	0,00	0,00	0,00
67	-0,75	-14,20	2,00	0,00	0,00	0,00
68	-0,75	-12,90	2,00	0,00	0,00	0,00
69	-0,75	-11,60	2,00	0,00	0,00	0,00
70	-0,75	-10,30	2,00	0,00	0,00	0,00
71	-0,75	-9,00	2,00	0,00	0,00	0,00
72	-0,75	-7,70	2,00	0,00	0,00	0,00
73	-0,75	-6,40	2,00	0,00	0,00	0,00
74	-0,75	-5,10	2,00	0,00	0,00	0,00
75	-0,75	-3,80	2,00	0,00	0,00	0,00
76	-0,75	-2,50	2,00	0,00	0,00	0,00
77	0,75	-16,80	2,00	0,00	0,00	0,00
78	0,75	-15,50	2,00	0,00	0,00	0,00
79	0,75	-14,20	2,00	0,00	0,00	0,00
80	0,75	-12,90	2,00	0,00	0,00	0,00
81	0,75	-11,60	2,00	0,00	0,00	0,00
82	0,75	-10,30	2,00	0,00	0,00	0,00
83	0,75	-9,00	2,00	0,00	0,00	0,00
84	0,75	-7,70	2,00	0,00	0,00	0,00
85	0,75	-6,40	2,00	0,00	0,00	0,00
86	0,75	-5,10	2,00	0,00	0,00	0,00
87	0,75	-3,80	2,00	0,00	0,00	0,00
88	0,75	-2,50	2,00	0,00	0,00	0,00
89	16,04	-18,11	2,00	0,00	0,00	0,00
90	16,04	-15,98	2,00	0,00	0,00	0,00
91	16,04	-13,85	2,00	0,00	0,00	0,00
92	16,04	-11,72	2,00	0,00	0,00	0,00
93	16,04	-9,59	2,00	0,00	0,00	0,00
94	16,04	-7,46	2,00	0,00	0,00	0,00
95	16,04	-5,33	2,00	0,00	0,00	0,00
96	16,04	-3,20	2,00	0,00	0,00	0,00
97	16,04	-1,07	2,00	0,00	0,00	0,00
98	16,04	1,06	2,00	0,00	0,00	0,00
99	16,04	3,19	2,00	0,00	0,00	0,00
100	16,04	5,32	2,00	0,00	0,00	0,00
101	16,04	7,45	2,00	0,00	0,00	0,00
102	16,04	9,58	2,00	0,00	0,00	0,00
103	16,04	11,71	2,00	0,00	0,00	0,00
104	16,04	13,84	2,00	0,00	0,00	0,00
105	16,04	15,97	2,00	0,00	0,00	0,00
106	16,04	18,10	2,00	0,00	0,00	0,00
107	17,54	-18,11	2,00	0,00	0,00	0,00
108	17,54	-15,98	2,00	0,00	0,00	0,00
109	17,54	-13,85	2,00	0,00	0,00	0,00
110	17,54	-11,72	2,00	0,00	0,00	0,00
112	17,54	-7,46	2,00	0,00	0,00	0,00
113	17,54	-5,33	2,00	0,00	0,00	0,00
114	17,54	-3,20	2,00	0,00	0,00	0,00
115	17,54	-1,07	2,00	0,00	0,00	0,00
116	17,54	1,06	2,00	0,00	0,00	0,00
117	17,54	3,19	2,00	0,00	0,00	0,00
118	17,54	5,32	2,00	0,00	0,00	0,00
119	17,54	7,45	2,00	0,00	0,00	0,00
121	17,54	11,71	2,00	0,00	0,00	0,00
122	17,54	13,84	2,00	0,00	0,00	0,00
123	17,54	15,97	2,00	0,00	0,00	0,00
124	17,54	18,10	2,00	0,00	0,00	0,00

TABLE D.2: Pile types in D-Foundations

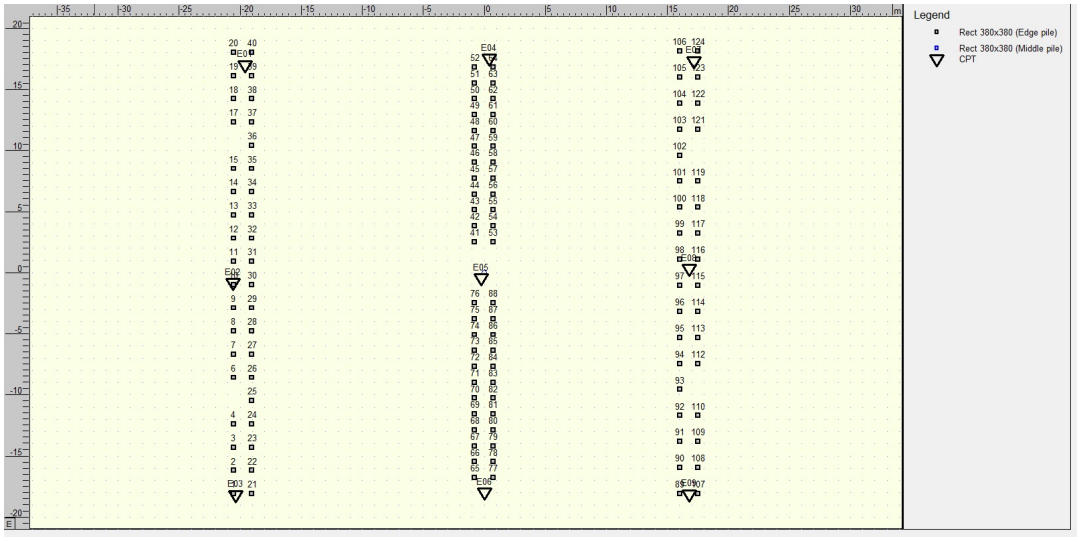

FIGURE D.9: Top view foundation in D-Foundations

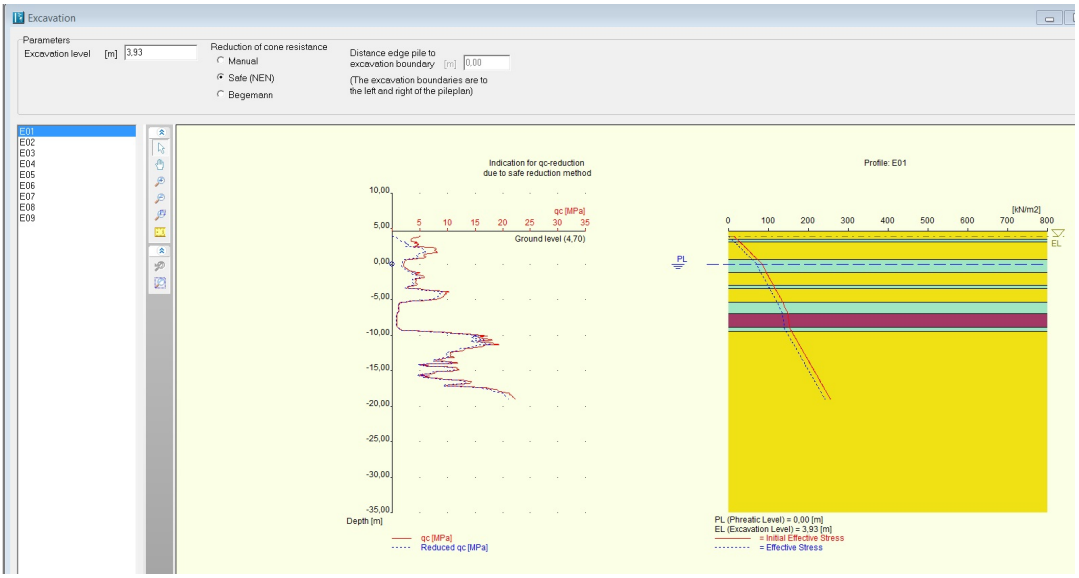

FIGURE D.10: Excavation window in D-Foundations

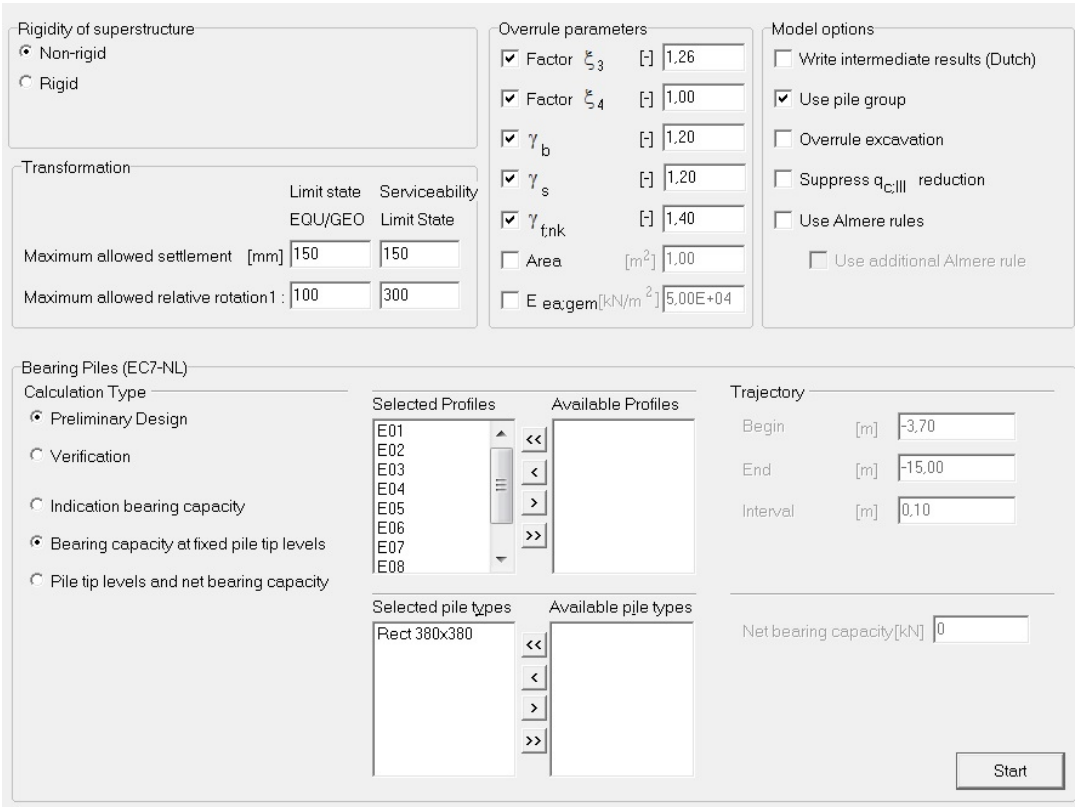

FIGURE D.11: Calculation window in D-Foundations

ever on the model input.

- Level IV:

  The newly preformed CPT set must be added to the old CPT set in the model, accompanied by the same input as described in subsection D.1.2. Furthermore, in the calculation window, the factors ξ_3 and ξ_4 change due to a higher amount of CPTs. In this case, the increase is minimal, since there were already 9 CPTs available and the maximum amount is equal to 10.
  Again, the choice for governing CPT does not influence the model input.

Weerstand	Symbool	Combinatie					
		R1	R2	R3			R4
Punt	γ_b	N.v.t.	N.v.t.	1,4 [a]	1,8 [b]	1,2 [c]	1,15 [d]	N.v.t.
Schacht (op druk)	γ_s	N.v.t.	N.v.t.	1,4 [a]	1,8 [b]	1,2 [c]	1,15 [d]	N.v.t.
Totaal/gecombineerd (op druk)	γ_t	N.v.t.	N.v.t.	1,4 [a]	1,8 [b]	1,2 [c]	1,15 [d]	N.v.t.
Schacht (op trek)	γ_{st}	N.v.t.	N.v.t.	–	–	1,35 [c]	1,25 [d]	N.v.t.

[a] Zonder onderzoek; hierbij moet gebruik zijn gemaakt van slagdiagrammen die bij het heien zijn opgenomen om de draagkracht te beoordelen.
[b] Zonder onderzoek.
[c] Afgeleid uit proefbelastingen of berekend uit sonderingen.
[d] Voor palen die zijn proefbelast.

TABLE D.3: γ-factors to be considered for calculations in D-Foundations

Correlatiefactoren ξ voor een niet-stijf bouwwerk							
ξ voor n =	1	2	3	4	5	7	10
ξ_3	1,39	1,32	1,30	1,28	1,28	1,27	1,25
ξ_4	1,39	1,32	1,30	1,03	1,03	1,01	1,00

TABLE D.4: ξ-factors to be considered for calculations in D-Foundations

D-Foundations, version 16.1.2.2
File : D:\Mijn Documenten\Merijn Stap - afstuderen\Afstuderen\4. Research Study (23-2 to ...)\2) Foundations\05) D-Foundations\Huntumdreef old
Date : 21-6-2017

Results of the option Preliminary Design, Bearing capacity at fixed pile tip levels

Results for pile type :
Rect 380x380

CPT name	Level [m R.L.]	Groundlevel [m R.L.]	Rb;cal;max [kN]	Rs;cal;max [kN]	Rc;cal;max [kN]	Rc;d [kN]	F;nst;rep [kN]	Fnst;d [kN]
E01	-10.65	4,70	833	238	1070	708	439	615
E02	-10.65	4,84	669	296	965	638	412	577
E03	-10.65	4,69	527	294	821	543	402	563
E04	-10.65	-1,13	1035	294	1329	879	86	121
E05	-10.65	-1,11	681	278	959	634	92	129
E06	-10.65	-1,07	572	265	837	554	83	116
E07	-10.65	4,79	621	190	810	536	429	601
E08	-10.65	5,03	1162	335	1497	990	418	585
E09	-10.65	5,00	1212	441	1654	1094	378	529

End of data

FIGURE D.12: Results for the bearing capacities of piles with a PTL at -10.65 m NAP in D-Foundations

D-Foundations, version 16.1.2.2
File : D:\Mijn Documenten\Merijn Stap - afstuderen\Afstuderen\4. Research Study (23-2 to ...)\2) Foundations\05) D-Foundations\Huntumdreef old
Date : 21-6-2017

Results of the option Preliminary Design, Bearing capacity at fixed pile tip levels

Results for pile type :
Rect 380x380

CPT name	Level [m R.L.]	Groundlevel [m R.L.]	Rb;cal;max [kN]	Rs;cal;max [kN]	Rc;cal;max [kN]	Rc;d [kN]	F;nst;rep [kN]	Fnst;d [kN]
E01	-10.50	4,70	879	204	1082	716	439	615
E02	-10.50	4,84	663	269	931	616	412	577
E03	-10.50	4,69	639	268	907	600	402	563
E04	-10.50	-1,13	1003	241	1244	823	86	121
E05	-10.50	-1,11	673	250	924	611	92	129
E06	-10.50	-1,07	577	231	808	534	83	116
E07	-10.50	4,79	655	162	818	541	429	601
E08	-10.50	5,03	1119	301	1420	939	418	585
E09	-10.50	5,00	1188	407	1595	1055	378	529

End of data

FIGURE D.13: Results for the bearing capacities of piles with a PTL at -10.65 m NAP in D-Foundations

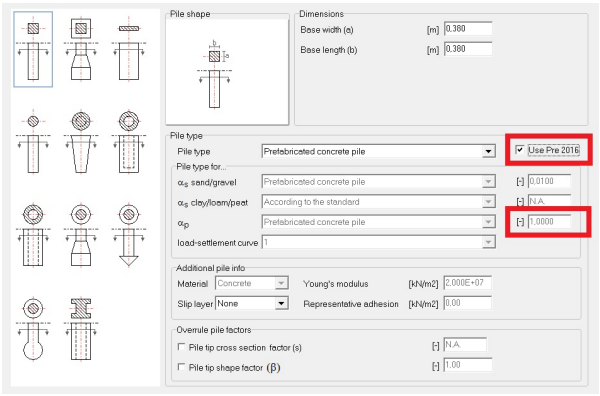

FIGURE D.14: Pile types in D-Foundations with α_p = 1.0

- Level V:
  If the old CPTs can be ignored, these can be removed from the model input.
- Level VI:

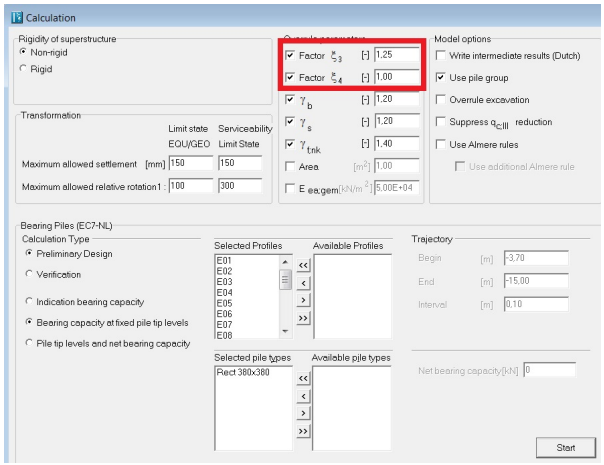

FIGURE D.15: Calculation window in D-Foundations with reduced ξ-factors

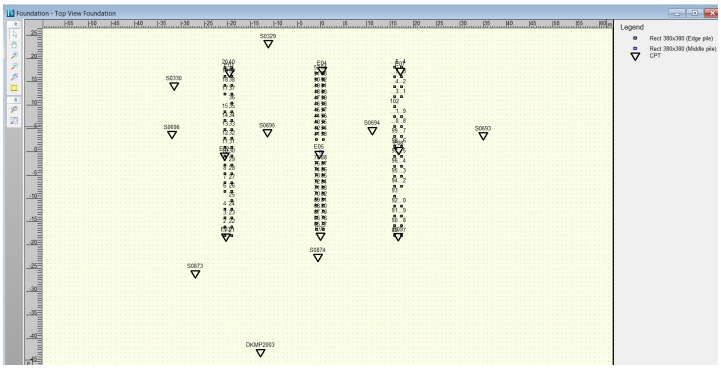

FIGURE D.16: Top view foundation in D-Foundations with both old and new CPT sets

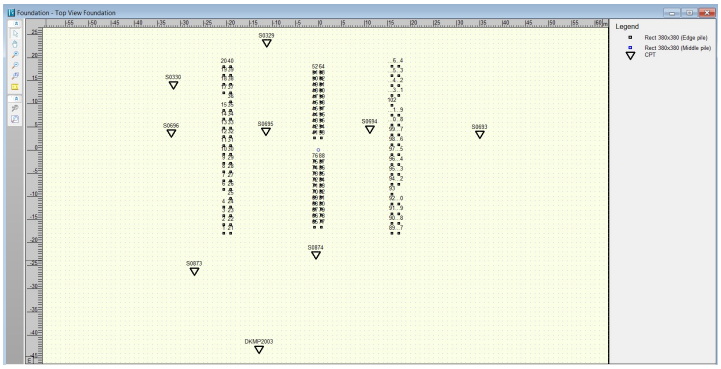

FIGURE D.17: Top view foundation in D-Foundations with new CPT set only

For the influence of set-up, the bearing capacity at fixed pile tip levels must be taken from the model results. There are however no changes to the model input.

D.3. RESULTS MODEL

The six levels of the geotechnical analysis lead to the results as presented in Figures D.18 to D.25.

Level I

D-Foundations, version 16.1.2.2
File : D:\Mijn Documenten\Merijn Stap - afstuderen\Afstuderen\4. Research Study (23-2 to ...)\2) Foundations\05) D-Foundations\Huntumdreef old
Date : 21-6-2017

Results of the option Preliminary Design, Bearing capacity at fixed pile tip levels

Results for pile type :
Rect 380x380

CPT name	Level [m R.L.]	Groundlevel [m R.L.]	Rb;cal;max [kN]	Rs;cal;max [kN]	Rc;cal;max [kN]	Rc;d [kN]	F;nsf;rep [kN]	Fnsf;d [kN]
E01	-10.65	4,70	833	238	1070	708	439	615
E02	-10.65	4,84	669	296	965	638	412	577
E03	-10.65	4,69	527	294	821	543	402	563
E04	-10.65	-1,13	1035	294	1329	879	86	121
E05	-10.65	-1,11	681	278	959	634	92	129
E06	-10.65	-1,07	572	265	837	554	83	116
E07	-10.65	4,79	621	190	810	536	429	601
E08	-10.65	5,03	1162	335	1497	990	418	585
E09	-10.65	5,00	1212	441	1654	1094	378	529

End of data

FIGURE D.18: Results for the Level I bearing capacities of piles with a PTL at -10.65 m NAP in D-Foundations

D-Foundations, version 16.1.2.2
File : D:\Mijn Documenten\Merijn Stap - afstuderen\Afstuderen\4. Research Study (23-2 to ...)\2) Foundations\05) D-Foundations\Huntumdreef old
Date : 21-6-2017

Results of the option Preliminary Design, Bearing capacity at fixed pile tip levels

Results for pile type :
Rect 380x380

CPT name	Level [m R.L.]	Groundlevel [m R.L.]	Rb;cal;max [kN]	Rs;cal;max [kN]	Rc;cal;max [kN]	Rc;d [kN]	F;nsf;rep [kN]	Fnsf;d [kN]
E01	-10.50	4,70	879	204	1082	716	439	615
E02	-10.50	4,84	663	269	931	616	412	577
E03	-10.50	4,69	639	268	907	600	402	563
E04	-10.50	-1,13	1003	241	1244	823	86	121
E05	-10.50	-1,11	673	250	924	611	92	129
E06	-10.50	-1,07	577	231	808	534	83	116
E07	-10.50	4,79	655	162	818	541	429	601
E08	-10.50	5,03	1119	301	1420	939	418	585
E09	-10.50	5,00	1188	407	1595	1055	378	529

End of data

FIGURE D.19: Results for the Level I bearing capacities of piles with a PTL at -10.65 m NAP in D-Foundations

Level II

See Level I.

Level III

D-Foundations, version 16.1.2.2
File : D:\Mijn Documenten\Merijn Stap - afstuderen\Afstuderen\4. Research Study (23-2 to ...)\2) Foundations\05) D-Foundations\Huntumdreef old
Date : 21-6-2017

Results of the option Preliminary Design, Bearing capacity at fixed pile tip levels

Results for pile type :
Rect 380x380

CPT name	Level [m R.L.]	Groundlevel [m R.L.]	Rb;cal;max [kN]	Rs;cal;max [kN]	Rc;cal;max [kN]	Rc;d [kN]	F;nsf;rep [kN]	Fnsf;d [kN]
E01	-10.65	4,70	1189	238	1427	944	439	615
E02	-10.65	4,84	955	296	1251	828	412	577
E03	-10.65	4,69	752	294	1046	692	402	563
E04	-10.65	-1,13	1479	294	1773	1172	86	121
E05	-10.65	-1,11	973	278	1251	827	92	129
E06	-10.65	-1,07	818	265	1082	716	83	116
E07	-10.65	4,79	887	190	1076	712	429	601
E08	-10.65	5,03	1660	335	1995	1319	418	585
E09	-10.65	5,00	1732	441	2173	1437	378	529

End of data

FIGURE D.20: Results for the Level III bearing capacities of piles with a PTL at -10.65 m NAP in D-Foundations

Level IV

D-Foundations, version 16.1.2.2
File : D:\Mijn Documenten\Merijn Stap - afstuderen\Afstuderen\4. Research Study (23-2 to ...)\2) Foundations\05) D-Foundations\Huntumdreef old
Date : 21-6-2017

Results of the option Preliminary Design, Bearing capacity at fixed pile tip levels

Results for pile type :
Rect 380x380

CPT name	Level [m R.L.]	Groundlevel [m R.L.]	Rb;cal;max [kN]	Rs;cal;max [kN]	Rc;cal;max [kN]	Rc;d [kN]	F;nst;rep [kN]	Fnst;d [kN]
E01	-10.50	4,70	1255	204	1459	965	439	615
E02	-10.50	4,84	946	269	1215	804	412	577
E03	-10.50	4,69	912	268	1181	781	402	563
E04	-10.50	-1,13	1433	241	1674	1107	86	121
E05	-10.50	-1,11	962	250	1212	802	92	129
E06	-10.50	-1,07	825	231	1055	698	83	116
E07	-10.50	4,79	936	162	1099	727	429	601
E08	-10.50	5,03	1599	301	1900	1256	418	585
E09	-10.50	5,00	1697	407	2104	1392	378	529

End of data

FIGURE D.21: Results for the Level III bearing capacities of piles with a PTL at -10.65 m NAP in D-Foundations

D-Foundations, version 16.1.2.2
File : D:\Mijn Documenten\Merijn Stap - afstuderen\Afstuderen\4. Research Study (23-2 to ...)\2) Foundations\05) D-Foundations\Huntumdreef old and new
Date : 21-6-2017

Results of the option Preliminary Design, Bearing capacity at fixed pile tip levels

Results for pile type :
Rect 380x380

CPT name	Level [m R.L.]	Groundlevel [m R.L.]	Rb;cal;max [kN]	Rs;cal;max [kN]	Rc;cal;max [kN]	Rc;d [kN]	F;nst;rep [kN]	Fnst;d [kN]
E01	-10.65	4,70	833	238	1070	714	439	615
E02	-10.65	4,84	669	296	965	643	412	577
E03	-10.65	4,69	527	294	821	547	402	563
E04	-10.65	-1,13	1035	294	1329	886	86	121
E05	-10.65	-1,11	681	278	959	639	92	129
E06	-10.65	-1,07	572	265	837	558	83	116
E07	-10.65	4,79	621	190	810	540	429	601
E08	-10.65	5,03	1162	335	1497	998	418	585
E09	-10.65	5,00	1212	441	1654	1102	378	529
S0329	-10.65	-0,50	957	305	1262	841	129	181
S0330	-10.65	4,10	1132	377	1509	1006	456	638
S0693	-10.65	4,18	1218	331	1549	1033	448	628
S0694	-10.65	-0,49	876	358	1234	823	121	170
S0695	-10.65	-0,58	796	336	1132	755	120	169
S0696	-10.65	4,19	695	312	1007	671	456	639
S0873	-10.65	1,94	737	405	1142	761	271	380
S0874	-10.65	-1,76	764	303	1067	712	79	110
DKMP2003		-10.65	-2,27	1571	472	2043	1362	67	93

End of data

FIGURE D.22: Results for the Level IV bearing capacities of piles with a PTL at -10.65 m NAP in D-Foundations

D-Foundations, version 16.1.2.2
File : D:\Mijn Documenten\Merijn Stap - afstuderen\Afstuderen\4. Research Study (23-2 to ...)\2) Foundations\05) D-Foundations\Huntumdreef old and new
Date : 21-6-2017

Results of the option Preliminary Design, Bearing capacity at fixed pile tip levels

Results for pile type :
Rect 380x380

CPT name	Level [m R.L.]	Groundlevel [m R.L.]	Rb;cal;max [kN]	Rs;cal;max [kN]	Rc;cal;max [kN]	Rc;d [kN]	F;nst;rep [kN]	Fnst;d [kN]
E01	-10.50	4,70	879	204	1082	721	439	615
E02	-10.50	4,84	663	269	931	621	412	577
E03	-10.50	4,69	639	268	907	605	402	563
E04	-10.50	-1,13	1003	241	1244	829	86	121
E05	-10.50	-1,11	673	250	924	616	92	129
E06	-10.50	-1,07	577	231	808	539	83	116
E07	-10.50	4,79	655	162	818	545	429	601
E08	-10.50	5,03	1119	301	1420	947	418	585
E09	-10.50	5,00	1188	407	1595	1063	378	529
S0329	-10.50	-0,50	942	271	1213	809	129	181
S0330	-10.50	4,10	1097	344	1441	960	456	638
S0693	-10.50	4,18	1187	297	1484	989	448	628
S0694	-10.50	-0,49	881	324	1205	803	121	170
S0695	-10.50	-0,58	797	301	1098	732	120	169
S0696	-10.50	4,19	748	290	1038	692	456	639
S0873	-10.50	1,94	750	376	1125	750	271	380
S0874	-10.50	-1,76	736	277	1013	676	79	110
DKMP2003		-10.50	-2,27	1530	438	1968	1312	67	93

End of data

FIGURE D.23: Results for the Level IV bearing capacities of piles with a PTL at -10.65 m NAP in D-Foundations

Level V

D-Foundations, version 16.1.2.2
File : D:\Mijn Documenten\Merijn Stap - afstuderen\Afstuderen\4. Research Study (23-2 to ...)\2) Foundations\05) D-Foundations\Huntumdreef new
Date : 21-6-2017

Results of the option Preliminary Design, Bearing capacity at fixed pile tip levels

Results for pile type :
Rect 380x380

CPT name	Level [m R.L.]	Groundlevel [m R.L.]	Rb;cal;max [kN]	Rs;cal;max [kN]	Rc;cal;max [kN]	Rc;d [kN]	F;nst;rep [kN]	Fnst;d [kN]
S0329	-10.65	-0,50	957	305	1262	835	129	181
S0330	-10.65	4,10	1132	377	1509	998	456	638
S0693	-10.65	4,18	1218	331	1549	1025	448	628
S0694	-10.65	-0,49	876	358	1234	816	121	170
S0695	-10.65	-0,58	796	336	1132	749	120	169
S0696	-10.65	4,19	695	312	1007	666	456	639
S0873	-10.65	1,94	737	405	1142	755	271	380
S0874	-10.65	-1,76	764	303	1067	706	79	110
DKMP2003		-10.65 -2,27	1571	472	2043	1351	67	93

End of data

FIGURE D.24: Results for the Level V bearing capacities of piles with a PTL at -10.65 m NAP in D-Foundations

D-Foundations, version 16.1.2.2
File : D:\Mijn Documenten\Merijn Stap - afstuderen\Afstuderen\4. Research Study (23-2 to ...)\2) Foundations\05) D-Foundations\Huntumdreef new
Date : 21-6-2017

Results of the option Preliminary Design, Bearing capacity at fixed pile tip levels

Results for pile type :
Rect 380x380

CPT name	Level [m R.L.]	Groundlevel [m R.L.]	Rb;cal;max [kN]	Rs;cal;max [kN]	Rc;cal;max [kN]	Rc;d [kN]	F;nst;rep [kN]	Fnst;d [kN]
S0329	-10.50	-0,50	942	271	1213	802	129	181
S0330	-10.50	4,10	1097	344	1441	953	456	638
S0693	-10.50	4,18	1187	297	1484	982	448	628
S0694	-10.50	-0,49	881	324	1205	797	121	170
S0695	-10.50	-0,58	797	301	1098	726	120	169
S0696	-10.50	4,19	748	290	1038	686	456	639
S0873	-10.50	1,94	750	376	1125	744	271	380
S0874	-10.50	-1,76	736	277	1013	670	79	110
DKMP2003		-10.50 -2,27	1530	438	1968	1302	67	93

End of data

FIGURE D.25: Results for the Level V bearing capacities of piles with a PTL at -10.65 m NAP in D-Foundations

Level VI
See Level I.

D.4. CPT FILES

In this section the CPT files used for the input of profiles in subsection D.1.2, for both the old and new CPT set, are given.

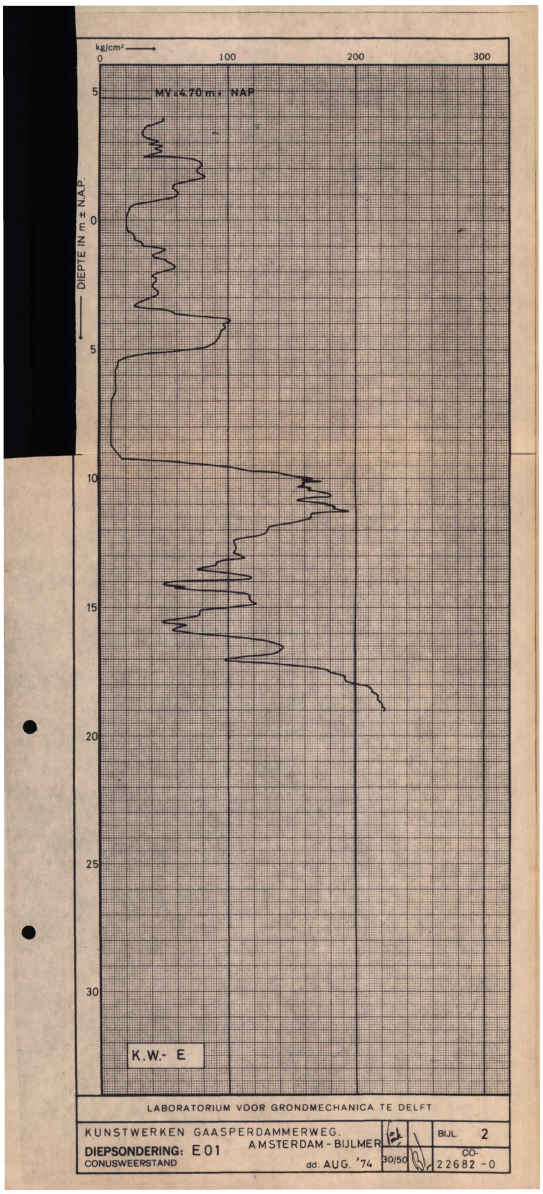

FIGURE D.26: CPT results for CPT E01 *[Laboratorium voor grondmechanica, 1975]*

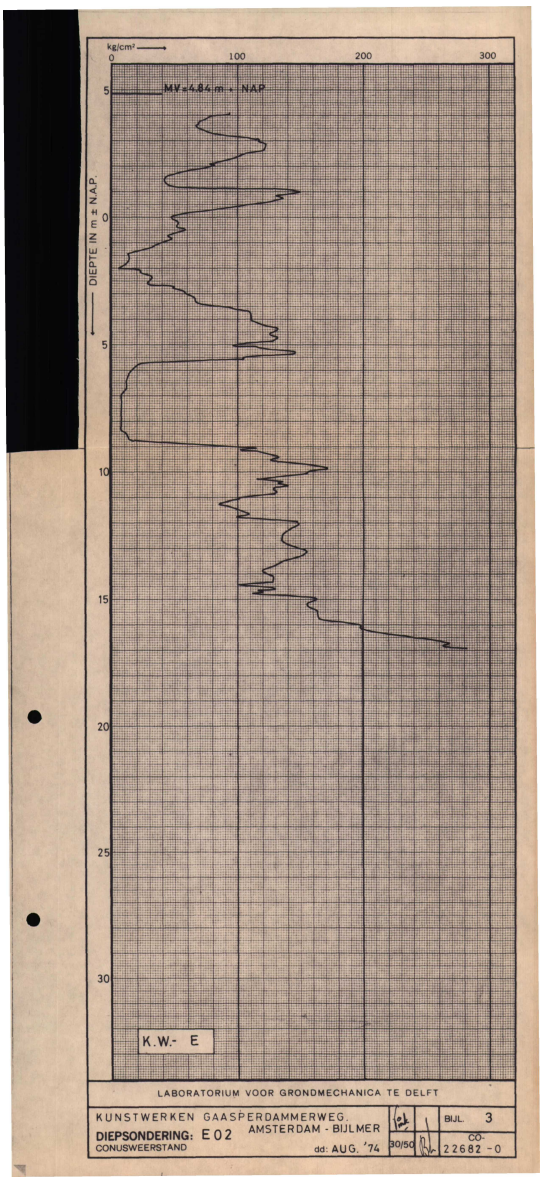

FIGURE D.27: CPT results for CPT E02 *[Laboratorium voor grondmechanica, 1975]*

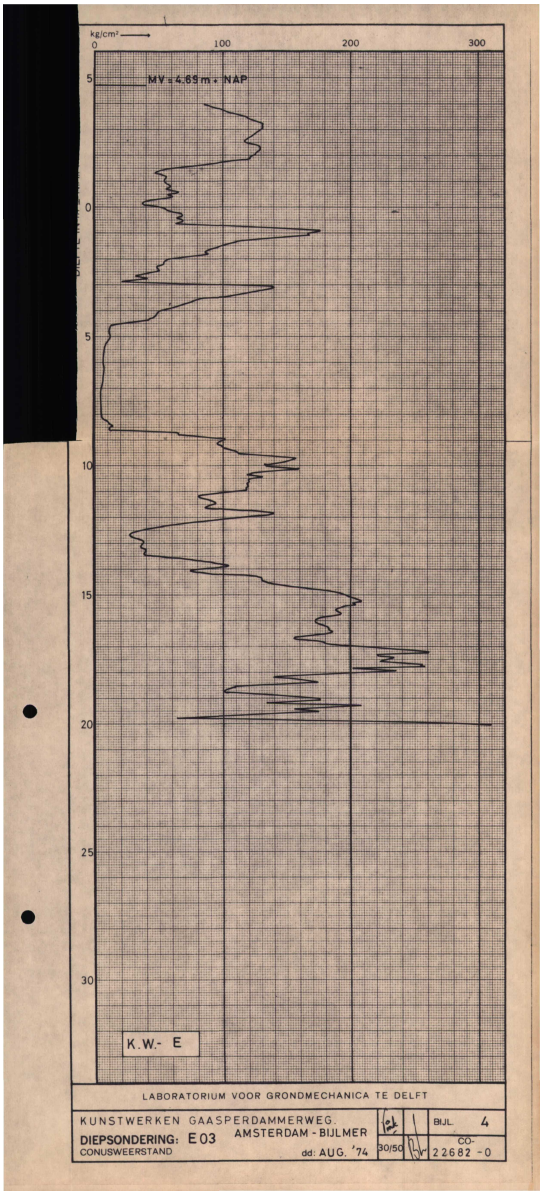

FIGURE D.28: CPT results for CPT E03 *[Laboratorium voor grondmechanica, 1975]*

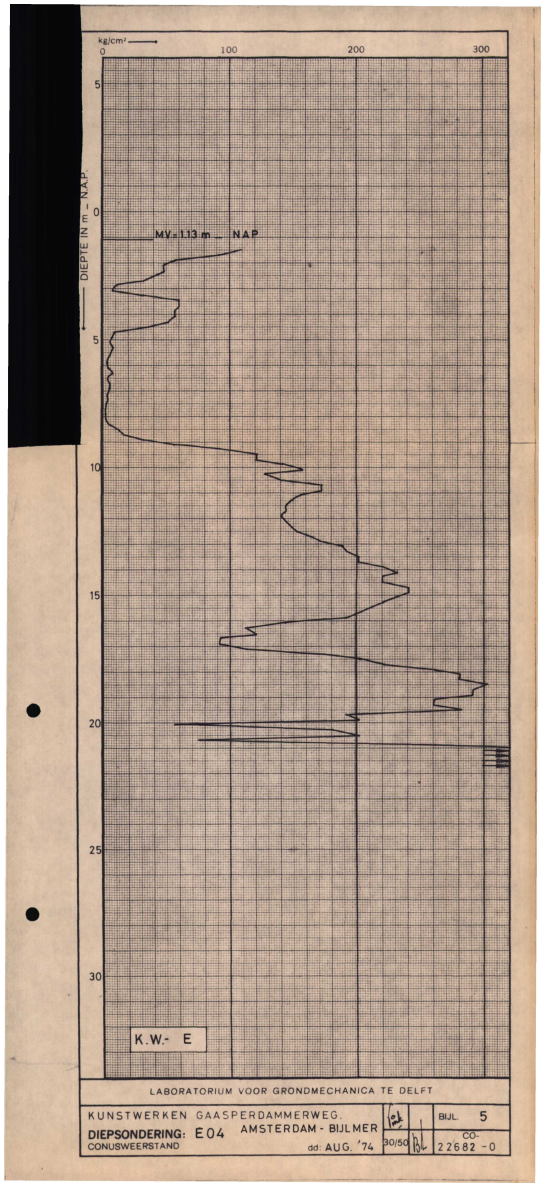

FIGURE D.29: CPT results for CPT E04 *[Laboratorium voor grondmechanica, 1975]*

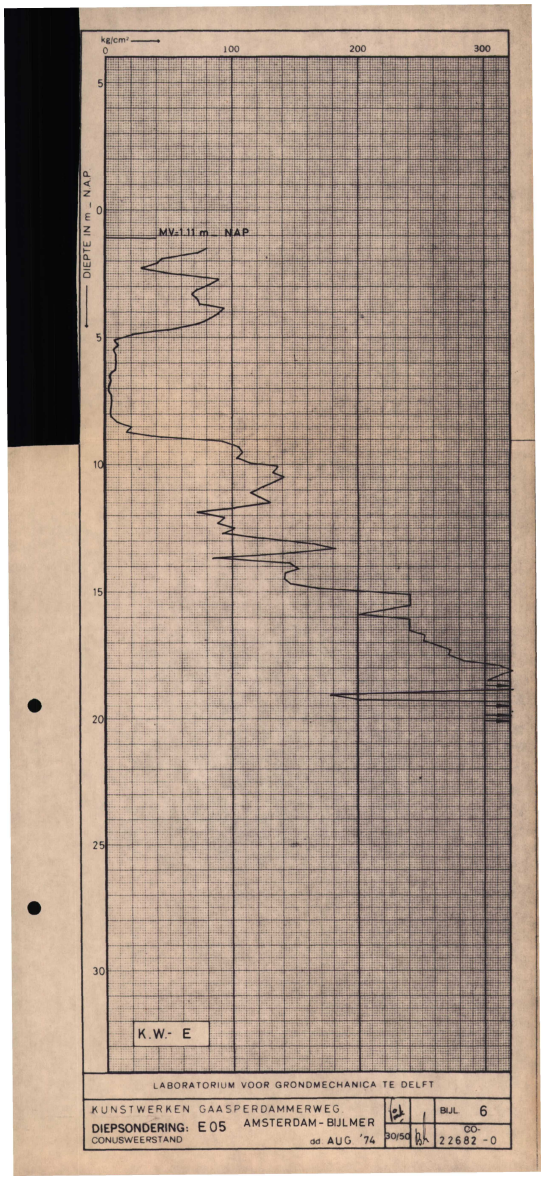

FIGURE D.30: CPT results for CPT E05 *[Laboratorium voor grondmechanica, 1975]*

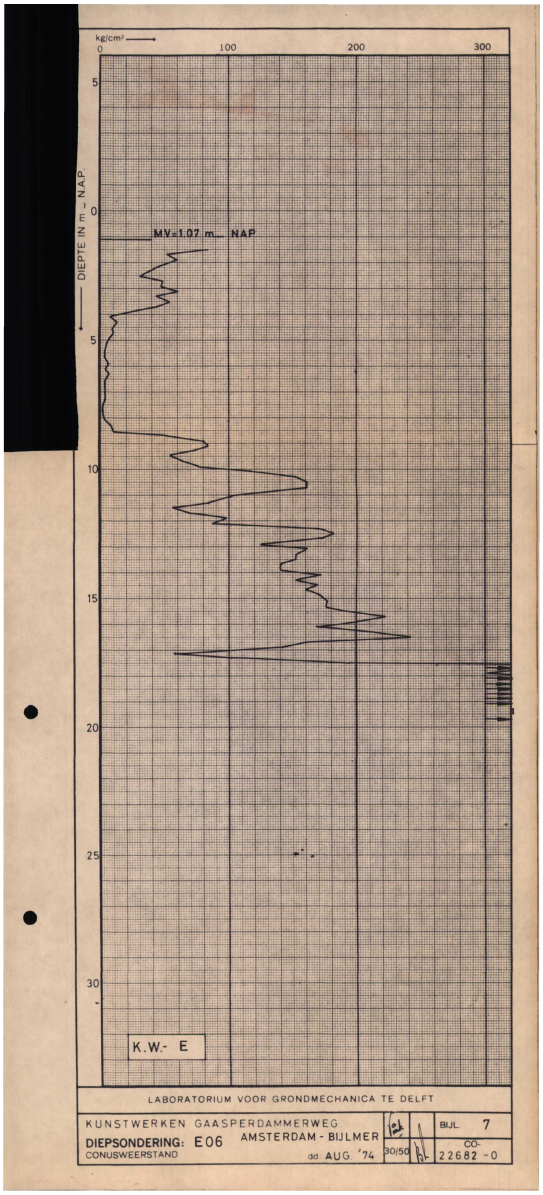

FIGURE D.31: CPT results for CPT E06 *[Laboratorium voor grondmechanica, 1975]*

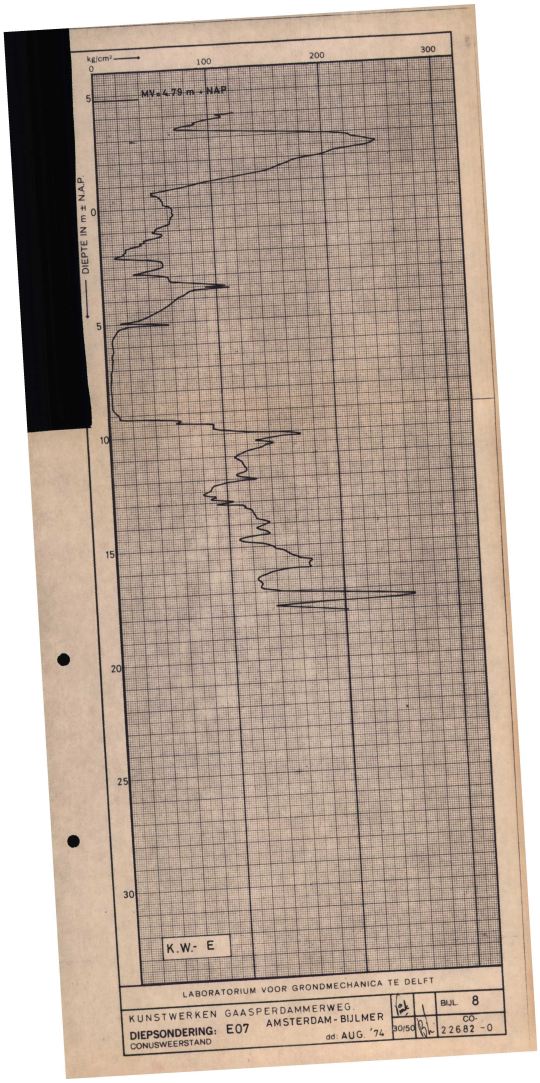

FIGURE D.32: CPT results for CPT E07 *[Laboratorium voor grondmechanica, 1975]*

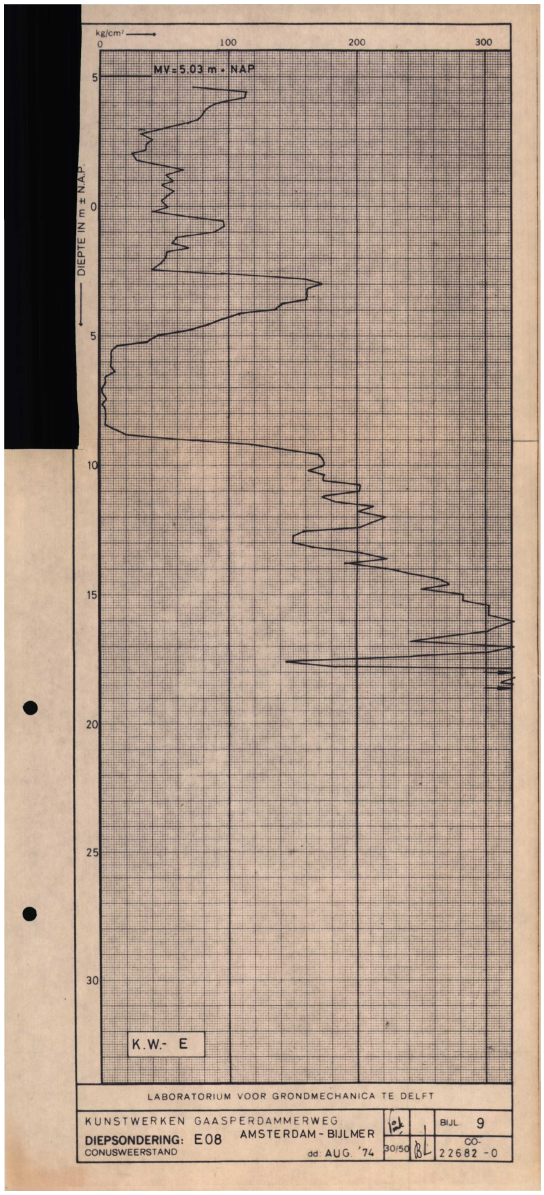

FIGURE D.33: CPT results for CPT E08 *[Laboratorium voor grondmechanica, 1975]*

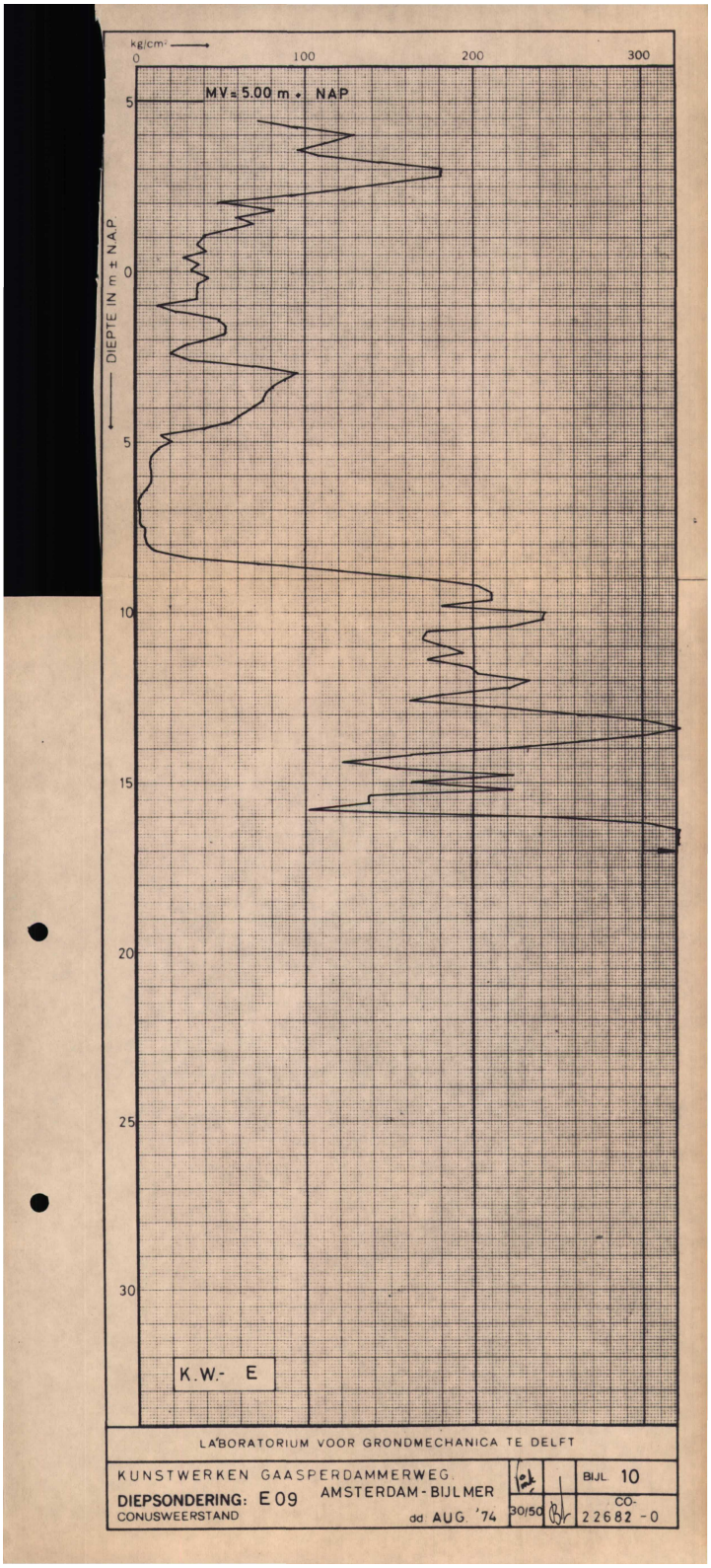

FIGURE D.34: CPT results for CPT E09 *[Laboratorium voor grondmechanica, 1975]*

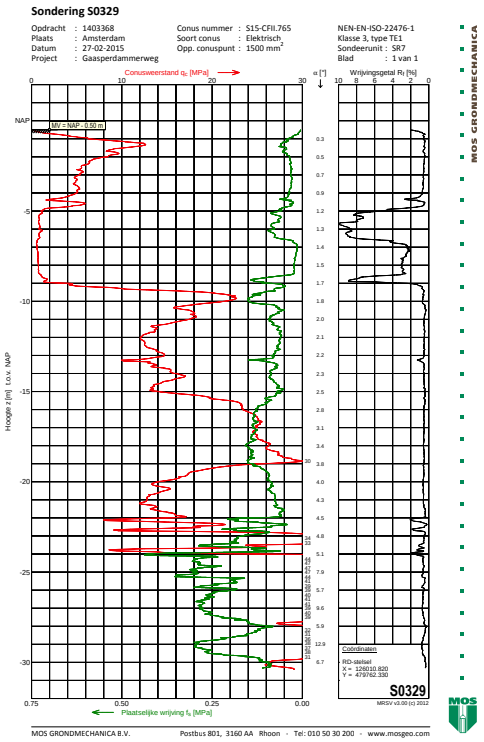

FIGURE D.35: CPT results for CPT S0329 *[Mos Grondmechanica, 2015]*

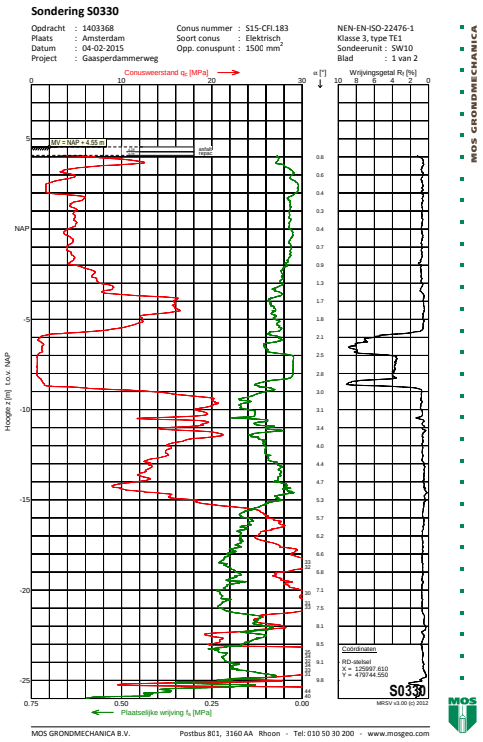

FIGURE D.36: CPT results for CPT S0330 *[Mos Grondmechanica, 2015]*

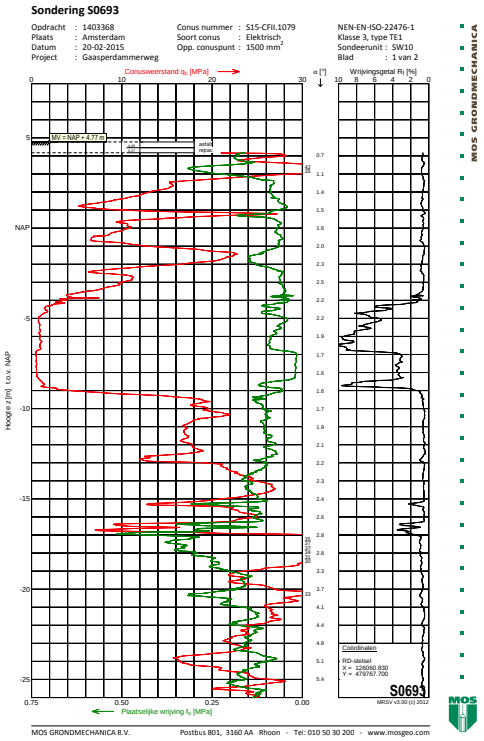

FIGURE D.37: CPT results for CPT S0693 *[Mos Grondmechanica, 2015]*

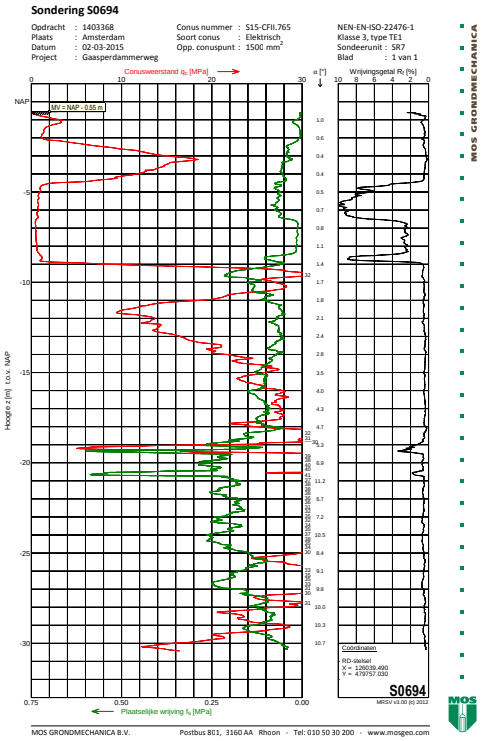

FIGURE D.38: CPT results for CPT S0694 *[Mos Grondmechanica, 2015]*

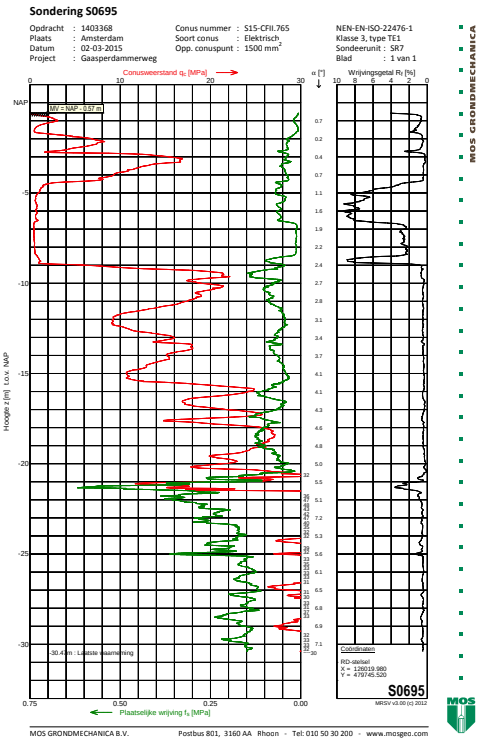

FIGURE D.39: CPT results for CPT S0695 *[Mos Grondmechanica, 2015]*

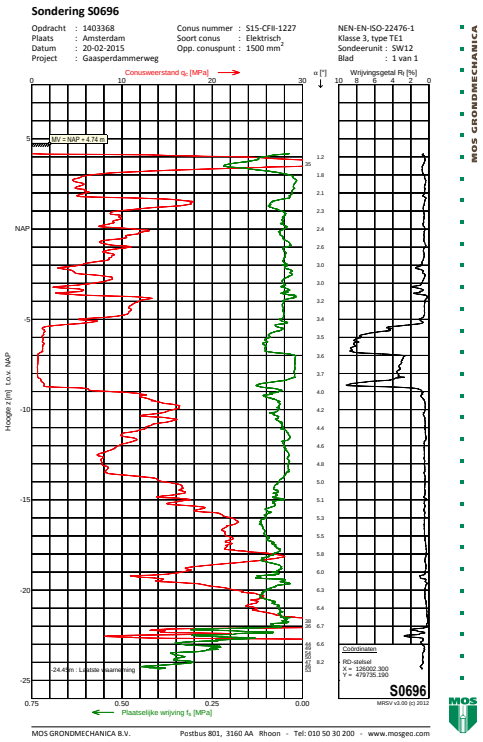

FIGURE D.40: CPT results for CPT S0696 *[Mos Grondmechanica, 2015]*

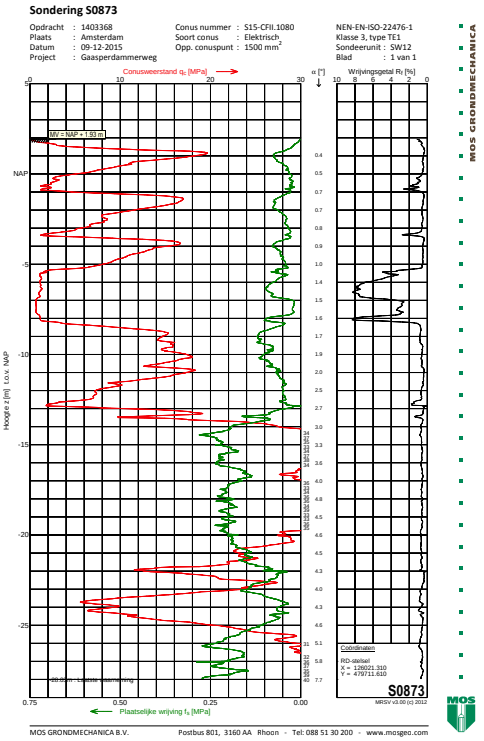

FIGURE D.41: CPT results for CPT S0873 *[Mos Grondmechanica, 2015]*

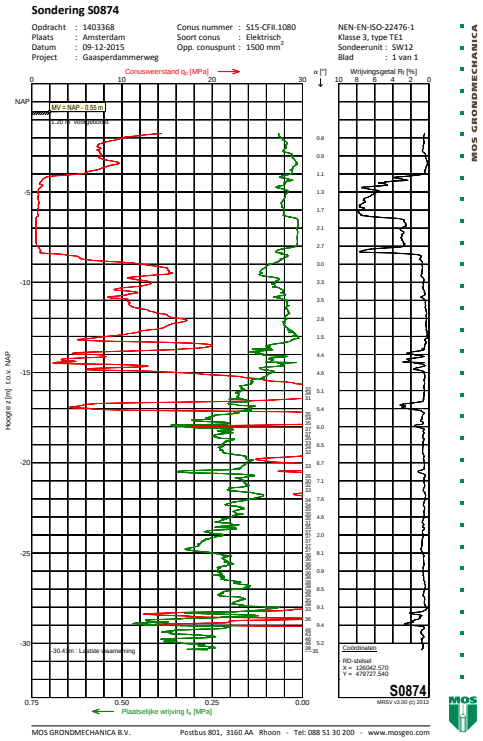

FIGURE D.42: CPT results for CPT S0874 *[Mos Grondmechanica, 2015]*

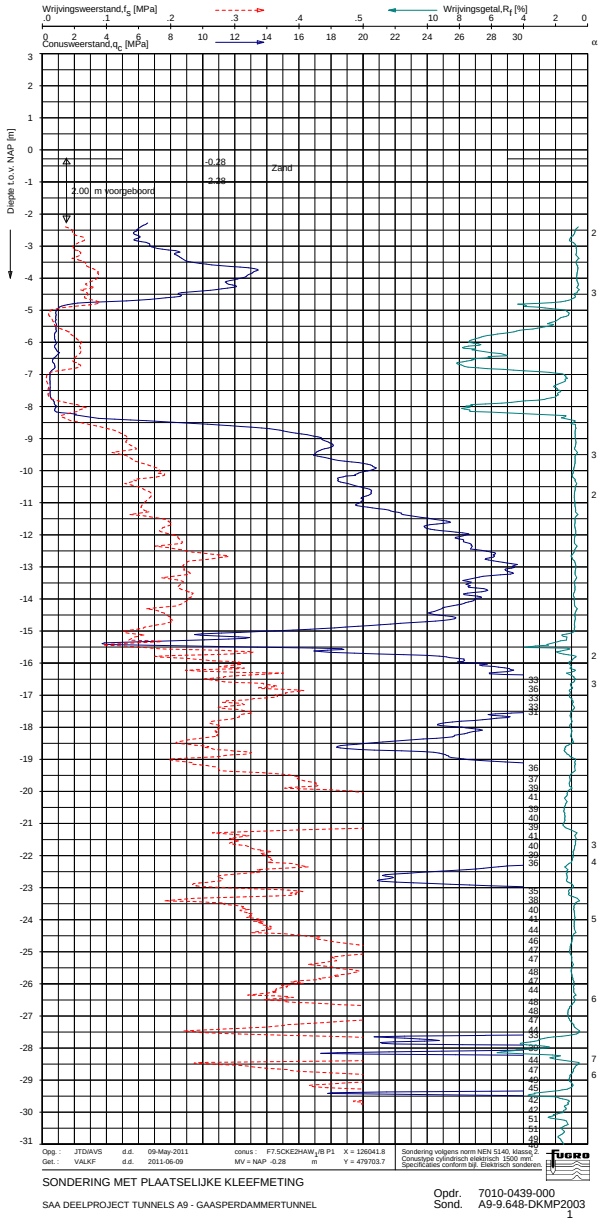

FIGURE D.43: CPT results for CPT DKMP2003 *[Fugro, 2011]*

Structural analysis - Conceptual design

E

CONCEPTUAL DESIGN TROUGH BRIDGE - DESIGN CONSIDERATIONS

In Appendices E to G the calculation procedure for a structural analysis of a trough bridge is discussed. First, in this appendix the general design considerations along with the applied parameters are discussed. Then, in Appendix F the design of a trough girder with massive floor girders and massive side girders will be treated. Following, the open structure design of a multicell box girder for the floor and a truss girder for the sides will be further elaborated in Appendix G.
To verify the load distributions used in this analytical design, use is made of some FEM models. The model input and comparison of results is handled in Appendices H and I.

The order of analysis is depicted in the Figure E.1.

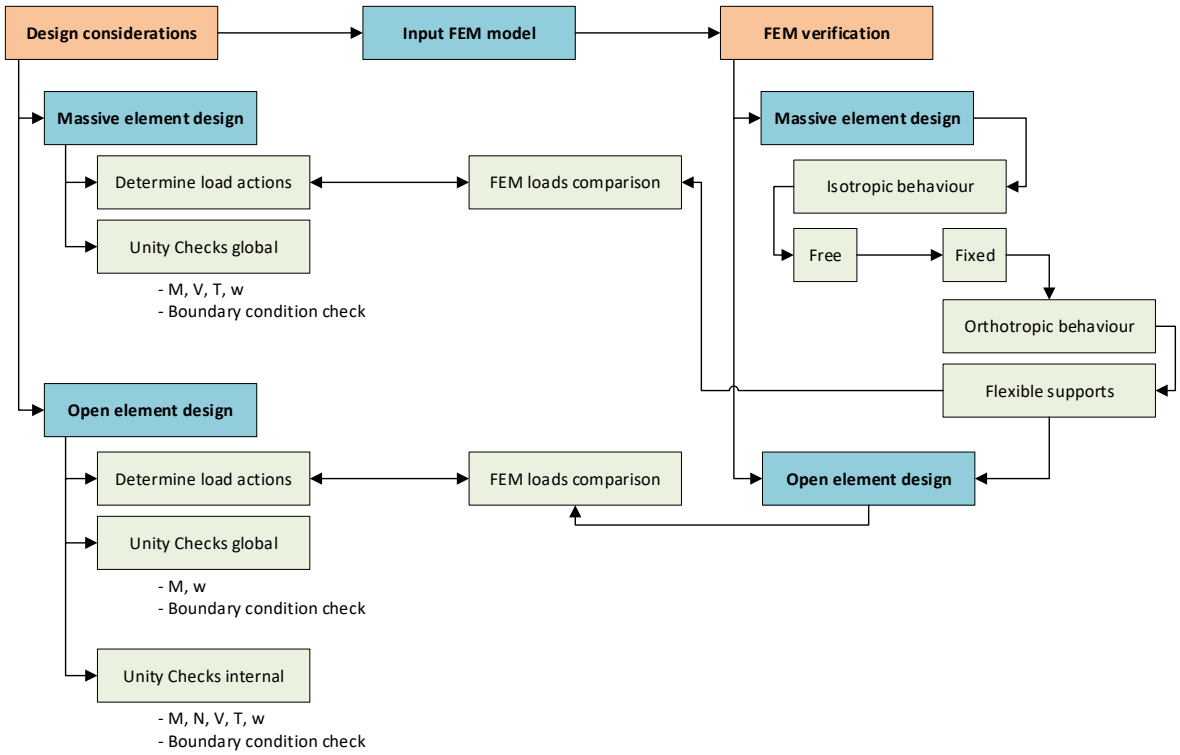

FIGURE E.1: Schematic representation of the design steps and their connection

E.1. DESIGN APPROACH

For this conceptual design of a trough girder for a normal traffic bridge use is made of analytical calculations supported by some Finite Element Model (FEM) verifications. For the analytical design, multiple calculation procedures were combined into an iterative Excel sheer based on a few input parameters. The general input parameters are discussed in section E.2 but there were also a number of variable parameters, such as the height of the side girder, on which all calculations depend.

For the main variable the prestress area in all structural elements is chosen. With the help of some adjustable parameters - like section height and compression zone height x_e - the prestress area is determined. Since all other parameters and calculations are based on this prestress area the accompanying Unity Checks and stresses in the outer fibres could be obtained. The outcomes were then matched to the pre-set boundary conditions, which also depend on the prestress area. In that way the input parameters could directly be linked to both the Unity Checks and the boundary conditions and thus the basis of this analytical calculation was formed.

E.2. DESIGN PARAMETERS

The applied geometric, material and load parameters for this analysis are given in Tables E.1, E.2 and E.3 respectively.

Geometry				
Overall				
	Span length	l_t	36,8	*m*
	Width roadway	w	15,57	*m*
	Nominal width driving lane	w_1	3	*m*
	Kerb width	w_0	1,3	*m*
	Kerb height	h_k	0,19	*m*
	Width bridge	l_f	18,17	*m*
Floor girder				
	Width girder	b_f	3	*m*
	Amount of girders	n_f	11	-
	Width end girder	b_{fe}	1,9	*m*
	Depth asphalt layer	h_a	0,14	*m*
	Height floor girder	h_f	0,61	*m*
Side girder				
	Width girder	b_t	1,2	*m*

TABLE E.1: Geometric parameters applied in this structural analysis

Material properties				
UHPC	**C170/200**			
	Characteristic compressive strength	f_{ck}	170	N/mm^2
	Characteristic cubic compressive strength	$f_{ck;cube}$	200	N/mm^2
	Characteristic tensile strength	f_{ctm}	8	N/mm^2
	Tensile strength at w = 0.3 mm	σ_{w03}	12	N/mm^2
	Material factor	γ_c	1,5	-
	Factor for long-term effects	α_{cc}	0,85	-
	Design compressive strength	f_{cd}	96,33	N/mm^2
	Density	ρ_c	25	kN/m^3
	Modulus of elasticity	E_c	50000	N/mm^2
	Poisson's ratio	ν	0,2	-
	Linear elastic compressive strain	ε_{c3}	2,3	‰
	Ultimate compressive strain	ε_{cu3}	2,6	‰
	Maximum aggregate size	D_{max}	8	*mm*
	Fibre length	l_{fi}	13	*mm*
	Fibre orientation factor (local)	K_{local}	1,75	-
	Fibre orientation factor (global)	K_{global}	1,25	-
Asphalt	**Hot-rolled**			
	Density	ρ_a	23	kN/m^3
Prestressing	**Y1860S7**			
	Characteristic tensile strength	f_{pk}	1860	N/mm^2
	Material factor	γ_p	1,1	-
	Design tensile strength	f_{pd}	1521,82	N/mm^2
	Modulus of elasticity	E_p	195000	N/mm^2
	Maximum prestress at t = 0	σ_{pm0}	1395	N/mm^2
	Time-dependent losses	Δ_p	0,15	-
	Maximum prestress at t = ∞	$\sigma_{pm\infty}$	1185,75	N/mm^2
	Strand diameter	Φ_{ps}	15,7	*mm*
	Strand area	A_{ps}	150	mm^2
Shear reinforcement	**B500S**			
	Characteristic tensile strength	f_{sk}	500	N/mm^2
	Material factor	γ_s	1,15	-
	Design tensile strength	f_{sd}	434,78	N/mm^2
	Modulus of elasticity	E_s	200000	N/mm^2

TABLE E.2: Material parameters applied in this structural analysis

Loading				
Design load factors				
	Permanent load actions	γ_G	1,4	-
	Variable load actions	γ_Q	1,5	-
	Accidental load actions	γ_A	1	-

TABLE E.3: Safety load factors applied in this structural analysis

E.3. LOAD COMBINATIONS

With the previous analysis conducted in Appendix A it is assumed that the combination in which the traffic load is governing, will be governing for all load combinations. Therefore, only the permanent load actions and the variable traffic load action will be taken into account.

Permanent loads

The permanent loads that are taken into account are:

Self-weight concrete:	$\rho_c = 25$ kN/m^2
Resting load asphalt layer:	$\rho_a = 23$ kN/m^2
	$h_a = 140$ mm
Resting load concrete kerbs:	$\rho_c = 25$ kN/m^2
	$h_k = 190$ mm

The design load factor for permanent loads is taken from Appendix A as $\gamma_P = 1.4$.

Traffic loads

The variable traffic load is considered according to Load Model 1 from the *[NEN-EN 1991-2, 2015]* Eurocode, as presented in Appendix A. For simplicity reasons, the horizontal component of this load is neglected. Since safety barriers are applied between side girder and highway the collision loads are also not considered in design. In a more detailed analysis, collision loads must be incorporated regarding the shear capacity of the side girders and the truss elements and also regarding the moment capacity of the floor-to-side connection.

- Vertical loads (LM1)
  According to Appendix A both uniformly distributed loads (UDL) and knife-edge loads (KEL) must be considered. For highways in the Netherlands the values as given in Table E.4 hold.

Lane	Q_{ik} [kN]	q_{ik} [kN/m^2]	α_{Qi}	α_{qi}	F_{KEL} [kN]	q_{UDL} [kN/m^2]
1	150	9	1,00	1,15	150	10,35
2	100	2,5	1,00	1,40	100	3,50
3	50	2,5	1,00	1,40	50	3,50
4	0	2,5	1,00	1,40	0	3,50
5	0	2,5	1,00	1,40	0	3,50
r	0	2,5	1,00	1,40	0	3,50

TABLE E.4: Traffic loads for Dutch highways according to Load Model 1 and *[NEN-EN 1991-2, 2015]*

The nominal lanes must be chosen to obtain the most governing load situation. For both the massive and the open structure, it holds that there are four situations to be considered:

1. Load situation 1: Maximum loads for the floor girder, at midspan (Figure E.2)
2. Load situation 2: Maximum loads for the floor girder, at end span (Figure E.3)
3. Load situation 3: Maximum loads for the side girder, at midspan (Figure E.4)
4. Load situation 4: Maximum loads for the side girder, at end span (Figure E.5)

The design load factor for variable traffic loads is taken from Appendix A as $\gamma_Q = 1.5$.

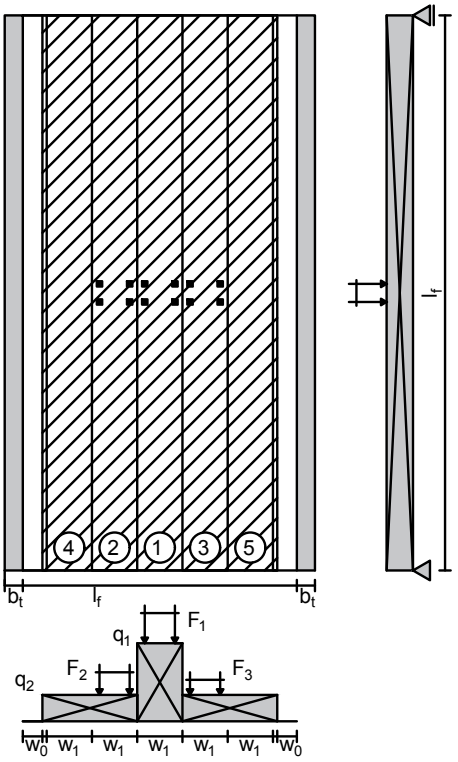

FIGURE E.2: Load situation 1 - traffic load configuration for maximum loads in the floor girder at midspan

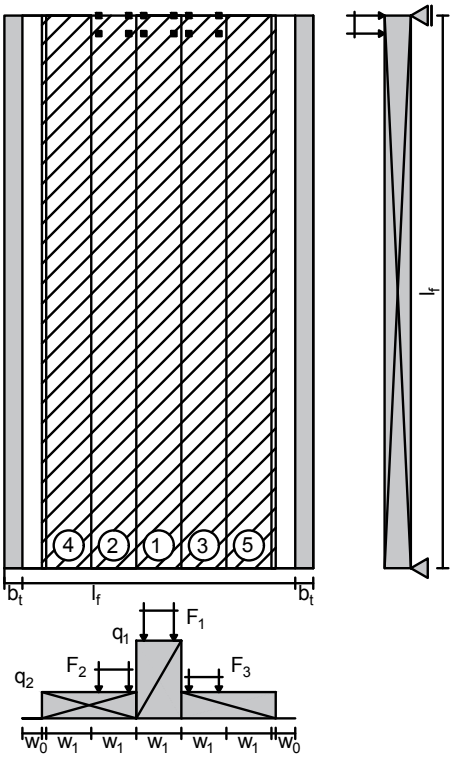

FIGURE E.3: Load situation 2 - traffic load configuration for maximum loads in the floor girder at end span

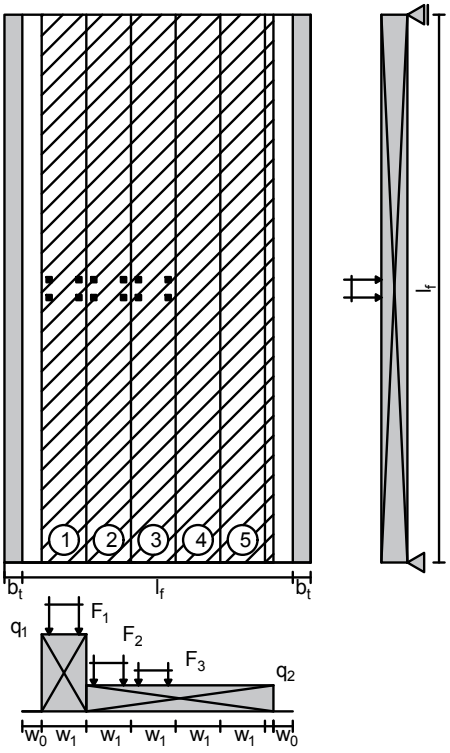

FIGURE E.4: Load situation 3 - traffic load configuration for maximum loads in the side girder at midspan

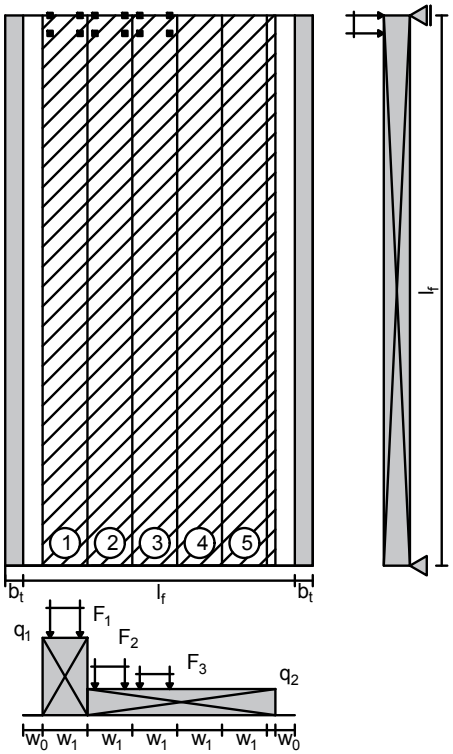

FIGURE E.5: Load situation 2 - traffic load configuration for maximum loads in the side girder at end span

E.4. MATERIAL BEHAVIOUR

Although other materials might be suitable for the design of a structural trough girder for a traffic bridge, in this thesis the possibilities for UHPC are a core subject and therefore no other materials will be considered in this analysis, with the exception of prestressing steel and reinforcement steel. The used materials and their properties are listed in Table E.2. These values are obtained from *[AFGC, 2013]*, *[Ketel et al., 2011]*, *[Walraven, 2010]* and *[Walraven and Braam, 2015]*.

As is the case for NSC, UHPC behaviour in compression can be described by a bilinear stress-strain diagram (Figure E.6). The tensile behaviour is more complicated than that of NSC, due to the addition of fibres and the accompanying strain-softening or strain-hardening behaviour. The exact behaviour depends on the fibre content and individual fibre length, but for design purposes the tensile stress-strain diagram can be simplified as shown in Figure E.7.

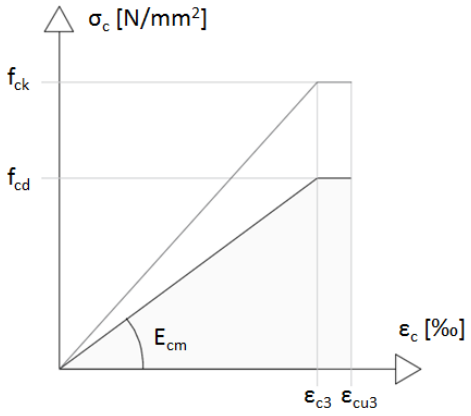

FIGURE E.6: Schematised compressive behaviour of UHPC

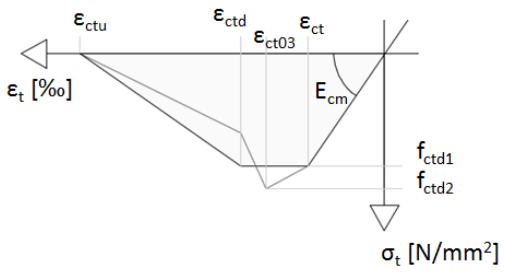

FIGURE E.7: Schematised tensile behaviour of UHPC concrete class C170/200

The E-modulus of the concrete is given by the secant of the stress-strain diagram and it thus reduces if crushing ($f_c > f_{cd}$) or cracking ($f_t > f_{ctd1}$) occurs.

Stress-strain diagrams for prestressing and reinforcement steel are given in Figure E.8 and E.9 respectively.

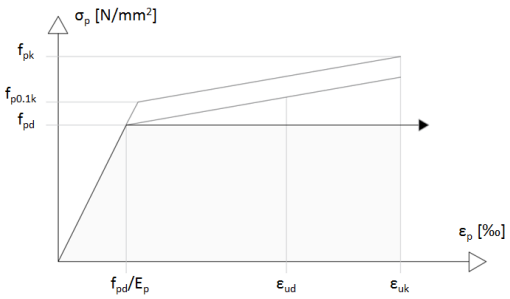

FIGURE E.8: Schematised tensile behaviour of prestressing steel Y1860S7

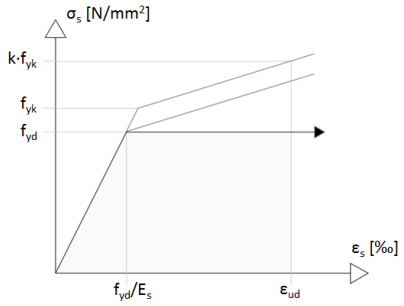

FIGURE E.9: Schematised tensile behaviour of reinforcement steel B500B

E.5. BOUNDARY CONDITIONS

The design of the structural elements is based on multiple boundary conditions, which are discussed below.

Strength and deformation capacity

All structural elements will have to be sufficiently designed to withstand all load actions taken into account. This is done by checking all relevant ultimate limit states (ULS) and serviceability limit states (SLS) *[NEN-EN*

1990, 2011]:

ULS: STR - All structural elements will have sufficient strength to withstand internal failure or excessive deformations
EQU (stability), FAT (fatigue), GEO (geotechnical failure), UPL (uplift) and HYD (erosion) are ultimate limit states that will not be considered in this analysis, either due to irrelevance or for reasons of simplicity.

SLS: Excessive deformations

Minimum concrete cover

A minimal concrete cover on prestressing and reinforcement elements is required to ensure adequate bonding and adequate durability. From *[NEN-EN 1992-1-1, 2005]* and *[AFGC, 2013]* it follows that:

$$c_{nom} = c_{min} = \Delta c_{dur}$$

$$\Delta c_{dur} = 5 \text{ mm}$$

$$c_{min} = \max\{c_{min;b}; c_{min;dur} + \Delta c_{dur;y} - \Delta c_{dur;st} - \Delta c_{dur;add}; c_{min;p}; 10\} \text{ [mm]}$$

The design service life is set at 100 years for traffic bridges, which results in Structural Class S6. The durability classes to be considered are:

XC4:	Corrosion induced by carbonation	Cyclic wet and dry
XD3:	Corrosion induced by chlorides	Cyclic wet and dry
XF4:	Freeze/thaw attack	High water saturation with de-icing agents or sea water

$c_{min;b}$:
- Reinforcement steel: $c_{min;b} = \phi_{sw}$
- Pre-tensioned steel: $c_{min;b} = \max\{2 \cdot \phi_s; D_{max}\}$
- Post-tensioned steel: $c_{min;b} = \max\{\phi_{eq;t}; 80\}$

$c_{min;dur}$:
- XC4:
  - Prestressing steel: $c_{min;dur} = 25$ mm
  - Reinforcement steel: $c_{min;dur} = 20$ mm
- XD3:
  - Prestressing steel: $c_{min;dur} = 30$ mm
  - Reinforcement steel: $c_{min;dur} = 25$ mm
- XF4: Requires special attention in concrete mixture, but is assumed adequate in normal situations.

$$\Delta c_{dur;y} = 0 \text{ mm}$$
$$\Delta c_{dur;st} = 0 \text{ mm}$$
$$\Delta c_{dur;add} = 0 \text{ mm}$$

$c_{min;p}$: Is only considered in case of prestressing:
$c_{min;p} = \max\{1.5 \cdot l_f; 1.5 \cdot D_{max}; \phi\}$

Summarising:

- For reinforcement steel: $c_{nom} = \max\{\phi_{sw}; 26\} + 5$ [mm]
- For pre-tensioned steel: $c_{nom} = 36.5$ [mm]
- For post-tensioned steel: $c_{nom} = \max\{\phi_{eq;t}; 80\} + 5$ [mm]

The minimal horizontal (e_h) and vertical (e_v) distance between two adjacent bars is given by:

$$e_h = e_v \geq e_{min} = \max\{\phi; D_{max} + 5; 1.5 \cdot l_f; 20\} = \max\{\phi; 26\} \text{ [mm]}$$

Prestressing conditions

There is a maximum and minimum amount of prestress area allowed in each element:

$$\max\{A_{p;min;1}; A_{p;min;2}\} \leq A_p \leq \min\{A_{p;max;1}; A_{p;max;2}\}$$

- $A_{p;max;1}$ is based on the maximal allowed compressive stress in the cross-section: $\sigma_c \leq 0.6 \cdot f_{ck}(t)$ *[NEN-EN 1992-1-1, 2005]*. Here, $f_{ck}(t)$ is the characteristic compressive strength of the concrete at the time of prestress release. For post-tensioning steel, this means the characteristic strength after 28 days, which is equal to $f_{ck} = 170$ N/mm^2. For pre-tensioned steel, however, release takes place in the first day after concrete pouring, at $t = 0.5$ day. In that case, $f_{ck}(t)$ is given by:

$$f_{ck}(t) = f_{cm}(t) - 8 \text{ [N/mm}^2\text{]}$$
$$f_{ck}(t) = \beta_{cc}(t) \cdot f_{ck}$$
$$\beta_{cc}(t) = e^{s \cdot \left\{1 - \sqrt{\frac{28}{t}}\right\}}$$
$$s = 0.2 \text{ (Cement class R)}$$

Thus for t = 28 days, $f_{ck}(t) = f_{ck} = 170$ N/mm^2 and for t = 0.5 days, $f_{ck}(t) = 0.27 \cdot f_{ck} = 46.5$ N/mm^2.

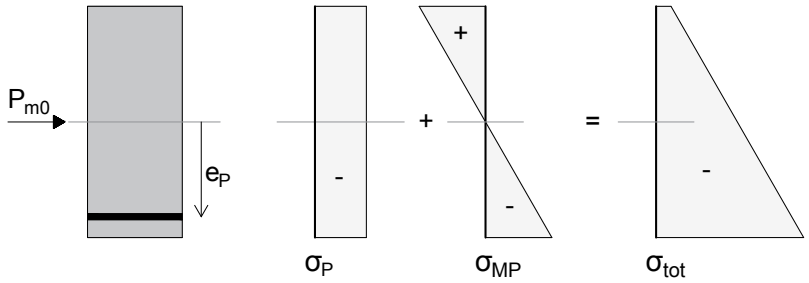

FIGURE E.10: Stress distribution for the maximum compressive stress in the concrete cross-section after prestress release at t = 0

$$A_{p;max;1} = \frac{A_c \cdot 0.6 cdot f_{ck}}{\sigma_{pm0}}$$

- $A_{p;max;2}$ is based on the maximum tensile strength in the top fibre, in order to prevent cracking of the top fibre during the construction stage as a result of the upwards directed prestress. It holds that:

$$\sigma_{ct;top} \leq f_{ctd1}$$

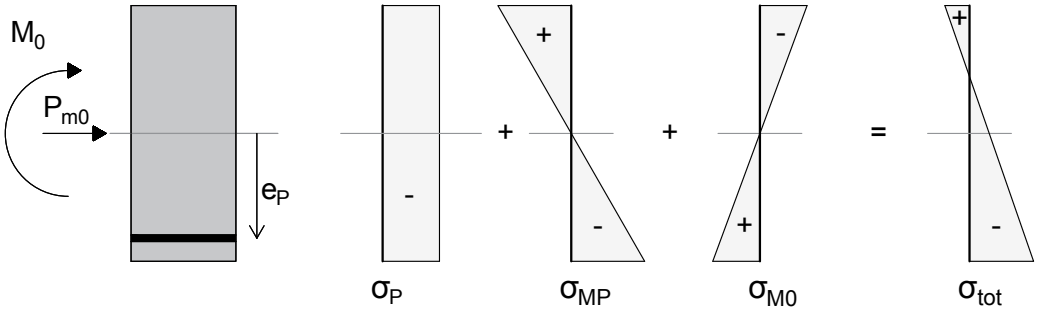

FIGURE E.11: Stress distribution for the maximum tensile stress in the concrete cross-section at t = 0

With: $\sigma_p = \frac{P_{m0}}{A_c}$ $\sigma_{M;P} = \frac{e_p \cdot P_{m0} \cdot z_t}{I_c}$ $\sigma_{M;t=0} = \frac{M_{t=0} \cdot z_t}{I_c}$

$$-\frac{P_{m0}}{A_c} + \frac{e_p \cdot P_{m0} \cdot z_t}{I_c} - \frac{M_{t=0} \cdot z_t}{I_c} \leq f_{ctd1}$$

Here Mt=0 consists of the moment due to the self-weight of the concrete and the upwards curvature pressure of the tendon profile. Furthermore, since cracking is considered, this is an SLS check.

It must be stated that the self-weight of the concrete is a parabolic function of the position, while the moment from prestressing is constant. Therefore multiple positions must be checked to verify whether this boundary condition is met:

1: $M_{t=0} = 0.125 \cdot q_{ck} \cdot {l_f}^2 - f \cdot P_{m0}$ (at midspan)
2: $M_{t=0} = -f \cdot P_{m0}$ (at support)

$$P_{m0;max} \leq \frac{f_{ctd1} \cdot I_c + q_{ck} \cdot x^2 \cdot z_t}{(f + e_p) \cdot z_t \cdot A_c \cdot I_c - {I_c}^2}$$

$$A_{p;max;2} = \frac{P_{m0;max}}{\sigma_{pm0}}$$

- $A_{p;min1}$ is based on the requirement that there is no tensile stress in the cross-section in SLS at any time. The most governing situation for this check is at t = ∞ in the bottom fibre of the concrete cross section:

$$\sigma_{c;bot} \leq \sigma_{res} \text{ [N/mm}^2\text{]}$$

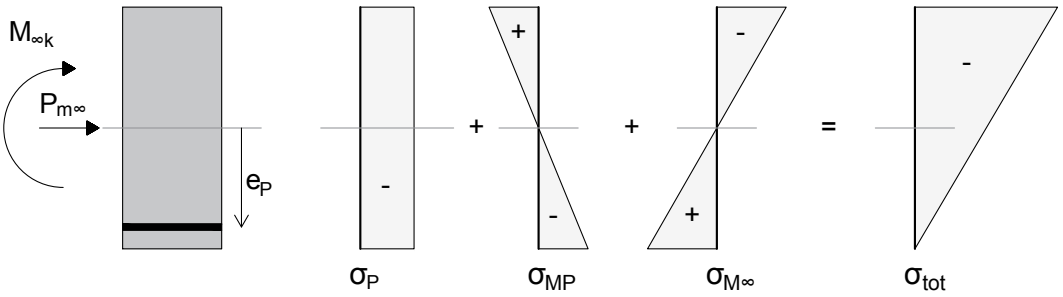

FIGURE E.12: Stress distribution for the minimum compressive stress in the concrete cross-section in SLS at t = ∞

With: $\sigma_p = \frac{P_{m\infty}}{A_c}$ $\sigma_{M;P} = \frac{e_p \cdot P_{m\infty} \cdot z_b}{I_c}$ $\sigma_{M;t=\infty} = \frac{M_{t=\infty} \cdot z_b}{I_c}$

$$-\frac{P_{m\infty}}{A_c} - \frac{e_p \cdot P_{m\infty} \cdot z_b}{I_c} + \frac{M_{t=\infty} \cdot z_b}{I_c} \leq f_{ctd1}$$

Here $M_{t=\infty}$ consists of the characteristic maximum moment in the cross section including the upwards curvature pressure of the tendon profile:

$$M_{t=\infty} = M_{Ek} - f \cdot P_{m\infty}$$

$$P_{m\infty;min} \geq \frac{\sigma_{res} \cdot I_c + M_{Ek} \cdot z_b}{(f + e_p) \cdot z_b \cdot A_c \cdot I_c + {I_c}^2}$$

$$A_{p;min} = \frac{P_{m\infty;min}}{\sigma_{pm\infty}}$$

- $A_{p;min2}$ is based on the transverse tensile stresses that are induced by the compressive prestresses:

$$A_{p\perp;min;2} = \nu \cdot A_{p//}$$

However, in a fixed floor system, both top and bottom prestress is required to resist both positive and negative moments. In that case, although the boundary conditions stay the same, the formula as presented above will differ:

- $A_{p;max;1} = \frac{A_c \cdot 0.6 \cdot f_{ck}(t)}{\sigma_{pm0}}$

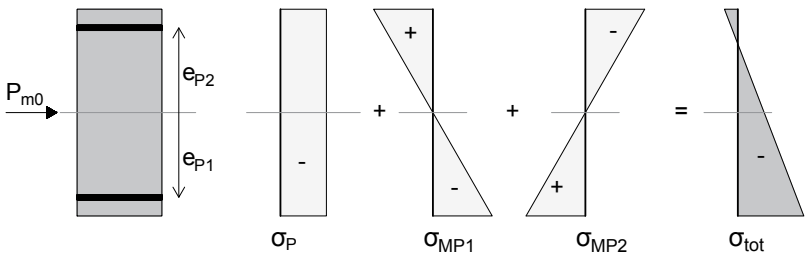

FIGURE E.13: Stress distribution for the maximum compressive stress in the concrete cross-section at t = 0 with double prestressing

- $A_{p;max;2} = \frac{P_{m0;max}}{\sigma_{pm0}}$

$$P_{m0;1;max} \leq \frac{f_{ctd1} \cdot I_c + \frac{1}{24} \cdot q_{ck} \cdot l_f{}^2 \cdot z_t}{(f + e_{p1}) \cdot z_t \cdot A_c \cdot I_c - I_c{}^2}$$

$$P_{m0;2;max} \leq \frac{f_{ctd1} \cdot I_c + \frac{1}{12} \cdot q_{ck} \cdot l_f{}^2 \cdot z_t}{(f + e_{p2}) \cdot z_t \cdot A_c \cdot I_c - I_c{}^2}$$

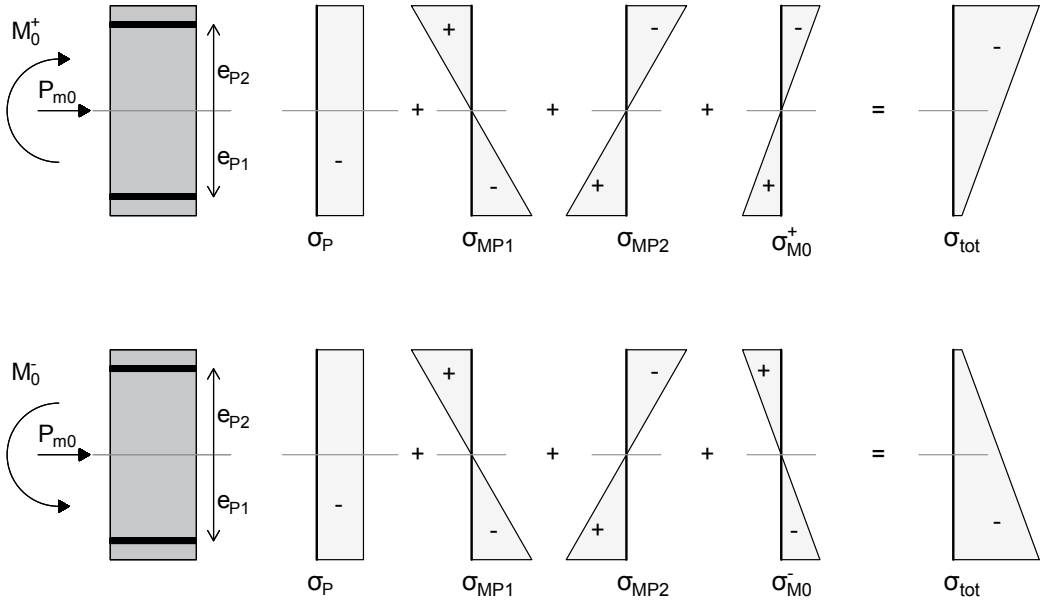

FIGURE E.14: Stress distribution for the maximum tensile stress in the concrete cross-section at t = 0 with double prestressing

- $A_{p;min} = \frac{P_{m\infty;max}}{\sigma_{pm\infty}}$

$$P_{m\infty;1;min} \geq \frac{M_{Ek}{}^{+} \cdot z_b \cdot (e_{p2} \cdot z_t \cdot A_c + I_c) + |M_{Ek}{}^{-}| \cdot z_t \cdot (e_{p2} \cdot z_b \cdot A_c - I_c)}{I_c \cdot (e_{p1} + e_{p2}) \cdot h}$$

$$P_{m\infty;2;min} \geq \frac{M_{Ek}{}^{+} \cdot z_b \cdot (e_{p1} \cdot z_t \cdot A_c - I_c) + |M_{Ek}{}^{-}| \cdot z_t \cdot (e_{p1} \cdot z_b \cdot A_c + I_c)}{I_c \cdot (e_{p1} + e_{p2} \cdot h}$$

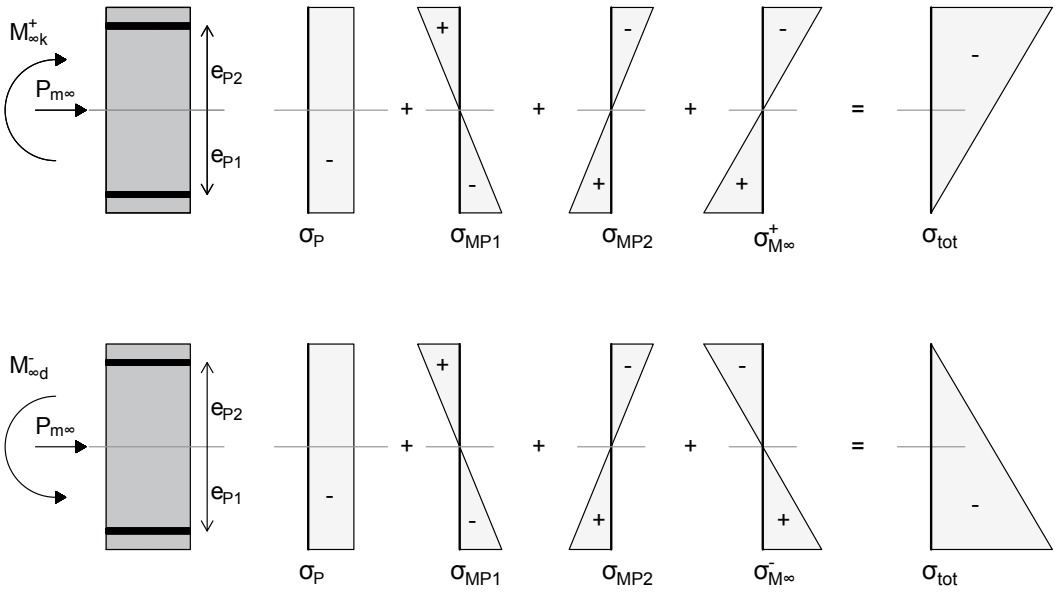

FIGURE E.15: Stress distribution for the minimum compressive stress in the concrete cross-section in SLS at t = ∞ with double prestressing

Ductility
In order to prevent brittle failure, each element should be designed in such a way that the structure gives a warning before failure occurs. This ductility is incorporated in the boundary conditions by requiring cracks to form in ULS loading. In formula:

$$\text{At } t = \infty: \quad \sigma_{c;top} \text{ or } \sigma_{c;bot} > f_{ctd1}$$

For single prestressing it holds:

- $A_{p;max;3} = \frac{P_{m\infty;max}}{\sigma_{pm\infty}}$

$$P_{m\infty;max} \leq \frac{-f_{ctd1} \cdot I_c + M_{Ed} \cdot z_b}{(f + e_{p1}) \cdot z_b \cdot A_c \cdot I_c + I_c^2}$$

Here $M_{t=\infty}$ consists of the design maximum moment in the cross section including the upwards curvature pressure of the tendon profile:

$$M_{t=\infty} = M_{Ed} - f \cdot P_{m\infty}$$

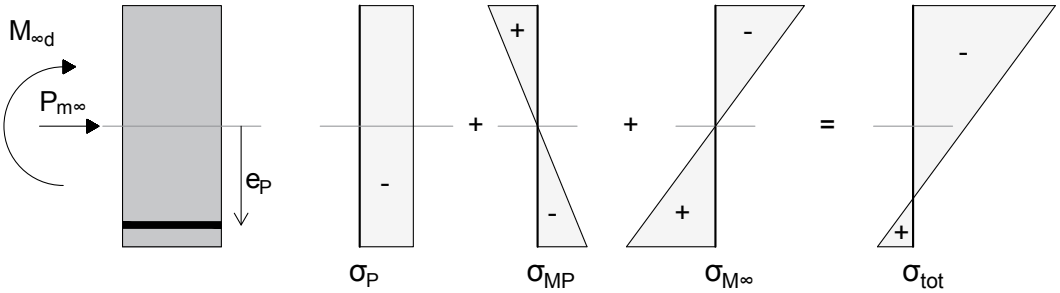

FIGURE E.16: Stress distribution for the minimum tensile stress in the concrete cross-section at in ULS t = ∞

For double prestressing it holds:

- $A_{p;max;3} = \frac{P_{m\infty;max}}{\sigma_{pm\infty}}$

$$P_{m\infty;1;max} \leq \frac{-f_{ctd1} \cdot e_{p2} \cdot A_c \cdot I_c \cdot h + M_{Ed}{}^{+} \cdot z_t \cdot (e_{p2} \cdot z_b \cdot A_c + I_c) + |M_{Ed}{}^{-}| \cdot z_b \cdot (e_{p2} \cdot z_t \cdot A_c - I_c)}{I_c \cdot (e_{p1} + e_{p2}) \cdot h}$$

$$P_{m\infty;2;max} \leq \frac{-f_{ctd1} \cdot e_{p1} \cdot A_c \cdot I_c \cdot h + M_{Ed}{}^{+} \cdot z_t \cdot (e_{p1} \cdot z_b \cdot A_c - I_c) + |M_{Ed}{}^{-}| \cdot z_b \cdot (e_{p1} \cdot z_t \cdot A_c + I_c)}{I_c \cdot (e_{p1} + e_{p2} \cdot h}$$

Ultimate strength compressive struts
Both shear capacity and torsion capacity are limited by the ultimate strength of the compressive struts:

$$V_{Rd;max} = \frac{2 \cdot 1.14 \cdot \frac{\alpha_{cc}}{\gamma_c} \cdot b_w \cdot z \cdot f_{ck}{}^{\frac{2}{3}}}{\cot(\theta) + \tan(\theta)}$$

$$T_{Rd;max} = 2 \cdot 1.14 \cdot \frac{\alpha_{cc}}{\gamma_c} \cdot f_{ck} \cdot 2 \cdot A_k \cdot t_{eff} \cdot \sin(\theta) \cdot \cos(\theta)$$

If both shear and torsion are present on a structural element, the following Unity Check must be fulfilled:

$$\frac{V_{Ed}}{V_{Rd;max}} + \frac{T_{Ed}}{T_{Rd;max}} \leq 1.0$$

E.6. CONNECTIONS

In this analysis, it is assumed that multiple floor girders are spanned between two side girders that consist of one single segment. This means that there are two connections to be considered, namely the floor-to-floor connection and the floor-to-side connection.

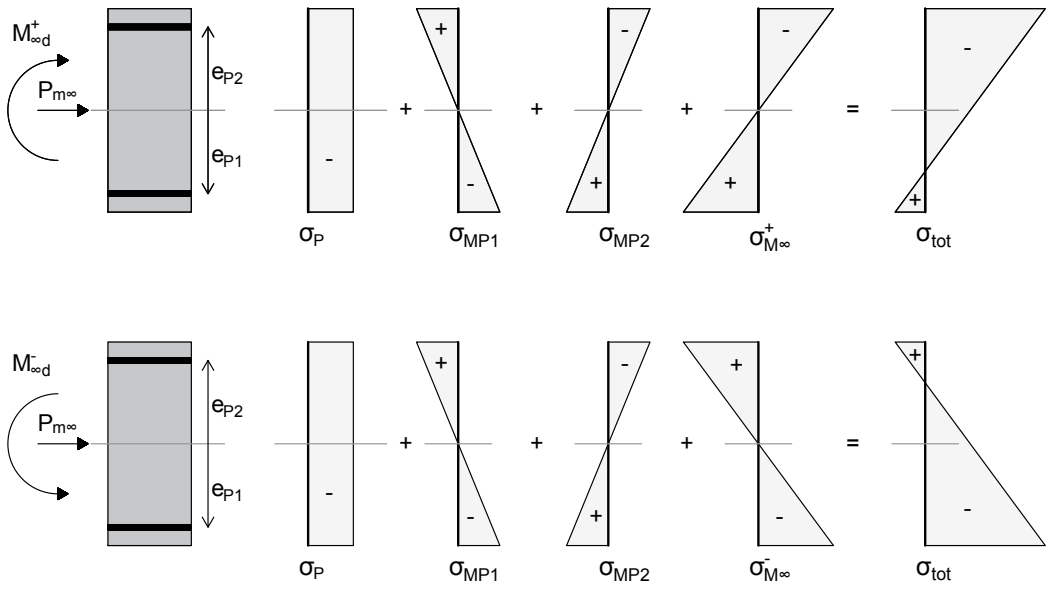

FIGURE E.17: Stress distribution for the minimum tensile stress in the concrete cross-section at in ULS t = ∞ with double prestressing

Floor-to-floor connection:
The floor girders are assumed to be connected through transversal prestressing at either the top only (Figure E.18) or at both the top and bottom of the girder (Figure E.19).

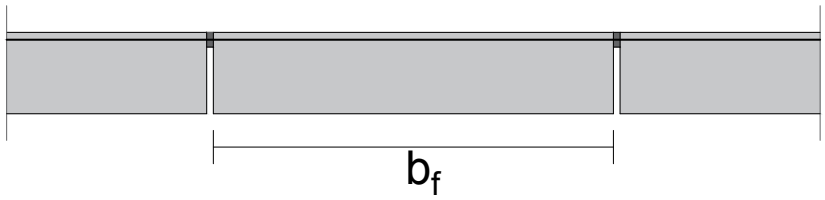

FIGURE E.18: Transverse floor-to-floor connection by single prestressing at the top of the cross-section

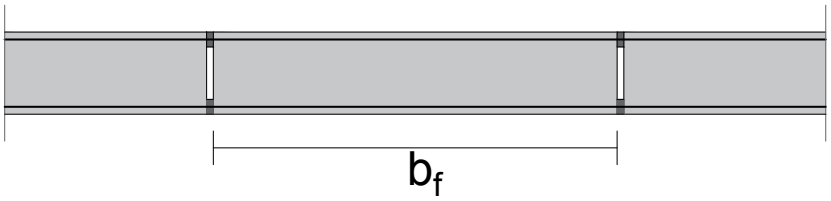

FIGURE E.19: Transverse floor-to-floor connection by double prestressing at both the top and the bottom of the cross-section

The choice for connection affects the structural integrity of the separate floor girders as a whole. The stiffness of the floor plate in transverse direction is directly dependent on the amount of connection points and thus the floor girders will act more as one plate if the connection consists of two contact points. To enhance the structural integrity of the floor girders a double floor-to-floor connection is assumed in this analysis.

Floor-to-side connection:
The floor-to-side connection determines the internal forces occurring in the floor girder and therefore the reaction forces in the side girder. Four connection types are distinguished. The types are characterised by their moment capacity and can either be classified as free ($k_\phi = 0$), fixed ($k_\phi = 1$) or being somewhere in between ($0 < k_\phi < 1$). For simplicity it is assumed that connection type A is free and all other three connection types are fixed.

A. Corbel
The biggest disadvantage of this connection type is that the floor girder is very prone to cracking in the location specified in Figure E.20. The dynamic behaviour of traffic loads in combination with the poor accessibility of this part of the structure makes this connection type undesirable. Furthermore, the amount of reinforcement needed in the floor girder at the connection might lead to bonding problems in the limited floor height.

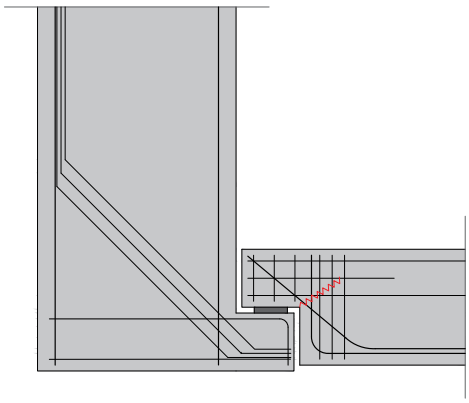

FIGURE E.20: Floor-to-side connection as a corbel, with $k_\phi = 0$

B. Suspension
This is an adequate connection type, but it might lead to problems when connecting the two prefabricated elements together. Either protruding suspension reinforcement will be required in the floor girders, which will complicate the transportation of those floor elements, or additional room for prestress cables will have to be incorporated in the side girder. The latter requires additional prestress ducts and thus a reduced concrete cross-section in the side girder. Also, protruding anchorages underneath the bridge deck will have to be manoeuvred away somehow.

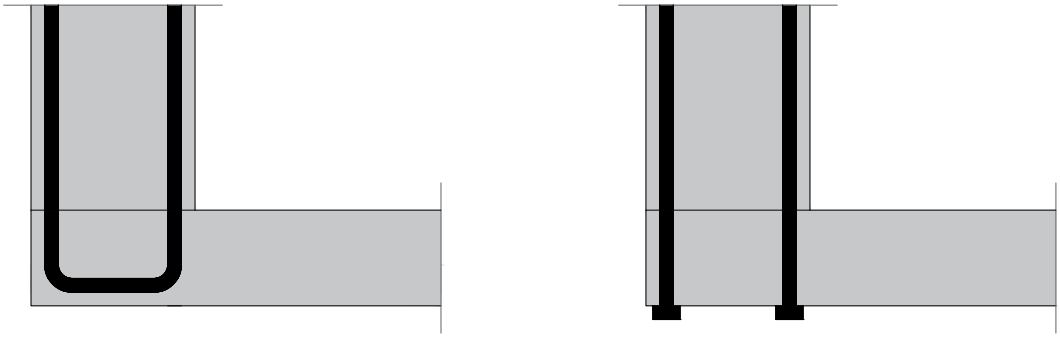

FIGURE E.21: Floor-to-side connection by suspension through prestressing, with $k_\phi = 1$

C. Clamped
All disadvantages of the Type B connection are not relevant in this connection type and therefore this is a very viable solution. Part of the pre-tensioned prestress required for the floor girders can be replaced by ducts for post-tensioning, which will be the same prestress required for the connection between the floor and the side girder. Thus no additional prestressing steel is needed. Furthermore, transportation is not hindered by protruding reinforcement bars and the protruding anchorages at the side of the side girders are also not a problem.

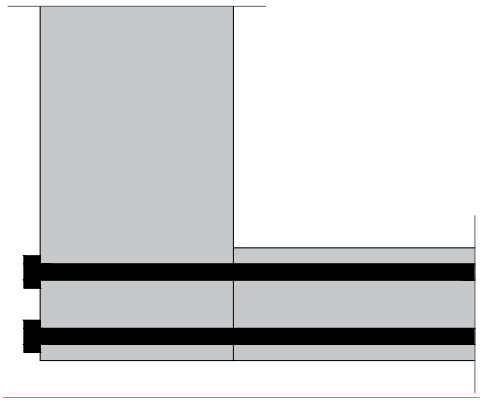

FIGURE E.22: Floor-to-side connection by prestressing, with $k_\phi = 1$

D. Monolithic
The fourth connection type consists of a monolithic connection between the floor and the truss girder. Compared to the other three types, it has the advantage of stability during the construction phase, eliminating the need for temporary scaffolding of the floor girders during construction.

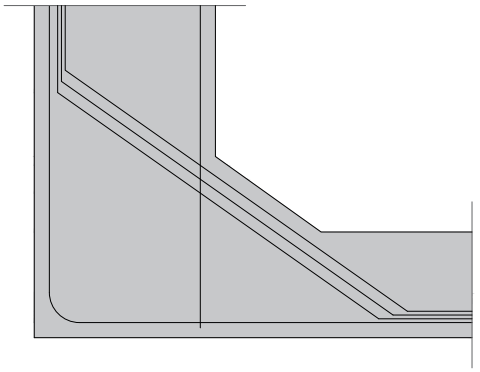

FIGURE E.23: Monolithic floor-to-side connection, with $k_\phi = 1$

However, in order to satisfy the transportation limitations the entire bridge will have to consist of segments containing both floor and side girder segments. The consequences are:

- The flexibility of fabrication is lost, as for every bridge the dimensions differ and an entirely different mould is required;
- For weight reduction of the structure a different solution than a truss girder an a multicell box girder will have to be sought;
- The connection between each segment will have to be considered.

Since this connection type requires a substantially different approach, it will not be considered in this analysis.

From the considerations discussed above, only connection type C, in which the floor girders are clamped between the side girders by means of prestressing, will be considered in this analysis. Therefore also the floor-to-side connection is modelled as fixed.

In terms of transportation and flexibility of design it would be preferable if the side girders were also built up out of several segments with size limitations. For reasons of simplicity this is however neglected in this analysis.

E.7. DESIGN CONSIDERATIONS AND ASSUMPTIONS

Several design considerations and assumptions have been determined in order to simplify the design analysis. They are listed below:

- Floor girder width:
  The width of the floor girders is chosen at b_f = 3.00 m as this coincides with normal transportation limits for road transport.
- Amount of floor girders:
  The amount of floor girders is based on the width of the floor girders and two end girders with sufficient width to transfer the loads to the abutments. It is assumed that the end girders are at least 2.0 m wide.
- Height asphalt layer:
  The height of the asphalt layer is h_a = 140 mm and based on the current regulations for designing bridges. Although it is expected that the thickness of this layer can be reduced when applying it to UHPC, in this design no adaptation is made.
- Width kerbs:
  The width of the kerbs is w_0 = 1.3 m and is based on the minimum space required for safety barriers according to the Dutch standard (w = 0.8 m) and walking space behind this barrier (w = 0.5 m) *[Spencer, 2009]*.
- Height concrete kerbs:
  According to standard details the height of the kerb should be at least 50 mm higher than the asphalt layer, thus h_k = 190 mm.
- Width side girder:
  The width of the side girder is chosen at b_t = 1.2 m, which is according to the design codes for railway trough bridges. This requirement is based on safety reasons so that the side can accommodate a safe escape route from passing trains. Although in this design safety barriers are used and the height of the side girders is too high for an escape route, the assumption is left unaltered as it seems a plausible starting point.
- Maximum aggregate diameter:
  The maximum aggregate diameter of 8 mm is based on cement mixes found in practice.
- Fibre length:
  The fibre length of 13 mm is based on cement mixes found in practice.
- Time-dependent prestress losses:
  The time-dependent prestress losses are assumed to be 15%.
- Crack widths:
  It is assumed that all crack widths that occur in ULS will be sufficiently small to satisfy all durability requirements.
- Reduced modulus of elasticity:
  If cracking occurs in ULS this also reduces the modulus of elasticity and the the orthotropic behaviour and deformation of the elements. For reasons of simplicity this reduction of E_c is neglected.
- Time-dependent behaviour:
  No time-dependent behaviour of concrete, like creep or relaxation, is taken into account in this analysis.
- Construction phase:
  Load actions that arise during the construction phase of the bridge will not be considered in this analysis.

F

CONCEPTUAL DESIGN TROUGH BRIDGE - MASSIVE ELEMENTS

In this appendix the analytical design method for a trough bridge with massive elements is considered.

F.1. SUMMARY

The resulting dimensions for the floor girders are given in Table F.1 and supported by Figures F.1 and F.2. For the side girders the same is done in Table F.2 and Figures F.3 to F.5.

Floor girder - massive			
Parameter		**Value**	**Unit**
Dimensions			
Height floor girder	h_f	0.61	*m*
Width floor girder	b_f	3.00	*m*
Length floor girder	l_f	18.17	*m*
Height top connection	h_{c1}	0.11	*m*
Height bottom connection	h_{c2}	0.11	*m*
Prestress			
Bottom; x-direction	$A_{p;x1}$	10700	mm^2
Eccentricity	$e_{p;x1}$	0.25	*m*
Top; x-direction	$A_{p;x2}$	13500	mm^2
Eccentricity	$e_{p;x2}$	0.25	*m*
Bottom; y-direction	$A_{p;y1}$	2600	mm^2
Eccentricity	$e_{p;y1}$	0.25	*m*
Bottom; y-direction	$A_{p;y2}$	2700	mm^2
Eccentricity	$e_{p;y2}$	0.25	*m*

TABLE F.1: Resulting dimensions for the floor girders in a massive element trough bridge design

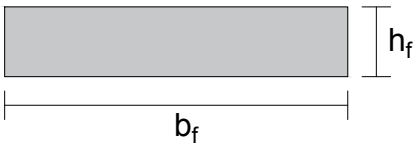

FIGURE F.1: Cross-sectional view of the massive floor girder in x-direction

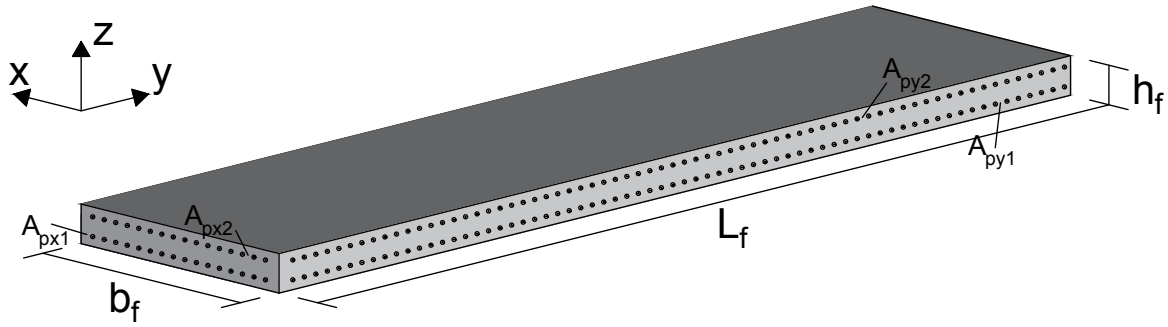

FIGURE F.2: Massive floor girders with the prestressing cables indicated (not to scale)

Side girder - massive			
Parameter		**Value**	**Unit**
Dimensions			
Height side girder	h_t	2.30	*m*
Width side girder	b_t	1.20	*m*
Length side girder	l_t	36.80	*m*
Prestress			
Bottom; y-direction - phase 1	$A_{p;y1}$	31000	mm^2
Bottom; y-direction - phase 2	$A_{p;y1}$	40600	mm^2
Eccentricity	$e_{p;y1}$	0.55	*m*
Drag	f_p	0.35	*m*
Top; y-direction - phase 1	$A_{p;y2}$	2600	mm^2
Top; y-direction - phase 2	$A_{p;y2}$	2600	mm^2
Eccentricity	$e_{p;y1}$	1.03	*m*
Drag	f_p	0.00	*m*

TABLE F.2: Resulting dimensions for the side girders in a massive element trough bridge design

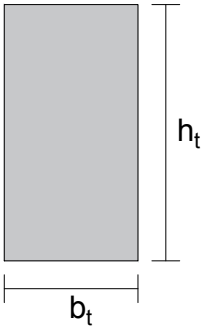

FIGURE F.3: Cross-sectional view of the massive side girder in y-direction

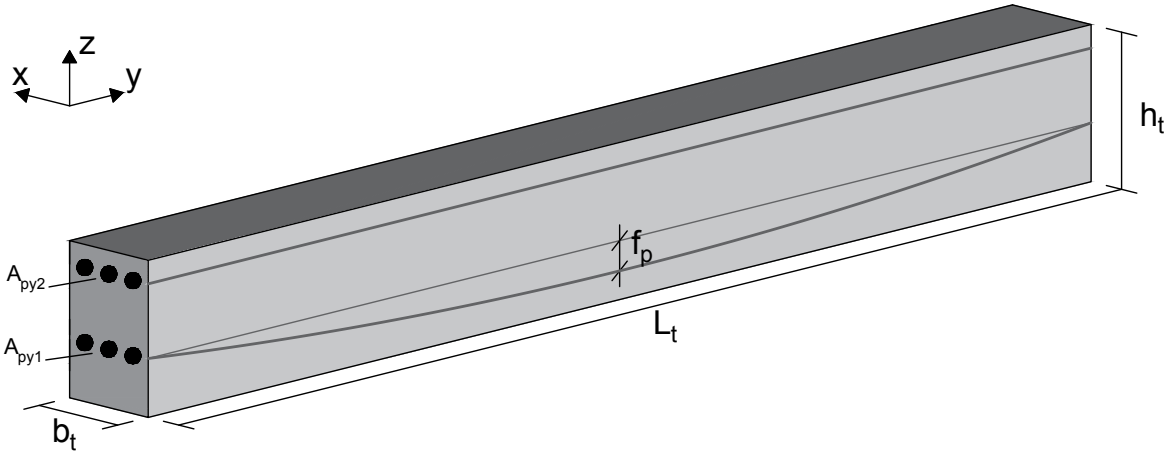

FIGURE F.4: Massive side girders with the prestressing cables indicated (not to scale)

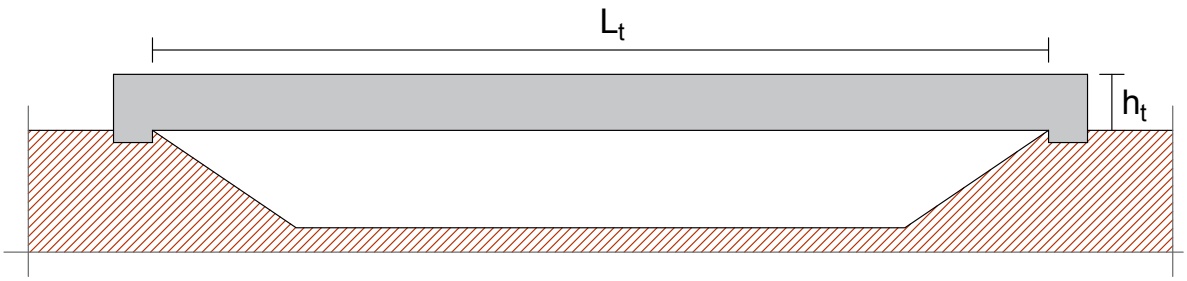

FIGURE F.5: Side view of the trough bridge in x-direction

F.2. FLOOR GIRDER

F.2.1. Geometry and specific considerations

The geometry for the massive floor girders is governed by the current total deck height and the required asphalt depth:

$h_f = 0.75 - 0.14 = 0.61$ m

Furthermore, the width of the floor girders is governed by transportation limits and is chosen as:

$b_f = 3.00$ m

The length of the floor girders is obtained from the current width of the roadway and an additional space for kerbs and safety barriers:

$l_f = 15.57 + 2 \cdot 1.30 = 18.17$ m

The connection to the side girder is assumed to be fixed as considered in Figure E.22.

For the prestressing, pre-tensioning cables with a straight tendon profile are assumed for both lower and upper prestressing.

F.2.2. Analytical load actions

In Figure F.6 the general model for the floor girder is given. In the analytical approach, each floor girder is considered as a beam supported at both ends. Since the connection between the side and the floor girder is assumed to be fixed, the supports are modelled as clamped.

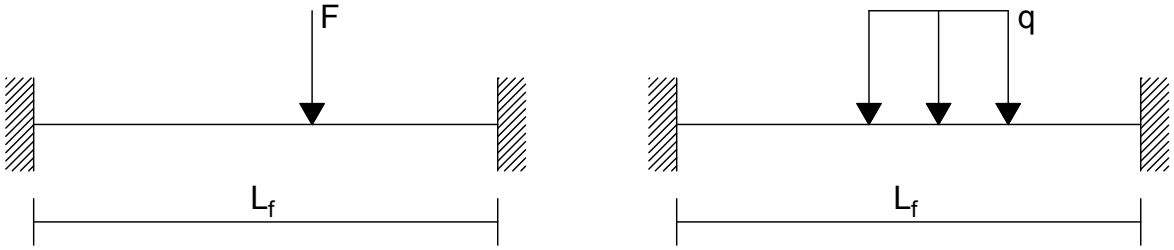

FIGURE F.6: General floor model for the calculation of point loads and distributed loads

Guyon-Massonnet method

In a plate, loads will be laterally distributed depending on the flexibility and stiffness of the plate in both longitudinal and transverse direction. For plates consisting of multiple beams, these reduced loads can be determined through application of the Guyon-Massonet method. This method is further elaborated below.
It must be stated, however, that the applicability of this Guyon-Massonet method is confined to beams which are simply supported. Since the connection between the floor and side girders is fixed, technically Guyon-Massonnet cannot be applied. For this analysis, however, it is assumed that the method is applicable nev-

ertheless but in Appendix I this assumption is checked in comparison to the FEM model. It can be seen that indeed, for a free floor-to-side connection the Guyon-Massonnet method is a very good estimate for the lateral load distribution, while for a fixed connection the analytical results differ slightly from the FEM results.

In the Guyon-Massonnet method, the flexural and torsional rigidity of the system is used to construct influence lines for loads located at specific reference stations. These influence lines are based on so-called K-values that can be obtained from standard graphs. From these influence lines at the reference points a new influence line can be constructed for the actual location of the load. The average K-value corresponding to this location can then be used to determine the reduced loads.

The bridge width is denoted as $2 \cdot b$, with nine reference stations at each $0.25 \cdot b$ (see Figure F.7).

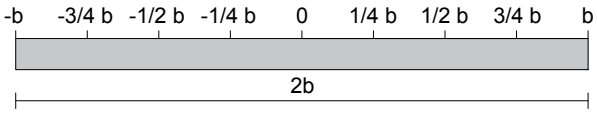

FIGURE F.7: Reference stations on a beam with a width of $2 \cdot b$

$$I_x = \frac{1}{12} \cdot b_f \cdot {h_f}^3 = 5.67 \cdot 10^{-2} \text{ m}^4$$

$$I_y = \frac{1}{12} \cdot b_{fe} \cdot ({h_{c1}}^3 + {h_{c2}}^3) + (z_t - 0.5 \cdot h_{c1})^2 \cdot b_{fe} \cdot h_{c1} + (z_b - 0.5 \cdot h_{c2})^2 \cdot b_{fe} \cdot h_{c2} = 1.89 \cdot 10^{-2} \text{ m}^4$$

Flexible rigidity per unit width:

$$\rho_x = \frac{\Sigma E \cdot I_x}{b_f} = 9.46 \cdot 10^8 \text{ kNm}^3$$

$$\rho_y = \frac{\Sigma E \cdot I_y}{l_f} = 6.99 \cdot 10^8 \text{ kNm}^3$$

Torsional rigidity per unit width:

$$\gamma_x = \frac{\Sigma G \cdot I_x}{b_f} = 3.94 \cdot 10^8 \text{ kNm}^3$$

$$\gamma_y = \frac{\Sigma G \cdot I_y}{l_f} = 2.91 \cdot 10^8 \text{ kNm}^3$$

Flexural stiffness:

$$\theta = \frac{b_f}{l_f} \cdot \sqrt[4]{\frac{\rho_x}{\rho_y}} = 0.178 \text{ rad}$$

Torsional stiffness:

$$\alpha = \frac{\gamma_x + \gamma_y}{2 \cdot \sqrt{\rho_x \cdot \rho_y}} = 0.421$$

For $\alpha = 0$ and $\alpha = 1$, standard graphs exist in which the K-values at each reference station can be determined for the established value of θ. The values from these table can be used to construct the K-values for the established torsional stiffness α by applying the following formula:

$$K_\alpha = K_0 + (K_1 - K_0) \cdot \sqrt{\alpha}$$

This gives the K-values as presented in Table F.3 and from this the influence lines for each reference station can be constructed (see Figure F.8).
Now, the location of the loads must be determined. For both load situation 1 and 3 (Figures E.2 and E.4), the considered beam lies at midspan of the side girder, thus at $0 \cdot b$. For load situations 2 and 4 (Figures E.3 and

K_0	- b	-3/4 b	-1/2 b	-1/4 b	0	1/4 b	1/2 b	3/4 b	b
- b	4,10	3,40	2,48	1,72	0,95	0,24	-0,53	-1,20	-1,91
-3/4 b	3,27	2,70	2,10	1,55	0,99	0,42	-0,14	-0,65	-1,20
-1/2 b	2,51	2,11	1,72	1,36	0,98	0,63	0,24	-0,15	-0,47
-1/4 b	1,73	1,56	1,33	1,19	1,02	0,84	0,63	0,42	0,23
0	0,95	0,97	0,99	1,03	1,05	1,03	0,99	0,97	0,95
1/4 b	0,23	0,42	0,63	0,84	1,02	1,19	1,33	1,56	1,73
1/2 b	-0,47	-0,15	0,24	0,63	0,98	1,36	1,72	2,11	2,51
3/4 b	-1,20	-0,65	-0,14	0,42	0,99	1,55	2,10	2,70	3,27
b	-1,91	-1,20	-0,53	0,24	0,95	1,72	2,48	3,40	4,10
K_1	**- b**	**-3/4 b**	**-1/2 b**	**-1/4 b**	**0**	**1/4 b**	**1/2 b**	**3/4 b**	**b**
- b	1,33	1,22	1,13	1,04	0,97	0,92	0,87	0,83	0,77
-3/4 b	1,20	1,16	1,09	1,03	0,99	0,95	0,90	0,86	0,83
-1/2 b	1,10	1,08	1,06	1,02	1,00	0,97	0,94	0,90	0,88
-1/4 b	1,02	1,02	1,01	1,00	1,00	0,99	0,98	0,94	0,92
0	0,97	0,98	1,00	1,01	1,03	1,01	1,00	0,98	0,97
1/4 b	0,92	0,94	0,98	0,99	1,00	1,00	1,01	1,02	1,02
1/2 b	0,88	0,90	0,94	0,97	1,00	1,02	1,06	1,08	1,10
3/4 b	0,83	0,86	0,90	0,95	0,99	1,03	1,09	1,16	1,20
b	0,77	0,83	0,87	0,92	0,97	1,04	1,13	1,22	1,33
K_α	**- b**	**-3/4 b**	**-1/2 b**	**-1/4 b**	**0**	**1/4 b**	**1/2 b**	**3/4 b**	**b**
- b	2,30	1,98	1,60	1,28	0,96	0,68	0,38	0,12	-0,17
-3/4 b	1,93	1,70	1,44	1,21	0,99	0,76	0,54	0,33	0,12
-1/2 b	1,59	1,44	1,29	1,14	0,99	0,85	0,69	0,53	0,41
-1/4 b	1,27	1,21	1,12	1,07	1,01	0,94	0,86	0,76	0,68
0	0,96	0,98	1,00	1,02	1,04	1,02	1,00	0,98	0,96
1/4 b	0,68	0,76	0,86	0,94	1,01	1,07	1,12	1,21	1,27
1/2 b	0,41	0,53	0,69	0,85	0,99	1,14	1,29	1,44	1,59
3/4 b	0,12	0,33	0,54	0,76	0,99	1,21	1,44	1,70	1,93
b	-0,17	0,12	0,38	0,68	0,96	1,28	1,60	1,98	2,30

TABLE F.3: K-values for $\alpha = 0$. $\alpha = 1$ and $\alpha = 0.417$

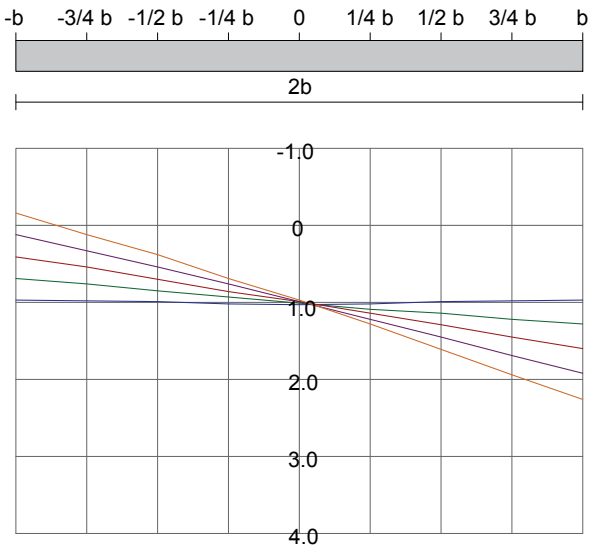

FIGURE F.8: Influence lines for each reference station for $\theta = 0.178$ rad and $\alpha = 0.417$

E.5), the considered beam lies at the end span, at 0.6 m from the edge or at $+0.97 \cdot b$. For both locations, the influence line is constructed from the nine reference station lines, as presented in Figures F.9 and F.10.
For this analysis, the UDL starts at $-b$ and ends at $+b$, while the KEL loads are located at -0.6 m and +0.6 m from the beam location.

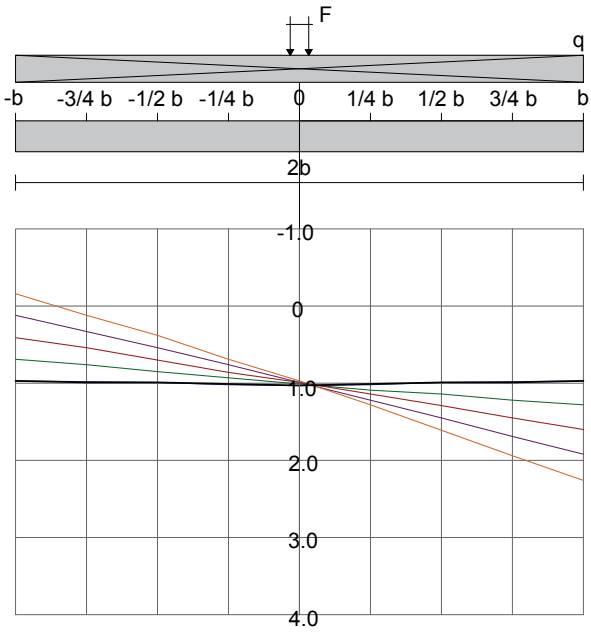

FIGURE F.9: Influence lines for loading at midspan (at $0 \cdot b$)

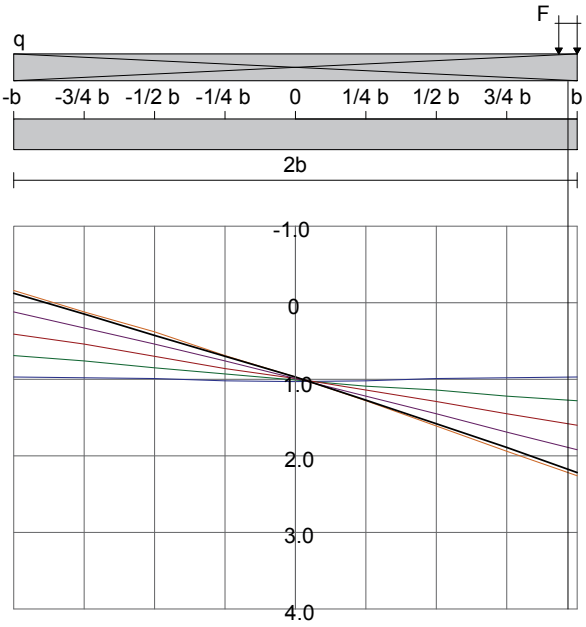

FIGURE F.10: Influence lines for loading at end span (at $+0.97 \cdot b$)

Then for the UDL loads it holds:

At $0 \cdot b$: $K_{mean} = 1.00$

$l_{UDL} = l_t = 36.8$ m

$f_{UDL} = \frac{q_{UDL} \cdot l_{UDL}}{l_t}$

$q_{f;UDL} = f_{UDL} \cdot K_{mean} \cdot b_f$

$q_{f;UDL;1} = \frac{10.35 \cdot 36.8}{36.8} \cdot 1.00 \cdot 3.00 = 30.97$ kN/m

$q_{f;UDL;2} = \frac{3.5 \cdot 36.8}{36.8} \cdot 1.00 \cdot 3.00 = 10.47$ kN/m

At $0.97 \cdot b$: $K_{mean} = 1.06$
$l_{UDL} = 34.64$ m (Conservative assumption: only the psitive part of the influence line is taken into account)

$q_{f;UDL;1} = \frac{10.35 \cdot 36.64}{36.8} \cdot 1.06 \cdot 3.00 = 30.96$ kN/m
$q_{f;UDL;2} = \frac{3.5 \cdot 36.8}{36.8} \cdot 1.06 \cdot 3.00 = 10.47$ kN/m

For the KEL loads it holds:
At $0 \cdot b$: $K_{mean} = 1.04$
$l_{KEL} = l_f = 12.0$ m (Assumption: the KEL loads will spread over only a part of the total width (see Appendix I))
$f_{KEL} = \frac{F_{KEL} \cdot l_{KEL}}{l_f}$
$F_{f;KEL} = f_{KEL} \cdot K_{mean} \cdot b_f$

$F_{f;KEL;1} = \frac{150 \cdot 12.0}{36.8} \cdot 1.02 \cdot 3.00 = 77.78$ kN
$F_{f;KEL;2} = \frac{100 \cdot 12.0}{36.8} \cdot 1.02 \cdot 3.00 = 51.85$ kN
$F_{f;KEL;3} = \frac{50 \cdot 12.0}{36.8} \cdot 1.02 \cdot 3.00 = 25.93$ kN

At $0.97 \cdot b$: $K_{mean} = 2.21$
$l_{KEL} = l_f = 10.0$ m (Assumption: the KEL loads will spread over only a part of the total width (see Appendix I))

$F_{f;KEL;1} = \frac{150 \cdot 12.0}{36.8} \cdot 1.02 \cdot 3.00 = 199.17$ kN
$F_{f;KEL;2} = \frac{100 \cdot 12.0}{36.8} \cdot 1.02 \cdot 3.00 = 132.78$ kN
$F_{f;KEL;3} = \frac{50 \cdot 12.0}{36.8} \cdot 1.02 \cdot 3.00 = 66.39$ kN

Slender analysis
By using slender analysis theory, the beam behaviour can be described as follows:

Distributed load:

Euler-Bernouilli beam: $EI \cdot v'''' = q_z$

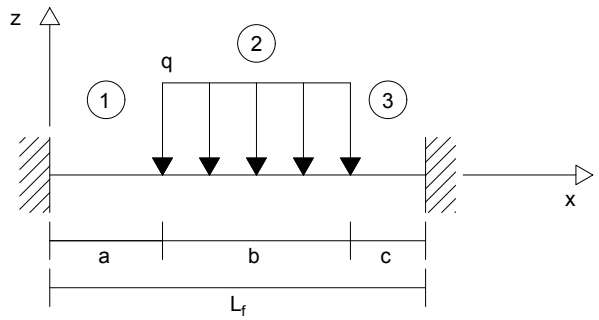

FIGURE F.11: Mechanical model for a distributed load on a clamped beam at an arbitrary distance a from the left support to an arbitrary distance c to the right support

Divide the beam into three fields: left of the distributed load (1), at the distributed load (2) and right of the distributed load (3). Each field is described by its own equations and constants:
$EI \cdot v_1'''' = 0$
$EI \cdot v_1''' = C_1$
$EI \cdot v_1'' = C_1 \cdot x + C_2$
$EI \cdot v_1' = \frac{1}{2} \cdot C_1 \cdot x^2 + C_2 \cdot x + C_3$
$EI \cdot v_1 = \frac{1}{6} \cdot C_1 \cdot x^3 + \frac{1}{2} \cdot C_2 \cdot x^2 + C_3 \cdot x + C_4$

$$EI \cdot v_2'''' = q_z$$
$$EI \cdot v_2''' = q_z \cdot x + C_5$$
$$EI \cdot v_2'' = \frac{1}{2} \cdot q_z \cdot x^2 + C_5 \cdot x + C_6$$
$$EI \cdot v_2' = \frac{1}{6} \cdot q_z \cdot x^3 + \frac{1}{2} \cdot C_5 \cdot x^2 + C_6 \cdot x + C_7$$
$$EI \cdot v_2 = \frac{1}{24} \cdot q_z \cdot x^4 + \frac{1}{6} \cdot C_5 \cdot x^3 + \frac{1}{2} \cdot C_6 \cdot x^2 + C_7 \cdot x + C_8$$

$$EI \cdot v_3'''' = 0$$
$$EI \cdot v_3''' = C_9$$
$$EI \cdot v_3'' = C_9 \cdot x + C_10$$
$$EI \cdot v_3' = \frac{1}{2} \cdot C_9 \cdot x^2 + C_10 \cdot x + C_11$$
$$EI \cdot v_1 = \frac{1}{6} \cdot C_9 \cdot x^3 + \frac{1}{2} \cdot C_10 \cdot x^2 + C_11 \cdot x + C_12$$

The following boundary conditions apply:

At x = 0:	$v_1 = 0$ (1)	At x = L:	$v_3 = 0$ (3)
	$M_1 = 0$ (2)		$M_3 = 0$ (4)
At x = a:	$v_1 = v_2$ (5)	At x = b:	$v_2 = v_3$ (9)
	$\phi_1 = \phi_2$ (6)		$\phi_2 = \phi_3$ (10)
	$M_1 = M_2$ (7)		$M_2 = M_3$ (11)
	$V_1 = V_2$ (8)		$V_2 = V_3$ (12)

With 12 unknown constants and 12 equations, this is a solvable system. The results are:

$C_1 = \frac{q}{2 \cdot L^3} \cdot (2 \cdot L^3 \cdot a - 2 \cdot L^3 \cdot b - 2 \cdot L \cdot a^3 + 2 \cdot L \cdot b^3 + a^4 - b^4)$
$C_2 = -\frac{q}{12 \cdot L^2} \cdot (6 \cdot L^2 \cdot a^2 - 6 \cdot L^2 \cdot b^2 - 8 \cdot L \cdot a^3 + 8 \cdot L \cdot b^3 + 3 \cdot a^4 - 3 \cdot b^4)$
$C_3 = 0$
$C_4 = 0$
$C_5 = -\frac{q}{2 \cdot L^3} \cdot (2 \cdot L^3 \cdot b + 2 \cdot L \cdot a^3 - 2 \cdot L \cdot b^3 - a^4 + b^4)$
$C_6 = \frac{q}{12 \cdot L^2} \cdot (6 \cdot L^2 \cdot b^2 + 8 \cdot L \cdot a^3 - 8 \cdot L \cdot b^3 - 3 \cdot a^4 + 3 \cdot b^4)$
$C_7 = -\frac{1}{6} \cdot q \cdot a^3$
$C_8 = \frac{1}{24} \cdot q \cdot a^4$
$C_9 = -\frac{q}{2 \cdot L^3} \cdot (2 \cdot L \cdot a^3 - 2 \cdot L \cdot b^3 - a^4 + b^4)$
$C_{10} = \frac{q}{12 \cdot L^2} \cdot (8 \cdot L \cdot a^3 - 8 \cdot L \cdot b^3 - 3 \cdot a^4 + 3 \cdot b^4)$
$C_{11} = -\frac{1}{6} \cdot q \cdot a^4 + \frac{1}{6} \cdot q \cdot b^4$
$C_{12} = \frac{1}{24} \cdot q \cdot a^4 - \frac{1}{24} \cdot q \cdot b^4 4$

By inserting these constants into the equations given for v, ϕ, M and V, all internal forces, deformations and rotations at every location of the beam can be determined.

Point load:

Euler-Bernouilli beam: $EI \cdot v'''' = q_z$

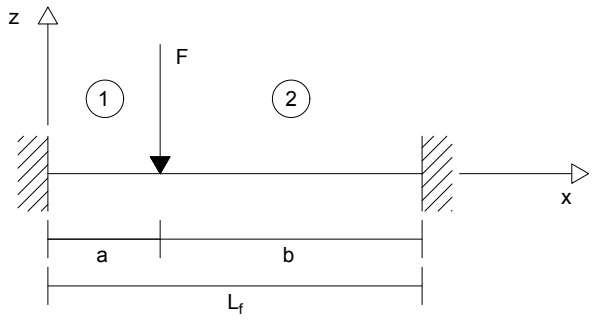

FIGURE F.12: Mechanical model for a point load on a clamped beam at an arbitrary distance a from the left support

Divide the beam into two fields: left of the point load (1) and right of the point load (2). Each field is described by its own equations and constants:

$$EI \cdot v_1'''' = 0$$
$$EI \cdot v_1''' = C_1$$
$$EI \cdot v_1'' = C_1 \cdot x + C_2$$
$$EI \cdot v_1' = \tfrac{1}{2} \cdot C_1 \cdot x^2 + C_2 \cdot x + C_3$$
$$EI \cdot v_1 = \tfrac{1}{6} \cdot C_1 \cdot x^3 + \tfrac{1}{2} \cdot C_2 \cdot x^2 + C_3 \cdot x + C_4$$

$$EI \cdot v_2'''' = 0$$
$$EI \cdot v_2''' = C_5$$
$$EI \cdot v_2'' = C_5 \cdot x + C_6$$
$$EI \cdot v_2' = \tfrac{1}{2} \cdot C_5 \cdot x^2 + C_6 \cdot x + C_7$$
$$EI \cdot v_2 = \tfrac{1}{6} \cdot C_5 \cdot x^3 + \tfrac{1}{2} \cdot C_6 \cdot x^2 + C_7 \cdot x + C_8$$

The following boundary conditions apply:

At x = 0:	$v_1 = 0$ (1)	At x = L:	$v_3 = 0$ (3)
	$M_1 = 0$ (2)		$M_3 = 0$ (4)
At x = a:	$v_1 = v_2$ (5)		
	$\phi_1 = \phi_2$ (6)		
	$M_1 = M_2$ (7)		
	$V_1 = V_2$ (8)		

With 8 unknown constants and 8 equations, this is a solvable system. The results are:

$C_1 = -\frac{F}{L^3} \cdot (L^3 - 3 \cdot L \cdot a^2 + 2 \cdot a^3)$
$C_2 = \frac{F \cdot a}{L^2} \cdot (L^2 - 2 \cdot L \cdot a + a^2)$
$C_3 = 0$
$C_4 = 0$
$C_5 = \frac{F \cdot a^2}{L^3} \cdot (3 \cdot L - 2 \cdot a)$
$C_6 = -\frac{F \cdot a^2}{L^2} \cdot (2 \cdot L - a)$
$C_7 = \frac{1}{2} \cdot F \cdot a^2$
$C_8 = -\frac{1}{6} \cdot F \cdot a^3$

By inserting these constants into the equations given for v, ϕ, M and V, all internal forces, deformations and rotations at every location of the beam can be determined.

Through the principle of superposition and the respective distance and value of each load, the beam behaviour can be determined in each position of the beam. This is done for situation 1 and 2 as presented in Figures E.2 and E.3 to obtain the maximum cross-sectional forces in the floor girder. The results are presented in Table F.4.

Floor	Char.	Design	
Shear	1289	1882	*kN*
Moment$^{+}_{x}$	596	878	*kNm*
Moment$^{-}_{x}$	-528	-761	*kNm*
Moment$^{+}_{y}$	2079	3123	*kNm*
Moment$^{-}_{Y}$	-3720	-5427	*kNm*
Deformation	15,1	-	*mm*

TABLE F.4: Resulting maximum load actions in the massive floor girders

Plate theory
Since the floor girder is modelled as a beam, only forces in the x-direction are considered. In reality however, the connection of the floor girders to each other constitutes plate behaviour and thus the cross-sectional forces in y-direction must also be considered.

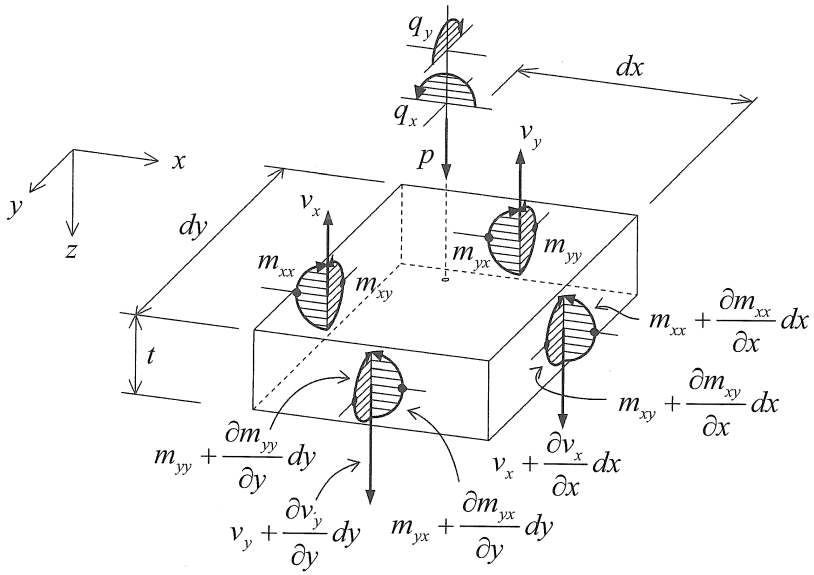

FIGURE F.13: Positive loads and stress distribution in a plate element *[Blauwendraad, 2006]*

In order to obtain the stresses in transverse direction, plate theory is used, for which all stresses and forces are depicted in Figure F.13. In pure bending, which occurs when only distributed loads act on the plate, the stresses in transverse direction can be determined by means of the Poissons ratio ν.

For a slab spanning in one direction it holds *[Walraven and Braam, 2015]*:

Maximum bending moment in a strip with width b_x	M_y	$= 0.125 \cdot q \cdot b_x \cdot {l_{eff}}^2$
Maximum tensile stress:	$\sigma_c(x)$	$= \pm \frac{M_y}{W_y}$
Maximum strain bottom fibre:	$\epsilon_c(x)$	$= \frac{\sigma_c(x)}{E_c} = \frac{M_y}{E_c \cdot W_y}$
In case of free deformation:	$\epsilon_c(y)$	$= -\nu \cdot \epsilon_c(x)$
Moment induced to restore compatibility:	M_x	$= E_c \cdot (-\epsilon_c(x)) \cdot W_x = \nu \cdot M_y \cdot \frac{W_x}{W_y}$
In a solid isotropic and uncracked slab:		$W_x = W_y$
Bending moment in transverse direction:	M_x	$= \nu \cdot M_y$

Pure shear loading, or a combination of bending and shear load actions, is much more difficult since shear deformation has to be taken into account. According to *[Steele and Balch, 2009]* pure shear loading gives a constant transverse shear and a linearly varying bending moment. The combination gives rise to warping of the normal but this effect is small when the length is larger than the thickness, which is definitely the case in this situation. The accompanying effect is further elaborated on in Appendix I.

F.2.3. FEM load actions

As a verification, the analytical results are compared to computational calculations by means of a finite element model (FEM). The program used is SCIA and the model input is listed in Appendix H An extensive comparison is conducted in Appendix I for all loading situations and for the different possible floor-to-floor and floor-to-side connections.

From these results it can thus be concluded that the analytically obtained cross-sectional forces are an ade-

quate representation of the forces to be expected from a FEM calculation. It can indeed be seen that although the Guyon-Massonnet method is adequate for a simply supported plate, the results for a fixed plate differ quite significantly. Furthermore, the influence of shear deformation has quite an impact on the transverse load distribution as a result of shear lading.
The orthotropic behaviour of the floor girders is calculated significantly different in the analytical model and the FEM model, causing large deviations in mainly the transverse floor stresses. Therefore it is not possible to compare both models adequately on this influence. Also, the flexibility of the side girder and thus of the floor supports has a significant effect on the cross-sectional forces. Due to the rotational capacity of the side girder the negative moments in longitudinal direction will decrease, but this also results in an increase of positive moments, transverse moments and the absolute and relative deflection of the floor girders.
These differences will however not be implemented in the analytical approach for reasons of simplicity.

F.2.4. Unity Checks

The floor girder will have to be designed with sufficient capacity to resist all loads, while fulfilling the boundary conditions as set in E.5.
From both the analytical calculation of the load actions and the FEM calculations it follows that the maximum internal forces in the floor in the x-direction occur at the end span, thus load situation 2, while in the y-direction they occur at midspan, thus load situation 1.

Moment capacity

The moment capacity is obtained by analysing moment equilibrium and horizontal force equilibrium in the cross-section. Since partial prestressing is applied, this is an iterative procedure in which the choice of compression height x_e is governing. The general calculation is first described, after which the Unity Checks for both positive and negative moments in both x- and y-direction are determined.

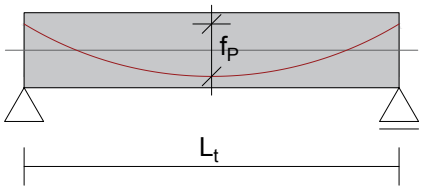

FIGURE F.14: Model schematisation of a beam on two supports with a curved prestress profile

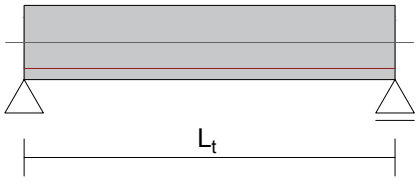

FIGURE F.15: Model schematisation of a beam on two supports with a straight prestress profile

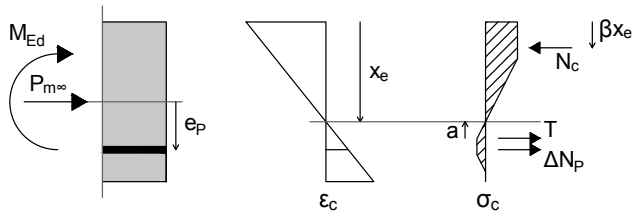

FIGURE F.16: Strain and stress distribution in concrete cross-section under positive bending moment action

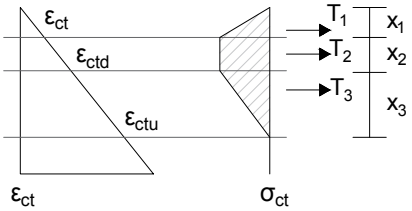

FIGURE F.17: Stress and strain distribution in the tensile zone of the concrete cross-section

For the stresses and strain in the tensile zone it holds:

$$
\begin{aligned}
f_{ctd1} &= \frac{f_{ctm}}{\gamma_c} \\
f_{ctd2} &= \frac{\sigma_{w03}}{K \cdot \gamma_c} \\
\epsilon_{ct} &= \frac{f_{ctd1}}{E_c} \\
\epsilon_{ctu} &= \frac{l_f}{4 \cdot l_c} \\
l_c &= \frac{2}{3} \cdot h \\
\epsilon_{ct03} &= \frac{w_{03}}{l_c} + \epsilon_{ct} \\
\epsilon_{ctd} &= \epsilon_{ct03} + \frac{f_{ctd2} - f_{ctd1}}{f_{ctd2}} \cdot (\epsilon_{ctu} - \epsilon_{ct03})
\end{aligned}
$$

In full prestressing the starting point for design is the assumption that the prestress has reached its yield strength before the concrete reaches its ultimate compressive strength:

$$\Delta E_p = \frac{1}{E_p} \cdot (f_{pd} - \sigma_{pm0}) = \frac{d_p - x_u}{x_u} \cdot \epsilon_{cu3}$$

$$\text{Thus: } x_u \leq \frac{\epsilon_{cu3}}{\frac{1}{E_p} \cdot (f_{pd} - \sigma_{pm0}) + \epsilon_{cu3}} \cdot d_p$$

First horizontal equilibrium is considered:

$$\Sigma F_x = 0 \quad \rightarrow \quad N_c = P_{m\infty} + T + \Delta N_p$$

$$\begin{aligned} N_c &= \alpha \cdot b \cdot f - cd \cdot x_u \\ \alpha &= \frac{\epsilon_{ecu3} - \frac{1}{2} \cdot \epsilon_{c3}}{\epsilon_{cu3}} \\ P_{m\infty} &= A_p \cdot \sigma_{pm0} \\ \Delta N_p &= A_p \cdot (f_{pd} - \sigma_{pm\infty}) \end{aligned}$$

$$\begin{aligned} T &= \Sigma T_i \qquad T_1 = \tfrac{1}{2} \cdot b \cdot f_{ctd1} \cdot x_1 \qquad x_1 = \frac{\epsilon_{ct}}{\epsilon_{cu3}} \cdot x_u \\ &\qquad\quad T_2 = b \cdot f_{ctd1} \cdot x_2 \qquad x_2 = \frac{\epsilon_{ctd} - \epsilon_{ct}}{\epsilon_{cu3}} \cdot x_u \\ &\qquad\quad T_3 = \tfrac{1}{2} \cdot b \cdot f_{ctd1} \cdot x_3 \qquad x_3 = \frac{\epsilon_{ctu} - \epsilon_{ctd}}{\epsilon_{cu3}} \cdot x_u \end{aligned}$$

$$T = \tfrac{1}{2} \cdot b \cdot f_{ctd1} \frac{\epsilon_{ctu} + \epsilon_{ctd} - \epsilon_{ct}}{\epsilon_{cu3}} \cdot x_u$$

$$\rightarrow A_p = \frac{N_c - T}{f_{pd}} = \frac{\alpha \cdot b \cdot f_{cd} \cdot x_u - \frac{1}{2} \cdot b \cdot f_{ctd1} \cdot (\epsilon_{ctu} + \epsilon_{ctd} - \epsilon_{ct}) \cdot x_u}{\epsilon_{cu3} \cdot f_{pd}}$$

Then moment equilibrium is considered:

$$\Sigma M = 0 \quad \rightarrow \quad M_{Rdc} = N_c \cdot (1 - \beta) \cdot x_u + T \cdot a + \Delta N_p \cdot (d_p - x_u) + P_{m\infty} \cdot (z_t - x_u)$$

$$\begin{aligned} \beta &= \frac{\frac{1}{2} \cdot {\epsilon_{cu3}}^3 + \frac{1}{6} \cdot {\epsilon_{c3}}^2 - \frac{1}{2} \cdot \epsilon_{cu3} \cdot \epsilon_{c3}}{\alpha \cdot {\epsilon_{cu3}}^2} \\ a &= \frac{\Sigma T_i \cdot a_i}{\Sigma T_i} \\ a_1 &= \tfrac{2}{3} \cdot x_1 \\ a_2 &= x_1 + \tfrac{1}{2} \cdot x_2 \\ a_3 &= x_1 + x_2 + \tfrac{1}{3} \cdot x_3 \end{aligned}$$

However, in this case not full prestressing is applied, but partial prestressing. In that case the starting assumption - that the prestress yields before ultimate concrete strength is reached - is not valid anymore and this calculation becomes an iterative procedure in which compression zone height x_e and required prestress area A_p depend on each other.

In this analysis, the compression zone x_e is taken as a variable input parameter from which all other parameters depend, including A_p. By comparing A_p to the maximum and minimum values as found in the boundary conditions, a sufficient moment capacity design can be found.

This results in:

In x-direction:

Positive:	Prestress area:	A_{px1}	= 10700 mm^2 (72 strands)
	Prestress eccentricity:	e_{p1}	= 0.25 m
	Compression zone height:	x_e	= 0.143 m
		α	= 0.5
		β	= 0.33
	Compression force:	N_c	= 20649 kN
	Prestress force:	P_{m01}	= 14930 kN
		$P_{m\infty 1}$	= 12690 kN
	Increase in prestress force:	ΔN_p	= 3597 kN
	Tensile force:	T	= 4362 kN
		a	= 0.16 m
	Moment capacity concrete:	M_{Rdc}	= 6185 kNm
	Moment capacity prestress:	M_{Rdp}	= 3173 kNm
	Total moment capacity:	M_{Rd}	= 9358 kNm
	$M_y{}^+$ in ULS:	M_{Ed}	= 3123 kNm
	Unity Check:	UC_M	= 0.33
Negative:	Prestress area:	A_{px2}	= 13500 mm^2 (90 strands)
	Prestress eccentricity:	e_{p2}	= 0.25 m
	Compression zone height:	x_e	= 0.180 m
		α	= 0.5
		β	= 0.33
	Compression force:	N_c	= 26053 kN
	Prestress force:	P_{m02}	= 18837 kN
		$P_{m\infty 2}$	= 16012 kN
	Increase in prestress force:	ΔN_p	= 4358 kN
	Tensile force:	T	= 5504 kN
		a	= 0.20 m
	Moment capacity concrete:	M_{Rdc}	= 7909 kNm
	Moment capacity prestress:	M_{Rdp}	= 4003 kNm
	Total moment capacity:	M_{Rd}	= 11912 kNm
	$M_y{}^-$ in ULS:	M_{Ed}	= 5427 kNm
	Unity Check:	UC_M	= 0.46

Check boundary conditions:

- Minimum concrete cover:

  For pre-tensioned steel: c_{com} = 36.5 mm

  $e_h = e_v$ = 26 mm

As shown in Figure F.18 and Table F.5, the boundary condition for minimum concrete cover is satisfied

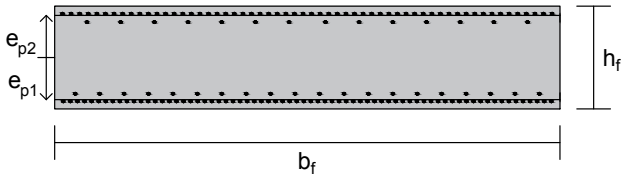

FIGURE F.18: Prestress configuration in the massive floor element in x-direction

x		n [-]	e [m]
e_{p1}	top	58	0.260
	bottom	14	0.210
	total	72	0.250
e_{p2}	top	20	0.215
	bottom	70	0.260
	total	90	0.250
Maximum		72	0.260

TABLE F.5: Prestress configuration in the massive floor element in x-direction

in this direction.

- Minimum prestress area:
  At t = ∞, the following stress distribution occurs at SLS loading:

$$\sigma_1 = -\frac{P_{m\infty 1}}{A_c} + \frac{e_{p1} \cdot P_{m\infty 1} \cdot z_t}{I_c} - \frac{P_{m\infty 2}}{A_c} - \frac{e_{p2} \cdot P_{m\infty 2} \cdot z_t}{I_c} - \frac{M_{t=\infty} \cdot z_t}{I_c}$$
$$\sigma_2 = -\frac{P_{m\infty 1}}{A_c} - \frac{e_{p1} \cdot P_{m\infty 1} \cdot z_b}{I_c} - \frac{P_{m\infty 2}}{A_c} + \frac{e_{p2} \cdot P_{m\infty 2} \cdot z_b}{I_c} + \frac{M_{t=\infty} \cdot z_t}{I_c}$$

Minimum presress			
	M_y^+	M_y^-	Unit
σ_1	-31.32	-0.15	N/mm^2
σ_2	-0.05	-31.22	N/mm^2

TABLE F.6: Boundary condition check for minimum prestress in x-direction

Since all end fibres are in compression, the condition for minimum prestress is met.

- Maximum prestress area:
  The maximum compression stress at t = 0 is given by:

$$\sigma_1 = -\frac{P_{m01}}{A_c} + \frac{e_{p1} \cdot P_{m01} \cdot z_t}{I_c} - \frac{P_{m02}}{A_c} - \frac{e_{p2} \cdot P_{m0} \cdot z_t}{I_c}$$
$$\sigma_2 = -\frac{P_{m\infty 1}}{A_c} - \frac{e_{p1} \cdot P_{m\infty 1} \cdot z_b}{I_c} - \frac{P_{m\infty 2}}{A_c} + \frac{e_{p2} \cdot P_{m\infty 2} \cdot z_b}{I_c}$$

Maximum prestress (comp)		
	M = 0	Unit
σ_1	-23.70	N/mm^2
σ_2	-13.20	N/mm^2

TABLE F.7: Boundary condition check for maximum prestress based on compression strength in x-direction

These are smaller than $0.6 \cdot f_{ck}(t) = 0.6 \cdot 46.5 = 27.9$ N/mm^2 and thus this condition is met.

The maximum tensile stress in the upper and lower fibre after prestressing is given by:

$$\sigma_1 = -\frac{P_{m01}}{A_c} + \frac{e_{p1} \cdot P_{m01} \cdot z_t}{I_c} - \frac{P_{m02}}{A_c} - \frac{e_{p2} \cdot P_{m0} \cdot z_t}{I_c} - \frac{M_{t=0} \cdot z_t}{I_c}$$
$$\sigma_2 = -\frac{P_{m\infty 1}}{A_c} - \frac{e_{p1} \cdot P_{m\infty 1} \cdot z_b}{I_c} - \frac{P_{m\infty 2}}{A_c} + \frac{e_{p2} \cdot P_{m\infty 2} \cdot z_b}{I_c} + \frac{M_{t=0} \cdot z_b}{I_c}$$

Maximum prestress (tension)			
	M_y^+	M_y^-	Unit
σ_1	-27.09	-16.94	N/mm^2
σ_2	-3.05	-33.50	N/mm^2

TABLE F.8: Boundary condition check for maximum prestress based on tension strength in x-direction

The boundary condition ($\sigma \leq f_{ctd1}$) is met at all locations.

- Ductility:
  The maximum stress in top and bottom fibre in the ULS is given by:

$$\sigma_1 = -\frac{P_{m\infty 1}}{A_c} + \frac{e_{p1} \cdot P_{m\infty 1} \cdot z_t}{I_c} - \frac{P_{m\infty 2}}{A_c} - \frac{e_{p2} \cdot P_{m\infty 2} \cdot z_t}{I_c} - \frac{M_{Ed} \cdot z_t}{I_c}$$
$$\sigma_2 = -\frac{P_{m\infty 1}}{A_c} - \frac{e_{p1} \cdot P_{m\infty 1} \cdot z_b}{I_c} - \frac{P_{m\infty 2}}{A_c} + \frac{e_{p2} \cdot P_{m\infty 2} \cdot z_b}{I_c} + \frac{M_{Ed} \cdot z_t}{I_c}$$

  It follows that for both cases the tensile stress in the concrete is larger than f_{ctd1} and thus cracking occurs. This means that the condition for ductility is met.

Maximum prestress (ductility)			
	M_y^+	M_y^-	Unit
σ_1	-36.93	9.02	N/mm^2
σ_2	5.56	-40.39	N/mm^2

TABLE F.9: Boundary condition check for maximum prestress based on ductility in x-direction

In y-direction:

Positive:	Prestress area:	A_{py1}	= 2600 mm^2 (18 strands per meter)
	Prestress eccentricity:	e_{p1}	= 0.25 m
	Compression zone height:	x_e	= 0.035 m
		α	= 0.50
		β	= 0.33
	Compression force:	N_c	= 5041 kN
	Prestress force:	P_{m0}	= 3625 kN
		$P_{m\infty}$	= 3082 kN
	Increase in prestress force:	ΔN_p	= 873 kN
	Tensile force:	T	= 1059 kN
		a	= 0.04 m
	Moment capacity concrete:	M_{Rdc}	= 1443 kNm
	Moment capacity prestress:	M_{Rdp}	= 770 kNm
	Total moment capacity:	M_{Rd}	= 2214 kNm
	M_x^+ in ULS:	M_{Ed}	= 878 kNm
	Unity Check:	UC_M	= 0.40
Negative:	Prestress area:	A_{py2}	= 2700 mm^2 (18 strands per meter)
	Compression zone height:	x_e	= 0.036 m
	Prestress eccentricity:	e_{p2}	= 0.25 m
		α	= 0.50
		β	= 0.33
	Compression force:	N_c	= 5216 kN
	Prestress force:	P_{m0}	= 3772 kN
		$P_{m\infty}$	= 3206 kN
	Increase in prestress force:	ΔN_p	= 909 kN
	Tensile force:	T	= 1102 kN
		a	= 0.04 m
	Moment capacity concrete:	M_{Rdc}	= 1502 kNm
	Moment capacity prestress:	M_{Rdp}	= 801 kNm
	Total moment capacity:	M_{Rd}	= 2304 kNm
	M_x^- in ULS:	M_{Ed}	= 761 kNm
	Unity Check:	UC_M	= 0.33

Check boundary conditions:

- Minimum concrete cover:
  For pre-tensioned steel: c_{com} = 36.5 mm
  $e_h = e_v$ = 26 mm
  As shown in Figure F.19 and Table F.10, the boundary condition for minimum concrete cover is satisfied in this direction.

- Minimum prestress area:
  At t = ∞, the following stress distribution occurs at SLS loading:

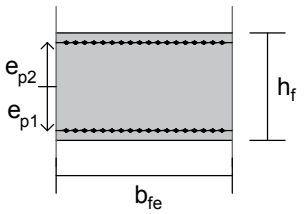

FIGURE F.19: Prestress configuration in the massive floor element in y-direction

y		n [-]	e [m]
e_{p1}	total	18	0.250
e_{p2}	total	18	0.250
Maximum		24	0.260

TABLE F.10: Prestress configuration in the massive floor element in y-direction

$$\sigma_1 = -\frac{P_{m\infty 1}}{A_c} + \frac{e_{p1} \cdot P_{m\infty 1} \cdot z_t}{I_c} - \frac{P_{m\infty 2}}{A_c} - \frac{e_{p2} \cdot P_{m\infty 2} \cdot z_t}{I_c} - \frac{M_{t=\infty} \cdot z_t}{I_c}$$
$$\sigma_2 = -\frac{P_{m\infty 1}}{A_c} - \frac{e_{p1} \cdot P_{m\infty 1} \cdot z_b}{I_c} - \frac{P_{m\infty 2}}{A_c} + \frac{e_{p2} \cdot P_{m\infty 2} \cdot z_b}{I_c} + \frac{M_{t=\infty} \cdot z_t}{I_c}$$

Minimum presress			
	M_x^+	M_x^-	Unit
σ_1	-20.42	-2.30	N/mm^2
σ_2	-0.20	-18.32	N/mm^2

TABLE F.11: Boundary condition check for minimum prestress in y-direction

Since all end fibres are in compression, the condition for minimum prestress is met.

- Maximum prestress area:
  The maximum compression stress at t = 0 is given by:

$$\sigma_1 = -\frac{P_{m01}}{A_c} + \frac{e_{p1} \cdot P_{m01} \cdot z_t}{I_c} - \frac{P_{m02}}{A_c} - \frac{e_{p2} \cdot P_{m0} \cdot z_t}{I_c}$$
$$\sigma_2 = -\frac{P_{m\infty 1}}{A_c} - \frac{e_{p1} \cdot P_{m\infty 1} \cdot z_b}{I_c} - \frac{P_{m\infty 2}}{A_c} + \frac{e_{p2} \cdot P_{m\infty 2} \cdot z_b}{I_c}$$

Maximum prestress (comp)		
	M = 0	Unit
σ_1	-12.72	N/mm^2
σ_2	-11.54	N/mm^2

TABLE F.12: Boundary condition check for maximum prestress based on compression strength in y-direction

These are smaller than $0.6 \cdot f_{ck}(t) = 0.6 \cdot 46.5 = 27.9$ N/mm^2 and thus this condition is met.

The maximum tensile stress in the upper and lower fibre after prestressing is given by:

$$\sigma_1 = -\frac{P_{m01}}{A_c} + \frac{e_{p1} \cdot P_{m01} \cdot z_t}{I_c} - \frac{P_{m02}}{A_c} - \frac{e_{p2} \cdot P_{m0} \cdot z_t}{I_c} - \frac{M_{t=0} \cdot z_t}{I_c}$$
$$\sigma_2 = -\frac{P_{m\infty 1}}{A_c} - \frac{e_{p1} \cdot P_{m\infty 1} \cdot z_b}{I_c} - \frac{P_{m\infty 2}}{A_c} + \frac{e_{p2} \cdot P_{m\infty 2} \cdot z_b}{I_c} + \frac{M_{t=0} \cdot z_b}{I_c}$$

Maximum prestress (tension)			
	M_x^+	M_x^-	Unit
σ_1	-16.10	-5.95	N/mm^2
σ_2	-1.39	-31.83	N/mm^2

TABLE F.13: Boundary condition check for maximum prestress based on tension strength in y-direction

The boundary condition ($\sigma \leq f_{ctd1}$) is met at all locations.

- Ductility:
  The maximum stress in top and bottom fibre in the ULS is given by:

$$\sigma_1 = -\frac{P_{m\infty 1}}{A_c} + \frac{e_{p1} \cdot P_{m\infty 1} \cdot z_t}{I_c} - \frac{P_{m\infty 2}}{A_c} - \frac{e_{p2} \cdot P_{m\infty 2} \cdot z_t}{I_c} - \frac{M_{Ed} \cdot z_t}{I_c}$$

$$\sigma_2 = -\frac{P_{m\infty 1}}{A_c} - \frac{e_{p1} \cdot P_{m\infty 1} \cdot z_b}{I_c} - \frac{P_{m\infty 2}}{A_c} + \frac{e_{p2} \cdot P_{m\infty 2} \cdot z_b}{I_c} + \frac{M_{Ed} \cdot z_t}{I_c}$$

Maximum prestress (ductility)			
	M_x^+	M_x^-	Unit
σ_1	-24.97	1.46	N/mm^2
σ_2	4.36	-22.08	N/mm^2

TABLE F.14: Boundary condition check for maximum prestress based on ductility in y-direction

It follows that for no case the tensile stress in the concrete is larger than f_{ctd1} and thus no cracking will occur in y-direction. However, since this condition is met in x-direction it is assumed sufficient anyway.

Shear capacity

The shear capacity consists of three components, which will be elaborated below. The maximum shear capacity has to be checked for load situation 2 only.

- Concrete capacity:

  $V_{Rdc} = \frac{0.24}{\gamma_{CF} \cdot \gamma_E} \cdot k \cdot \sqrt{f_{ck}} \cdot b_w \cdot z$

  $k = 1 + 3 \cdot \frac{\sigma_{cp}}{f_{ck}}$ for $\sigma_{cp} \geq 0$
  $k = 1 + 0.7 \cdot \frac{\sigma_{cp}}{f_{ck}}$ for $\sigma_{cp} < 0$
  $\sigma_{cp} = \frac{N_{Ed}}{A_c}$ > 0 for compression
  $\gamma_{CF} \cdot \gamma_E = 1.5$
  $b_w = b_f - \Sigma\Phi_{duct}$
  $z = 0.9 \cdot d_p$

- Fibre capacity:

  $V_{Rdf} = \frac{A_{vf} \cdot \sigma_{Rdf}}{\tan(\theta)}$

  $A_{vf} = b_w \cdot z$
  For strain-softening and low strain-hardening UHPC:
  $\sigma_{Rdf} = \frac{1}{K \cdot \gamma_{CF} \cdot w_{lim}} \cdot \int \sigma_f(w) dw$
  $w_{lim} = \max\{w_u; w_{max}\}$
  $w_u = 0.3$ mm
  $w_{max} = 0.20$ mm
  $\int \sigma_f(w) dw = 0.5 \cdot \frac{\epsilon_{ctu} + \epsilon_{ctd} - \epsilon_{ct}}{\epsilon_{cu3}} \cdot f_{ctd1}$
  $\gamma_{CF} = 1.3$ for durable/transient situations
  $K = K_{global}$ for $h, b > 5 \cdot l_{fibre}$
  $K = K_{local}$ for $h, b < 5 \cdot l_{fibre}$

- Reinforcement capacity:

  $V_{Rds} = \frac{A_{sw}}{s} \cdot z \cdot f_{ywd} \cdot \cot(\theta)$

Then the shear capacity of the cross-section is given by:

$$V_{Rd} = V_{Rdc} + V_{Rdf} + V_{Rds}$$

Normal force from prestress:	N_{Ed}	= 13290 kN
Working width of cross-section:	b_w	$= b_f$ = 3.00 m
Concrete shear capacity:	V_{Rdc}	= 3582 kN

Fibre shear strength:	σ_{Rdf}	= 5.10 N/mm^2
Fibre shear capacity:	V_{Rdf}	= 13440 kN
Shear reinforcement diameter:	Φ_{sw}	= 20 mm
Number of bars over width:	n_{sw}	= 2
Bar spacing:	s	= 100 mm
Reinforcement capacity:	V_{Rds}	= 2401 kN
Total shear capacity:	V_{Rd}	= 19423 kN
Maximum shear in cross-section:	V_{Ed}	1882 kN
Unity Check:	UC_V	= 0.10

Check boundary conditions:

- Minimum concrete cover:
  For reinforcement steel: c_{com} = 31 mm
  $e_h = e_v$ = 26 mm
  The requirement for minimum concrete cover is met as a bar spacing of s_y = 100 mm > e_h = 26 mm is used and the application of two shear bars for every meter length results in a spacing of $s_x = \frac{b}{2}$ = 500 mm > e_h.

- Ultimate strength compressive struts:
  From the boundary conditions given in E.5 it follows that the compressive struts have an ultimate strength that limits the shear capacity of the concrete:

  $V_{Rd;max}$ = 2613 kN

  Since V_{Rd} is larger than $V_{Rd;max}$, this capacity is too optimistic and must be replaced by $V_{Rd;max}$. The Unity Check then becomes:

  Unity Check: UC_V = 0.72

Deformation capacity
The maximum deformation must be checked according to *[NEN-EN 1992-1-1, 2005]* for load situation 2, since the maximum deformation occurs when loading the end span.

Maximum allowable deformation:	$w_{k;max}$	$= \frac{l_f}{250}$ = 73 mm
Maximum deformation:	w_{Ek}	= 27 mm
Unity Check:	UC_w	= 0.37

F.3. SIDE GIRDER

F.3.1. Geometry and specific considerations

The width of the side girder is chosen as:
b_t = 1.2 m
This width is based on the regulations for railway trough bridges, in which the side girder acts as an escape route. Although in this design safety barriers are used and the height of the side girders is too high for an escape route, the assumption is left unaltered as it seems a plausible starting point.

The length of the side girders is obtained from the current total span length of the bridge:
l_t = 36.8 m

The height of the side girder h_t is to be determined in the calculations to satisfy all Unity Checks. It follows that a height of h_t = 2.3 m provides an adequate structural performance of the side girder.

The connection to the floor girders is fixed, but the side girders themselves are simply supported.

For the prestressing, Double post-tensioning is assumed, in which the lower prestress has curved tendons and the upper prestress has straight tendons.

F.3.2. Analytical load actions

For the maximum load in the side girder load situations 3 (Figure E.4) and 4 (Figure E.5) apply.
For the load distribution to the side girder a different approach is used than the Guyon-Massonnet approach for the floor girder. Instead, the stiffness ratio of the two load-carrying directions is used to determine the effective width over which the loads are spread. This spreading is only applicable for the KEL loads since the distributed traffic loads and permanent loads are present over the entire span length of the bridge.

With an isotropic plate, the loads will spread evenly in both directions and thus the effective width will be equal to the distance of the concentrated loads to the side girder (see Figures F.20 and F.21). In this case, however, the plate consists of several floor girders connected to each other and the stiffness of this connection is lower than that of the massive plate itself, depending on the height of the connection. The resulting distribution is illustrated in Figures F.22 and F.23 and it can be seen that the loads will be distributed over a smaller width than in the first case.

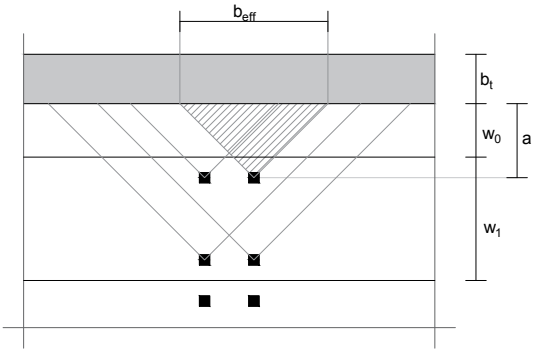

FIGURE F.20: Load spreading towards the side girder at midspan in an isotropic floor plate

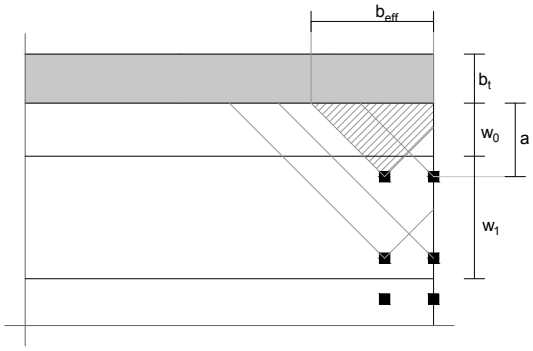

FIGURE F.21: Load spreading towards the side girder at end span in an isotropic floor plate

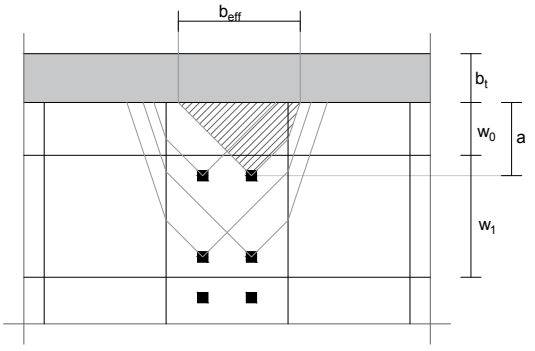

FIGURE F.22: Load spreading towards the side girder at midspan in an orthotropic floor plate

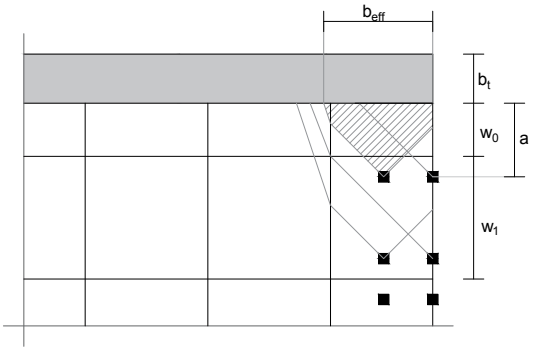

FIGURE F.23: Load spreading towards the side girder at end span in an orthotropic floor plate

The analytical calculation of the loads which are transferred from the floor girders onto the side girders requires the same approach as the slender analysis calculation presented in subsection F.2.2. It will therefore

not be repeated here. In Table F.15 the results from the KEL distribution and the slender analysis are presented for the side girder.

Truss	Char.	Design	
Shear	6172	8819	*kN*
Moment$_y$	5494	8088	*kNm*
Moment$_x$	54910	78324	*kNm*
Deformation	124	-	*mm*

TABLE F.15: Resulting maximum load actions in the massive side girders

These loads must be transferred from the connection point with the floor girder to the top of the side girder through suspension reinforcement. It is common practice to design this reinforcement based on just half of the tensile strength of the steel to provide for unknown dynamical and fatigue loads *[Allaart, 1994]*.

F.3.3. FEM load actions

Again, the analytical model is verified by means of a FEM calculation. The FEM model input and interpretation of the results can be found in Appendices H and I respectively.

It follows that both models differ significantly, due to two reasons. The first reason has to do with the incorporation of orthotropic behaviour in both models. Since the calculation methods differ substantially also the results give a large differentiation. It is thus not possible to compare both models adequately on this influence.
The second reason comes from the structural enhancement of the entire system, that is not taken into account in the analytical approach. In the analytical calculations the side girder is considered separately, while in reality its deformational behaviour depends on the presence of the floor girders and the other side girder. The result is that in reality the bending moment and deformation observed are respectively 60% and 50% lower than incorporated in the analytical approach. This difference is excepted in order to obtain a conservative design.

F.3.4. Unity Checks

The side girder will have to be designed with sufficient capacity to resist all loads, while fulfilling the boundary conditions as set in section E.5.
From both the analytical calculation of the load actions and the FEM calculations it follows that the maximum moment and maximum deformation in the side girder occur at midspan, thus load situation 3 (Figure E.4), while the maximum shear load occurs at the end span, thus situation 4 (Figure E.5).

Suspension reinforcement

Since the connection of floor and side girder is situated at the bottom of the side girder, all load actions working on the side beam must first be transferred to the top of the beam. As stated before, *[Allaart, 1994]* prescribes a reduced tensile strength of the suspension reinforcement to account for unknown dynamical and fatigue loads. It thus holds that:

Maximum distributed load acting on the side girder:	$q_{max;d}$	= 924 kN/m
Tensile strength suspension reinforcement:	$f_{yd;sus}$	= $\frac{1}{2}\cdot 435$ = 218 N/mm^2
Required suspension reinforcement area:	$A_{sus,req}$	= 4249 mm^2/m
Suspension reinforcement diameter:	Φ_{sw}	= 20 mm
Number of bars over width:	n_{sw}	= 2
Bar spacing:	s	= 120 mm
Applied suspension reinforcement area:	S_{sus}	= 5236 mm^2/m
Unity Check:	UC_{sus}	= 0.81

Moment capacity
As for the floor girder, the moment capacity is obtained by analysing moment equilibrium and horizontal force equilibrium in the cross-section. Again, partial prestressing is applied, in which the compressive zone height x_e is used as a variable input parameter for this iterative procedure.

The specifically determined parameters for the side girder are:

h_t = 2.3 m
e_{p1} = 0.55 m
f_{p1} = 0.35 m
e_{p2} = 1.03 m
f_{p2} = 0.00 m

It turns out that, in order to fulfil all boundary conditions, prestressing must be done in two phases because otherwise cracks will occur at $t = \infty$ in the upper fibre of the cross-section due to the upwards curvature pressure of the lower prestressing.
This results in:

Phase 1:	Lower prestress area:	A_{py1}	= 30900 mm^2 (11 tendons)
	Lower prestress eccentricity:	e_{p1}	= 0.55 m
	Lower prestress curvature drag:	f_p	= 0.35 m
	Compression zone height:	x_e	= 0.862 m
	Upper prestress area:	A_{py2}	= 2600 mm^2 (1 tendon)
	Upper prestress eccentricity:	e_{p2}	= 1.00 m
		α	= 0.50
		β	= 0.33
	Compression force:	N_c	= 49800 kN
	Lower prestress force:	P_{m01}	= 43105 kN
		$P_{m\infty1}$	= 36640 kN
	Upper prestress force:	P_{m02}	= 3627 kN
		$P_{m\infty2}$	= 3083 kN
	Increase in prestress force:	ΔN_p	= 10385 kN
	Tensile force:	T	= 2776 kN
		a	= 0.26 m
	Moment capacity concrete:	M_{Rdc}	= 48584 kNm
	Moment capacity prestress:	M_{Rdp}	= 12824 kNm
	Total moment capacity:	M_{Rd}	= 68749 kNm
	$M_x{}^+$ in ULS:	M_{Ed}	= 56584 kNm
	$M_x{}^-$ in ULS:	M_{Ed}	= 12866 kNm
	Unity Check:	UC_M	= 0.64
Phase 2:	Lower prestress area:	A_{py1}	= 40600 mm^2 (15 tendons)
	Compression zone height:	x_e	= 1.015 m
	Upper prestress area:	A_{py2}	= 2600 mm^2 (1 tendon)
		α	= 0.55
		β	= 0.34
	Compression force:	N_c	= 65061 kN
	Lower prestress force:	P_{m01}	= 56641 kN
		$P_{m\infty1}$	= 48145 kN
	Upper prestress force:	P_{m02}	= 3627 kN
		$P_{m\infty2}$	= 3083 kN
	Increase in prestress force:	ΔN_p	= 13645 kN
	Tensile force:	T	= 3271 kN
		a	= 0.30 m

Moment capacity concrete:	M_{Rdc}	= 60477 kNm
Moment capacity prestress:	M_{Rdp}	= 26480 kNm
Total moment capacity:	M_{Rd}	= 86957 kNm
$M_x{}^+$ in ULS:	M_{Ed}	= 78324 kNm
$M_x{}^-$ in ULS:	M_{Ed}	= 16851 kNm
Unity Check:	UC_M	= 0.71

Check boundary conditions:

- Minimum concrete cover:
  For post-tensioned steel: c_{com} = 85 mm
  $e_h = e_v$ = 60 mm
  As shown in Figure F.24 and Table F.16, the boundary condition for minimum concrete cover is satisfied

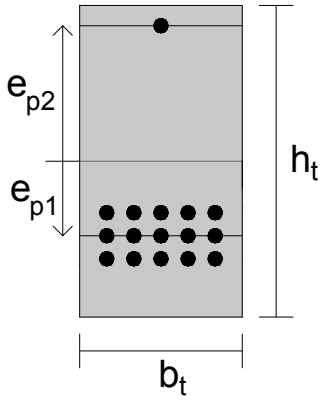

FIGURE F.24: Prestress configuration in the massive side element in y-direction

y		n [-]	e [m]
e_{p1}	top	5	0.380
	middle	5	0.550
	bottom	5	0.720
	total	15	0.550
e_{p2}	total	1	1.000
Maximum		6	1.010

TABLE F.16: Prestress configuration in the massive side element in y-direction

in this direction.

- Minimum prestress area:
  At t = ∞, the following stress distribution occurs at SLS loading:

$$\sigma_1 = -\frac{P_{m\infty 1}}{A_c} + \frac{e_{p1}\cdot P_{m\infty 1}\cdot z_t}{I_c} - \frac{P_{m\infty 2}}{A_c} - \frac{e_{p2}\cdot P_{m\infty 2}\cdot z_t}{I_c} - \frac{M_{t=\infty}\cdot z_t}{I_c} + \frac{f_{p1}\cdot P_{m\infty 1}\cdot z_t}{I_c}$$
$$\sigma_2 = -\frac{P_{m\infty 1}}{A_c} - \frac{e_{p1}\cdot P_{m\infty 1}\cdot z_b}{I_c} - \frac{P_{m\infty 2}}{A_c} + \frac{e_{p2}\cdot P_{m\infty 2}\cdot z_b}{I_c} + \frac{M_{t=\infty}\cdot z_t}{I_c} - \frac{f_{p1}\cdot P_{m\infty 1}\cdot z_b}{I_c}$$

Minimum presress		
Phase 1	x = 0.5 L	Unit
σ_1	-24.34	N/mm^2
σ_2	-4.44	N/mm^2

TABLE F.17: Boundary condition check for minimum prestress in y-direction in the first tensioning phase

Minimum presress		
Phase 2	x = 0.5 L	Unit
σ_1	-32.42	N/mm^2
σ_2	-4.70	N/mm^2

TABLE F.18: Boundary condition check for minimum prestress in y-direction in the second tensioning phase

It can be seen that for the two tensioning phases all end fibres are in compression and thus the condition for minimum prestress is met.

- Maximum prestress area:
  The maximum compression stress at t = 0 is given by:

$$\sigma_1 = -\frac{P_{m01}}{A_c} + \frac{e_{p1}\cdot P_{m01}\cdot z_t}{I_c} - \frac{P_{m02}}{A_c} - \frac{e_{p2}\cdot P_{m0}\cdot z_t}{I_c}$$
$$\sigma_2 = -\frac{P_{m\infty 1}}{A_c} - \frac{e_{p1}\cdot P_{m\infty 1}\cdot z_b}{I_c} - \frac{P_{m\infty 2}}{A_c} + \frac{e_{p2}\cdot P_{m\infty 2}\cdot z_b}{I_c}$$

It follows that these are smaller than $0.6\cdot f_{ck}(t) = 0.6\cdot 170 = 102$ N/mm^2 and thus this condition is met.

The maximum tensile stress in the upper and lower fibre after prestressing is given by:

$$\sigma_1 = -\frac{P_{m01}}{A_c} + \frac{e_{p1}\cdot P_{m01}\cdot z_t}{I_c} - \frac{P_{m02}}{A_c} - \frac{e_{p2}\cdot P_{m0}\cdot z_t}{I_c} - \frac{M_{t=0}\cdot z_t}{I_c} + \frac{f_{p1}\cdot P_{m01}\cdot z_t}{I_c}$$

Maximum prestress (comp)		
Phase 1		Unit
σ_1	2.05	N/mm^2
σ_2	-35.91	N/mm^2

TABLE F.19: Boundary condition check for maximum prestress based on compressive strength in y-direction in the first tensioning phase

Maximum prestress (comp)		
Phase 2		Unit
σ_1	4.18	N/mm^2
σ_2	-47.85	N/mm^2

TABLE F.20: Boundary condition check for maximum prestress based on compressive strength in y-direction in the second tensioning phase

$$\sigma_2 = -\frac{P_{m\infty 1}}{A_c} - \frac{e_{p1} \cdot P_{m\infty 1} \cdot z_b}{I_c} - \frac{P_{m\infty 2}}{A_c} + \frac{e_{p2} \cdot P_{m\infty 2} \cdot z_b}{I_c} + \frac{M_{t=0} \cdot z_b}{I_c} - \frac{f_{p1} \cdot P_{m01} \cdot z_b}{I_c}$$

Maximum prestress (tension)			
Phase 1	x = 0	x = 0.5 L	Unit
σ_1	2.05	5.27	N/mm^2
σ_2	-35.91	-39.13	N/mm^2

TABLE F.21: Boundary condition check for maximum prestress based on tensile strength in y-direction in the first tensioning phase

Maximum prestress (tension)			
Phase 2	x = 0	x = 0.5 L	Unit
σ_1	4.18	-15.28	N/mm^2
σ_2	-47.85	-28.39	N/mm^2

TABLE F.22: Boundary condition check for maximum prestress based on tensile strength in y-direction in the second tensioning phase

The boundary condition ($\sigma \leq f_{ctd1}$) is met at all locations.

- Ductility:
  The maximum stress in top and bottom fibre in the ULS is given by:

$$\sigma_1 = -\frac{P_{m\infty 1}}{A_c} + \frac{e_{p1} \cdot P_{m\infty 1} \cdot z_t}{I_c} - \frac{P_{m\infty 2}}{A_c} - \frac{e_{p2} \cdot P_{m\infty 2} \cdot z_t}{I_c} - \frac{M_{Ed} \cdot z_t}{I_c} + \frac{f_{p1} \cdot P_{m\infty 1} \cdot z_t}{I_c}$$

$$\sigma_2 = -\frac{P_{m\infty 1}}{A_c} - \frac{e_{p1} \cdot P_{m\infty 1} \cdot z_b}{I_c} - \frac{P_{m\infty 2}}{A_c} + \frac{e_{p2} \cdot P_{m\infty 2} \cdot z_b}{I_c} + \frac{M_{Ed} \cdot z_t}{I_c} - \frac{f_{p1} \cdot P_{m\infty 1} \cdot z_b}{I_c}$$

Maximum prestress (ductility)		
Phase 1	x = 0.5 L	Unit
σ_1	-39.62	N/mm^2
σ_2	10.84	N/mm^2

TABLE F.23: Boundary condition check for maximum prestress based on ductility in y-direction in the first tensioning phase

Maximum prestress (ductility)		
Phase 2	x = 0.5 L	Unit
σ_1	-54.55	N/mm^2
σ_2	17.43	N/mm^2

TABLE F.24: Boundary condition check for maximum prestress based on ductility in y-direction in the second tensioning phase

It follows that for both tensioning phases the tensile stress in the concrete is larger than f_{ctd1} and thus cracking will occur in y-direction.

Shear capacity

The shear capacity is determined in the same manner as was the case for the floor girder. The largest difference in this calculation is that the effective width of the girder has to be reduced due to the lower bond characteristics of grouted prestress cables. Therefore the configuration of prestress ducts near the supports is chosen wisely in order to have an adequate cross-sectional width (Figure F.25).

Also, *[AFGC, 2013]* prescribes that a reduction of shear force may be applied if the shear load is located within a certain distance of the end support, see also Figure F.26. However, since in this case a distributed load is applied and not a concentrated point load this reduction cannot be taken into account.

The shear capacity of the cross-section is given by:

$$V_{Rd} = V_{Rdc} + V_{Rdf} + V_{Rds}$$

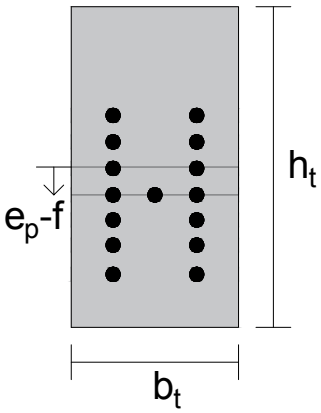

FIGURE F.25: Configuration of the post-tensioning ducts at the end span to obtain a maximum effective width for shear capacity

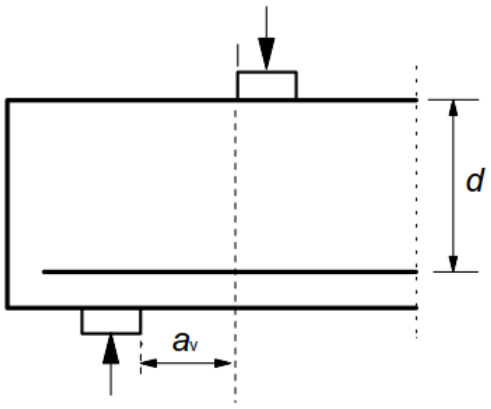

FIGURE F.26: Possible shear force reduction if shear force is positioned within a distance $0.5 \cdot d \leq a_v \leq 2 \cdot d$ *[NEN-EN 1992-1-1, 2005]*

Normal force from prestress:	N_{Ed}	= 48145 kN
Working width of cross-section:	b_w	$= b_f$ = 1.00 m
Concrete shear capacity:	V_{Rdc}	= 3684 kN
Fibre shear strength:	σ_{Rdf}	= 5.37 N/mm^2
Fibre shear capacity:	V_{Rdf}	= 12560 kN
Shear reinforcement diameter:	Φ_{sw}	= 20 mm
Number of bars over width:	n_{sw}	= 2
Bar spacing:	s	= 100 mm
Reinforcement capacity:	V_{Rds}	= 6414 kN
Total shear capacity:	V_{Rd}	= 22658 kN
Maximum shear in cross-section:	V_{Ed}	= 8819 kN
Unity Check:	UC_V	= 0.39

Check boundary conditions:

- Minimum concrete cover:
  For reinforcement steel: c_{com} = 31 mm
  $e_h = e_v$ = 26 mm
  The requirement for minimum concrete cover is met as a bar spacing of s_x = 100 mm > e_h = 26 mm is used and the application of two shear bars for every meter length results in a spacing of $s_y = \frac{b}{2}$ = 500 mm > e_h.

- Ultimate strength compressive struts:
  From the boundary conditions given in E.5 it follows that the compressive struts have an ultimate strength that limits the shear capacity of the concrete:

  $V_{Rd;max}$ = 2318 kN

  Since V_{Rd} is larger than $V_{Rd;max}$, this capacity is too optimistic and must be replaced by $V_{Rd;max}$. The Unity Check then becomes:

  Unity Check: UC_V = 3.71

  Clearly, the cross-section does not satisfy the shear capacity Unity Check. In order to increase the Unity

Check, the ultimate strength of the compressive struts must be increased. When looking at the formula for $V_{Rd;max}$, it can be seen that the only parameters that can be changed are the cross-sectional width and heigh-section.
It follows that a massive cross-sectional area is required to fulfil this condition, with b_t = 2.0 m and h_t = 4.0 m. Then, the Unity Check for shear capacity becomes:

Unity Check: UC_V = 0.91

However, since this analysis is based on several consumptions and for instance important load actions like fatigue are not considered, it is advised to incorporate a double shear force capacity (n = 2). Then:
$V_{Ed} = n \cdot V_{Ed}$ = 17440 kN
In that case, the dimensions of the cross-section at the supports would become b_t = 2.5 m and h_t = 5.5 m.
Unity Check: UC_V = 0.98

It is thus evident that the shear capacity is a large problem in designing trough girders for traffic bridges.

Torsion capacity
Torsion occurs in the side girders due to the eccentrically supported floor girders. The torsional moment induces shear stresses in the outer shell of the cross-section, as depicted in Figure F.27. The cross-section has a certain torsional capacity before cracking occurs and reinforcement has to be applied. The cracking moment is given by:

$$T_{Rdc} = 2 \cdot A_k \cdot t_eff \cdot f_{ctd}$$

In which:
$A_k = b_m \cdot h_m$
$t_{eff} = \frac{A_c}{u}$

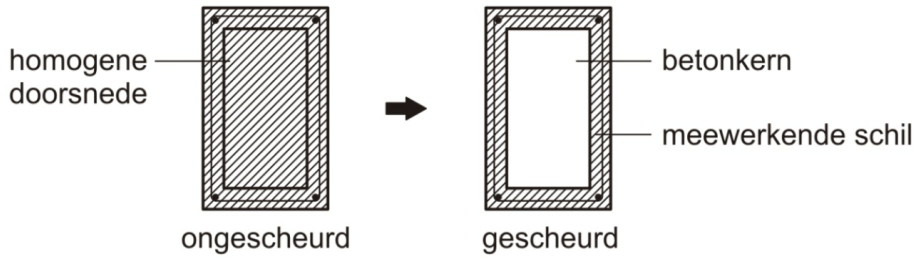

FIGURE F.27: Effective shell for torsion resistance in a massive cross-section *[Hoogenboom, 2014]*

If the cracking moment T_{Rdc} is exceeded, shear reinforcement is required, given by:

$$T_{Rds} = \frac{2 \cdot A_k}{\cot(\theta)} \cdot \frac{\Sigma A_{sl} \cdot f_{ywd} + A_k \cdot \sigma_{Rdf}}{u_k}$$

The result is:

Cross-sectional capacity:	T_{Rdc}	= 2615 kNm
Maximum torsional moment:	T_{Ed}	= 8088 kNm
Thus additional reinforcement is required		

Shear reinforcement diameter:	Φ_{sw}	= 20 mm
Maximum shear bars over width:	n_{max}	7
Number of bars over width:	n_{sw}	= 7
Minimum bar spacing:	s_{min}	= 26 mm
Bar spacing:	s	= 26 mm
Reinforcement capacity:	T_{Rds}	= 6866 kNm
Total torsion capacity:	T_{Rd}	= T_{Rds} = 6866 kNm
Unity Check:	UC_V	= 1.18

It follows that the torsional capacity is insufficient for the maximum load situation, due to the restricted amount of reinforcement possible in the cross-section. If this is to be increased to fulfil the Unity Check, the cross-sectional area of the side girder should be increased to b_t = 1.4 m and h_t = 2.3 m. In this, mainly widening of the cross-section has a positive effect.

Check boundary conditions:

- Minimum concrete cover:
  For reinforcement steel: c_{com} = 31 mm
  $e_h = e_v$ = 26 mm
  The maximum amount of bars and minimum bar spacing have already been incorporated in the design and therefore this boundary condition is met.

- Ultimate strength compressive struts:
  From the boundary conditions given in E.5 it follows that the compressive struts have an ultimate strength that limits the torsion capacity of the concrete:

  $T_{Rd;max}$ = 62687 kNm

  Since T_{Rd} is smaller than $T_{Rd;max}$, this boundary condition is fulfilled.

  However, for the ultimate strength of the compressive struts the combination of shear and torsion must also be taken into account, since they constitute shear stresses in the same direction (Figure F.28).

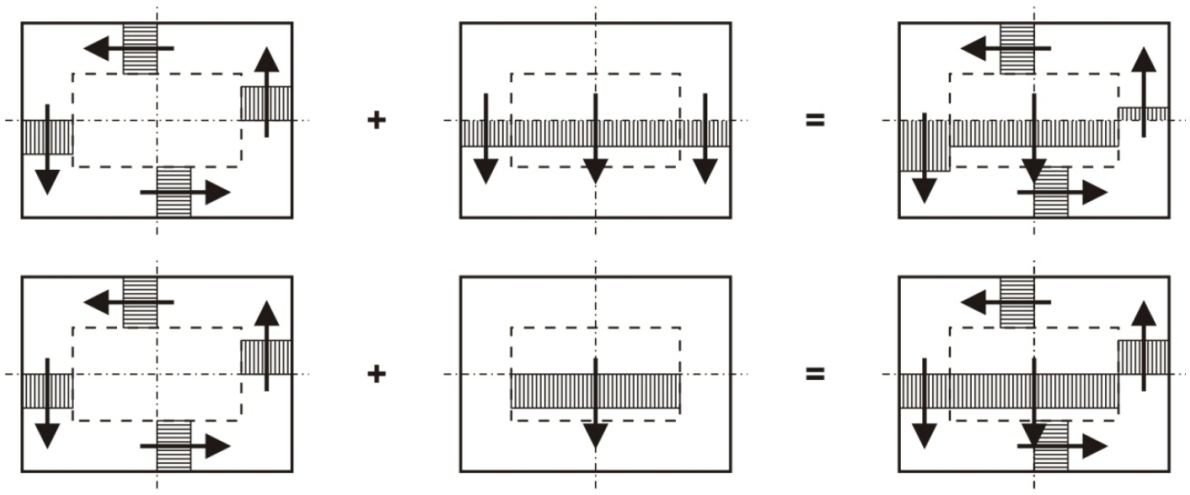

FIGURE F.28: Possible shear stress configurations for the combination of shear and torsion loading *[Hoogenboom, 2014]*

$$\frac{V_{Ed}}{V_{Rd;max}} + \frac{T_{Ed}}{T_{Rd;max}} \leq 1.0$$

Applying this to the cross-section with a width of b_t = 1.2 m and a height of h_t = 2.3 m will result in:

Unity Check: UC_{V+T} = 3.98

This was to be expected, since the Unity Check for pure shear is already insufficient.

Deformation capacity

The maximum deformation must be checked according to *[NEN-EN 1992-1-1, 2005]* for load situation 2, since the maximum deformation occurs when loading the end span. In this case, however, a positive effect is also observed as a result of the upwards curvature pressure from the prestress.

Maximum allowable deformation:	$w_{k;max}$	$= \frac{l_t}{250}$ = 147 mm
Maximum deformation:	w_{Ek}	= 124 mm
Upwards deflection from prestress:	w_{Pk}	= 104 mm
Unity Check:	UC_w	= 0.14

G

CONCEPTUAL DESIGN TROUGH BRIDGE - OPEN STRUCTURE DESIGN

In the previous appendix the design for a trough bridge with massive elements was presented, from which it follows that shear and torsion cause major problems in design.

In this appendix the design for an open element trough bridge will be given. The main reasons for applying an open structure are:

- Weight reduction:
  To decrease the load actions on the existing foundations, to increase the ease of transportation and the speed of erection and to reduce the material costs.
- Tunnel effect:
  Drivers can experience a so-called tunnel effect when approaching a passage with high walls, which will cause them to slow down unknowingly. This behaviour can be subdued by opening up the side girders as much as possible.
- Ice formation: Shaded areas should be avoided as much as possible to prevent ice-formation in winter.

The reduction in self-weight of the structure might also diminish the problems regarding shear and torsion capacity in the side girders.

G.1. SUMMARY

The resulting dimensions for the floor girders are given in Table G.1 and supported by Figures G.2 and G.1. For the side girders the same is done in Table G.2 and Figures G.3 to G.7.

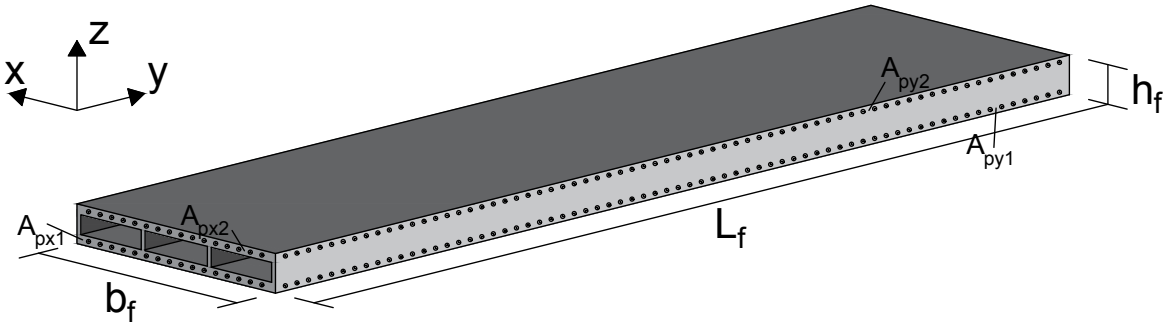

FIGURE G.1: Open floor girders with the prestressing cables indicated (not to scale)

Floor girder - open			
Parameter		**Value**	**Unit**
Dimensions			
Height floor girder	h_f	0.61	*m*
Width floor girder	b_f	3.00	*m*
Length floor girder	l_f	18.17	*m*
Height top flange	t_{ft}	0.13	*m*
Height bottom flange	t_{fb}	0.12	*m*
Thickness webs	t_w	0.09	*m*
Number of box cells	n_b	3	-
Height top connection	h_{c1}	0.13	*m*
Height bottom connection	h_{c2}	0.12	*m*
Prestress			
Bottom; x-direction	$A_{p;x1}$	5500	mm^2
Eccentricity	$e_{p;x1}$	0.24	*m*
Top; x-direction	$A_{p;x2}$	7600	mm^2
Eccentricity	$e_{p;x2}$	0.25	*m*
Bottom; y-direction	$A_{p;y1}$	1300	mm^2
Eccentricity	$e_{p;y1}$	0.24	*m*
Bottom; y-direction	$A_{p;y2}$	1600	mm^2
Eccentricity	$e_{p;y2}$	0.25	*m*

TABLE G.1: Resulting dimensions for the floor girders in an open element trough bridge design

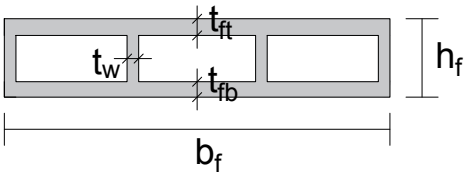

FIGURE G.2: Cross-sectional view of the multicell-box floor girder in x-direction

Side girder - open			
Parameter		**Value**	**Unit**
Dimensions			
Height side girder	h_t	2.30	*m*
Width side girder	b_t	1.20	*m*
Span side girder	l_t	36.80	*m*
Length side girder	l_{tot}	40.00	*m*
Height top beam	h_{tt}	0.40	*m*
Height lower beam	h_{tb}	0.80	*m*
Thickness verticals	d_{tv}	0.30	*m*
Thickness diagonals	d_{td}	0.30	*m*
Length segment	l_{ts}	2.50	*m*
Number of segments	n_{ts}	14	-
Length end segment	l_{tse}	2.50	*m*
Prestress			
Bottom; y-direction	$A_{p;y1}$	20000	mm^2
Eccentricity	$e_{p;y1}$	0.57	*m*
Drag	f_p	0.00	*m*
Top; y-direction	$A_{p;y2}$	8000	mm^2
Eccentricity	$e_{p;y1}$	1.13	*m*
Drag	f_p	0.00	*m*

TABLE G.2: Resulting dimensions for the truss girders in an open element trough bridge design

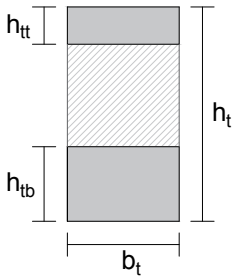

FIGURE G.3: Cross-sectional view of the open truss girder in y-direction

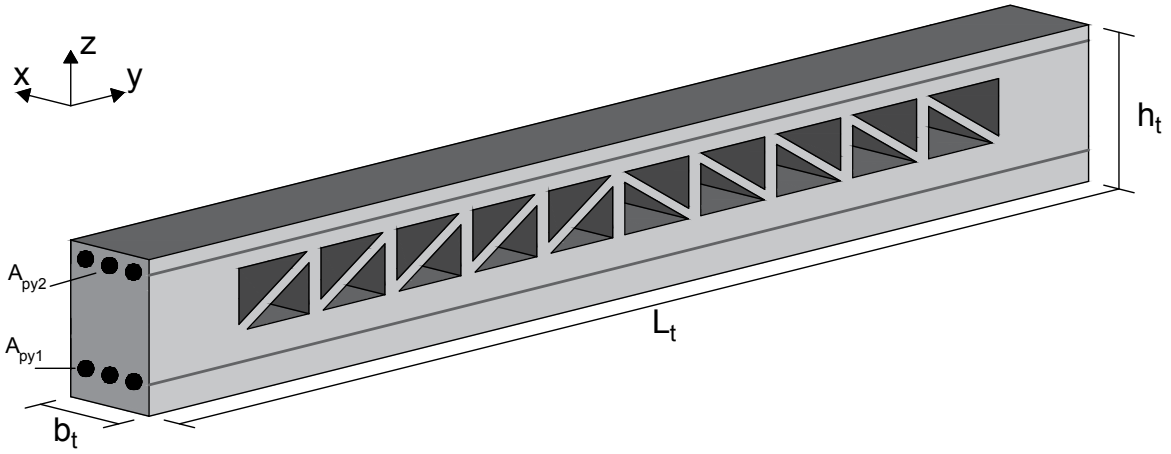

FIGURE G.4: Truss girders with the prestressing cables indicated (not to scale)

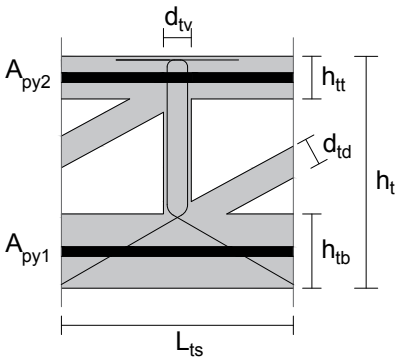

FIGURE G.5: Detail of a middle truss segment with prestressing and suspension reinforcement indicated

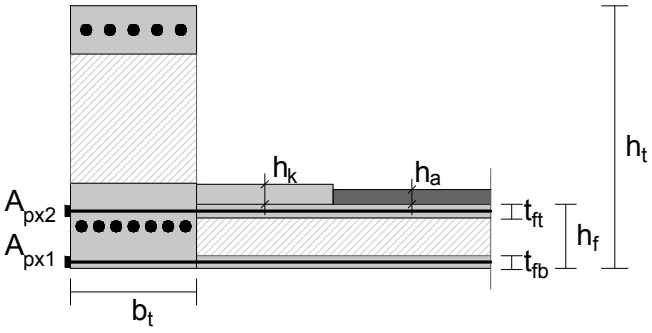

FIGURE G.6: Detail for the floor-to-side connection in an open element trough bridge

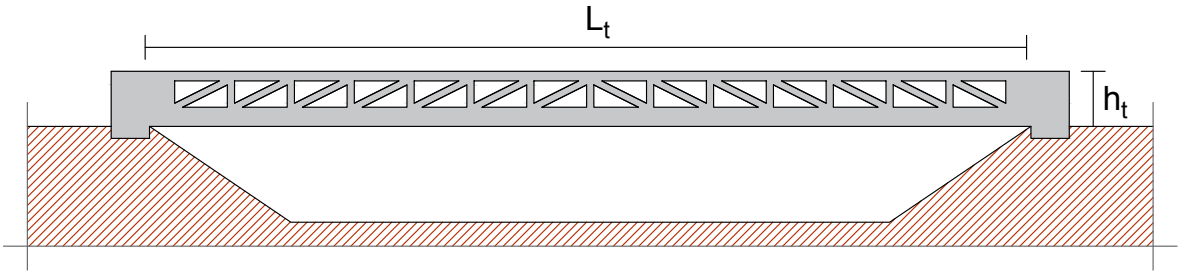

FIGURE G.7: Side view of the trough bridge in x-direction

G.2. MULTICELL BOX GIRDER

G.2.1. Geometry and specific considerations

The total deck height is equal to that of the massive floor structure, thus h_f = 0.61 m. The same holds for the width and length of the floor girder, b_f = 3.0 m and l_f = 18.17 m.

There are different open-structure girder types that can be considered, such as the four types depicted in Figure G.8.
Although T-beams are generally adequate to withstand bridge load actions, in Dutch design codes the open underside of the bridge is considered as a problem as the risk of collision is too large. Therefore, only the multicell box girder is designed in this analysis.

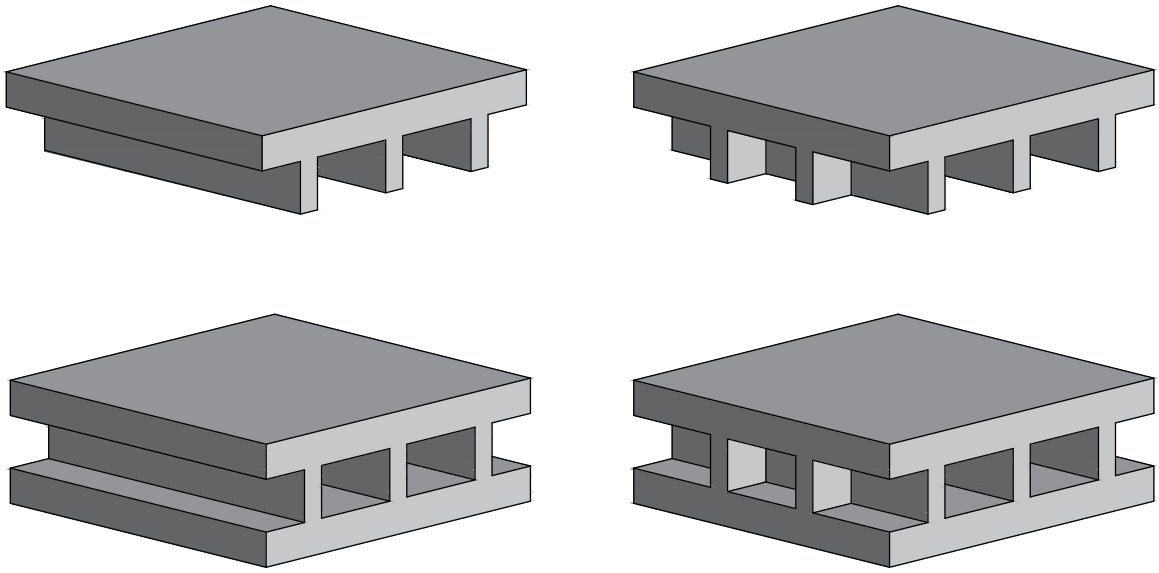

FIGURE G.8: Different types for an open floor structure: T-beams in one direction, box beams in one direction and both options in a honeycomb structure

The honeycomb box structure is not considered due to simplicity reasons, but it is to be expected that the orthotropic behaviour of the honeycomb structure will lead to a better distribution of loads and thus in a more slender structure than the box structure with webs in one direction only.

It is assumed that the box girders consist of three cells. The following dimensions are then found for an adequate structural behaviour:

t_{ft} = 0.13 m
t_{fb} = 012 m
t_w = 0.09 m

Straight pre-tensioned cables will be used in both upper and top flange, in both x- and y-directions and partial prestressing will be applied.

As in the case for massive floor girders, both the connection between floor and truss girder and two floor girders is assumed to be fixed.

G.2.2. Analytical load actions

The general approach for the determination of load actions in the floor girder is equal to that of the massive floor girder. This means that the Guyon-Massonnet method will be used to determine the load distribution and slender analysis will be used to determine beam behaviour in bending, shear and deflection.

The largest difference in this respect is the reduced self-weight of the concrete and the different stiffnesses in x- and y-direction due to the one-directional box structure. As a result, the flexural and torsional stiffness differ.

For the Guyon-Massonet method this leads to:

$$I_x = \frac{1}{12}\cdot b_f\cdot({t_{ft}}^3+{t_{fb}}^3)+4\cdot\frac{1}{12}\cdot t_w\cdot(h_f-t_{ft}-t_{fb})^3+(z_t-0.5\cdot t_{ft})^2\cdot b_f\cdot t_{ft}+(z_b-0.5\cdot t_{fb})^2\cdot b_f\cdot t_{fb} = 4.64\cdot10^{-2}\ \text{m}^4$$

$$I_y = \frac{1}{12}\cdot b_{fe}\cdot({t_{ft}}^3+{t_{fb}}^3)+(z_t-0.5\cdot t_{ft})^2\cdot b_{fe}\cdot t_{ft}+(z_b-0.5\cdot t_{fb})^2\cdot b_{fe}\cdot t_{fb} = 1.50\cdot10^{-2}\ \text{m}^4$$

Flexible rigidity per unit width:

$$\rho_x = \frac{\Sigma E \cdot I_x}{b_f} = 7.74 \cdot 10^8 \text{ kNm}^3$$

$$\rho_y = \frac{\Sigma E \cdot I_y}{l_f} = 7.50 \cdot 10^8 \text{ kNm}^3$$

Torsional rigidity per unit width:

$$\gamma_x = \frac{\Sigma G \cdot I_x}{b_f} = 3.22 \cdot 10^8 \text{ kNm}^3$$

$$\gamma_y = \frac{\Sigma G \cdot I_y}{l_f} = 3.13 \cdot 10^8 \text{ kNm}^3$$

Flexural stiffness:

$$\theta = \frac{b_f}{l_f} \cdot \sqrt[4]{\frac{\rho_x}{\rho_y}} = 0.166 \text{ rad}$$

Torsional stiffness:

$$\alpha = \frac{\gamma_x + \gamma_y}{2 \cdot \sqrt{\rho_x \cdot \rho_y}} = 0.417$$

This is an iterative procedure, since θ and α depend on the dimensions of the floor girder and the dimensions of the floor girder in turn depend on the load action and thus on θ and α. The influence of α can be directly incorporated in the determination of K_α but the influence of θ has to be manually obtained from the design graphs. In this analysis it is therefore assumed that the influence of different dimensions on the value for θ is negligible and thus no iterative procedure for θ is required.

The resulting reduced loads are presented in Table G.3 for load situations 1 and 2 (Figures E.2 and E.3) that apply for maximum loading in the floor girders.

Load situation 1		
F_{f1}	77,30	*kN*
F_{f2}	51,53	*kN*
F_{f3}	25,77	*kN*
q_{f1}	30,99	*kN/m*
q_{f2}	10,48	*kN/m*

Load situation 1		
F_{f1}	195,58	*kN*
F_{f2}	130,38	*kN*
F_{f3}	65,19	*kN*
q_{f1}	30,97	*kN/m*
q_{f2}	10,47	*kN/m*

TABLE G.3: Load reduction for load situations 1 and 2 following from the Guyon-Massonnet method

The beam behaviour is described by the same slender analysis theory as explained in F.2.2. Through the principle of superposition and the respective distance and value of each load, the beam behaviour can be determined in each position of the beam. This is done for situation 1 and 2 to obtain the maximum cross-sectional forces in the floor girder. The results are presented in Table G.4.

Floor	Char.	Design	
Shear	1145	1680	*kN*
Moment^+_x	554	819	*kNm*
Moment^-_x	-447	-648	*kNm*
Moment^+_y	1867	2746	*kNm*
Moment^-_y	-3289	-4820	*kNm*
Deformation	14	-	*mm*

TABLE G.4: Resulting maximum load actions in the multicell box girders

Internal loads

Apart from the global load actions on the floor girder, also the internal load actions must be analysed. The top flange must be able to resist all loads acting on the bridge deck and in this case the loads are not reduced through stress distribution. The ultimate load situation is given in Figure G.9 for a floor segment with a length of b_{fe} = 1.0 m.

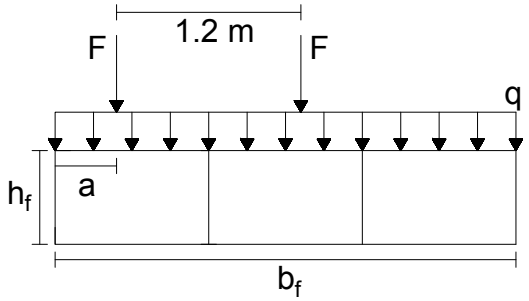

FIGURE G.9: Floor section model for the internal load calculation

The top flange will thus be loaded in bending, shear and compression. To determine the behaviour of the top flange, an adequate model must be composed.

The model applied determines for a great deal to what extent the webs and lower flange are loaded. Several models (Figures G.10 to G.14) have been investigated.

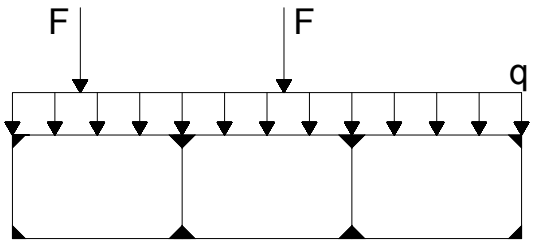

FIGURE G.10: Internal floor model 1

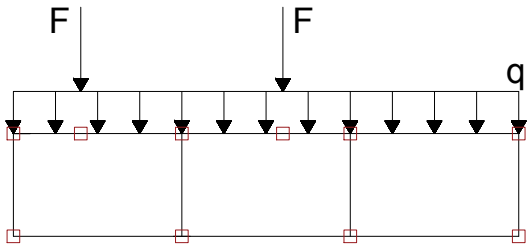

FIGURE G.11: Position of the different boundary conditions in internal floor model 1

The first case was rejected due to its complexity. It could be solved by applying slender analysis and coupling all fields through adequate boundary conditions, but this would result in a system of 40 equations and 40 unknown constants. Although this model is solvable, the calculations would be too comprehensive for this analysis.

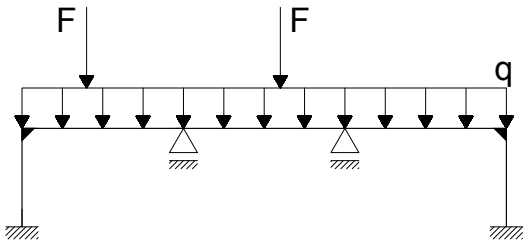

FIGURE G.12: Internal floor model 2 with fixed web-to-lower-flange connection

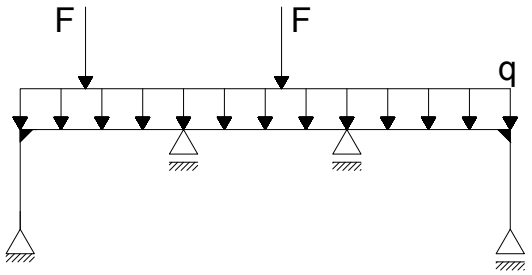

FIGURE G.13: Internal floor model 2 with free web-to-lower-flange connection

The second model is a more simplified case, in which it is assumed that the upper flange and outer webs are rigidly connected. This means that the load distribution depends on the stiffness ratio between both elements. It also leads to rather thick web and upper flanges due to the moment induced in the connection. The thickness of the webs is needed to resist this bending moment. In order to limit the web dimensions,

adequate normal stress should be present, which is in turn governed by the thickness of the top flange. It turns out that equilibrium is reached at rather thick elements (t_{ft} = 0.27 m and t_w = 0.10 m).

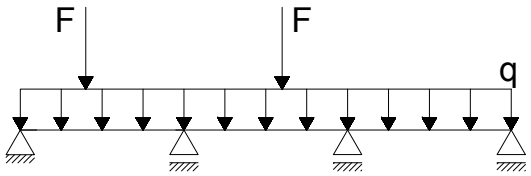

FIGURE G.14: Internal floor model 3

Therefore, the third case is analysed, where the top flange is decoupled from the webs and only normal and shear forces can be transferred. This leads to higher moments in the top flange but the overall thickness of the top flange is limited to t_{ft} = 0.13 m.
Ultimately, any model between the first case and the last case can be used to describe the internal loads within this floor girder.

So, in this analysis the floor girder is modelled as presented in the third case in Figure G.15. Through statically determinate elements with adequate boundary conditions all internal forces can be determined. This is further elaborated below:

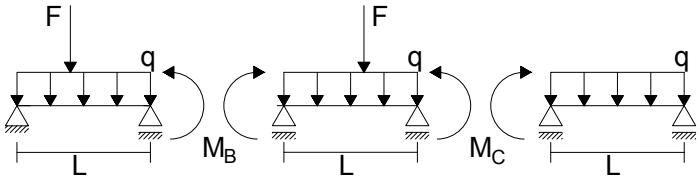

FIGURE G.15: Statically determinate system for the internal floor model

The statically indeterminate system is divided into statically determined sections, as showed in Figure G.15. The internal support moments at B and C now become external moments. The working loads will cause the beam to deform:

$$\begin{aligned}
\phi_B{}^{(1)} &= \frac{M_B \cdot L}{3 \cdot EI} + \frac{F \cdot a \cdot b \cdot (L+a)}{6 \cdot L \cdot EI} + \frac{q \cdot L^3}{24 \cdot EI} \\
\phi_B{}^{(2)} &= -\frac{M_B \cdot L}{3 \cdot EI} - \frac{M_C \cdot L}{6 \cdot EI} - \frac{F \cdot a \cdot b \cdot (L+b)}{6 \cdot L \cdot EI} - \frac{q \cdot L^3}{24 \cdot EI} \\
\phi_C{}^{(1)} &= \frac{M_B \cdot L}{6 \cdot EI} + \frac{M_C \cdot L}{3 \cdot EI} + \frac{F \cdot a \cdot b \cdot (L+a)}{6 \cdot L \cdot EI} + \frac{q \cdot L^3}{24 \cdot EI} \\
\phi_C{}^{(2)} &= -\frac{M_C \cdot L}{3 \cdot EI} - \frac{q \cdot L^3}{24 \cdot EI}
\end{aligned}$$

To restore compatibility the following boundary conditions have to be applied:

$$\phi_B{}^{(1)} = \phi_B{}^{(2)}$$
$$\phi_C{}^{(1)} = \phi_C{}^{(2)}$$

This gives a system of 2 equations with 2 unknowns (M_B and M_C) which can thus be solved. The resulting loads are listed in Table G.5.

G.2.3. FEM load actions

As for the massive element structure, the analytical approach is compared to the results of a FEM model for verification. The FEM model input parameters and result interpretation are presented in Appendices H and I respectively.

For the open structure design the same conclusions can be drawn as for the massive structure design. The only difference is the incorporation of orthotropic behaviour, but since it was already stated that this behaviour cannot be compared adequately - due to different calculation methods - the conclusion for the analytical approach remain unaltered.

Elements		Char.	Design	
Upper flange	Shear	277	415	*kN*
	Moment$^{+}_{x}$	46	69	*kNm*
	Moment$^{-}_{x}$	-40	-60	*kNm*
	Normal	-	3287	*kN*
	Deformation	0.30	-	*mm*
Lower flange	Shear	9	14	*kN*
	Moment	0	0	*kNm*
	Normal	-	1139	-
Webs	Shear	0	0	*kN*
	Moment	0	0	*kNm*
	Normal^{+}	-9	-14	*kN*
	Normal^{-}	277	415	*kN*

TABLE G.5: Resulting maximum internal load actions in the multicell box girders

G.2.4. Unity Checks

The floor girder will have to be designed with sufficient capacity to resist all loads, while fulfilling the boundary conditions as set in E.5. From both the analytical calculation of the load actions and the FEM calculations it follows that the maximum internal forces in the floor in the x-direction occur at the end span, thus load situation 2, while in the y-direction they occur at midspan, thus load situation 1.

First the global loads and capacities will be investigated, followed by the internal forces and capacities.

Global analysis - Moment capacity

The moment capacity is obtained by analysing moment equilibrium and horizontal force equilibrium in the cross-section. Since partial prestressing is applied, this is an iterative procedure in which the choice of compression height x_e is governing. The general calculation is first described, after which the Unity Checks for both positive and negative moments in both x- and y-direction are determined.

The general calculation is based on the same approach as for the massive floor, with the difference that it must first be determined which part of the compression and tension zone can actually be used. This is illustrated in Figure G.16.

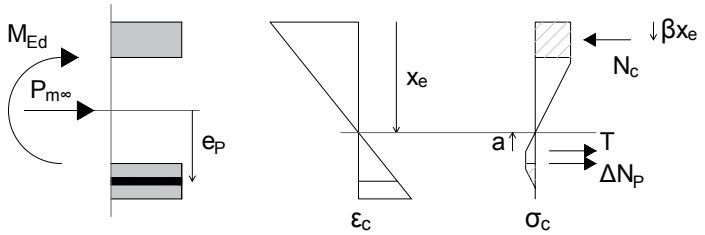

FIGURE G.16: Strain and stress distribution in open concrete cross-section under positive bending moment action

This results in:

In x-direction:

Positive:	Prestress area:	A_{px1}	= 5500 mm^2 (37 strands)
	Prestress eccentricity:	e_{p1}	= 0.24 m
	Compression zone height:	x_e	= 0.097 m
		α	= 0.50
		β	= 0.33
	Compression force:	N_c	= 10135 kN
	Prestress force:	P_{m01}	= 7669 kN
		$P_{m\infty 1}$	= 6519 kN
	Increase in prestress force:	ΔN_p	= 1848 kN
	Tensile force:	T	= 1769 kN
		a	= 0.15 m
	Moment capacity prestress:	M_{Rdp}	= 1562 kNm
	Total moment capacity:	M_{Rd}	= 4539 kNm
	$M_y{}^+$ in ULS:	M_{Ed}	= 2746 kNm
	Unity Check:	UC_M	= 0.60
Negative:	Prestress area:	A_{px2}	= 7600 mm^2 (51 strands)
	Prestress eccentricity:	e_{p2}	= 0.25 m
	Compression zone height:	x_e	= 0.186 m
		α	= 0.50
		β	= 0.33
	Compression force:	N_c	= 13321 kN
	Prestress force:	P_{m02}	= 10590 kN
		$P_{m\infty 2}$	= 9001 kN
	Increase in prestress force:	ΔN_p	= 2551 kN
	Tensile force:	T	= 1769 kN
		a	= 0.15 m
	Moment capacity concrete:	M_{Rdc}	= 4221 kNm
	Moment capacity prestress:	M_{Rdp}	= 2209 kNm
	Total moment capacity:	M_{Rd}	= 6430 kNm
	$M_y{}^-$ in ULS:	M_{Ed}	= 4820 kNm
	Unity Check:	UC_M	= 0.75

Check boundary conditions:

- Minimum concrete cover:
  For pre-tensioned steel: c_{com} = 36.5 mm
  $e_h = e_v$ = 26 mm
  As shown in Figure G.17 and Table G.6, the boundary condition for minimum concrete cover is satisfied

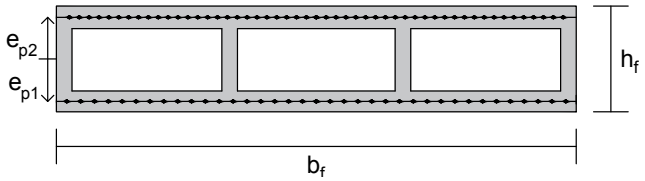

FIGURE G.17: Prestress configuration in the open floor element in x-direction

x		n [-]	e [m]
e_{p1}	total	37	0.240
e_{p2}	total	51	0.250
Maximum		72	0.260

TABLE G.6: Prestress configuration in the open floor element in x-direction

in this direction.

- Minimum prestress area:

At t = ∞, the following stress distribution occurs at SLS loading:

$$\sigma_1 = -\frac{P_{m\infty 1}}{A_c} + \frac{e_{p1} \cdot P_{m\infty 1} \cdot z_t}{I_c} - \frac{P_{m\infty 2}}{A_c} - \frac{e_{p2} \cdot P_{m\infty 2} \cdot z_t}{I_c} - \frac{M_{t=\infty} \cdot z_t}{I_c}$$
$$\sigma_2 = -\frac{P_{m\infty 1}}{A_c} - \frac{e_{p1} \cdot P_{m\infty 1} \cdot z_b}{I_c} - \frac{P_{m\infty 2}}{A_c} + \frac{e_{p2} \cdot P_{m\infty 2} \cdot z_b}{I_c} + \frac{M_{t=\infty} \cdot z_t}{I_c}$$

Minimum presress			
	M_y^+	M_y^-	Unit
σ_1	-34.37	-0.06	N/mm^2
σ_2	-0.31	-35.86	N/mm^2

TABLE G.7: Boundary condition check for minimum prestress in x-direction

Since all end fibres are in compression, the condition for minimum prestress is met.

- Maximum prestress area:
  The maximum compression stress at t = 0 is given by:

$$\sigma_1 = -\frac{P_{m01}}{A_c} + \frac{e_{p1} \cdot P_{m01} \cdot z_t}{I_c} - \frac{P_{m02}}{A_c} - \frac{e_{p2} \cdot P_{m0} \cdot z_t}{I_c}$$
$$\sigma_2 = -\frac{P_{m\infty 1}}{A_c} - \frac{e_{p1} \cdot P_{m\infty 1} \cdot z_b}{I_c} - \frac{P_{m\infty 2}}{A_c} + \frac{e_{p2} \cdot P_{m\infty 2} \cdot z_b}{I_c}$$

Maximum prestress (comp)		
	M = 0	Unit
σ_1	-25.82	N/mm^2
σ_2	-15.51	N/mm^2

TABLE G.8: Boundary condition check for maximum prestress based on compression strength in x-direction

These are smaller than $0.6 \cdot f_{ck}(t) = 0.6 \cdot 46.5 = 27.9$ N/mm^2 and thus this condition is met.

The maximum tensile stress in the upper and lower fibre after prestressing is given by:

$$\sigma_1 = -\frac{P_{m01}}{A_c} + \frac{e_{p1} \cdot P_{m01} \cdot z_t}{I_c} - \frac{P_{m02}}{A_c} - \frac{e_{p2} \cdot P_{m0} \cdot z_t}{I_c} - \frac{M_{t=0} \cdot z_t}{I_c}$$
$$\sigma_2 = -\frac{P_{m\infty 1}}{A_c} - \frac{e_{p1} \cdot P_{m\infty 1} \cdot z_b}{I_c} - \frac{P_{m\infty 2}}{A_c} + \frac{e_{p2} \cdot P_{m\infty 2} \cdot z_b}{I_c} + \frac{M_{t=0} \cdot z_b}{I_c}$$

Maximum prestress (tension)			
	M_y^+	M_y^-	Unit
σ_1	-27.84	-21.80	N/mm^2
σ_2	-13.50	-19.54	N/mm^2

TABLE G.9: Boundary condition check for maximum prestress based on tension strength in x-direction

The boundary condition ($\sigma \leq f_{ctd1}$) is met at all locations.

- Ductility:
  The maximum stress in top and bottom fibre in the ULS is given by:

$$\sigma_1 = -\frac{P_{m\infty 1}}{A_c} + \frac{e_{p1} \cdot P_{m\infty 1} \cdot z_t}{I_c} - \frac{P_{m\infty 2}}{A_c} - \frac{e_{p2} \cdot P_{m\infty 2} \cdot z_t}{I_c} - \frac{M_{Ed} \cdot z_t}{I_c}$$
$$\sigma_2 = -\frac{P_{m\infty 1}}{A_c} - \frac{e_{p1} \cdot P_{m\infty 1} \cdot z_b}{I_c} - \frac{P_{m\infty 2}}{A_c} + \frac{e_{p2} \cdot P_{m\infty 2} \cdot z_b}{I_c} + \frac{M_{Ed} \cdot z_t}{I_c}$$

Maximum prestress (ductility)			
	M_y^+	M_y^-	Unit
σ_1	-40.22	10.13	N/mm^2
σ_2	5.75	-46.42	N/mm^2

TABLE G.10: Boundary condition check for maximum prestress based on ductility in x-direction

It follows that for both cases the tensile stress in the concrete is larger than f_{ctd1} and thus cracking occurs. This means that the condition for ductility is met.

In y-direction:

Positive:	Prestress area:	A_{py1}	= 1300 mm^2 (9 strands per meter)
	Prestress eccentricity:	e_{p1}	= 0.24 m
	Compression zone height:	x_e	= 0.076 m
		α	= 0.50
		β	= 0.33
	Compression force:	N_c	= 3367 kN
	Prestress force:	P_{m0}	= 1817 kN
		$P_{m\infty}$	= 1544 kN
	Increase in prestress force:	ΔN_p	= 438 kN
	Tensile force:	T	= 1386 kN
		a	= 0.12 m
	Moment capacity concrete:	M_{Rdc}	= 866 kNm
	Moment capacity prestress:	M_{Rdp}	= 370 kNm
	Total moment capacity:	M_{Rd}	= 1236 kNm
	$M_x{}^+$ in ULS:	M_{Ed}	= 819 kNm
	Unity Check:	UC_M	= 0.66
Negative:	Prestress area:	A_{py2}	= 1600 mm^2 (11 strands per meter)
	Prestress eccentricity:	e_{p2}	= 0.25 m
	Compression zone height:	x_e	= 0.072 m
		α	= 0.50
		β	= 0.33
	Compression force:	N_c	= 3762 kN
	Prestress force:	P_{m0}	= 2242 kN
		$P_{m\infty}$	= 1906 kN
	Increase in prestress force:	ΔN_p	= 540 kN
	Tensile force:	T	= 1316 kN
		a	= 0.11 m
	Moment capacity concrete:	M_{Rdc}	= 1020 kNm
	Moment capacity prestress:	M_{Rdp}	= 468 kNm
	Total moment capacity:	M_{Rd}	= 1488 kNm
	$M_x{}^-$ in ULS:	M_{Ed}	= 648 kNm
	Unity Check:	UC_M	= 0.44

Check boundary conditions:

- Minimum concrete cover:
  For pre-tensioned steel: c_{com} = 36.5 mm
  $e_h = e_v$ = 26 mm
  As shown in Figure G.18, the boundary condition for minimum concrete cover is satisfied in this direction.

- Minimum prestress area:
  At t = ∞, the following stress distribution occurs at SLS loading:
  $$\sigma_1 = -\frac{P_{m\infty 1}}{A_c} + \frac{e_{p1}\cdot P_{m\infty 1}\cdot z_t}{I_c} - \frac{P_{m\infty 2}}{A_c} - \frac{e_{p2}\cdot P_{m\infty 2}\cdot z_t}{I_c} - \frac{M_{t=\infty}\cdot z_t}{I_c}$$
  $$\sigma_2 = -\frac{P_{m\infty 1}}{A_c} - \frac{e_{p1}\cdot P_{m\infty 1}\cdot z_b}{I_c} - \frac{P_{m\infty 2}}{A_c} + \frac{e_{p2}\cdot P_{m\infty 2}\cdot z_b}{I_c} + \frac{M_{t=\infty}\cdot z_t}{I_c}$$
  Since all end fibres are in compression, the condition for minimum prestress is met.

- Maximum prestress area:
  The maximum compression stress at t = 0 is given by:

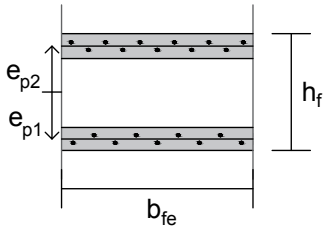

FIGURE G.18: Prestress configuration in the open floor element in y-direction

y		n [-]	e [m]
e_{p1}	total	9	0.240
e_{p2}	total	11	0.250
Maximum		24	0.260

TABLE G.11: Prestress configuration in the open floor element in y-direction

Minimum presress			
	M_x^+	M_x^-	Unit
σ_1	-26.81	-6.82	N/mm^2
σ_2	-0.32	-21.03	N/mm^2

TABLE G.12: Boundary condition check for minimum prestress in y-direction

$$\sigma_1 = -\frac{P_{m01}}{A_c} + \frac{e_{p1} \cdot P_{m01} \cdot z_t}{I_c} - \frac{P_{m02}}{A_c} - \frac{e_{p2} \cdot P_{m0} \cdot z_t}{I_c}$$
$$\sigma_2 = -\frac{P_{m\infty 1}}{A_c} - \frac{e_{p1} \cdot P_{m\infty 1} \cdot z_b}{I_c} - \frac{P_{m\infty 2}}{A_c} + \frac{e_{p2} \cdot P_{m\infty 2} \cdot z_b}{I_c}$$

Maximum prestress (comp)		
	M = 0	Unit
σ_1	-18.53	N/mm^2
σ_2	-13.86	N/mm^2

TABLE G.13: Boundary condition check for maximum prestress based on compression strength in y-direction

These are smaller than $0.6 \cdot f_{ck}(t) = 0.6 \cdot 46.5 = 27.9$ N/mm^2 and thus this condition is met.

The maximum tensile stress in the upper and lower fibre after prestressing is given by:

$$\sigma_1 = -\frac{P_{m01}}{A_c} + \frac{e_{p1} \cdot P_{m01} \cdot z_t}{I_c} - \frac{P_{m02}}{A_c} - \frac{e_{p2} \cdot P_{m0} \cdot z_t}{I_c} - \frac{M_{t=0} \cdot z_t}{I_c}$$
$$\sigma_2 = -\frac{P_{m\infty 1}}{A_c} - \frac{e_{p1} \cdot P_{m\infty 1} \cdot z_b}{I_c} - \frac{P_{m\infty 2}}{A_c} + \frac{e_{p2} \cdot P_{m\infty 2} \cdot z_b}{I_c} + \frac{M_{t=0} \cdot z_b}{I_c}$$

Maximum prestress (tension)			
	M_x^+	M_x^-	Unit
σ_1	-19.20	-17.19	N/mm^2
σ_2	-13.19	-15.20	N/mm^2

TABLE G.14: Boundary condition check for maximum prestress based on tension strength in y-direction

The boundary condition ($\sigma \leq f_{ctd1}$) is met at all locations.

- Ductility:
  The maximum stress in top and bottom fibre in the ULS is given by:
  $$\sigma_1 = -\frac{P_{m\infty 1}}{A_c} + \frac{e_{p1} \cdot P_{m\infty 1} \cdot z_t}{I_c} - \frac{P_{m\infty 2}}{A_c} - \frac{e_{p2} \cdot P_{m\infty 2} \cdot z_t}{I_c} - \frac{M_{Ed} \cdot z_t}{I_c}$$
  $$\sigma_2 = -\frac{P_{m\infty 1}}{A_c} - \frac{e_{p1} \cdot P_{m\infty 1} \cdot z_b}{I_c} - \frac{P_{m\infty 2}}{A_c} + \frac{e_{p2} \cdot P_{m\infty 2} \cdot z_b}{I_c} + \frac{M_{Ed} \cdot z_t}{I_c}$$
  It follows that for no case the tensile stress in the concrete is larger than f_{ctd1} and thus no cracking will occur in y-direction. However, since this condition is met in x-direction it is assumed sufficient anyway.

Global analysis - Shear capacity

The shear capacity is checked in the same manner as is done for the massive floor girder. The biggest difference is the fact that in the open structure all shear forces will be carried by the webs. It follows that:

Maximum prestress (ductility)			
	M_x^+	M_x^-	Unit
σ_1	-32.11	-2.81	N/mm^2
σ_2	5.17	25.18	N/mm^2

TABLE G.15: Boundary condition check for maximum prestress based on ductility in y-direction

Normal force from prestress:	N_{Ed}	= 3858 kN
Working width of cross-section:	b_w	= b_f = 0.36 m
Concrete shear capacity:	V_{Rdc}	= 480 kN
Fibre shear strength:	σ_{Rdf}	= 5.10 N/mm^2
Fibre shear capacity:	V_{Rdf}	= 1745 kN
Shear reinforcement diameter:	Φ_{sw}	= 20 mm
Number of bars over width:	n_{sw}	= 2
Bar spacing:	s	= 100 mm
Reinforcement capacity:	V_{Rds}	= 2598 kN
Total shear capacity:	V_{Rd}	= 4823 kN
Maximum shear in cross-section:	V_{Ed}	= 1680 kN
Unity Check:	UC_V	= 0.35

Check boundary conditions:

- Minimum concrete cover:
  For reinforcement steel: c_{com} = 31 mm
  $e_h = e_v$ = 26 mm
  The requirement for minimum concrete cover is met as a bar spacing of s_y = 100 mm > e_h = 26 mm is used and the application of two shear bars for every meter length results in a spacing of $s_x = \frac{b}{2}$ = 500 mm > e_h.

- Ultimate strength compressive struts:
  From the boundary conditions given in E.5 it follows that the compressive struts have an ultimate strength that limits the shear capacity of the concrete:

  $V_{Rd;max}$ = 339 kN

  Since V_{Rd} is larger than $V_{Rd;max}$, this capacity is too optimistic and must be replaced by $V_{Rd;max}$. The Unity Check then becomes:

  Unity Check: UC_V = 4.95

  Clearly, the cross-section does not satisfy the shear capacity Unity Check. It follows that the web width should be gradually increased towards the end of the span to a width of t_w is 0.50 m. In that case, the Unity Check for shear capacity becomes:

  Unity Check: UC_V = 0.89

Global analysis - Deformation capacity
The maximum deformation must be checked according to *[NEN-EN 1992-1-1, 2005]* for load situation 2, since the maximum deformation occurs when loading the end span.

Maximum allowable deformation:	$w_{k;max}$	$= \frac{l_f}{250} = 73$ mm
Maximum deformation:	w_{Ek}	= 26 mm
Unity Check:	UC_w	= 0.36

Internal analysis - Upper flange
The upper flange will have to be checked on moment capacity, shear capacity, normal capacity and deformation.

- The moment capacity is given by a simplified calculation in which it is assumed that no tensile stress will occur in the cross-section (see Figure G.19):

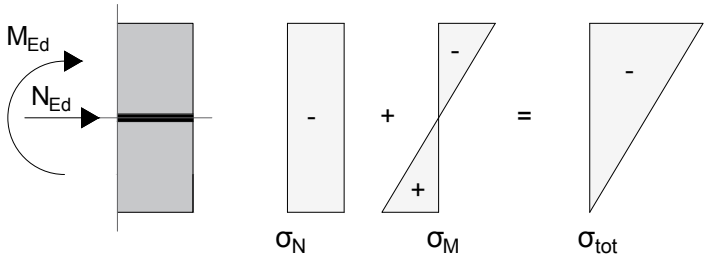

FIGURE G.19: Moment capacity in prestressed upper flange in compression

$$\sigma_2 = -\frac{N_{Ed}}{A_c t} + \frac{M_{Rdc} \cdot z_b}{I_c} \leq 0$$
$$M_{Rdc} \leq N_{Ed} \cdot \frac{I_c}{A_c \cdot z_b} = \frac{1}{6} \cdot N_{Ed} \cdot h_{ft}$$

This results in:

Bending moment:	M_{Ed}	= 69 kNm
Compressive force:	N_{Ed}	= 3287 kN
Moment capacity:	M_{Rdc}	= 71.2 kNm
Unity Check:	UC_M	= 0.96

- The shear capacity is calculated in the same manner as before and it follows that the ultimate compressive strut strength is again governing. It holds:

Shear force:	V_{Ed}	= 415 kN
Shear capacity:	$V_{Rd;max}$	= 857 kN
Unity Check:	UC_V	= 0.48

- The upper flange is in compression and thus the element must be checked on compressive strength and buckling capacity. The calculation procedure is as follows:

$$\sigma_c = \frac{N_{Ed}}{A_{ct}}$$

This results in:

Compressive force:	N_{Ed}	= 3287 kN
Compressive stress:	σ_c	= 25.28 N/mm^2
Compressive strength:	f_{cd}	= 96.33 N/mm^2
Unity Check:	UC_{N^-}	= 0.26

In elements in compression also buckling failure should be considered. This is a second order check, which only has to be preformed when the critical slenderness λ_{lim} is reached. The critical slenderness is calculated through *[Braam, 2010]*:

$\lambda_{lim} = \frac{20 \cdot A \cdot B \cdot C}{\sqrt{n}}$

A = $\frac{1}{1+0.2 \cdot \phi_{ef}}$

ϕ_{ef} is the effective creep coefficient: $\phi_{ef} = \phi(\infty, t_0) \cdot \frac{M_{0Eqp}}{M_{0Ed}}$

$\phi(\infty, t_0)$ is the ultimate value for the creep coefficient

M_{0Eqp} is the first order bending moment in the quasi-permanent load combination

M_{0Ed} is the first order bending moment in the ULS

$B = \sqrt{1+2 \cdot \omega} = \sqrt{1+2 \cdot \frac{A_s \cdot f_{yd}}{A_c \cdot f_{cd}}}$

A_s is the total cross-sectional area of longitudinal reinforcement

$C = 1.7 - r_m$ for braced structures

$C = 0.7$ for unbraced structures

$n = \frac{N_{Ed}}{A_c \cdot f_{cd}}$ is the relative normal force

This critical slenderness has to be compared to the slenderness of the element, which is calculated by **??**[Cement stabiliteit]:

$\lambda = \frac{l_0}{i}$

l_0 is the effective or buckling length

$i = \sqrt{\frac{I_c}{A_c}}$

This results in:

Element slenderness:	λ	= 26.65
Factor A:	A	= $\frac{1}{1+0.2 \cdot 0.8}$ = 0.86
Factor B:	B	= $\sqrt{1+2 \cdot \frac{A_p \cdot f_{yd}}{A_c \cdot f_{cd}}}$ = 3.34 $\cdot 10^5$
Factor C:	C	= 0.7
Critical slenderness:	λ_{lim}	= 7.87 $\cdot 10^6$
Unity Check:	UC_{buc}	= 0.00

Thus no second order calculation has to be performed to investigate the buckling behaviour.

- The deformation of the upper flange must be conform the maximum allowable deformation in SLS. It holds that:

Maximum allowable deformation:	$w_{k;max}$	= $\frac{l_{box}}{250}$ = 4 mm
Maximum deformation:	w_{Ek}	= 0.30 mm
Unity Check:	UC_w	= 0.07

Internal analysis - Webs

Due to the applied model for the upper flange (Figure G.14) only normal loads are transferred to the webs.

As a result of the governing load situation in the upper flange the maximum normal forces in the webs are indicated in Figure G.20. It can be seen that both compressive and tensile stresses occur. In this, the self-weight of the webs is neglected.

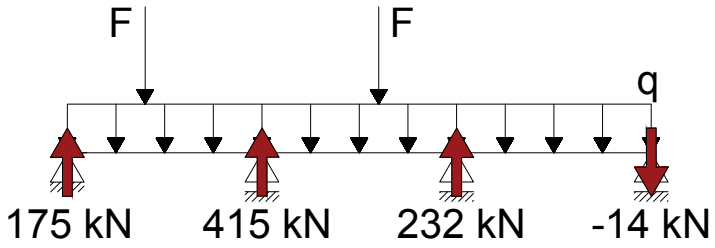

FIGURE G.20: Normal forces in the webs from upper flange load actions

The capacity for compression is calculated through the approach as discussed in the upper flange calculations.

This results in:

Compressive force:	N_{Ed}	= 415.0 kN
Compressive stress:	σ_c	= 4.61 N/mm^2
Compressive strength:	f_{cd}	= 96.33 N/mm^2
Unity Check:	$UC_N{}^-$	= 0.05

Again, it is investigated whether buckling has to be checked:

Element slenderness:	λ	= 13.86
Factor A:	A	$= \frac{1}{1+0.2 \cdot 0.8} = 0.86$
Factor B:	B	$= \sqrt{1 + 2 \cdot \frac{0 \cdot f_{yd}}{A_c \cdot f_{cd}}} = 1$
Factor C:	C	= 0.7
Critical slenderness:	λ_{lim}	= 55.16
Unity Check:	UC_{buc}	= 0.25

Thus no second order calculation has to be performed to investigate the buckling behaviour.

The capacity for tension is calculated through the following approach:

$$\sigma_c = \frac{N_{Ed}}{A_{cw}}$$

This results in:

Tensile force:	N_{Ed}	= 13.8 kN
Tensile stress:	σ_c	= 0.15 N/mm^2
Tensile strength:	$\lvert f_{ctd1}$	= 5.33 N/mm^2
Unity Check:	$UC_N{}^+$	= 0.03

Thus no additional longitudinal reinforcement is required to fulfil the Unity Check for normal capacity in the webs. However, some suspension reinforcement is required to transfer the loads from the lower flange due to the self-weight of concrete to the upper flange.

Since the tensile force following from the self-weight of the lower flange is equal to just $R_{c;fb}$ = 1.5 kN it is assumed this will not cause any problems. The required minimal concrete cover does determine the minimum web thickness however:

For reinforcement steel:	c_{nom}	= 31 mm
Reinforcement diameter:	Φ_{sw}	= 20 mm
Minimal web thickness:	$t_{w;min}$	= 0.09 m

Internal analysis - Lower flange
As for the webs, the self-weight of the lower flange is neglected as it is assumed that the cross-sectional area of the flange is sufficient to carry this load. It is also assumed that collision forces from underneath will not cause any problems to the structural behaviour of the floor girder and therefore it does not have to be taken into account.
Since no other load actions occur on the lower flange no Unity Check will need to be performed.

The minimum flange thickness follows from the minimum concrete cover required on the pre-tensioning steel that is present in both directions:

For pre-tensioning steel:	c_{nom}	= 36.5 mm
Strand diameter:	Φ_{ps}	= 15.7 mm
Minimal flange thickness:	$t_{fb;min}$	= 0.12 m

G.3. TRUSS GIRDER

G.3.1. Geometry and specific considerations

The length of the side girder is still l_f = 36.8 m and the width of the truss girder is chosen equal to that of the massive side girder: b_t = 1.2 m.

For a heavily loaded side girder a truss is a promising solution, designed such that the diagonals are in compression and the verticals are in tension (see Figure G.21). Prestressing will be present in both lower and upper beam and these will consist of straight post-tensioned cables throughout the structure. In contradiction to the massive side girder, prestressing does not have to be executed in two stages.

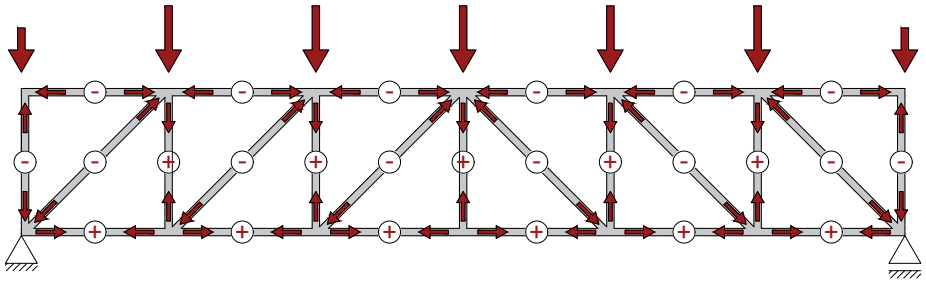

FIGURE G.21: Normal forces in the truss elements from general load action

The following dimensions give an adequate structural performance of the truss:

h_t = 2.3 m
h_{tt} = 0.40 m
h_{tb} = 0.80 m
d_{td} = 0.30 m
d_{tv} = 0.30 m
l_{ts} = 2.5 m
l_{tse} = 0.9 m to the support, but will extend to 1.6 m beyond the support

The connection to the floor girders is fixed, but the side girders themselves are simply supported.

G.3.2. Analytical load actions

Global load actions
The same approach to determine the load action from the floor girders is used for the truss girder as explained in F.3.2. Again, the effective width of the concentrated loads depends on the stiffness ratio in both directions. The results that follow are presented in Table G.16.
Again, these loads have to be transferred from the bottom of the truss girder, through the lower beam and the verticals, to the top of the truss girder. The required suspension reinforcement is calculated according to the

Truss	Char.	Design	
Shear	4386	6319	*kN*
Moment$_x$	38501	55357	*kNm*
Moment$_y$	2670	3917	*kNm*
Deformation	109	-	*mm*

TABLE G.16: Resulting maximum load actions in the truss girders

regulations given in *[Allaart, 1994]* in which half the tensile strength is assumed.

Internal load actions

The normal compressive and tensile loads in the upper and lower beam result from global moment equilibrium, but the loads in the verticals and diagonals must be obtained in another way. This is done through global and internal force equilibrium within a part of the structure, as illustrated in Figures G.22 to G.24.

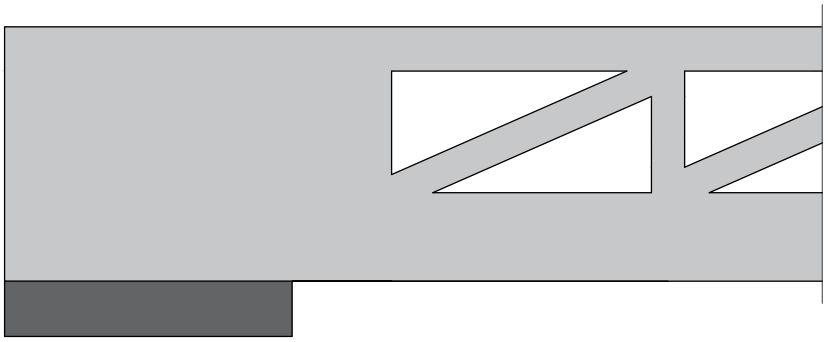

FIGURE G.22: Detail of the end segment in a truss girder

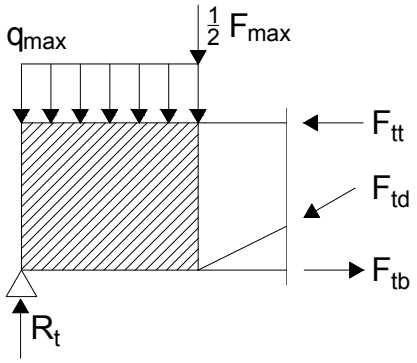

FIGURE G.23: Internal and external force equilibrium for the calculation of the internal load action in the diagonals

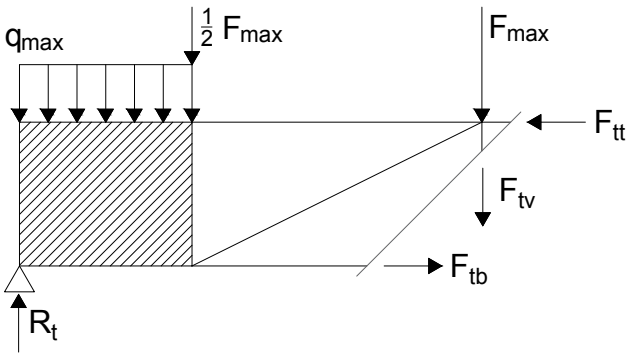

FIGURE G.24: Internal and external force equilibrium for the calculation of the internal load action in the verticals

Furthermore, the lower beam is loaded in bending and shear from the connection with the floor girders. In Figure G.25, the two limit states for an adequate structural model are given, one with clamped ends and one with free ends.
In reality, there will be a certain rotational stiffness from the rest of the lower beam and the verticals and diagonals, but for reasons of simplicity this analysis is confined to these two cases.

The resulting internal element loads are listed in Table G.17.

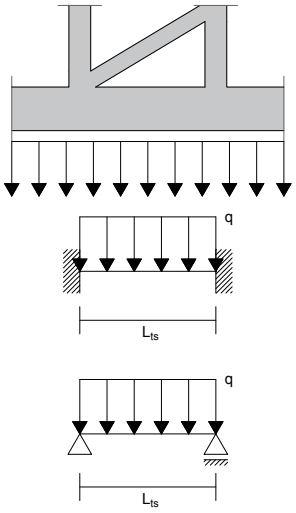

FIGURE G.25: Internal load model for load actions on the lower truss beam

Elements		Char.	Design	
Upper beam	Normal	-	11590	*kN*
Lower beam	Shear	867	1285	*kN*
	$Moment^{+}_{x}$	181	268	*kNm*
	$Moment^{-}_{x}$	-361	-535	*kNm*
	Normal	301	-931	*kN*
	Deformation	0,14	-	*mm*
Vertical beam	Normal	-	-3975	*kN*
Diagonal beam	Normal	-	3694	*kN*
End segment	Shear	-	1941	*kN*

TABLE G.17: Resulting maximum internal load actions in the truss girders

G.3.3. FEM load actions

As for the massive element structure, the analytical approach is compared to the results of a FEM model for verification. The FEM model input parameters and result interpretation are presented in Appendices H and I respectively.

For the open structure design the same conclusions can be drawn as for the massive structure design. The difference in the incorporation of orthotropic behaviour will not alter the analytical approach.

G.3.4. Unity Checks

The side girder will have to be designed with sufficient capacity to resist all loads, while fulfilling the boundary conditions as set in E.5.
From both the analytical calculation of the load actions and the FEM calculations it follows that the maximum moment and maximum deformation in the side girder occur at midspan, thus load situation 3, while the maximum shear load occurs at the end span, thus situation 4.

First, the global bending and deformation capacity will be checked after which the internal elements will be checked according to their loading situations.

Suspension reinforcement

Since the connection of floor and side girder is situated at the bottom of the side girder, all load actions working on the side beam must first be transferred trough the lower beam ad the verticals to the top of the

beam. As stated before, *[Allaart, 1994]* prescribes a reduced tensile strength of the suspension reinforcement to account for unknown dynamical and fatigue loads.
Also, the segment length is chosen as such to accommodate the suspension reinforcement positioned over an angle of 30° in the lower beam towards the verticals (see Figure G.26).

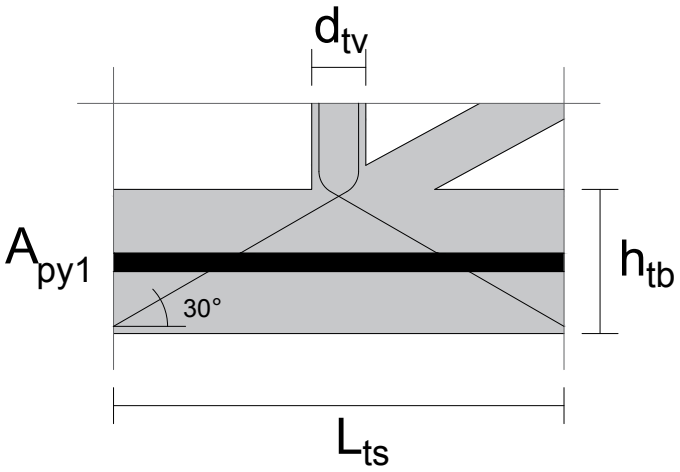

FIGURE G.26: Layout of the suspension reinforcement in the lower truss beam and vertical (not to scale)

For the lower beam it holds that:

Maximum distributed load acting on the side girder:	$q_{max;d}$	= 924 kN/m
Resultant of the distributed load over a 30° angle:	$R_{max;d}$	= 1371 kN
Tensile strength suspension reinforcement:	$f_{yd;sus}$	$= \frac{1}{2} \cdot 435 = 218$ N/mm^2
Required suspension reinforcement area:	$A_{sus,req}$	= 6290 mm^2
Suspension reinforcement diameter:	Φ_{sw}	= 20 mm
Number of bars over width:	n_{sw}	= 4
Bar spacing:	s	= 150 mm
Applied suspension reinforcement area:	S_{sus}	= 8378 mm^2
Unity Check:	UC_{sus}	= 0.75

For the verticals it holds that:

Resultant of the distributed load:	$R_{max;d}$	= 739 kN
Tensile strength suspension reinforcement:	$f_{yd;sus}$	$= \frac{1}{2} \cdot 435 = 218$ N/mm^2
Required suspension reinforcement area:	$A_{sus,req}$	= 3391 mm^2
Suspension reinforcement diameter:	Φ_{sw}	= 20 mm
Number of bars over width:	n_{sw}	= 4
Bar spacing:	s	= 150 mm
Applied suspension reinforcement area:	S_{sus}	= 8378 mm^2
Unity Check:	UC_{sus}	= 0.40

Check boundary conditions:

- Minimum concrete cover:
  For reinforcement steel: $c_{com} = 31$ mm
  $e_h = e_v = 26$ mm

  The requirement for minimum concrete cover in both lower beam and vertical is met. For the lower beam a distance of $\frac{h_{tb}}{\cos(\theta)} = 0.92$ m is available. With 4 bars this results in a possible spacing of 260 mm

between each bar is possible which is more than the required e_h = 26 mm. For the verticals the same holds as the 4 bars can be divided over the thickness d_{tv} with a spacing of 50 mm > e_h = 26 mm.

Global analysis - Moment capacity

The moment capacity of a truss is calculated differently to that of a full beam or to that of the floor, since only normal forces are present in the elements. The stress distribution is illustrated in Figure G.27.

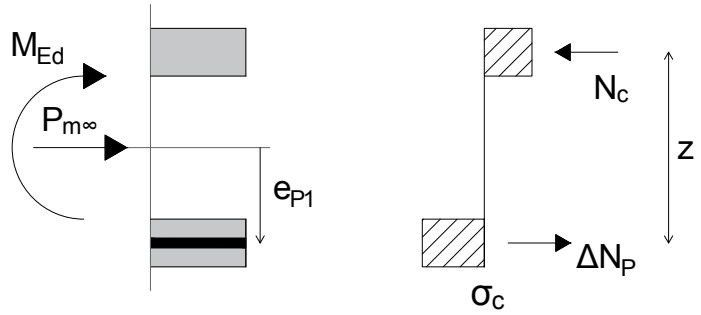

FIGURE G.27: Moment capacity and internal loads in a truss structure

Again, the equilibrium conditions are considered:

$$\Sigma F_x = 0 \quad \rightarrow \quad N_c = P_{m\infty} + \Delta N_p$$

$$N_c = b_t \cdot h_{tt} \cdot \sigma_c$$

$$\sigma_c = \frac{A_{py1} \cdot f_{pd} + A_{py2} \cdot \sigma_{pm\infty}}{b_t \cdot h_{tt}}$$

$$\Sigma M = 0 \quad \rightarrow \quad M_{Rdc} = N_c \cdot (z_t - 0.5 \cdot h_{tt}) + \Delta N_p \cdot (z_b - 0.5 \cdot h_{tb})$$

$$M_{Rdp} = e_{p1} \cdot P_{m\infty 1}$$

The results are given below:

Lower prestress area:	A_{py1}	= 21500 mm^2 (8 tendons)
Lower prestress eccentricity:	e_{p1}	= 0.57 m
Upper prestress area:	A_{py2}	= 8000 mm^2 (3 tendons)
Upper prestress eccentricity:	e_{p2}	= 1.13 m
Compressive force:	N_c	= 42205 kN
Lower prestress force:	P_{m01}	= 29993 kN
	$P_{m\infty 1}$	= 25494 kN
Upper prestress force:	P_{m01}	= 11160 kN
	$P_{m\infty 1}$	= 9486 kN
Increase in prestress force:	ΔN_p	= 7225 kN
Moment capacity concrete:	M_{Rdc}	= 51927 kNm
Moment capacity prestress:	M_{Rdp}	= 14446 kNm
Total moment capacity:	M_{Rd}	= 66373 kNm
$M_x{}^+$ in ULS:	M_{Ed}	= 55498 kNm
Unity Check:	UC_M	= 0.84

Check boundary conditions:

- Minimum concrete cover:
  For post-tensioned steel: c_{com} = 85 mm
  $e_h = e_v$ = 60 mm

  As shown in Figure G.28, the boundary condition for minimum concrete cover is satisfied in this direction.

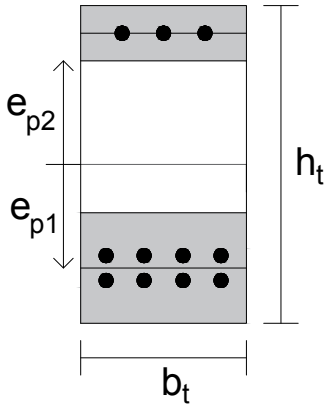

FIGURE G.28: Prestress configuration in the open truss element in y-direction

y		n [-]	e [m]
e_{p1}	top	4	0.480
	bottom	4	0.660
	total	8	0.570
e_{p2}	total	3	1.130
Maximum		6	1.190

TABLE G.18: Prestress configuration in the open truss element in y-direction

- Minimum prestress area:
  At t = ∞, the following stress distribution occurs at SLS loading:

$$\sigma_1 = -\frac{P_{m\infty 1}}{A_c} + \frac{e_{p1}\cdot P_{m\infty 1}\cdot z_t}{I_c} - \frac{P_{m\infty 2}}{A_c} - \frac{e_{p2}\cdot P_{m\infty 2}\cdot z_t}{I_c} - \frac{M_{t=\infty}\cdot z_t}{I_c}$$
$$\sigma_2 = -\frac{P_{m\infty 1}}{A_c} - \frac{e_{p1}\cdot P_{m\infty 1}\cdot z_b}{I_c} - \frac{P_{m\infty 2}}{A_c} + \frac{e_{p2}\cdot P_{m\infty 2}\cdot z_b}{I_c} + \frac{M_{t=\infty}\cdot z_t}{I_c}$$

Minimum presress		
	x = 0.5 L	Unit
σ_1	-62.54	N/mm^2
σ_2	-5.17	N/mm^2

TABLE G.19: Boundary condition check for minimum prestress in y-direction

It can be seen that all end fibres are in compression and thus the condition for minimum prestress is met.

- Maximum prestress area:
  The maximum compression stress at t = 0 is given by:

$$\sigma_1 = -\frac{P_{m01}}{A_c} + \frac{e_{p1}\cdot P_{m01}\cdot z_t}{I_c} - \frac{P_{m02}}{A_c} - \frac{e_{p2}\cdot P_{m0}\cdot z_t}{I_c}$$
$$\sigma_2 = -\frac{P_{m\infty 1}}{A_c} - \frac{e_{p1}\cdot P_{m\infty 1}\cdot z_b}{I_c} - \frac{P_{m\infty 2}}{A_c} + \frac{e_{p2}\cdot P_{m\infty 2}\cdot z_b}{I_c}$$

Maximum prestress (comp)		
		Unit
σ_1	-17.92	N/mm^2
σ_2	-33.91	N/mm^2

TABLE G.20: Boundary condition check for maximum prestress based on compressive strength in y-direction

It follows that these are smaller than $0.6\cdot f_{ck}(t) = 0.6\cdot 170 = 102$ N/mm^2 and thus this condition is met.

The maximum tensile stress in the upper and lower fibre after prestressing is given by:

$$\sigma_1 = -\frac{P_{m01}}{A_c} + \frac{e_{p1}\cdot P_{m01}\cdot z_t}{I_c} - \frac{P_{m02}}{A_c} - \frac{e_{p2}\cdot P_{m0}\cdot z_t}{I_c} - \frac{M_{t=0}\cdot z_t}{I_c}$$
$$\sigma_2 = -\frac{P_{m\infty 1}}{A_c} - \frac{e_{p1}\cdot P_{m\infty 1}\cdot z_b}{I_c} - \frac{P_{m\infty 2}}{A_c} + \frac{e_{p2}\cdot P_{m\infty 2}\cdot z_b}{I_c} + \frac{M_{t=0}\cdot z_b}{I_c}$$

The boundary condition ($\sigma \le f_{ctd1}$) is met at all locations.

Maximum prestress (tension)			
	x = 0	x = 0.5 L	Unit
σ_1	-17.92	-27.10	N/mm^2
σ_2	-33.91	-24.73	N/mm^2

TABLE G.21: Boundary condition check for maximum prestress based on tensile strength in y-direction

- Ductility:
  The maximum stress in top and bottom fibre in the ULS is given by:

$$\sigma_1 = -\frac{P_{m\infty 1}}{A_c} + \frac{e_{p1} \cdot P_{m\infty 1} \cdot z_t}{I_c} - \frac{P_{m\infty 2}}{A_c} - \frac{e_{p2} \cdot P_{m\infty 2} \cdot z_t}{I_c} - \frac{M_{Ed} \cdot z_t}{I_c}$$

$$\sigma_2 = -\frac{P_{m\infty 1}}{A_c} - \frac{e_{p1} \cdot P_{m\infty 1} \cdot z_b}{I_c} - \frac{P_{m\infty 2}}{A_c} + \frac{e_{p2} \cdot P_{m\infty 2} \cdot z_b}{I_c} + \frac{M_{Ed} \cdot z_t}{I_c}$$

Maximum prestress (ductility)		
	x = 0.5 L	Unit
σ_1	-83.25	N/mm^2
σ_2	5.19	N/mm^2

TABLE G.22: Boundary condition check for maximum prestress based on ductility in y-direction

It follows that the tensile stress in the concrete is smaller than f_{ctd1} and thus cracking will not occur in y-direction. This is however intended, since the lower beam will have to be sufficient for internal bending moments as well. For that, at least part of the lower beam should be uncracked as a result from global bending so that certain compression zone is present. Since the global bending moment causes a pure normal tension stress in the concrete it follows that this stress must be smaller than f_{ctd1}. It should however be checked in the internal analysis of the lower beam if the ductility requirement is met in ULS.

Global analysis - Deformation capacity

The maximum deformation is checked according to the same approach mentioned for the floor girder.

Maximum allowable deformation:	$w_{k;max}$	$= \frac{l_t}{250} = 147$ mm
Maximum deformation:	w_{Ek}	$= 102$ mm
Unity Check:	UC_w	$= 0.69$

Internal analysis - Upper beam

The upper beam will have to be checked on its normal capacity since a compression force results from both the prestressing and the global moment.

This results in:

Compressive force:	N_{Ed}	$= 10822$ kN
Compressive stress:	σ_c	$= 22.55$ N/mm^2
Compressive strength:	f_{cd}	$= 96.33$ N/mm^2
Unity Check:	UC_{N^-}	$= 0.23$

Again, it is investigated whether buckling has to be checked:

Element slenderness:	λ	= 21.65
Factor A:	A	$= \frac{1}{1+0.2 \cdot 0.8} = 0.86$
Factor B:	B	$= \sqrt{1 + 2 \cdot \frac{0 \cdot f_{yd}}{A_c \cdot f_{cd}}} = 1$
Factor C:	C	= 0.7
Critical slenderness:	λ_{lim}	= 24.95
Unity Check:	UC_{buc}	= 0.87

Thus no second order calculation has to be performed to investigate the buckling behaviour.

Internal analysis - Lower beam

The lower beam must be checked on moment capacity, shear capacity, torsion capacity, normal capacity and deformation.

- The moment capacity depends on the stress that is already present in the cross-section from global bending moment actions. As stated in the global analysis, this stress must be below the tensile strength of the concrete since otherwise the entire cross-section would be cracked and no additional loads can be taken up. The moment capacity of the lower beam itself must be such that the stresses that follow from either positive or negative bending moments do give rise to rack formation, in order to fulfil the ductility requirement.
  Again, the starting point for this analysis is that the reinforcement steel must yield before the concrete reaches its ultimate compression strength. According to Figure G.29 it can be seen that this results into:

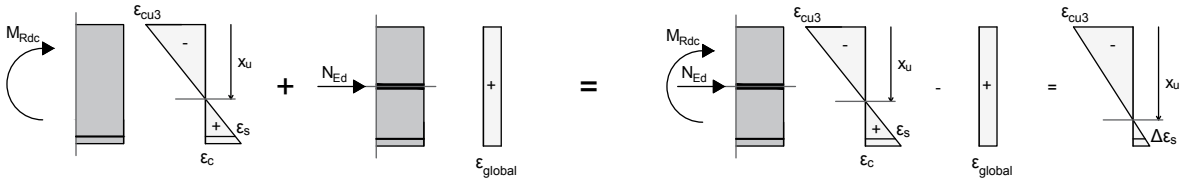

FIGURE G.29: Strain distribution and maximum moment capacity in the lower truss beam

$$x_u = \frac{\epsilon_{cu3}}{\Delta\epsilon_s + \epsilon_{cu3}} \cdot d_s$$

The moment capacity is then calculated according to Figure G.30. In this a simplification is applied, by neglecting the tensile capacity of the fibres in the concrete. Also it is assumed that the compression height is such that the concrete is still in its linear-elastic state. This has to be checked later on. The equilibrium conditions give:

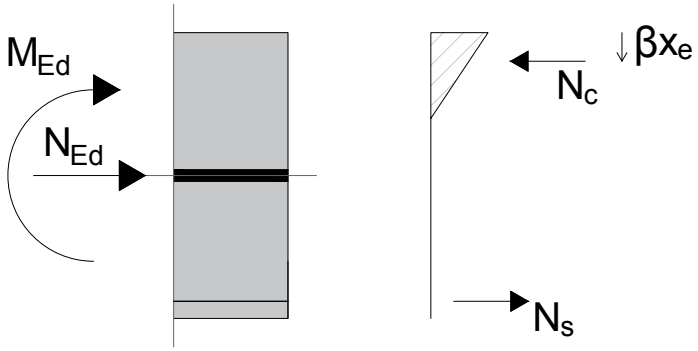

FIGURE G.30: Moment capacity in the lower beam due to internal bending moments

$$\Sigma F_x = 0 \quad \rightarrow \quad N_c = N_{Ed} + N_s$$
$$N_c = \alpha \cdot b_t \cdot {f_{cd}}^* \cdot x_e$$
$${f_{cd}}^* = \frac{f_{cd} \cdot x_e}{\frac{\epsilon_{c3}}{\epsilon_{cu3}} \cdot x_u}$$
$$x_e = \sqrt{\frac{(N_{Ed}+N_s) \cdot \frac{\epsilon_{c3}}{\epsilon_{cu3}} \cdot x_u}{\alpha \cdot b_t \cdot f_{cd}}}$$

$$\Sigma T = 0 \quad \rightarrow \quad M_{Rdc} = N_c \cdot (1-\beta) \cdot x_e + N_s \cdot (d_s - x_e) + N_{Ed} \cdot (z_t - x_e)$$

The result is:

Assumed arm for reinforcement:	d_s	= 0.75 m
Assumed normal reinforcement area:	A_s	= 11624 mm^2
Ultimate stress from global load actions:	σ_c	= 5.19 N/mm^2
Residual strain in steel:	$\Delta\epsilon_s$	= 2.07 ‰
Ultimate compression zone height:	x_u	= 0.42 m
Normal force in lower beam (tension):	N_{Ed}	= 4979 kN
Tensile force in steel:	N_s	= 5054 kN
	α	= 0.50
	β	= 0.33
Compression zone height:	x_e	= 0.02 m
Compression force:	N_c	= 1437 kN
Bending moment capacity:	M_{Rdc}	= 2116 kNm
Positive bending moment:	${M_{Ed}}^+$	= 268 kNm
Unity Check:	${UC_M}^+$	= 0.13
Negative bending moment:	${M_{Ed}}^-$	= 535 kNm
Unity Check:	${UC_M}^-$	= 0.33

In Table G.23 the resulting stresses in the lower beam cross-section are given as a result of ULS loading and it can be seen that the requirement for ductility is met.

Maximum prestress (ductility)			
	M_x^+	M_x^-	Unit
σ_1	3.09	9.37	N/mm^2
σ_2	7.28	1.00	N/mm^2

TABLE G.23: Boundary condition check for maximum prestress based on ductility in the lower beam in y-direction

- For the shear capacity in the lower beam it holds that the ultimate compressive strength of the struts is governing:

Normal force from prestress:	N_{Ed}	= 622 kN
Working width of cross-section:	b_w	= b_f = 0.51 m
Concrete shear capacity:	V_{Rdc}	= 782 kN
Fibre shear strength:	σ_{Rdf}	= 6.68 N/mm^2
Fibre shear capacity:	V_{Rdf}	= 4288 kN
Shear reinforcement diameter:	Φ_{sw}	= 20 mm
Number of bars over width:	n_{sw}	= 0
Bar spacing:	s	= 100 mm
Reinforcement capacity:	V_{Rds}	= 0 kN

Total shear capacity:	V_{Rd}	= 5070 kN
Maximum shear capacity:	$V_{Rd;max}$	= 636 kN
Maximum shear in cross-section:	V_{Ed}	= 1285 kN
Unity Check:	UC_V	= 2.02

- Since all load from the floor is transferred to the truss by the lower beam, this lower beam also takes up all the torsional moments. Its capacity is:

Cross-sectional capacity:	T_{Rdc}	= 590 kNm
Maximum torsional moment:	T_{Ed}	= 7077 kNm
Thus additional reinforcement is required		
Shear reinforcement diameter:	Φ_{sw}	= 20 mm
Maximum shear bars over width:	n_{max}	12
Number of bars over width:	n_{sw}	= 12
Minimum bar spacing:	s_{min}	= 26 mm
Bar spacing:	s	= 26 mm
Reinforcement capacity:	T_{Rds}	= 8063 kNm
Total torsion capacity:	T_{Rd}	= T_{Rds} = 8063 kNm
Unity Check:	UC_V	= 0.88

- So the torsion capacity is sufficient, but the combination of shear and torsion must also be considered with respect to the ultimate strength of the compressive struts.

  Unity Check: UC_{V+T} = 2.90

  This was to be expected, since the Unity Check for pure shear is already insufficient.

- The lower beam will be in tension due to the global bending moment. For reasons of ductility with regard to the bending moment in the lower beam, it was already showed that the tensile force is such that the stresses are below the tensile strength of the concrete and thus no additional reinforcement is required.

- The deformation of the lower beam must also be checked:

Maximum allowable deformation:	$w_{k;max}$	= $\frac{l_{ts}}{250}$ = 10 mm
Maximum deformation:	w_{Ek}	= 0.14 mm
Unity Check:	UC_w	= 0.01

Internal analysis - Verticals

The verticals will have to be checked on their normal capacity since a tensile force results from global load actions.

	Tensile force:	N_{Ed}	= 3989 kN
	Tensile stress:	σ_c	= 11.08 N/mm^2
This results in:	Tensile strength:	f_{ctd1}	= 5.33 N/mm^2
	Unity Check:	$UC_N{}^+$	= 2.08

It thus follows that additional longitudinal reinforcement is required to fulfil the Unity Check for normal capacity in the verticals. However there is also suspension reinforcement present in the verticals thus it must

be checked whether the minimum concrete cover still satisfies the boundary conditions.

The force that has to be transferred trough suspension reinforcement is equal to that of the reaction force on the lower beam over the truss segment length. This has to be taken up entirely by reinforcement:

Reaction load on lower beam:	$q_{max;d}$	= 1028 kNm
Suspension load:	N_{Ed}	= 2415 kN
Required suspension reinforcement area:	$A_{req;sus}$	= 5555 mm^2

For the normal reinforcement it holds:

Tensile force:	N_{Ed}	= 3989 kN
Required normal reinforcement area:	$A_{req;s}$	= 9174 mm^2

Combined this leads to:

Total reinforcement area required:	A_{req} = 14728 mm^2	
Applied reinforcement diameter:	Φ_s	= 20 mm
Maximum amount of reinforcement bars:	$n_{s;max}$	= 5
Minimum bar spacing:	s_{min}	= 26 mm
Applied bar spacing:	s	= 100 mm
Reinforcement area:	$A_{s;max}$	= 18850 mm^2
Unity Check:	UC_A	= 0.78

Internal analysis - Diagonals

The diagonals will have to be checked on their normal capacity since a compression force results from global load action.

This results in:

Compressive force:	N_{Ed}	= 3643 kN
Compressive stress:	σ_c	= 1.31 N/mm^2
Compressive strength:	f_{cd}	= 96.33 N/mm^2
Unity Check:	UC_{N^-}	= 0.01

Again, it is investigated whether buckling has to be checked:

Element slenderness:	λ	= 31.54
Factor A:	A	$= \frac{1}{1+0.2 \cdot 0.8} = 0.86$
Factor B:	B	$= \sqrt{1+2 \cdot \frac{0 \cdot f_{yd}}{A_c \cdot f_{cd}}} = 1$
Factor C:	C	= 0.7
Critical slenderness:	λ_{lim}	= 37.23
Unity Check:	UC_{buc}	= 0.85

Thus no second order calculation has to be performed to investigate the buckling behaviour.

Internal analysis - End segment

In a pure truss structure, no shear would occur as it would be taken up by the vertical truss elements as normal force. In this case, however, the closed end segment still has to be tested on shear.

The shear capacity is determined in the same manner as was done previously in the massive elements and the floor girder. The effective width of the girder has to be reduced due to the lower bond characteristics of grouted prestress cables.

In contrary to the situation with the massive side girder, the shear force now acts as a concentrated load at a distance of 0.9 m from the supports (see Figure G.22 and thus a reduction might be applied. This reduction

$\beta = \frac{a_v}{d}$ is however only valid if compared to the concrete shear capacity ($V_{Rdc} + V_{Rdf}$) and not if the capacity is governed by the ultimate strength of the compressive struts $V_{Rd;max}$. Since it turns out the latter is indeed governing, also in this situation no reduction of shear force may be applied.

The shear capacity of the cross-section is given by:

$$V_{Rd} = V_{Rdc} + V_{Rdf} + V_{Rds}$$

Normal force from prestress:	N_{Ed}	= 3273 kN
Working width of cross-section:	b_w	= b_f = 0.51 m
Concrete shear capacity:	V_{Rdc}	= 1411 kN
Fibre shear strength:	σ_{Rdf}	= 5.37 N/mm^2
Fibre shear capacity:	V_{Rdf}	= 7180 kN
Shear reinforcement diameter:	Φ_{sw}	= 20 mm
Number of bars over width:	n_{sw}	= 2
Bar spacing:	s	= 100 mm
Reinforcement capacity:	V_{Rds}	= 7468 kN
Total shear capacity:	V_{Rd}	= 16058 kN
Maximum shear in cross-section:	V_{Ed}	= 8819 kN
Unity Check:	UC_V	= 0.55

Check boundary conditions:

- Minimum concrete cover:
  For reinforcement steel: c_{com} = 31 mm
  $e_h = e_v$ = 26 mm
  The requirement for minimum concrete cover is met as a bar spacing of s_x = 100 mm > e_h = 26 mm is used and the application of two shear bars for every meter length results in a spacing of $s_y = \frac{l_{tse}}{2}$ = 450 mm > e_h.

- Ultimate strength compressive struts:
  From the boundary conditions given in E.5 it follows that the compressive struts have an ultimate strength that limits the shear capacity of the concrete:

  $V_{Rd;max}$ = 1394 kN

  Since V_{Rd} is larger than $V_{Rd;max}$, this capacity is too optimistic and must be replaced by $V_{Rd;max}$. The Unity Check then becomes:

  Unity Check: UC_V = 1.39

  Thus the cross-section does not satisfy the shear capacity Unity Check. In order to increase the Unity Check, the ultimate strength of the compressive struts must be increased. When looking at the formula for $V_{Rd;max}$, it can be seen that the only parameters that can be changed are the cross-sectional width and heigh-section.
  It follows that a cross-sectional area is required to fulfil this condition, with b_t = 1.4 m and h_t = 2.4 m. Then, the Unity Check for shear capacity becomes:

  Unity Check: UC_V = 0.97

  However, since this analysis is based on several consumptions and for instance important load actions like fatigue are not considered, it is advised to incorporate a double shear force capacity (n = 2). Then:
  $V_{Ed} = n \cdot V_{Ed}$ = 3884 kN

In that case, the dimensions of the cross-section at the supports would become b_t = 2.0 m and h_t = 2.8 m.

Unity Check: UC_V = 0.94

Thus despite the weight reduction of the open structure trough bridge compared to the massive structure design, shear capacity of the end segment and combined shear and torsion capacity of the lower beam are still a problem.

Structural analysis - FEM verification

H

FEM ANALYSIS TROUGH BRIDGE - FEM MODEL (SCIA)

In order to verify the analytical calculations used to determine the design for a trough girder, multiple finite element models were constructed in SCIA Engineer.
For the global load distribution in the floor and side girders, a basic plate is used with different supports and orthotropic behaviour to analyse all situations. As in the analytical calculation, the floor girder supports are assumed to be rigid and thus the result of the load distribution can be evenly compared. This is done for a massive plate, but also for plates with orthotropic behaviour to simulate both the connection between the floor girders and the stiffness of the open multicell box girder.
However, in reality, the supports for the floor girder are not rigid, but in fact flexible according to the bending and torsional stiffness of the side girder. Therefore a comparison is made between the rigidly supported plate model and the plate model supported on two side girders. Again, this is done for both isotropic and orthotropic plate behaviour.
Thus a clear comparison can be made between the load distribution assumed in the analytical calculation and the more realistic load distribution obtained through FEM analysis.

In this appendix the different FEM models in SCIA Engineer will be discussed according to their input and model considerations. These models will be used in the verification of the analytical calculations which is performed in Appendix I.

H.1. FLOOR MODEL

The basis of this FEM model consists of a two-dimensional plate that represents the floor girders. It has a length of 36.8 m, a width of 18.17 m and a depth of 0.61 m, which coincide with the outer dimensions of the bridge deck.
The x-direction is chosen - in accordance to the analytical analysis - along the width of the plate and the y-direction is chosen along the length of the plate (Figure H.1).

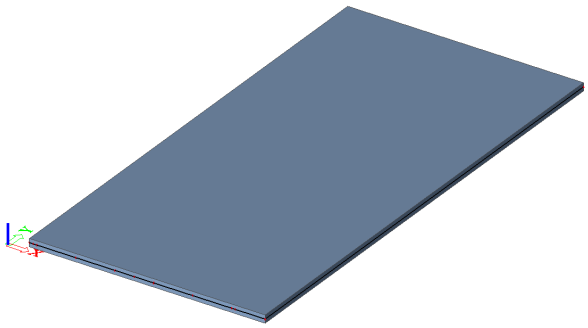

FIGURE H.1: Plate model for concrete deck construction in SCIA with global coordinates

A new material is made that represents UHPC concrete class C170/200, according to the parameters used in the analytical analysis (Appendix E, Table E.2).

The loads applied on the model are:

- Permanent loads:
  - Self-weight concrete
    The self-weight of the plate is automatically generated from the chosen material (ρ_c) and the depth of the plate. In the case of an open structure, the self-weight is naturally lower and this can be resolved by adapting the mass of the material ρ_c to an equivalent value. Thus:
    Massive: ρ_c = 2500 kg/m^3
    Open: ρ_c = 733 kg/m^3
  - Resting load asphalt layer:
    q_{ak} = -3.22 kN/m^2
  - Resting load concrete kerbs:
    q_{kk} = -4.75 kN/m^2

- Variable loads (Load Model 1):
  - Uniformly distributed loads (UDL):
    $q_{UDL;1}$ = -10.35 kN/m^2
    $q_{UDL;2}$ = -3.5 kN/m^2
  - Concentrated point loads (KEL):
    $F_{KEL;1}$ = -150 kN
    $F_{KEL;2}$ = -100 kN
    $F_{KEL;3}$ = -50 kN

The loads and their position are equal to those used in the analytical approach and they are illustrated in Figures H.2 to H.9.

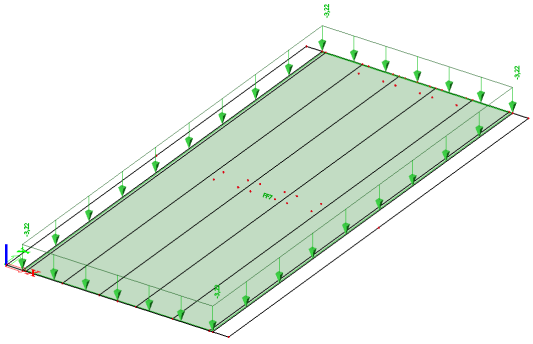

FIGURE H.2: Load configuration for the permanent resting load from the asphalt layer in SCIA

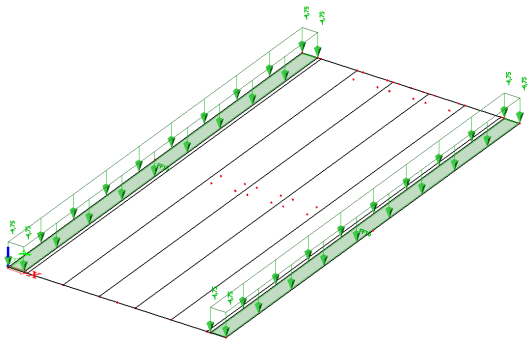

FIGURE H.3: Load configuration for the permanent resting load from the concrete kerbs in SCIA

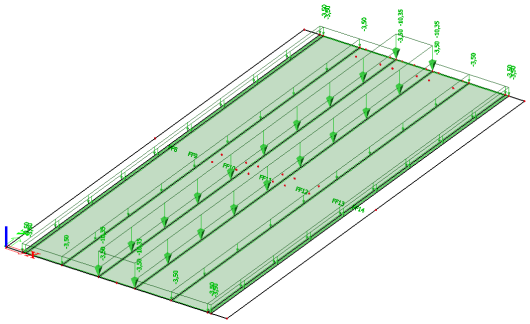

FIGURE H.4: Load configuration for the variable UDL traffic load for load situation 1 and 2

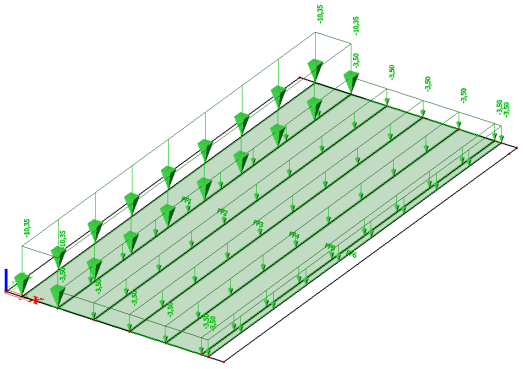

FIGURE H.5: Load configuration for the variable UDL traffic load for load situation 3 and 4

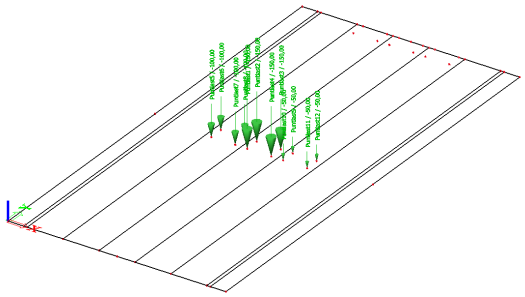

FIGURE H.6: Load configuration for the variable KEL traffic load for load situation 1

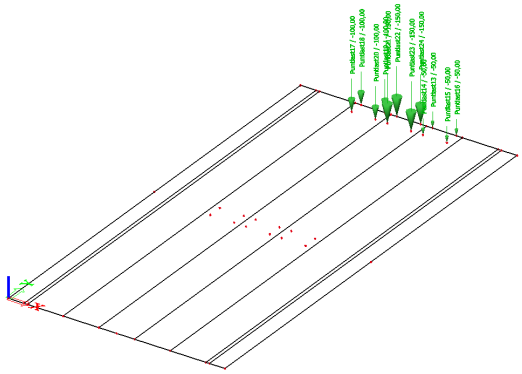

FIGURE H.7: Load configuration for the variable KEL traffic load for load situation 2

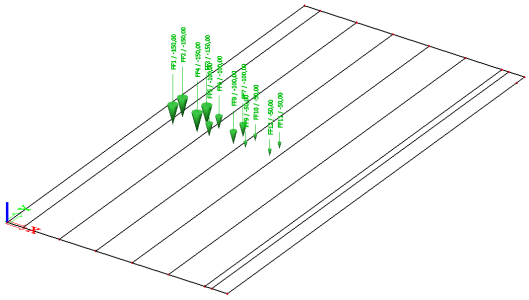

FIGURE H.8: Load configuration for the variable KEL traffic load for load situation 3

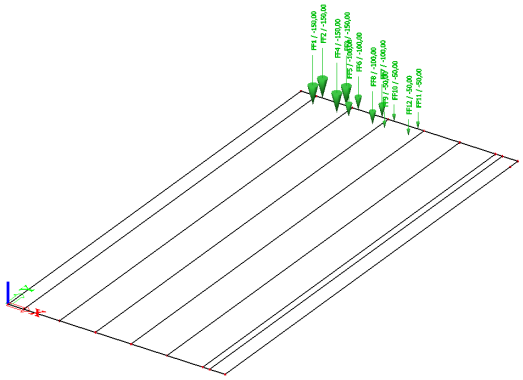

FIGURE H.9: Load configuration for the variable KEL traffic load for load situation 4

H.2. RIGID SUPPORTS

In the analytical analysis, the floor girders are fixed to the side girders and rigidly supported. In this FEM model, two line supports are modelled to simulate this.

The line supports have free translation in x- and y-direction and are fixed in z-direction. The rotation is free in x- and z-direction and fixed in y-direction. A detail of this line support is presented in Figure H.11.

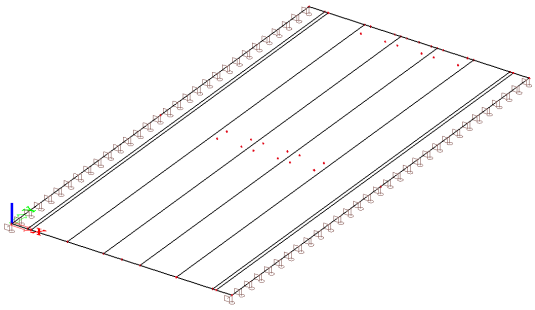

FIGURE H.10: Rigid line supports in SCIA

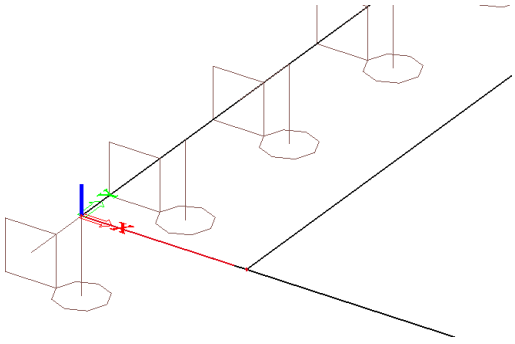

FIGURE H.11: Detailed view of the rigid line supports in SCIA

H.3. ORTHOTROPIC BEHAVIOUR

The orthotropic behaviour of both the massive floor girders and the multicell box girders is modelled by applying an orthotropic FEM model and adapting the corresponding stiffness matrix. The calculation of this stiffness matrix is done according to *[Spanbeton, nd]* and the results are given in Table H.1 for the massive floor girders and in Table H.2 for the open structure floor girders.

$$D_{11} = K_x = \frac{E_{//} \cdot I_x}{b_x} \quad \text{[MNm]}$$

$$D_{22} = K_y = \frac{M_x \cdot b_x}{2 \cdot \phi_y \cdot b_y} \quad \text{[MNm]}$$

$$D_{12} = \nu \cdot K_y \quad \text{[MNm]}$$

$$D_{33} = \frac{(K_{xy} + K_{yx})}{4} \quad \text{[MNm]}$$

$$K_{xy} = \frac{G_{//} \cdot I_t}{b_x} \quad \text{[MNm]}$$

$$K_{yx} = \frac{G_{\perp} \cdot I_y}{b_y} \quad \text{[MNm]}$$

$$D_{44} = \frac{G_{//} \cdot A_z}{b_x} \quad \text{[MN/m]}$$

$$D_{55} = \eta \cdot G_{\perp} \cdot h_c \quad \text{[MN/m]}$$

D_{11}	941.7	*MNm*
D_{22}	645.5	*MNm*
D_{12}	129.1	*MNm*
D_{33}	410.7	*MNm*
D_{44}	12500.0	*MN/m*
D_{55}	3819.4	*MN/m*

TABLE H.1: FEM stiffness matrix for orthotropic behaviour in the massive floor girders

D_{11}	773.5	*MNm*
D_{22}	122.5	*MNm*
D_{12}	24.5	*MNm*
D_{33}	233.4	*MNm*
D_{44}	1500.0	*MN/m*
D_{55}	2256.9	*MN/m*

TABLE H.2: FEM stiffness matrix for orthotropic behaviour in the open structure floor girders

In these calculations, it is assumed that the concrete remains uncracked. In reality though, the elements are designed to allow crack formation in ULS, in order to warn before failure and thus create a ductile design. This crack formation has an influence on the stiffness matrix, since the modulus of elasticity E_c is reduced and therefore also the shear modulus G_c will have to be adapted. The influence of cracking must therefore be investigated in further research in this topic.

H.4. FLEXIBLE SUPPORTS

The flexural and torsional stiffness of the side girder determines the flexibility of the line supports. However, since these stiffnesses can be described by a parabola, a variable stiffness has to be appointed to the line supports, which is not possible. Therefore, instead of line supports, one-dimensional beams supported at their ends will be used to simulate the flexibility of the side girders.

The one-dimensional beams have cross-sectional areas that coincide with the dimensions of the side girders in both cases. This means that for both the massive side girder and the open truss girder a width of 1200 mm and a height of 2300 mm is applied.
In the truss girder, the unit mass has to be adapted to match the reduced self-weight of the open structure, leading to $\rho_c = 1948$ kg/m^3. Also, the flexural and torsional stiffness must be modelled accurately. This is done by adapting the modulus of elasticity E_c and the shear modulus G_c from 50.000 N/mm^2 and 20.833 N/mm^2 to 38.518 N/mm^2 and 6.328 N/mm^2 respectively.

The one-dimensional beams are supported by point supports with a certain vertical spring stiffness to simulate the spring stiffness of the foundation piles. For this the same piles as in Appendix B are used, with a cross-sectional area of $380x380$ mm^2 and a length of 13.15 m. When applying NSC with a E-modulus of 34000 N/mm^2 this results in a spring stiffness of $E_c \cdot A_c / l_p = 373$ MN/m. An adequate guess for the number of piles underneath one support is based on the total reaction force of the model on a fixed support and the bearing capacity of one pile as calculated in Appendix B. It then follows that:

$$k_z = \frac{n_p \cdot E_c \cdot A_c}{l_p} = \frac{F_{Sd}}{R_{Cd}} \cdot \frac{E_c \cdot A_c}{l_p} = \frac{8820}{542} \cdot 373 = 6076 \quad \text{MN/m}$$

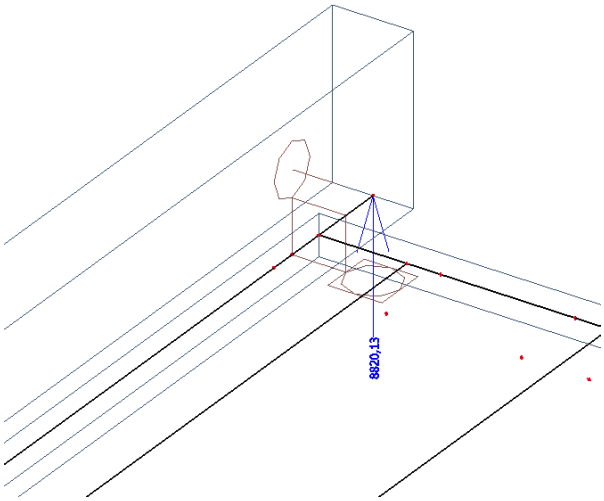

FIGURE H.12: Reaction force on the point support from bridge loading

To guarantee stability, the point supports are also fixed for translation in x-direction and for rotation over the y-axis.

The resulting model is presented in Figure H.13.

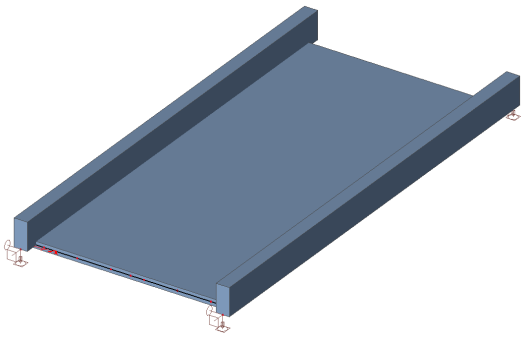

FIGURE H.13: SCIA model for a floor plate supported on flexible side girders

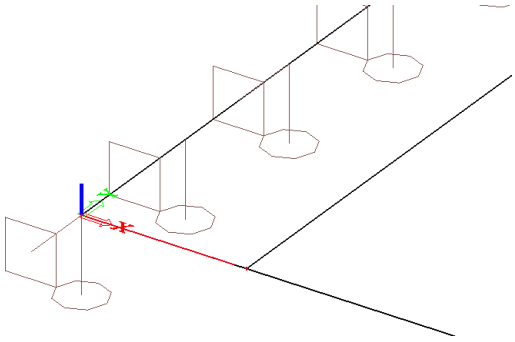

FIGURE H.14: Detailed view of the point supports for the flexible side girder

FEM ANALYSIS TROUGH BRIDGE - VERIFICATION OF ANALYTICAL RESULTS

The verification of the analytical calculations by means of a FEM model will be executed according to the following steps:

1. Massive trough bridge design
   a) Isotropic plate behaviour (section I.1)
      - Freely supported plate (section I.1.1)
      - Fixed supports (section I.1.2)
   b) Orthotropic plate behaviour (section I.2)
   c) Flexible supports (section I.3)
2. Open structure trough bridge design (section I.4)
3. Summarising conclusions on FEM verification (section I.5)

For each FEM model a comparison is made to the results from the analytical calculations with respect to the bending moment stresses, shear forces, deflections and torsion in the floor girders and side girders. Found differences will be investigated and explained and where necessary changes will be incorporated into the analytical model.

I.1. ISOTROPIC PLATE BEHAVIOUR

The first step is to analyse the plate model as an isotropic plate. For this, the Guyon-Massonnet input parameters are calculated:

$$I_x = \frac{1}{12} \cdot b_f \cdot {h_f}^3 = 5.67 \cdot 10^{-2} \text{ m}^4$$

$$I_y = \frac{1}{12} \cdot b_{fe} \cdot {h_f}^3 = 1.89 \cdot 10^{-2} \text{ m}^4$$

Flexible rigidity per unit width:

$$\rho_x = \frac{\Sigma E \cdot I_x}{b_f} = 9.46 \cdot 10^8 \text{ kNm}^3$$

$$\rho_y = \frac{\Sigma E \cdot I_y}{l_f} = 9.46 \cdot 10^8 \text{ kNm}^3$$

Torsional rigidity per unit width:

$$\gamma_x = \frac{\Sigma G \cdot I_x}{b_f} = 3.94 \cdot 10^8 \text{ kNm}^3$$

$$\gamma_y = \frac{\Sigma G \cdot I_y}{l_f} = 3.94 \cdot 10^8 \text{ kNm}^3$$

Flexural stiffness:

$$\theta = \frac{b_f}{l_f} \cdot \sqrt[4]{\frac{\rho_x}{\rho_y}} = 0.165 \text{ rad}$$

Torsional stiffness:

$$\alpha = \frac{\gamma_x + \gamma_y}{2 \cdot \sqrt{\rho_x \cdot \rho_y}} = 0.421$$

The concentrated KEL loads will be distributed evenly along an angle of 45° towards the side girder.

I.1.1. Freely supported plate

Several load distribution parameters have been compared and the results are shown in Figures I.1 to I.6 and Table I.1. A distinction is made between KEL loading at midspan (load situation 1 (Figure E.2)) and KEL loading at the end span (load situation 2 (Figure E.3)).

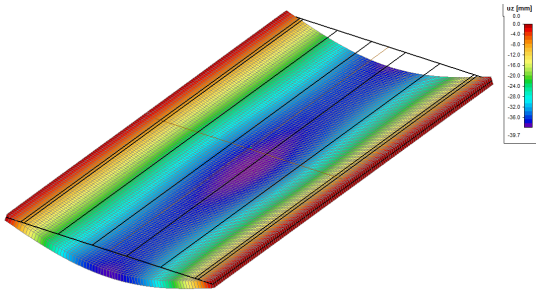

FIGURE I.1: Deformation of the isotropic, freely supported floor plate due to load situation 1

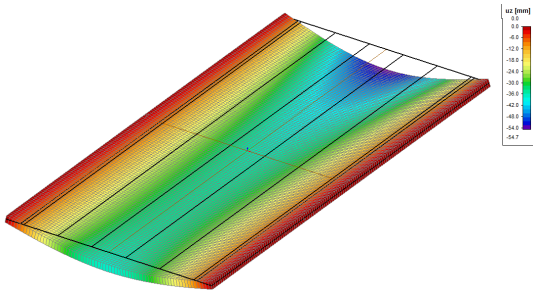

FIGURE I.2: Deformation of the isotropic, freely supported floor plate due to load situation 2

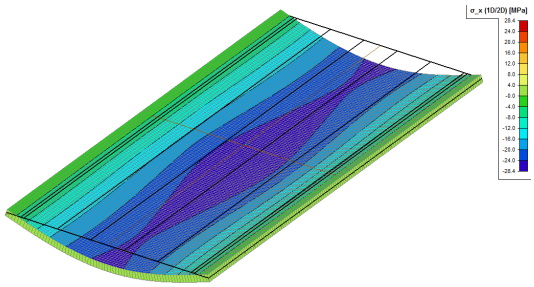

FIGURE I.3: Bending stresses in x-direction of the isotropic, freely supported floor plate due to load situation 1

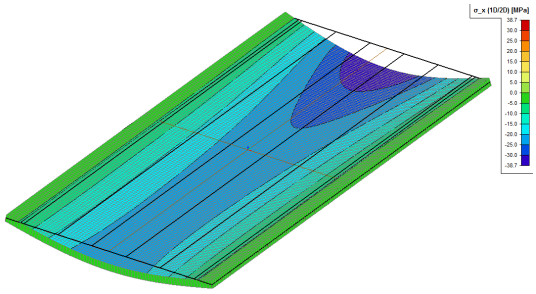

FIGURE I.4: Bending stresses in x-direction of the isotropic, freely supported floor plate due to load situation 2

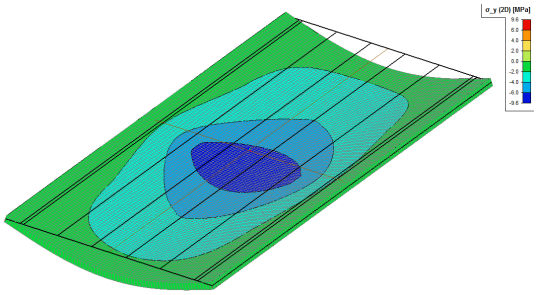

FIGURE I.5: Bending stresses in y-direction of the isotropic, freely supported floor plate due to load situation 1

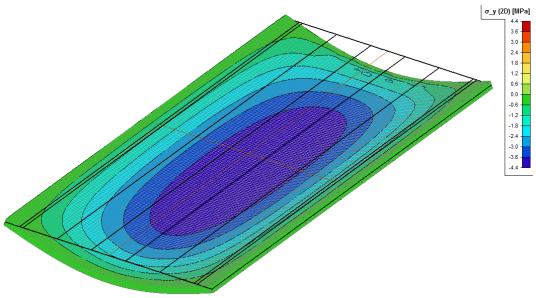

FIGURE I.6: Bending stresses in y-direction of the isotropic, freely supported floor plate due to load situation 2

Parameter	Situation 1			Situation 2			Unit
	FEM	Analytical	Δ [%]	FEM	Analytical	Δ [%]	
$\sigma_{x;max}$	28.0	28.5	1.8	38.7	45.1	16.5	N/mm^2
$\sigma_{y;max}$	9.2	5.7	38.0				N/mm^2
R_z	372.1	375.2	0.8	8242.7	447.6	94.6	kN/m
w_z	39.7	44.3	11.6	54.7	69.2	26.5	mm

TABLE I.1: Comparison between the analytical analysis and the FEM results for a freely supported isotropic floor plate

It can be seen that these values differ quite significantly. Several explanations can be found for these differences:

- First of all, it seems that the bending moment in transverse direction is much larger in the FEM analysis than in the analytical approach. In Table I.2 the comparison is made for all loads separately and it can clearly be seen that this large deviation is governed by the KEL loading.

$\sigma_{y;max}$	Situation 1			Unit
Load	FEM	Analytical	Δ [%]	
Self-weight	2.0	2.0	1.6	N/mm^2
Asphalt	0.4	0.4	4.8	N/mm^2
Kerbs	0.0	0.0	0.0	N/mm^2
UDL	0.7	0.7	4.4	N/mm^2
KEL	3.2	0.8	76.1	N/mm^2

TABLE I.2: Separate contributions to the bending stresses in y-direction for a freely supported isotropic floor plate in load situation 1

An explanation can be found in the plate theory for pure shear loading. In the analytical approach, shear deformation is neglected since the thickness to span ratio is very small. In reality, however, warping of a plate element occurs, thus giving rise to additional shear forces and moments in the transverse direction *[Steele and Balch, 2009]*.
It is found that if a transverse coefficient of 0.8 is used for KEL loading, the FEM and analytical analysis coincide quite neatly for both the KEL contribution (see Table I.3). It must be stated though that this is a somewhat arbitrary value since it depends on the model refinement and assumptions.

$\sigma_{y;max}$	Situation 1			Unit
Load	FEM	Analytical	Δ [%]	
Total	9.2	9.2	0.2	N/mm^2
KEL	3.2	3.2	4.3	N/mm^2

TABLE I.3: Result of adapting the transverse coefficient of point loads for a freely supported isotropic floor plate in load situation 1

- Secondly, the assumed distribution length $x_{L;F}$ used in the Guyon-Massonnet method must be checked. For load situation 1 it can be concluded that the stresses in both analyses coincide quite well, thus the assumption of $x_{L;F}$ = 18.17 m seems legitimate. For load situation 2, however, the stresses differ significantly (Δ =16.5%) and thus the question arises whether the assumption of $x_{L;F}$ = 9.685 m is correct.
Again the contribution every load is looked at separately and the results are shown in Table I.4. The largest deviation is again caused by the KEL loading. Since the reduction of KEL loads is governed by the distribution length taken into account, adapting this distribution length would be a logical explanation. It is found that, for an increased distribution length of $x_{L;F}$ = 14 m this deviation is removed and the stresses in both analyses are comparable again.
This adaptation also influences the analytical results of the maximum deflection in situation 2. The result is presented in Table I.5.

$\sigma_{x;max}$	Situation 2			
Load	**FEM**	**Analytical**	**Δ [%]**	**Unit**
Self-weight	10.4	10.1	2.4	N/mm^2
Asphalt	2.2	2.1	4.7	N/mm^2
Kerbs	0.1	0.1	35.5	N/mm^2
UDL	3.8	3.7	3.8	N/mm^2
KEL	10.3	15.1	46.9	N/mm^2

TABLE I.4: Separate contributions to the bending stresses in x-direction for a freely supported isotropic floor plate in load situation 2

$\sigma_{x;max}$	Situation 2			
Load	**FEM**	**Analytical**	**Δ [%]**	**Unit**
Total	38.7	38.3	1.0	N/mm^2
KEL	10.3	10.5	1.7	N/mm^2

TABLE I.5: Result of adapting the load distribution length for a freely supported isotropic floor plate in load situation 2

- Nevertheless, the difference in maximum deflection in both load situation 1 and 2 are quite significant. Again, the largest deviation comes from the KEL loading and it seems that the FEM analysis takes a larger load distribution into account than the analytical analysis. An explanation for this difference could be that the analytical analysis is based on beam theory, while the FEM analysis is based on plate theory. In a plate, the deflection of a strip will be retained by the material surrounding this strip and which has lower cross-sectional stresses and strains. In a beam, there is no material adjacent to the beam and thus there is no retaining influence on the deflection of the beam.

- At last, the very large differences in support reaction in load situation 2 must be addressed. The reason for this deviation must be sought in the FEM model, not the analytical model, since in load situation 1 no problems occur.
  In the FEM model, very large peak stresses occur at the end of the line supports that disturb the actual support reactions from the acting loads. They occur at every separate load action and thus the explanation must be sought in the general model parameters.
  These peak stresses are the result of transverse contraction in a plate element, that would not be present in a beam. Due to this transverse contraction, the plate wants to bend in a direction parallel to the line supports. This bending is however prohibited by the rigid line supports and therefore bending moments appear. But at the edges the moment must be equal to zero and thus the plate wants to deform. The rigid supports prevent this downwards translation and thus high peak stresses occur *[SCIA Engineer, 2015]*.

k_z	Load situation 1		Load situation 2		
[MN/m]	**FEM**	**Analytical**	**FEM**	**Analytical**	**Unit**
10	130.03	138.55	160.01	138.55	*kN/m*
100	134.06	138.55	201.68	138.55	*kN/m*
500	134.48	138.55	263.21	138.55	*kN/m*
1000	134.53	138.55	302.44	138.55	*kN/m*
∞	136.57	138.55	1440.36	138.55	*kN/m*

TABLE I.6: Influence of the support spring stiffness on the support reaction forces at midspan and end span

These peak stresses can be limited by allowing a realistic spring stiffness in the line supports. A quick investigation into the effect of this spring stiffness leads to the conclusion that the peak stresses can indeed be limited to some extent. The results will however never coincide with the analytical solution. In Table I.6 and Figures I.7 to I.16 this spring stiffness analysis is presented. It was performed on the self-weight of the floor girder.

It can be seen that the peak stresses indeed reduce significantly when appointing a spring stiffness to the line supports. The lower the spring stiffness, the smaller the difference between the FEM model and the analytical approach. The result is however also that at midspan the difference increases with decreasing spring stiffness and thus this must be taken into consideration as well.

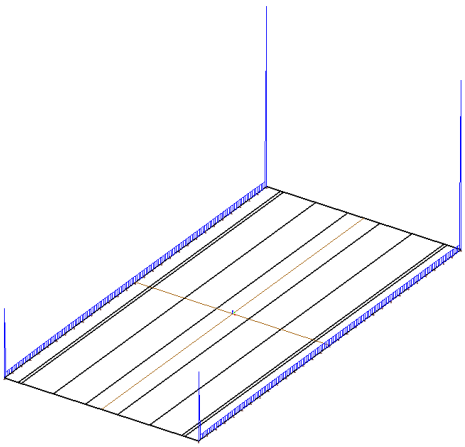

FIGURE I.7: Line support reaction for load situation 1 with a spring stiffness of $k_z = \infty$

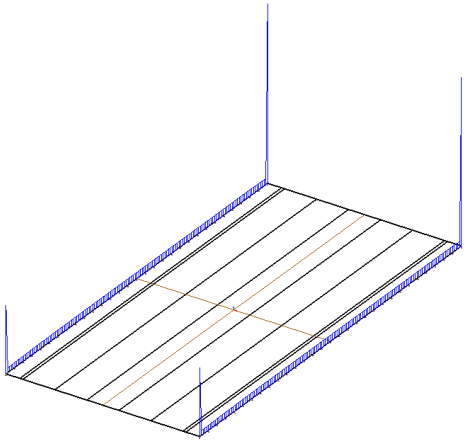

FIGURE I.8: Line support reaction for load situation 2 with a spring stiffness of $k_z = \infty$

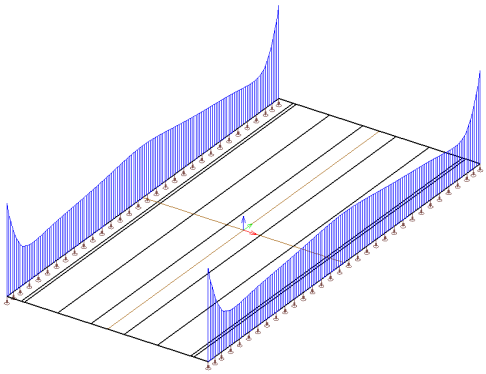

FIGURE I.9: Line support reaction for load situation 1 with a spring stiffness of $k_z = 1000$ MN/m

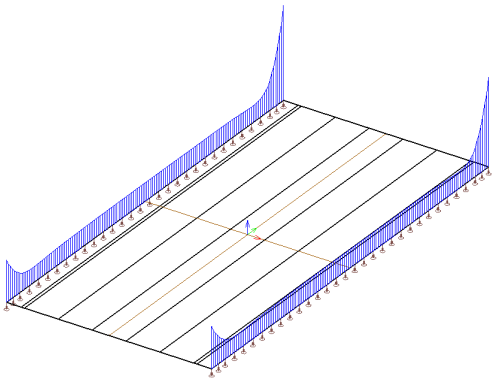

FIGURE I.10: Line support reaction for load situation 2 with a spring stiffness of $k_z = 1000$ MN/m

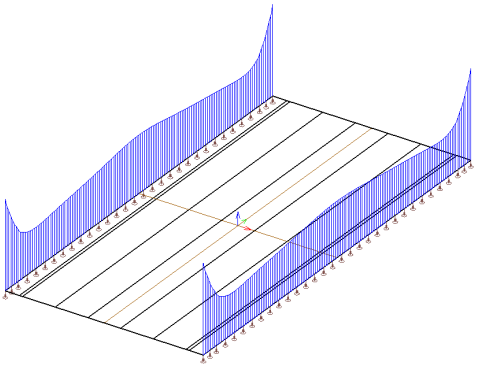

FIGURE I.11: Line support reaction for load situation 1 with a spring stiffness of $k_z = 500$ MN/m

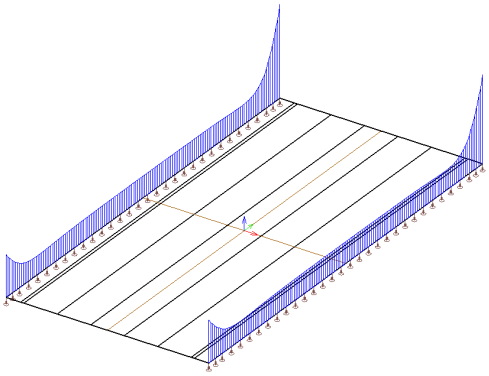

FIGURE I.12: Line support reaction for load situation 2 with a spring stiffness of $k_z = 500$ MN/m

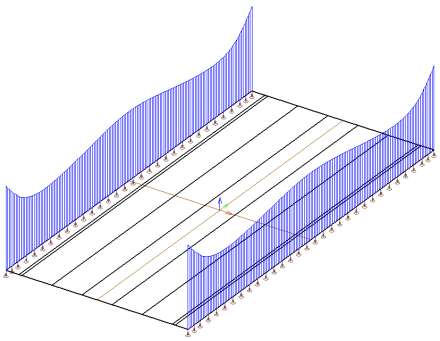

FIGURE I.13: Line support reaction for load situation 1 with a spring stiffness of k_z = 100 MN/m

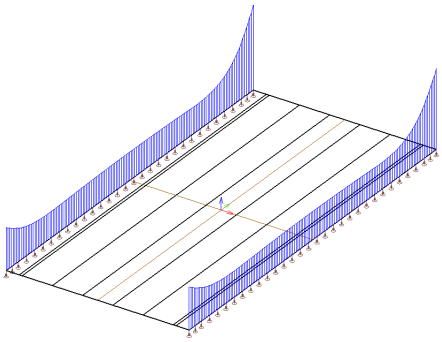

FIGURE I.14: Line support reaction for load situation 2 with a spring stiffness of k_z = 100 MN/m

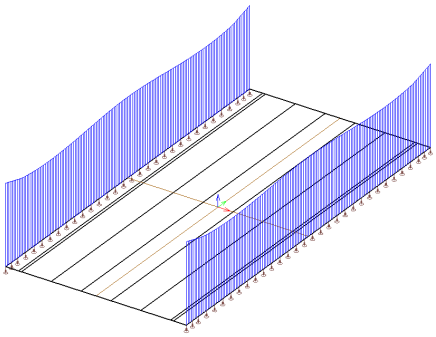

FIGURE I.15: Line support reaction for load situation 1 with a spring stiffness of k_z = 10 MN/m

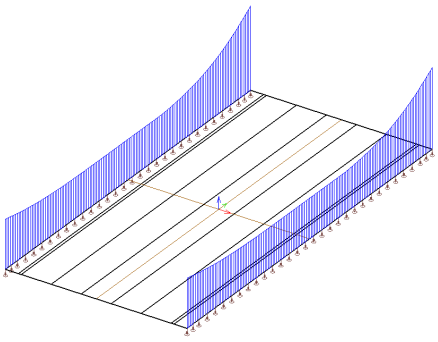

FIGURE I.16: Line support reaction for load situation 2 with a spring stiffness of k_z = 10 MN/m

Overall, the FEM plate model behaves as expected and the differences with the analytical model can be explained. In general it can be stated that the Guyon-Massonnet method is an adequate tool for the analytical approach, given that the right distribution lengths are chosen. Furthermore, the shear contribution of the concentrated KEL loads to the transverse moments cannot be ignored. And finally, the support reactions at midspan are adequate for comparison but due to the high peak stresses at the edge of the line supports this cannot be said about the support reactions in load situation 2.

I.1.2. Fixed supports

With the freely supported plate analysis the FEM model is verified. The next step is to look at line supports with prohibited rotation over the y-axis to simulate the floor girders clamped between the side girders. Again, several load parameters are discussed and a distinction is made between KEL loading at midspan (load situation 1 (Figure E.2)) and KEL loading at the end span (load situation 2 (Figure E.3)). The results are shown in Figures I.17 to I.22 and Table I.7.

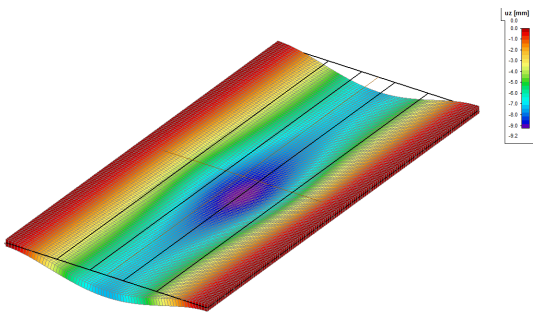

FIGURE I.17: Deformation of the isotropic, fixed floor plate due to load situation 1

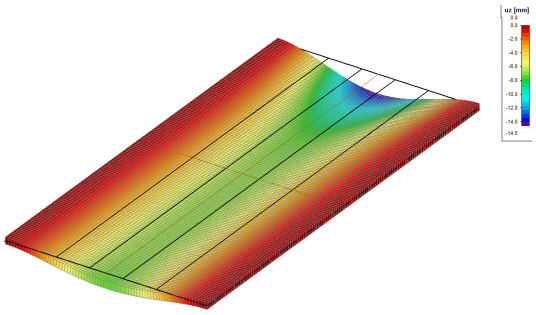

FIGURE I.18: Deformation of the isotropic, fixed floor plate due to load situation 2

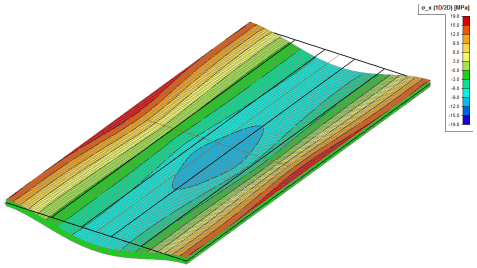

FIGURE I.19: Bending stresses in x-direction of the isotropic, fixed floor plate due to load situation 1

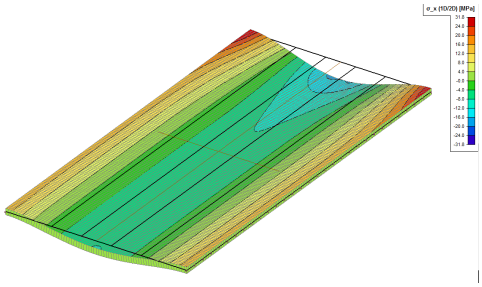

FIGURE I.20: Bending stresses in x-direction of the isotropic, fixed floor plate due to load situation 2

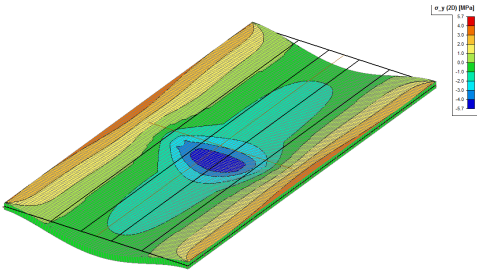

FIGURE I.21: Bending stresses in y-direction of the isotropic, fixed floor plate due to load situation 1

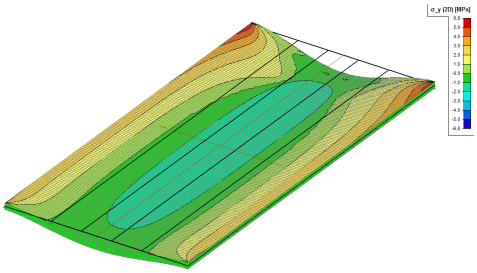

FIGURE I.22: Bending stresses in y-direction of the isotropic, fixed floor plate due to load situation 2

Parameter	Situation 1			Situation 2			Unit
	FEM	Analytical	Δ [%]	FEM	Analytical	Δ [%]	
$\sigma_{x;max}^{+}$	11.4	10.1	11.1	18.2	11.6	36.3	N/mm^2
$\sigma_{x;max}^{-}$	19.8	18.5	6.5	27.4	21.0	23.4	N/mm^2
$\sigma_{y;max}^{+}$	5.2	2.0	61.0				N/mm^2
$\sigma_{y;max}^{-}$	4.0	3.7	7.3				N/mm^2
R_z	399.8	385.0	3.7	2437.0	454.7	81.3	kN/m
w_z	9.2	9.4	2.2	14.5	10.8	25.5	mm

TABLE I.7: Comparison between the analytical analysis and the FEM results for a fixed isotropic floor plate

Again, it can be seen that these values differ quite significantly. Several explanations can be found for these differences:

- Larger differences can be observed in the stress distribution in x-direction in a fixed plate than in a freely supported plate (see Table I.1). This is mainly caused by the bad representation of KEL loads, as can be seen in Tables I.8 and I.9.

$\sigma_{x;max}$	Situation 1 - Positive			Unit
Load	FEM	Analytical	Δ [%]	
Self-weight	3.3	3.4	2.4	N/mm^2
Asphalt	0.7	0.7	1.4	N/mm^2
Kerbs	0.0	0.0	0.0	N/mm^2
UDL	1.4	1.4	0.6	N/mm^2
KEL	2.7	1.6	42.3	N/mm^2

TABLE I.8: Separate contributions to the positive bending stresses in x-direction for a fixed isotropic floor plate in load situation 1

$\sigma_{x;max}$	Situation 1 - Negative			
Load	FEM	Analytical	Δ [%]	Unit
Self-weight	6.6	6.8	2.5	N/mm^2
Asphalt	1.4	1.4	0.9	N/mm^2
Kerbs	0.1	0.1	40.9	N/mm^2
UDL	2.2	2.2	2.1	N/mm^2
KEL	3.4	2.4	28.9	N/mm^2

TABLE I.9: Separate contributions to the negative bending stresses in x-direction for a fixed isotropic floor plate in load situation 1

Since in the fixed supports have a higher stiffness than a free support, more load is drawn towards the support and less load is distributed in transverse direction. Therefore one could argue that the distribution length $x_{L;F}$ should be smaller than l_f = 18.17 m. A small analysis on the influence of $x_{L;F}$ on the accuracy of the stresses in x-direction shows that a reduction of distribution length to $x_{L;F}$ = 12 m gives an adequate representation of the load distributions as found in the FEM model. For the stresses in x-direction the adapted values are given in Tables I.10 and I.11.

$\sigma_{x;max}$	Situation 1 - Positive			
Load	FEM	Analytical	Δ [%]	Unit
Total	11.4	11.3	1.1	N/mm^2
KEL	2.7	2.3	15.2	N/mm^2

TABLE I.10: Result on the positive bending stresses in x-direction of adapting the load distribution length for a fixed isotropic floor plate in load situation 1

$\sigma_{x;max}$	Situation 1 - Negative			
Load	FEM	Analytical	Δ [%]	Unit
Total	19.8	20.4	3.2	N/mm^2
KEL	3.4	3.7	8.8	N/mm^2

TABLE I.11: Result on the negative bending stresses in x-direction of adapting the load distribution length for a fixed isotropic floor plate in load situation 1

- For the loads in transverse direction it again holds that the large differences are caused by the concentrated KEL loads (see Tables I.12 and I.13).

$\sigma_{y;max}$	Situation 1 - Positive			
Load	FEM	Analytical	Δ [%]	Unit
Self-weight	0.7	0.7	3.3	N/mm^2
Asphalt	0.1	0.1	39.7	N/mm^2
Kerbs	0.0	0.0	0.0	N/mm^2
UDL	0.3	0.3	6.8	N/mm^2
KEL	2.4	0.3	87.0	N/mm^2

TABLE I.12: Separate contributions to the positive bending stresses in y-direction for a fixed isotropic floor plate in load situation 1

$\sigma_{y;max}$	Situation 1 - Negative			
Load	FEM	Analytical	Δ [%]	Unit
Self-weight	1.3	1.4	4.2	N/mm^2
Asphalt	0.3	0.3	6.8	N/mm^2
Kerbs	0.0	0.0	0.0	N/mm^2
UDL	0.4	0.5	12.9	N/mm^2
KEL	0.7	0.5	30.1	N/mm^2

TABLE I.13: Separate contributions to the negative bending stresses in y-direction for a fixed isotropic floor plate in load situation 1

It appears that for the positive stress distribution, again the influence of shear deformations on the plate elements has to be taken into account. An adequate ratio of longitudinal and transverse stress for the concentrated loads is found at 0.9. This is however not the case for the negative stress distributions, where the deviation in the transverse direction is of the same order of the deviation in the longitudinal direction. This is probably due to the prevention of shear deformation near the fixed edge of the plate. The result are given in Tables I.14 and I.15 for a distribution length of $x_{L;F}$ = 12 m.

$\sigma_{y;max}$	Situation 1 - Positive			
Load	FEM	Analytical	Δ [%]	Unit
Total	5.2	4.7	9.6	N/mm^2
KEL	2.4	2.1	14.0	N/mm^2

TABLE I.14: Result on the positive bending stresses in y-direction of adapting the transverse coefficient of point loads for a fixed isotropic floor plate in load situation 1

$\sigma_{y;max}$	Situation 1 - Negative			
Load	FEM	Analytical	Δ [%]	Unit
Total	4.0	4.1	2.1	N/mm^2
KEL	0.7	0.7	6.0	N/mm^2

TABLE I.15: Result on the negative bending stresses in y-direction of adapting the transverse coefficient of point loads for a fixed isotropic floor plate in load situation 1

Although the deviation for the KEL load in the positive region is still somewhat large, it is of the same order of magnitude as the deviation in stresses in x-direction.

- The deviation in stress distribution in load situation 2 can also be accounted for by adaptation of the distribution length. Again, the distribution of KEL loads has the highest contribution to this difference (Tables I.16 and I.17).

$\sigma_{x;max}$	Situation 2 - Positive			
Load	FEM	Analytical	Δ [%]	Unit
Self-weight	3.5	3.4	3.4	N/mm^2
Asphalt	0.7	0.7	1.4	N/mm^2
Kerbs	0.0	0.0	0.0	N/mm^2
UDL	1.5	1.4	6.1	N/mm^2
KEL	7.0	2.5	63.8	N/mm^2

TABLE I.16: Separate contributions to the positive bending stresses in x-direction for a fixed isotropic floor plate in load situation 2

A quick analysis shows that the highest accuracy is obtained when applying a distribution length of $x_{L;F}$ = 10 m. The results are shown in Tables I.18 and I.19.

$\sigma_{x;max}$	Situation 2 - Negative			
Load	FEM	Analytical	Δ [%]	Unit
Self-weight	5.8	6.6	16.7	N/mm^2
Asphalt	1.2	1.4	15.6	N/mm^2
Kerbs	0.1	0.1	40.9	N/mm^2
UDL	2.0	2.2	12.3	N/mm^2
KEL	10.1	4.1	59.5	N/mm^2

TABLE I.17: Separate contributions to the negative bending stresses in x-direction for a fixed isotropic floor plate in load situation 2

$\sigma_{x;max}$	Situation 2 - Positive			
Load	FEM	Analytical	Δ [%]	Unit
Total	18.2	16.2	11.0	N/mm^2
Self-weight	3.5	3.4	3.4	N/mm^2
Asphalt	0.7	0.7	1.4	N/mm^2
Kerbs	0.0	0.0	0.0	N/mm^2
UDL	1.5	1.4	6.1	N/mm^2
KEL	7.0	5.8	17.2	N/mm^2

TABLE I.18: Result on the positive bending stresses in x-direction of adapting the transverse coefficient of point loads for a fixed isotropic floor plate in load situation 2

$\sigma_{x;max}$	Situation 2 - Negative			
Load	FEM	Analytical	Δ [%]	Unit
Total	27.4	28.9	5.5	N/mm^2
Self-weight	5.8	6.8	16.7	N/mm^2
Asphalt	1.2	1.4	15.6	N/mm^2
Kerbs	0.1	0.1	40.9	N/mm^2
UDL	2.0	2.2	12.3	N/mm^2
KEL	10.1	9.4	7.3	N/mm^2

TABLE I.19: Result on the negative bending stresses in x-direction of adapting the transverse coefficient of point loads for a fixed isotropic floor plate in load situation 2

The effect of this reduced distribution load is also positive for the deviation found in the deflection at end span. The results are shown in Table I.20.

w_z	Situation 2			
Load	FEM	Analytical	Δ [%]	Unit
Total	14.5	15.0	3.4	N/mm^2
KEL	7.2	7.9	9.7	N/mm^2

TABLE I.20: Result on the negative bending stresses in x-direction of adapting the transverse coefficient of point loads for a fixed isotropic floor plate in load situation 2

- At last, there is again the matter of the peak stresses that coincide with the support reactions at end span in the FEM model. This issue has been addresses in paragraph I.1.1 and will not be repeated here.

Overall it can be concluded that, although the Guyon-Massonnet method is not quite as accurate for the fixed plate as for the freely supported plate, it is suitable for use. The largest difference is the reduction of transverse distribution length due to the higher stiffness of the line supports. Also, the contribution of the concentrated KEL loads to the transverse moments is different in negative and positive stress regions.

I.2. ORTHOTROPIC PLATE BEHAVIOUR

Since the bridge deck does not consist of one plate but of multiple floor girders connected in transverse direction through prestressing, the bridge deck features orthotropic behaviour. For the massive floor girder this means that, although within one floor girder the material still behaves isotropic, the total load distribution will be less in transverse direction than in longitudinal direction.

In the FEM plate model it is possible to adapt the orthotropic behaviour of the plate by modifying the stiffness matrix. It is however not possible to incorporate both isotropic floor girder behaviour and orthotropic bridge deck behaviour. Or it would be possible, but that requires multiple plates with the width of one floor girder connected by springs with the correct translational and rotational stiffness. For simplicity reasons this analysis is not performed.
For the load distribution in the floor plate this will not give large deviations from the analytical analysis, since the same limitation holds for the Guyon-Massonnet method. It does however differ from the analytical method to determine the support reactions, since the effective widths in this approach are based on bilateral characteristics of the floor girders (see Figures I.23 and I.24).

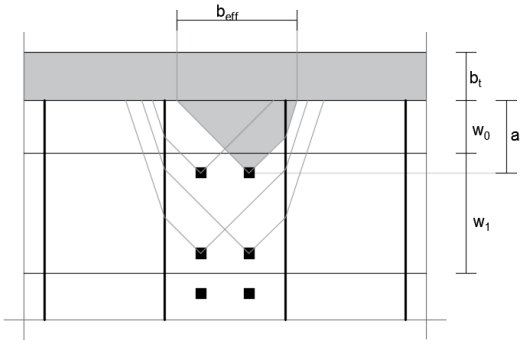

FIGURE I.23: Load distribution towards side girder in load situation 1 for massive floor girders with orthotropic behaviour

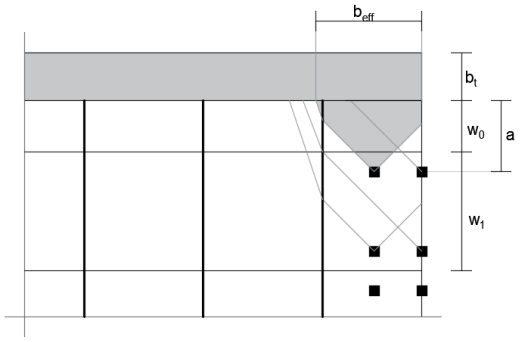

FIGURE I.24: Load distribution towards side girder in load situation 2 for massive floor girders with orthotropic behaviour

First, the stress distribution in the floor plate will be compared to that of the analytically determined stress distributions for orthotropic plate behaviour. Then the same will be done for the load distribution towards the side girders to determine the deviation in both models.

I.2.1. Load distribution in floor girder

For a good comparison, the load distribution found in the previous paragraph will be used. Thus it holds:

- For longitudinal stresses at midspan: $x_{L;F} = 12$ m
- For positive transverse stresses at midspan: $x_{L;F} = 12$ m $\quad M_{x;KEL} = 0.9 \cdot M_{y;KEL}$
- For negative transverse stresses at midspan: $x_{L;F} = 12$ m $\quad M_{x;KEL} = 0.2 \cdot M_{y;KEL}$
- For longitudinal stresses at end span: $x_{L;F} = 10$ m

The flexural and torsional stiffness used in the Guyon-Massonnet method are (see also paragraph I.1):

Flexible rigidity per unit width:

$$\rho_x = \frac{\Sigma E \cdot I_x}{b_f} = 9.46 \cdot 10^8 \text{ kNm}^3$$

$$\rho_y = \frac{\Sigma E \cdot I_y}{l_f} = 6.99 \cdot 10^8 \text{ kNm}^3$$

Torsional rigidity per unit width:

$$\gamma_x = \frac{\Sigma G \cdot I_x}{b_f} = 3.94 \cdot 10^8 \text{ kNm}^3$$

$$\gamma_y = \frac{\Sigma G \cdot I_y}{l_f} = 2.91 \cdot 10^8 \text{ kNm}^3$$

Flexural stiffness:

$$\theta = \frac{b_f}{l_f} \cdot \sqrt[4]{\frac{\rho_x}{\rho_y}} = 0.178 \text{ rad}$$

Torsional stiffness:

$$\alpha = \frac{\gamma_x + \gamma_y}{2 \cdot \sqrt{\rho_x \cdot \rho_y}} = 0.417$$

The stiffness matrix to be used in SCIA is presented in Table H.1 *[Spanbeton, nd]*. From these values it can already be seen that the methods for determining the flexural and torsional stiffness differ considerably in both models.

The results for both load situation 1 (loading at midspan (Figure E.2)) and load situation 2 (loading at end span (Figure E.3)) are given in Figures I.25 to I.30 and Table I.21.

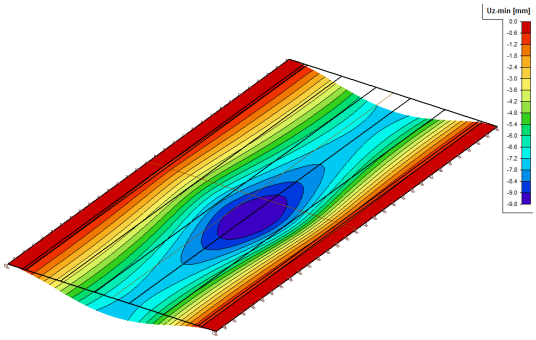

FIGURE I.25: Deformation of the orthotropic, fixed floor plate due to load situation 1

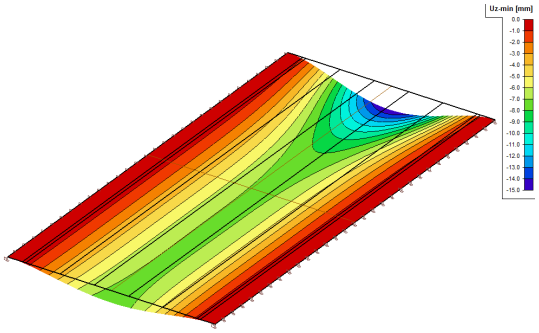

FIGURE I.26: Deformation of the orthotropic, fixed floor plate due to load situation 2

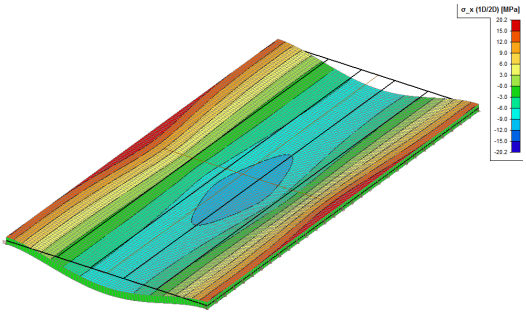

FIGURE I.27: Bending stresses in x-direction of the orthotropic, fixed floor plate due to load situation 1

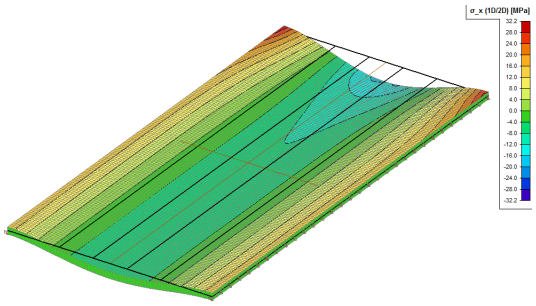

FIGURE I.28: Bending stresses in x-direction of the orthotropic, fixed floor plate due to load situation 2

Apart from the large deviation in support reactions at end span, which are caused by the occurrence of peak stresses, only the transverse bending stresses in both positive and negative moment regions differ significantly between FEM and analytical approach.
It can however be seen in Tables I.22 and I.23 that the deviations in this case are not only due to the concentrated loads but also due to the permanent and evenly distributed loads. The problem thus does not lie in the load distribution length or the transverse contraction coefficient for the concentrated loads. Instead, it

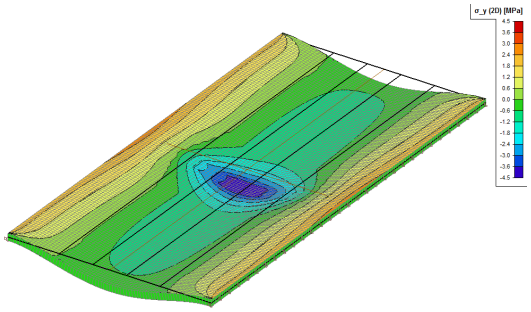

FIGURE I.29: Bending stresses in y-direction of the orthotropic, fixed floor plate due to load situation 1

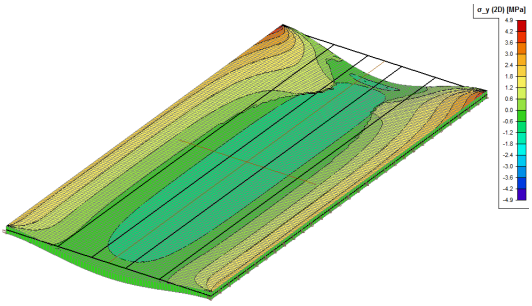

FIGURE I.30: Bending stresses in y-direction of the orthotropic, fixed floor plate due to load situation 2

Parameter	Situation 1			Situation 2			Unit
	FEM	Analytical	Δ [%]	FEM	Analytical	Δ [%]	
$\sigma_{x;max}^{+}$	11.5	11.3	1.9	18.0	16.2	10.0	N/mm^2
$\sigma_{x;max}^{-}$	20.2	20.4	1.1	29.2	28.4	2.7	N/mm^2
$\sigma_{y;max}^{+}$	4.0	4.7	17.6				N/mm^2
$\sigma_{y;max}^{-}$	2.8	4.1	46.1				N/mm^2
R_z	414.8	391.3	5.7	1332.5	638.4	52.1	kN/m
w_z	10.1	10.5	4.0	14.9	15.5	4.0	mm

TABLE I.21: Comparison between the analytical analysis and the FEM results for a fixed orthotropic floor plate

$\sigma_{y;max}$	Situation 1 - Positive			Unit
Load	FEM	Analytical	Δ [%]	
Self-weight	0.5	0.7	35.4	N/mm^2
Asphalt	0.1	0.1	39.7	N/mm^2
Kerbs	0.0	0.0	0.0	N/mm^2
UDL	0.2	0.3	39.7	N/mm^2
KEL	2.0	2.1	3.7	N/mm^2

TABLE I.22: Separate contributions to the positive bending stresses in y-direction for a fixed orthotropic floor plate in load situation 1

$\sigma_{y;max}$	Situation 1 - Negative			Unit
Load	FEM	Analytical	Δ [%]	
Self-weight	0.9	1.4	50.5	N/mm^2
Asphalt	0.2	0.3	39.7	N/mm^2
Kerbs	0.0	0.0	0.0	N/mm^2
UDL	0.3	0.5	50.5	N/mm^2
KEL	0.5	0.7	49.4	N/mm^2

TABLE I.23: Separate contributions to the negative bending stresses in y-direction for a fixed orthotropic floor plate in load situation 1

seems that the earlier found differences between the stiffnesses from Guyon-Massonnet and *[Spanbeton, nd]* are the cause of this. This is supported by Tables I.24 and I.25 in which the bending stresses for the isotropic and orthotropic case according to the analytical approach are given.

It appears that the changes in orthotropic behaviour are too small to have any significant influence on the flexural and torsional stiffness parameters in the Guyon-Massonnet method:

$\sigma_{y;max}$	Situation 1 - Negative			
Load	FEM	Analytical	Δ [%]	Unit
Total	4.1	4.1	0.1	N/mm^2
Self-weight	1.4	1.4	0.0	N/mm^2
Asphalt	0.3	0.3	0.0	N/mm^2
Kerbs	0.0	0.0	0.0	N/mm^2
UDL	0.5	0.5	0.0	N/mm^2
KEL	0.7	0.7	0.7	N/mm^2

TABLE I.24: Comparison of the positive bending stress in y-direction in load situation 1 for both isotropic and orthotropic plate behaviour

$\sigma_{y;max}$	Situation 1 - Negative			
Load	Isotropic	Orthotropic	Δ [%]	Unit
Total	4.1	4.1	0.1	N/mm^2
Self-weight	1.4	1.4	0.0	N/mm^2
Asphalt	0.3	0.3	0.0	N/mm^2
Kerbs	0.0	0.0	0.0	N/mm^2
UDL	0.5	0.5	0.0	N/mm^2
KEL	0.7	0.7	0.7	N/mm^2

TABLE I.25: Comparison of the negative bending stress in y-direction in load situation 1 for both isotropic and orthotropic plate behaviour

Isotropic behaviour:

$$\alpha = 0.417$$

$$\theta = 0.165 \text{ rad}$$

Orthotropic behaviour:

$$\alpha = 0.421$$

$$\theta = 0.178 \text{ rad}$$

Furthermore, in the analytical approach the Guyon-Massonnet method is only used to determine the spreading of traffic loads since all permanent loads are present over the entire length of the bridge.

Thus the orthotropic behaviour of permanent and evenly distributed loads are not taken into account in the analytical method and therefore a difference occurs in relation to the orthotropic behaviour described by the FEM plate model. This difference is excepted since the analytical approach, on which the cross-sectional dimensions are based, is conservative compared to the FEM plate model.

I.2.2. Load distribution to side girder

It is already shown in Table I.21 but it seems that the load distribution towards the side girder according to the effective width coincides quite neatly ($\Delta = 5.7\%$) with the distribution in the FEM plate model.
When looking at load situation 3 (Figure I.27) however, it can be seen that this conclusion does not hold. The explanation can be found in the distribution of loads over the effective width and the FEM model considerations. As stated earlier, in reality the massive floor girders show bilateral behaviour but for simplicity reasons this is not taken into account in the FEM analysis. Therefore in the FEM model the loads are distributed over a smaller angle over the entire width, while in the analytical approach the isotropic behaviour of the floor girder is considered over the first part (see Figure I.31). Therefore the FEM model will give higher support loads than the analytical approach, but since the latter is more realistic this difference will also be neglected.
It can also explained according from Figure I.31 that for maximum floor loading these results seem to coincide neatly. The larger the distance of the load to the side girder, the smaller the influence of the isotropic behaviour on the total effective width at the supporting side girder.

R_z	Situation 1			
Load	FEM	Analytical	Δ [%]	Unit
Total	414.8	391.3	5.7	N/mm^2
Self-weight	135.9	138.6	1.9	N/mm^2
Asphalt	25.8	25.1	2.9	N/mm^2
Kerbs	6.2	6.1	0.6	N/mm^2
UDL	38.6	36.6	5.2	N/mm^2
KEL	83.0	65.8	20.7	N/mm^2

TABLE I.26: Separate contributions to the support reaction for a fixed orthotropic floor plate in load situation 1

R_z	Situation 3			
Load	FEM	Analytical	Δ [%]	Unit
Total	596.1	459.3	23.0	N/mm^2
Self-weight	135.9	138.6	1.9	N/mm^2
Asphalt	25.1	25.1	0.0	N/mm^2
Kerbs	6.2	6.1	0.6	N/mm^2
UDL	46.4	36.6	21.1	N/mm^2
KEL	195.0	111.2	43.0	N/mm^2

TABLE I.27: Separate contributions to the support reaction for a fixed orthotropic floor plate in load situation 3

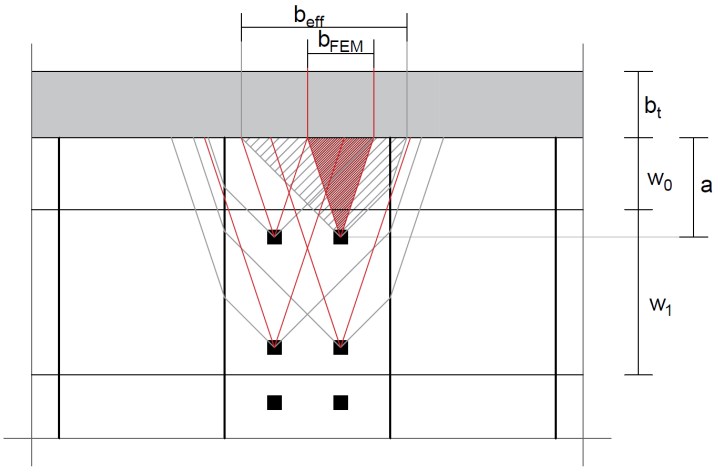

FIGURE I.31: Bilateral isotropic and orthotropic behaviour of the floor plate in distributing loads towards the side girder

I.3. INFLUENCE OF FLEXIBLE SUPPORTS

Although the analytical analysis for the floor girders is based on rigid supports, this is not an accurate model for reality. Since the floor girders are supported by the side girders and the side girders have a certain flexural and torsional stiffness, the support should have a vertical spring stiffness and rotational capacity over the y-axis that simulates this side girder. The stiffness of the side girder is however not constant over its length but both flexural and torsional stiffness is described by a parabolic curve. To model this in SCIA is quite extensive – it is better to construct the side girders as one-dimensional beams with the correct stiffness.

For this, side girders with a width of b_t = 1.2 m and height of h_t = 2.3 m are modelled to coincide with the dimensions of the massive side girders as found in section G.3.

I.3.1. Isotropic massive floor girders

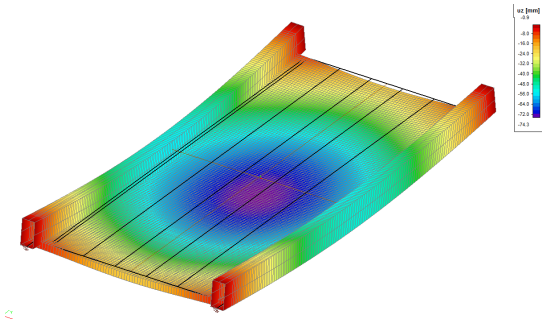

FIGURE I.32: Deformation of the isotropic, fixed floor plate on flexible supports due to load situation 1

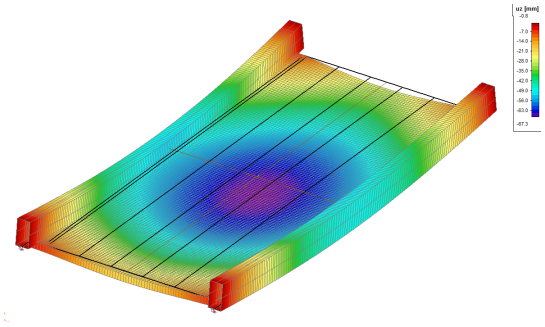

FIGURE I.33: Deformation of the isotropic, fixed floor plate on flexible supports due to load situation 2

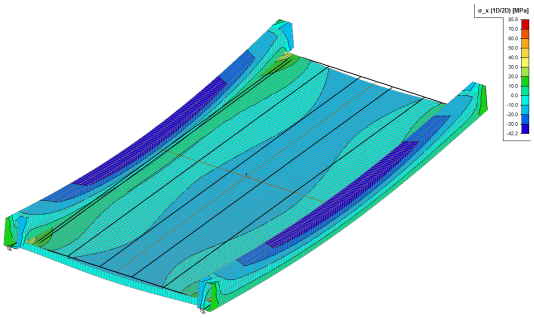

FIGURE I.34: Bending stresses in x-direction of the isotropic, fixed floor plate on flexible supports due to load situation 1

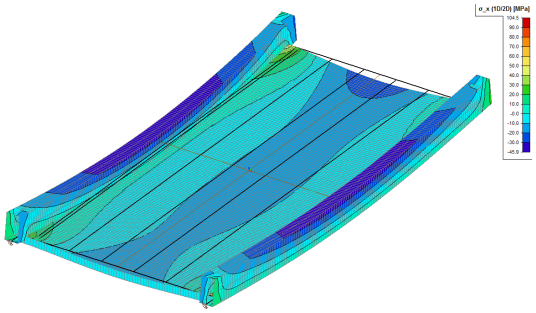

FIGURE I.35: Bending stresses in x-direction of the isotropic, fixed floor plate on flexible supports due to load situation 2

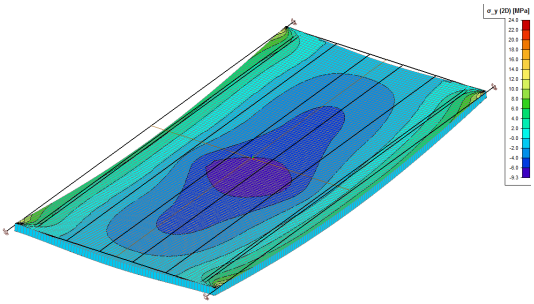

FIGURE I.36: Bending stresses in y-direction of the isotropic, fixed floor plate on flexible supports due to load situation 1

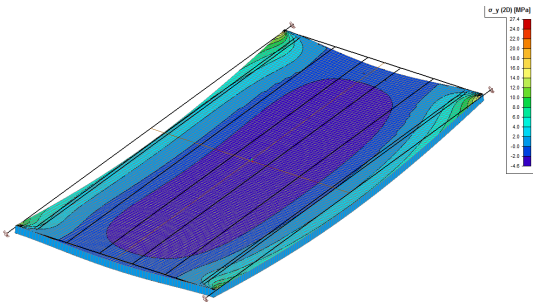

FIGURE I.37: Bending stresses in y-direction of the isotropic, fixed floor plate on flexible supports due to load situation 2

Floor plate behaviour

The results of the isotropic massive floor plate with flexible supports are compared to the plate behaviour on rigid supports. In paragraph I.1 it was showed that by taking the correct distribution lengths and shear behaviour into account, the isotropic FEM model and the isotropic analytical model give comparable results. It is thus possible to compare both support configurations in the FEM model in order to determine the differences in load distribution. The results are shown in Table I.28.

It can be seen that overall the flexible supports have a large influence on the load distribution in the floor plate.

- If you look at the stress in x-direction in both positive and negative moment regions, it can be seen that the negative moment is much smaller in case of a flexible support than in a rigid support. This difference is caused by the torsional flexibility of the side girder, which will rotate over the y-axis due

Parameter	Situation 1			Situation 2			Unit
	Flexible	Rigid	Δ [%]	Flexible	Rigid	Δ [%]	
$\sigma_{x;max}^{+}$	16.7	11.4	31.7	29.2	18.2	37.7	N/mm^2
$\sigma_{x;max}^{-}$	7.5	19.8	164.0	104.5	27.4	73.8	N/mm^2
$\sigma_{y;max}^{+}$	8.8	5.2	40.9				N/mm^2
$\sigma_{y;max}^{-}$	5.1	4.0	21.6				N/mm^2
R_z	367.0	399.8	9.0	3125.2	2437.0	22.0	kN/m
w_z	74.3	9.2	87.6	27.8	14.5	47.8	mm
Δw_z	20.6	9.2	55.3	21.7	14.5	33.2	mm

TABLE I.28: Comparison between the analytical analysis and the FEM results for a fixed isotropic floor plate on flexible supports

to the load action on the floors. Therefore, the connection between floor and side girder is no longer fixed and a reduction of negative moment and an increase in positive moment can be observed. In fact, Table I.29 shows that the rotational capacity of the connection lies somewhere between the boundaries of a fixed plate ($r_\phi = 1$) and a freely supported plate ($r_\phi = 0$).

Parameter	Situation 1			Situation 2			Unit
	Rigid (fixed)	Flexible	Rigid (free)	Rigid (fixed)	Flexible	Rigid (free)	
$\sigma_{x;max}^{+}$	11.4	16.7	28.0	18.2	29.2	38.7	N/mm^2
$\sigma_{x;max}^{-}$	19.8	7.5	0.0	27.4	104.5	0.0	N/mm^2

TABLE I.29: Degree of rotation of an isotropic flexible supported floor girder compared to fixed ($r_\phi = 1$) and free ($r_\phi = 0$) supports

This holds for both load situations, with the exception of the negative stress found in load situation 2. Here, a large increase of stress can be observed which is contradictory to the explanation given above. The reason for this must be sought in the transverse contraction of a plate model, which causes peak stresses at the corners of the plate. For a full explanation of this phenomenon reference is made to paragraph I.1.

- The stresses in y-direction are larger than in the case of rigid supports. This is due to the fact that a flexible element is less capable of distributing loads than a stiff element and therefore the spreading of loads is also smaller in the floor plate.

- Since flexible elements will result into a lower spread of loads over transverse direction it is expected that the shear force in the floor girders will be higher at midspan than in the case of rigid supports. From Table I.28 however, it follows that the opposite is the case and a lower shear force is observed at midspan near the connection between floor and side girders. This can be explained by the fact that the stiffness of an element determines the amount of load it attracts. Thus a flexible side girder will attract less loads from the floor girder than a rigid side support. It appears that this mechanism is governing for the overall value of the shear load.

- The deflections of the floor girder (w_z) are much higher in the case of a flexible support than in the case of a rigid support. There are two reasons for this:
  - First, not only the floor girders but also the side girders will undergo a certain deflection. This deflection is largest at midspan.
  - Second, due to the rotation of the side girder following from the torsional flexibility the floor girders will experience a larger relative deflection to the supports. This can be seen as well in Table I.28, where the relative deflection – the difference in defection between floor girder and side girder) is denoted by Δw_z.

Side girder behaviour
With the FEM analysis using flexible supports, the analytical load determination for the side girders can now also be verified. The results are given in Table I.30.

Parameter	Situation 1			Situation 2			Unit
	FEM	Analytical	Δ [%]	FEM	Analytical	Δ [%]	
M_y^+	29646.4	71756.3	142.0				N/mm^2
φ_x	4.1	5.2	26.8				N/mm^2
R_z				8658.3	8782.0	1.4	kN/m
w_z	57.3	123.0	114.7				mm

TABLE I.30: Comparison between the analytical analysis and the FEM results for a flexible side girder

It can be seen that the calculated shear force in both analytical and FEM analysis coincide very neatly, but the bending moment, torsional rotation and deflection show a large difference.

- The rotation of the side girder over the x-axis – as a result of torsion from the eccentric floor loads – is somewhat smaller in the FEM calculation than in the analytical calculation. This can be explained by looking at the torsional rigidity of the side girder over its length, which depends on the distance to the supports. Therefore the side girder is most flexible in the middle and stiffer at a location nearer to the support and the rotation of the side girder in the middle is somewhat prohibited by the stiffer parts next to it. In the analytical calculation this has not been taken into account and thus the rotation as a result of torsion will be higher.
- The difference in bending moment and deflection are much higher. This difference is caused by the stiffening effect the floor plate has on the entire structural system. This can be seen by comparing the side girder behaviour as a single beam (see Figure I.38) and as incorporated with a floor plate (see Figure I.39). The results are given in Table I.31 and differences with the same order of magnitude are observed.

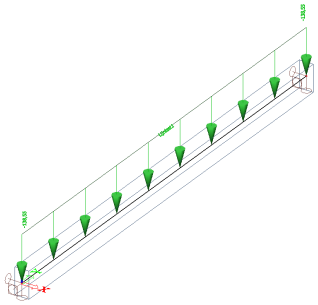

FIGURE I.38: Beam model of the flexible side girder with self-weight of concrete floor girders

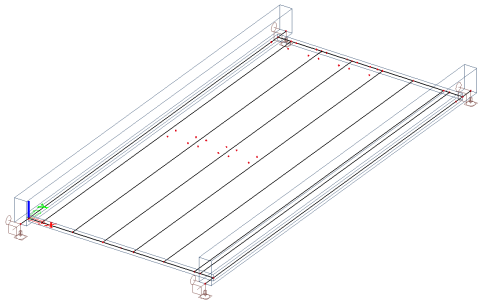

FIGURE I.39: Plate model of the flexible side girder

I.3.2. Orthotropic massive floor girders

It is interesting to investigate the influence of orthotropic behaviour on the plate model with flexible supports. The results are shown in Figures I.40 to I.45 and Table I.32.
As for the analysis on orthotropic plate behaviour for rigid supports, it can be seen that mainly the transverse stresses deviate from isotropic behaviour (Table I.28). This is caused by a difference in calculation methods of the flexibility in the analytical Guyon-Massonnet method and the stiffness matrix for the FEM model. A more elaborate explanation can be found in paragraph I.2.

I.3.3. Influence on element design calculations

Although the influence of the flexible supports has been neglected in designing the trough bridge elements, it is nevertheless interesting to investigate the effects of this flexibility.

Parameters		Analytical	FEM (beam)	Δ [%]	FEM (plate)	Δ [%]	Unit
M_y^+	Total	35133.4	34912.1	0.6	13374.1	61.7	*kNm*
	Truss	11680.3	11458.4	1.9			*kNm*
	Floor	23453.1	23453.7	0.0			*kNm*
w_z	Total	81.5	81.7	0.2	37.8	53.7	*mm*
	Truss	27.1	26.8	1.1			*mm*
	Floor	54.4	54.9	0.9			*mm*

TABLE I.31: Comparison between the FEM results for a flexible side girder as a beam model and as a plate model

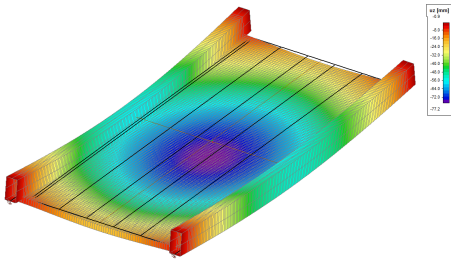

FIGURE I.40: Deformation of the orthotropic, fixed floor plate on flexible supports due to load situation 1

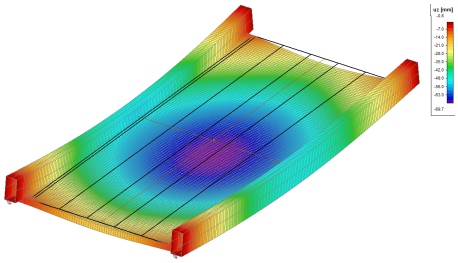

FIGURE I.41: Deformation of the orthotropic, fixed floor plate on flexible supports due to load situation 2

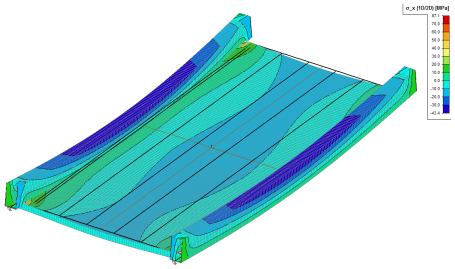

FIGURE I.42: Bending stresses in x-direction of the orthotropic, fixed floor plate on flexible supports due to load situation 1

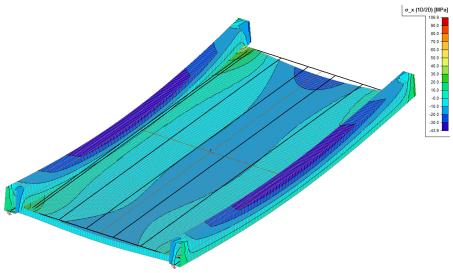

FIGURE I.43: Bending stresses in x-direction of the orthotropic, fixed floor plate on flexible supports due to load situation 2

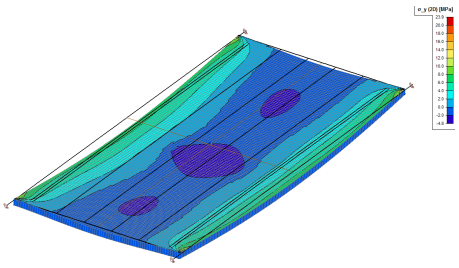

FIGURE I.44: Bending stresses in y-direction of the orthotropic, fixed floor plate on flexible supports due to load situation 1

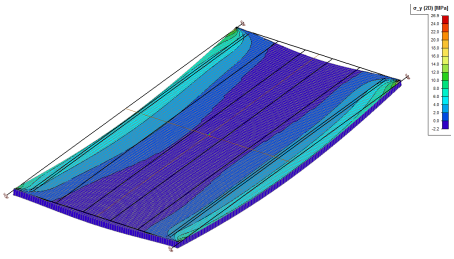

FIGURE I.45: Bending stresses in y-direction of the orthotropic, fixed floor plate on flexible supports due to load situation 2

In the floor girders, the flexible supports result in a higher positive moment in x-direction, lower negative moment in x-direction and a higher positive and negative moment in y-direction. Therefore the top prestress in x-direction (A_{px2}) might be reduced but the other prestresses (A_{px1},A_{py1} and A_{py2}) should be increased. Whether or not this is possible within the limited deck construction height of h_f = 0.61 m has to be investigated. For the shear force a slight decrease is observed which would be beneficial for design purposes. The deflection, on the other hand, increases significantly and might become a problem for overall design. With

Parameter	Situation 1			Situation 2			Unit
	Isotropic	Orthotropic	Δ [%]	Isotropic	Orthotropic	Δ [%]	
$\sigma_{x;max}^{+}$	16.5	16.7	1.2	28.5	29.2	2.4	N/mm^2
$\sigma_{x;max}^{-}$	8.5	7.5	11.8	106.9	104.5	2.2	N/mm^2
$\sigma_{y;max}^{+}$	4.5	8.8	48.9				N/mm^2
$\sigma_{y;max}^{-}$	7.8	5.1	34.6				N/mm^2
R_z	385.4	367.0	4.8	3376.9	3125.2	7.5	kN/m
w_z	77.2	74.3	3.9	27.8	27.8	0.0	mm
Δw_z	22.3	20.6	7.6	21.6	21.7	0.5	mm

TABLE I.32: Comparison between the analytical analysis and the FEM results for a fixed orthotropic floor plate on flexible supports

a span length of l_f = 18.17 m, the maximum allowed deflection is w_{max} = 73 mm. If this is valid for the relative deflection (Δw_z = 21.7 mm) this will not cause trouble but if the absolute value has to be taken into account (w_z = 74.3 mm) it exceeds the maximum value. A positive influence will be that the lower prestress is increased and the higher prestress is decreased but it will still be close to the maximum allowable deflection.

For the side girders it is observed that the analytical approach, in which the side girder is modelled as a beam on two supports, significantly overestimates the maximum bending moment and deflection at midspan. In reality, the side girders and floor girders form a connected system that reduces the bending moment by 60% and the deflection by 50%. This would mean that the design of the side girders could become even more slender. However, the shear force in the side girder is not influenced by the floor system and therefore the analytical and FEM model coincide quite neatly.

I.4. BEHAVIOUR OF AN OPEN STRUCTURE TROUGH BRIDGE

All influencing factors for the massive floor girder with respect to FEM modelling have been discussed in the previous paragraphs. The same is done for the open structure design, but only the results will be shown here.

The main differences in design are the flexural and torsional stiffness of both floor girders and side girders, together with the self-weight of the elements per unit width. From the analysis on orthotropic behaviour in the massive floor girders it is expected that these differences will only increase, since the difference in stiffness parameters between FEM model and Guyon-Masonnet method will also increase.

Guyon-Massonnet:

Flexible rigidity per unit width:

$$\rho_x = \frac{\Sigma E \cdot I_x}{b_f} = 7.74 \cdot 10^8 \text{ kNm}^3$$

$$\rho_y = \frac{\Sigma E \cdot I_y}{l_f} = 7.50 \cdot 10^8 \text{ kNm}^3$$

Torsional rigidity per unit width:

$$\gamma_x = \frac{\Sigma G \cdot I_x}{b_f} = 3.22 \cdot 10^8 \text{ kNm}^3$$

$$\gamma_y = \frac{\Sigma G \cdot I_y}{l_f} = 3.13 \cdot 10^8 \text{ kNm}^3$$

Flexural stiffness:

$$\theta = \frac{b_f}{l_f} \cdot \sqrt[4]{\frac{\rho_x}{\rho_y}} = 0.166 \text{ rad}$$

Torsional stiffness:

$$\alpha = \frac{\gamma_x + \gamma_y}{2 \cdot \sqrt{\rho_x \cdot \rho_y}} = 0.421$$

For the applied FEM stiffness matrix reference is made to Table H.2. The results are shown in Table I.33 for the floor girders.

Parameter	Situation 1			Situation 2			Unit
	FEM	Analytical	Δ [%]	FEM	Analytical	Δ [%]	
$\sigma_{x;max}^{+}$	14.5	8.6	40.7	24.0	13.8	42.5	N/mm^2
$\sigma_{x;max}^{-}$	5.6	15.5	63.9	82.2	24.0	70.8	N/mm^2
$\sigma_{y;max}^{+}$	8.4	4.1	51.2				N/mm^2
$\sigma_{y;max}^{-}$	7.3	3.1	57.5				N/mm^2
R_z	330.4	376.6	12.3	3933.3	546.7	86.1	kN/m
w_z	69.9	8.2	88.3	26.3	13.2	49.8	mm
Δw_z	25.1	8.2	67.3	21.5	13.2	38.6	mm

TABLE I.33: Comparison between the analytical analysis and the FEM results for an open structure, fixed orthotropic floor plate on flexible supports

As was the case in the flexible support verification for massive floor girders with orthotropic behaviour, the FEM model results differ significantly from the analytical analysis. However, all differentiations can be explained by the same phenomena as was done in the massive girders (section I.3) and therefore these differences are not discussed again.
The same holds for the truss girder results as presented in Table I.34.

Parameter	Situation 1			Situation 2			Unit
	FEM	Analytical	Δ [%]	FEM	Analytical	Δ [%]	
M_y^{+}	19840.1	57750.6	65.5				N/mm^2
φ_x	5.6	25.1	77.7				N/mm^2
R_z				8658.3	8782.0	12.2	kN/m
w_z	49.6	296.0	83.2				mm

TABLE I.34: Comparison between the analytical analysis and the FEM results for a flexible truss girder

Again, in Table I.35 large deviations can be seen in bending moment ($M_y{}^+$) and deflection (w_z) which can be explained by the stiffening behaviour of the plate system (Table I.31).

Parameters		Analytical	FEM (beam)	Δ [%]	FEM (plate)	Δ [%]	Unit
M_y^{+}	Total	20373.6	20200.1	0.9	5917.0	70.7	kNm
	Truss	11272.9	11272.4	0.0			kNm
	Floor	9100.7	8927.8	1.9			kNm
w_z	Total	61.3	62.2	1.4	22.4	64.0	mm
	Truss	33.9	34.7	2.3			mm
	Floor	27.4	27.5	0.4			mm

TABLE I.35: Comparison between the FEM results for a flexible truss girder as a beam model and as a plate model

In this case, however, also the rotation of the truss over its longitudinal axis (ϕ_x) shows a large difference in results. This difference with the massive girder comparison comes from the lower rotational capacity of the truss girder, which is taken into account differently in the analytical analysis and FEM analysis.

I.5. SUMMARISING CONCLUSIONS OF FEM VERIFICATION

Overall, the following conclusions can be drawn on the verification of the analytical design method by a FEM model:

1. The Guyon-Massonet method is applicable in both freely supported an fixed plates, as long as the distribution lengths and transverse shear action are correctly adapted. In this, it must be stated that the adaptation depends significantly on the FEM input parameters such as mesh size and calculation method.

2. The FEM model gives large peak stresses at corners due to the transition of 2D elements to 1D elements. By adapting the flexibility of the supports this can somewhat be corrected but it will nonetheless interfere with the results at this location.

3. The orthotropic behaviour of the floor girders is calculated significantly different in the analytical model and the FEM model, causing large deviations in mainly the transverse floor stresses. Therefore it is not possible to compare both models adequately on this influence.

4. The flexible side girder as a support has mostly a negative influence on the stresses and loads in the floor girders. Due to its rotational capacity the negative moments in longitudinal direction will decrease, but this also results in an increase of the positive moments, the transverse moments and the absolute and relative deflection of the floor girders.

5. The analytical approach does not take into account the stiffness of the floor system when calculating the side girder load actions. It turns out that this has a large positive influence on both the bending moment and the deflection, which can be reduced by 60% and 50% respectively. Overall, this could lead to a more slender and thus lightweight structure.

6. When comparing the analytical approach to the final FEM model with fixed floor-to-side connection, orthotropic behaviour and flexible supports, the following must be considered:
    - The positive and negative bending moment stresses in the floor girders will be higher than incorporated into the design, with the exception of the negative bending moment in longitudinal direction.
    - The deflection of the floor girders – both relative and absolute - will be higher than considered in the design.
    - The shear force in the floor girders will be somewhat smaller in reality, which could be beneficial for design.
    - The floor girders have a stiffening effect on the side girders, giving rise to much lower bending moments and deflections. Incorporating these differences into the design could lead to more slender side elements.
    - The shear force taken into account in the analytical approach for the side girders is somewhat conservative, which might turn out beneficial for design.
    - The torsional capacity of the side girder is significantly underestimated in the analytical approach.

It can thus be concluded that the analytical design of the floor girders is too optimistic with respect to the bending moments and deflections, but it is expected that these increases can be overcome within the maximum construction height. For the side girders a highly conservative design for bending moments and deflections is obtained through the analytical calculations which could lead to a higher slenderness.
However, it turns out that the shear and torsional capacity are governing for design and according to the analytical calculations both massive and open structure designs do not meet the requirements already. This might be solved by a slightly less conservative approach for shear and torsion loads that follows from the FEM model, but an even more slender side girder is therefore most likely not an option.